



University of
Stavanger

Faculty of Science and Technology

MASTER'S THESIS

Study program/Specialization: <i>Mechanical and structural engineering and material science / Mechanical engineering</i>	Spring semester, 2013 Open/ Restricted access
Writer: <i>Gunnar Haarr</i>	_____ (Writer's signature)
Faculty supervisor: <i>Vidar Hansen</i> External supervisor(s): <i>Atle Sjølyst-Kverneland</i>	
Title of thesis: <i>Low temperature thermo mechanical treatment of corrosion resistant alloys.</i>	
Credits (ECTS): <i>30</i>	
Key words: <i>UNS S31803 duplex stainless steel; Surface hardening; Erosion wear; Tensile test; Charpy impact test; Hardness test; Corrosion test; Metallographic examination.</i>	Pages: <u>114</u> + enclosure <u>14+CD</u> Stavanger, <u>12.06.2013</u> Date/year

Abstract

Wear deteriorates materials and are a widespread problem in many areas of industry. To some extent, all physical materials experience wear in one form or another by moving gas, particles, fluids or a combination of these substances relative to the material in focus. More specifically, there must be an interaction between two objects in order to achieve an extent of material displacement or removal. Change of physical dimensions due to wear may have serious consequences with loss of functionality of a part. There are different methods available in order to minimize the effect of wear. The interaction between the two objects may be prevented, the relative motion and the velocity may be reduced and more. The preventive action is strongly dependent of the particular application, and in some cases the best method might be to enhance the wear resistance of a part. This may be done by changing material, heat treatment of base material or by some sort of surface engineering. This may include surface finishing, plating, coating or surface modification process by heat treatment.

Present work has focused on the low temperature surface treatment of corrosion resistant alloys as a mean to increase the resistance against erosive wear. Duplex stainless steel have been used as base material and a total of four different surface treatments have been evaluated and tested against erosive wear. These include two low temperature nitriding and/or carburizing methods called Expanite and Kolsterising, one thermal spray method called high velocity oxygen fuel (HVOF) coating with tungsten carbide and one nitriding method called Sursulf. In order to evaluate the possible effect on base material and confirm the existence of the surface, experimental tests have been performed in addition to the erosion test. Tensile test, Charpy impact test, hardness test, corrosion test and some metallographic examination are among the tests supporting the evaluation of the surface treatments.

Erosion tests showed that there is no surface treatment which is superior to the other treatments. There are advantages and disadvantages subjected to each of the surface treatment in question. Nevertheless, Expanite and Kolsterising showed an improvement on erosion rates relative to untreated duplex for particle impact angles in the range from 0° to somewhere between 30° and 90°, both at low and high particle velocity. HVOF and Sursulf, however, only showed superior good erosion rates when testing with high particle velocity. At 90° particle impact angle, untreated duplex was as good as the surface treated duplex, or even better, both at low and high velocity. Only HVOF could match and get lower erosion rate than untreated duplex at this angle, but only at high particle velocity.

In terms of the possible effect the surface treatments had on base material properties, the experimental results revealed several problems associated with precipitation of unwanted phases, brittleness and non homogeneous surface layer. Expanite and Kolsterising are heat treatments involving temperatures around 400°C. Even at this temperature, a close to 100 % brittle fracture was experienced on the Charpy impact test. Metallographic examinations also revealed precipitation of nitrides and/or carbides on these samples, and a non homogeneous surface layer was revealed on the Expanite samples. Precipitates were also found in samples treated with Sursulf method, but Charpy impact test did not show the same brittleness behavior. HVOF did not result in any significant change in microstructure. This surface treatment showed relative good results for all experiments, but the binder material may be subjected to corrosion reactions and material degradation under specific environments.

Table of contents

ABSTRACT	II
TABLE OF CONTENTS	III
ACKNOWLEDGEMENT	V
1 INTRODUCTION	1
1.1 ROXAR SUBSEA CHEMICAL INJECTION VALVE	1
1.2 CHALLENGE ON THE RECEPTACLE ASSEMBLY	2
1.3 TEST MATRIX	3
1.4 OIL AND GAS STANDARDS.....	4
1.4.1 Norsok M-001 Material selection	4
1.4.2 Norsok M-630 Material data sheets and element data sheets for piping	4
1.4.3 ISO 15156 Materials for use in H ₂ S-containing environments in oil and gas production.....	5
1.4.4 ISO 10423 Drilling and production equipment-Wellhead and christmas tree equipment	7
1.4.5 ISO 13628 Design and operation of subsea production systems	7
1.4.6 DNV-RP-F112 Design of duplex stainless steel subsea equipment exposed to cathodic protection	8
2 THEORY	9
2.1 METALLURGICAL PRINCIPLES.....	9
2.1.1 Alloying additions.....	10
2.2 DUPLEX STAINLESS STEEL.....	14
2.2.1 Structural changes and precipitates	16
2.2.2 Heat treatment	20
2.3 TRIBOLOGY	22
2.3.1 Abrasive wear	25
2.3.2 Solid particle erosion.....	30
2.4 SURFACE HARDENING.....	35
2.4.1 Diffusion methods of surface hardening.....	37
2.4.2 Thermal spray coating	43
2.5 APPLICABLE SURFACE TREATMENT METHODS	44
2.5.1 Expanite	44
2.5.2 Bodycote Kolsterising.....	45
2.5.3 High velocity oxygen fuel	46
2.5.4 Sursulf	48
3 EXPERIMENTS	49
3.1 MATERIAL DETAILS	49
3.2 MATERIAL PREPARATION	51
3.3 TENSILE TEST	54
3.4 CHARPY TEST.....	56
3.5 HARDNESS TEST	57
3.6 EROSION TEST.....	61
3.7 G48 CORROSION TEST.....	64
3.8 METALLOGRAPHIC EXAMINATION	66

4	EXPERIMENTAL RESULTS	69
4.1	TENSILE TEST	69
4.2	CHARPY TEST	70
4.3	HARDNESS TEST	73
4.4	EROSION TEST.....	75
4.5	CORROSION G48	81
4.6	METALLOGRAPHIC EXAMINATION	84
5	DISCUSSION	89
5.1	TENSILE TEST	89
5.2	CHARPY TEST	91
5.3	HARDNESS TEST	93
5.4	EROSION TEST.....	96
5.5	CORROSION G48	102
5.6	METALLOGRAPHIC EXAMINATION	106
6	CONCLUSION	109
7	REFERENCES	111
	ATTACHMENT A: MATERIAL CERTIFICATES	115
	ATTACHMENT B: SEM IMAGES OF EROSION SURFACES	120
	ATTACHMENT C: SEM IMAGES OF HVOF SURFACE – CORROSION G48	125
	ATTACHMENT D: OPTICAL MICROGRAPHS OF NAOH ETCHED SPECIMENS	128

Acknowledgement

This thesis has been an informative, interesting and challenging experience. A lot of work has been done practically, experimentally and theoretically. Much of this work could not be accomplished with the degree of completion without the support and help from a number of resources.

First of all, I would like to thank my external supervisor at Roxar, Atle Sjølyst-Kverneland, and my department supervisor at University of Stavanger, Vidar Hansen. They have supported me and guided me throughout the fulfillment of this Master thesis.

The material is provided by Scana Steel Stavanger. This Master thesis could not be done without material available. Further, for the preparation of all test specimens and for the performance of various experimental tests, I would like to thank laboratory personnel at University of Stavanger for support and training of the various tools and machinery I have used. I am also thankful to Jan Kåre Bording for helping me making the final turning of the tensile test specimens and to Ingunn Cecilie Oddsen for help and use of the scanning electron microscope.

I owe special thanks to all surface treatment suppliers for surface treating the duplex stainless steel. This includes Expanite AS, Bodycote, Trio Oil and Bauer Hydraulic Motors AS. I appreciate the presentation and visit from Expanite and also the surface technology discussions per telephone. I will also give a special thank to Trio Oil for their guided tour at their facilities.

This Master thesis could neither been accomplished without the support from Roxar RFM, both financially and for using their production facilities. In this matter, I want to acknowledge Jan Ivar Nygaard and Rune Sandnes.

Erosion testing at Det Norske Veritas in Høvik was an important and big part of this Master thesis with respect to wear testing. In this matter, two weeks were spent at their facilities with support from Tor Jo Landheim and his colleagues.

Tension test was performed at Quality Lab in Forsand with the help of Petter Lunde. Per Morten Bjørheim from this company has also been involved regarding technical discussion around metallographic examinations. I appreciate your support and kindness.

1 Introduction

1.1 Roxar subsea Chemical Injection valve

Roxar is a business unit of Emerson Process Management and, based on their web page, a leading international technology solutions provider covering the entire reservoir optimization value chain. The objectives are to help oil and gas operators increase oil and gas recovery from their reservoirs, reduce uncertainty and make improved field management decisions [10].

Flow assurance is a term commonly used to cover a wide range of flow-related issues. These issues typically include hydrate formation, wax formation, asphaltene formation, emulsions, foaming, scale formation, sand production, slugging and material-related issues. All of these issues are directly related to either the specific reservoir and/or fluid properties of the field being developed [11]. Roxar provides a complete flow assurance solution for the oil and gas industry, where chemical injection control is an important area within this topic. Roxar provides a flow control valve to control flow and dosage rates in subsea chemical injection applications with high degree of precision to prevent hydrates. This product is called Roxar subsea Chemical Injection valve.

The Roxar subsea Chemical Injection valve is a remote operated, subsea retrievable high flow throttle valve illustrated in Figure 1. Its main purpose is to provide precise control and measurement of chemical dosage rates into the production process to counter flow assurance threats like hydrates, scaling, corrosion, wax and asphaltene build-up. Hydrate is a crystalline combination of natural gas and water that forms under particular combinations of low temperature and high pressure.

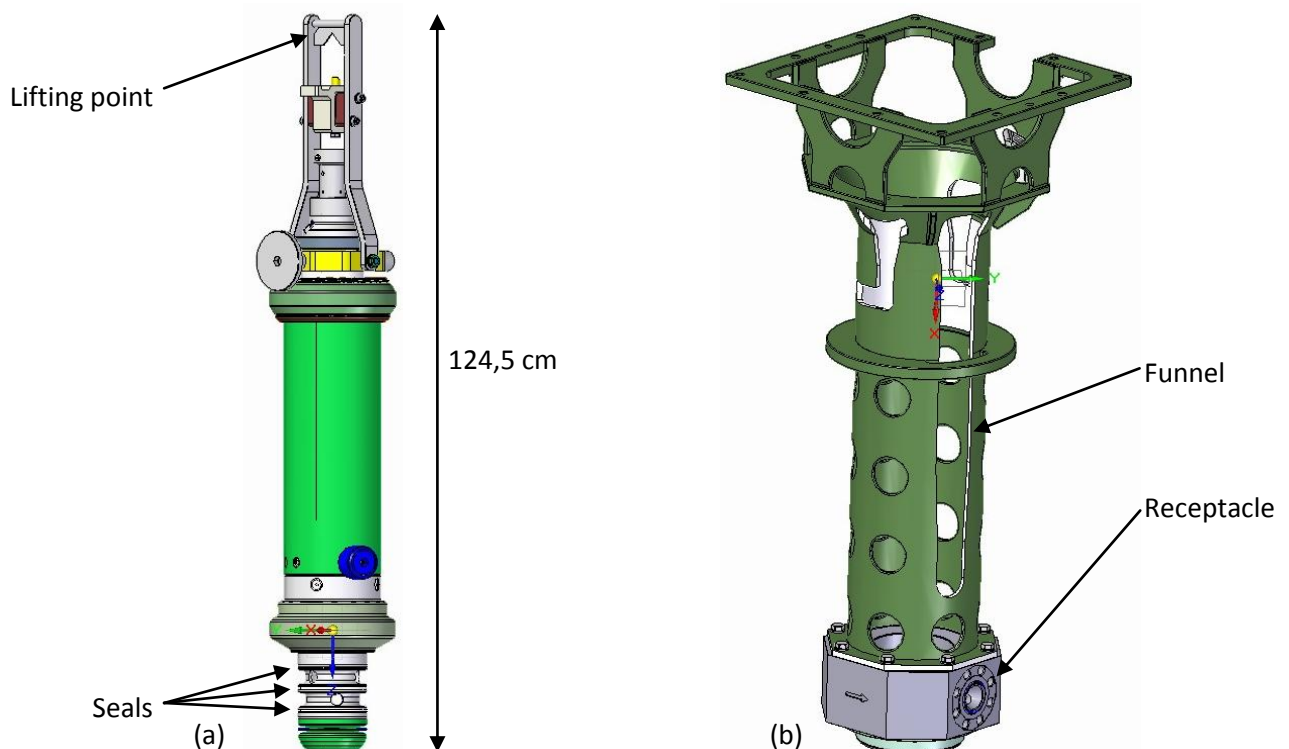


Figure 1. Illustration of the Roxar subsea Chemical Injection valve where (a) is showing the retrievable valve assembly and (b) is showing the fixed part, namely the funnel and receptacle assembly. The retrievable section is to be lifted by crane or equivalent by the handle assembly shown in (a). Three seals are engaged into the receptacle for sealing purpose.

1.2 Challenge on the receptacle assembly

The receptacle is part of the fixed assembly of the Roxar subsea Chemical Injection valve. It consists of a receptacle and a sleeve as shown in Figure 2.

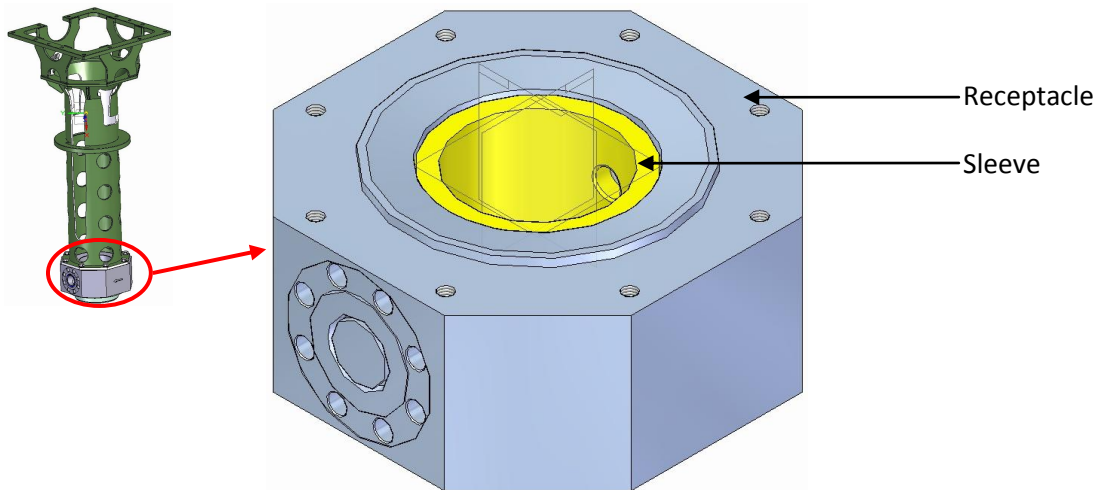


Figure 2. Detail view of receptacle and sleeve. Bolt holes on top are for mounting the funnel.

Wear is a term associated with some kind of material degradation by physical attrition. The sleeve is subjected to mainly two mechanisms wearing the outer surface:

1. Erosive wear due to the chemical fluid flow which contains a certain amount of particles at a certain velocity. The fluid will be directed along the inside surface of the sleeve.
2. Abrasive wear due to the insertion and extraction of the retrievable section of the valve. This movement will lead to a vertical movement of non-metallic seals, see Figure 1 (a), scratching the inside of the sleeve.

In addition, there is a possibility of sleeve being subjected to hydrocarbons and other chemicals from the oil and gas production which has a corrosive effect on the sleeve. All these factors benefit a material with hard surface and which is corrosion resistant. To comply with tensile and compressive stresses, a relatively high strength material is required as well. Based on the assumptions above, properties similar to a ceramic are beneficial but not sufficient. Typical ceramic properties are [9]:

- **Material degradation (corrosion):**
Ceramic materials are exceedingly immune to corrosion by almost all environments.
- **Hardness:**
One of the hardest known materials is ceramics which make them suitable when an abrasive or grinding action is required.
- **Stress-strain behavior:**
The flexural strength, also called fracture strength or bend strength, is an important mechanical parameter for brittle ceramics. Tensile strengths of ceramics are about 1:10 of their compressive strengths, and ceramics fail typically after only 0,1 % strain.
- **Toughness:**
The ability of a ceramic to absorb energy up to fracture is limited. Their toughness is low with a brittle fracture behavior.

Due to the stress-strain behavior and the toughness of the ceramics, ceramic material is disregarded. An eventually brittle fracture on a ceramic may have a negative consequence when operating with pressures up to 1050 bar¹ on hydrostatic pressure tests. Therefore, a study of hardening an ordinary steel to enhance wear properties is of great interest.

This Master thesis will examine and compare different heat treatment techniques applied on duplex stainless steel UNS S31803 in terms of increasing wear resistance and evaluate possible effects on base material properties. UNS S31803 is initially chosen since this material is compatible with the materials used both on the receptacle and the retrievable valve. Further, duplex is extensively used in the subsea market for more than 25 years [12] and is also the material used for a variety of subsea products in Roxar. It has a relatively high strength, ductility, toughness and it is good in terms of corrosion resistance. This makes the use of duplex as a safe and reliable choice. However, this steel has relatively low hardness and low wear resistance [13].

In order to examine and compare the different surface treatments applied on the duplex stainless steel, test specimens will be made in order to perform experiments like hardness, erosion, corrosion, strength, impact toughness in addition to some metallographic examinations by use of optical and electron microscope. Based on the experimental results, a conclusion will be made, if any, for the final recommendation of surface treatment for the sleeve of the Roxar subsea Chemical Injection valve.

1.3 Test matrix

An overview of the surface treatment methods used in this document is shown in Table 1. These surface treatments will make up the foundation for the experimental tests creating the basis of the analysis and ranking of treatments. The base material is duplex stainless steel UNS S31803 according to Norsok MDS D47.

Table 1. Selected surface treatments of duplex stainless steel UNS S31803.

#	Surface treatment	Technology	Company
0	Untreated	Base material	Not applicable
1	Expanite	Low temperature nitriding/carburizing	Expanite AS
2	Kolsterising	Low temperature carburizing	Bodycote
3	High velocity oxygen fuel	Thermal spray of tungsten carbide	Trio Oil Tech Service
4	Sursulf	Nitriding	Bauer Hydraulic Motors AS

Test specimens will be made for performing the selected experiments in order to come up with data sufficient to perform a comparison analysis between the surface treatments. An overview of the selected experiments is shown in Table 2. All experiments will be performed by the author of this Master thesis.

Table 2. Selected experiments to be performed.

#	Experiment	Based on	Location
A	Tension test	ISO6892-1	Q-lab.
B	Charpy impact test	ASTM A370	UiS
C	Hardness test	Rockwell B/C and micro Vickers	Roxar and UiS
D	Corrosion test	ASTM G48	UiS
E	Erosion test	DNV Høvik	DNV Høvik
F	Metallographic examination	Optical and electron microscope	UiS

¹ 1050 bar is based on 1,5 times the design pressure of 690 bar + 15 bar according to ISO 13628-6 (11.2.2).

Chemical composition of material designated as percent of a particular element represent weight percent relative to the total alloy weight in this document. If needed to express composition of an alloy in atom percent or mass per unit volume, this will be specified specifically.

1.4 Oil and gas standards

The Roxar subsea Chemical Injection valve shall comply with certain oil and gas standards in order to be qualified and accepted in the industry. There are hundreds of standards available for which all of them describe a confined area of service. Roxar have made a system requirement specification document listing all applicable documents to which the Roxar subsea Chemical Injection valve must comply. Some of them describe requirements for the mechanical strength and integrity, other give requirements in terms of material issues and other in terms of electrical applications and more. In terms of mechanical requirements involving material related issues, the following standards are applicable:

- Norsok M-001 Material selection
- Norsok M-630 Material data sheets and element data sheets for piping
- ISO 15156 Materials for use in H₂S-containing environments in oil and gas production
- ISO 10423 Drilling and production equipment-Wellhead and Christmas tree equipment
- ISO 13628 Design and operation of subsea production systems
- DNV-RP-F112 Design of duplex stainless steel subsea equipment exposed to cathodic protection

1.4.1 Norsok M-001 Material selection

This Norsok standard provides general principles, engineering guidance and requirements for materials selection and corrosion protection for hydrocarbon production and processing facilities and supporting systems for fixed offshore installations. The standard also applies for onshore terminals, except for structural and civil works [14].

Among the specific applications specified in this standard, the duplex stainless steel UNS S31803 is an often recommended material for use in e.g. subsea production and flow line systems. There are also some design limitations for materials listed below:

- For submerged parts that may be exposed to cathodic protection, resistance against hydrogen embrittlement shall be controlled by specifying that the actual hardness of material is less than 300 HV₁₀ for duplex stainless steel base material.
- For pressure retaining purposes, the materials shall resist general corrosion, localized corrosion in the form of pitting and crevice corrosion and environmental cracking in the form of chloride induced corrosion cracking (CSCC) and sulphide stress cracking (SSC) where specified H₂S limits are given. The minimum design temperature is -46°C for 22Cr duplex stainless steel.

1.4.2 Norsok M-630 Material data sheets and element data sheets for piping

This Norsok standard includes material requirement in a collection of material data sheets for use in piping systems, selected according to Norsok L-001. The material data sheets can also be applied for components other than piping, e.g. pressure vessels, pumps, strainer, etc. [15]. Norsok M-630 contains two data sheets of special interest:

1. Material data sheet D47

The material data sheet D47 contains specifications concerning type 22Cr duplex stainless steel with the product form bar. The grade UNS S31803 and UNS S32205 is specifically specified and involve standard ASTM A479 and ASTM A988. Below are some important specifications from MDS D47:

- Bar shall have maximum section thickness of 300 mm without special agreements.
- Nitrogen content to be within 0,14-0,20 %.
- Charpy testing is required according to ASTM A370 at -46°C. The minimum absorbed energy shall satisfy 45 J average and 35 J single.
- The ferrite content shall be determined to ASTM E562 or equivalent and shall be within 35-55 %.
- The microstructure, as examined at minimum 400 X magnification on a suitable etched specimen shall be free from intermetallic phases and precipitates.

2. Element data sheet NHF2

The element data sheet NHF2 contains specifications concerning hardfacing by thermal spraying of tungsten carbide. High velocity oxygen fuel (HVOF) or equivalent process is specified as the thermal spraying process where the use of TAFA/Praxair JP 5000/8000 is considered to be a typical, accepted equipment. Below are some important details from EDS NHF2:

- The coating shall be of cermet type based tungsten carbide and a metallic binder, where the binder shall be based on Co and/or Ni which shall be alloyed with Cr or Cr and Mo.
- The coating shall be in the range 0,15-0,25 mm after grinding and lapping.
- The average hardness shall be minimum 1000 HV_{0,3}.

1.4.3 ISO 15156 Materials for use in H₂S-containing environments in oil and gas production

This standard consists of the following parts:

Part 1: General principles for selection of cracking-resistant materials

Part 2: Cracking-resistant carbon and low-alloy steels, and the use of cast irons

Part 3: Cracking-resistant corrosion resistant alloys and other alloys

ISO 15156-1 General principles for selection of cracking-resistant alloys

This part of ISO 15156 describes general principles and gives requirements and recommendations for the selection and qualification of metallic materials for service in equipment used in oil and gas production and in natural-gas sweetening plants in H₂S-containing environments, where the failure of such equipment can pose a risk to the health and safety of the public and personnel or to the environment [16]. In general, this part references the material selection to follow the requirements and recommendations of ISO 15156-2 or ISO 15156-3, as appropriate.

ISO 15156-2 Cracking-resistant carbon and low-alloy steels, and the use of cast irons

This part of ISO 15156 focuses on carbon and low-alloy steel and is therefore not applicable for the purpose of this document since the material considered for examination is a duplex stainless steel.

ISO 15156-3 Cracking resistant corrosion-resistant alloys and other alloys

This part of ISO 15156 gives requirements and recommendations for the selection and qualification of corrosion-resistant alloys and other alloys for service in equipment used in oil and natural gas production and natural gas treatment plants in H₂S-containing environments, whose failure can pose a risk to the health and safety of the public and personnel or to the environment [17]. Specifications of special interest from this standard include:

- Requirements for overlays, surface treatments, plating, coatings, linings, etc.
 - i. Metallic coatings, conversion coating, plastic coatings or linings may be used but are not acceptable for preventing cracking.
 - ii. The effect of their application on the cracking resistance of the substrate shall be considered.
 - iii. Nitriding with a maximum case depth of 0,15 mm is an acceptable surface treatment if conducted at a temperature below the lower critical temperature of the alloy being treated. The use of nitriding as a means of preventing cracking in sour service is not acceptable.

- Environmental and materials limits for the uses of duplex stainless steel.
 - i. Maximum temperature to be 232°C and maximum partial pressure of H₂S to be 10 kPa for pitting-resistance equivalent number (PREN) in the range of 30-40 and Mo >1,5 %.
 - ii. Wrought and cast duplex stainless steel shall have ferrite content of between 35 % and 65 % and shall not have undergone ageing heat-treatments.

- Cladding, overlays and wear-resistant alloys.
 - i. Hard facing may be used.
 - ii. Surface layers specifically designed to provide hard facing is not specified in ISO 15156. No production limits for temperature, partial pressure of H₂S, Cl⁻ or in situ pH have been established.
 - iii. Unless the user can demonstrate and document the likely long-term in-service integrity of the hard-facing materials, the base material after application of the hard-facing material shall comply with ISO 15156-2 or ISO 15156-3 as applicable.

- Chemical composition of duplex stainless steel UNS S31803 is specified with maximum percentage mass fraction reproduced and shown in Table 3.

Table 3. Maximum percentage mass fraction for the chemical composition of duplex stainless steel UNS S31803 according to ISO 15156-3.

Carbon C	Manganese Mn	Phosphorus P	Sulfur S	Silicon Si	Chromium Cr	Nickel Ni	Nitrogen N	Molybdenum Mo
0,030	2,00	0,030	0,020	1,00	21,0-23,0	4,5-6,5	0,08-0,20	2,5-3,5

1.4.4 ISO 10423 Drilling and production equipment-Wellhead and christmas tree equipment

This standard specifies requirements and gives recommendations for the performance, dimensional and functional interchangeability, design, materials, testing, inspection, welding, marking, handling, storing, shipment, purchasing, repair and remanufacture of wellhead and Christmas tree equipment for use in the petroleum and natural gas industries [18].

In terms of material general requirements for bodies, bonnets, end and outlet connection, there are some material property requirements depending on the pressure rating and material designation of the product in question. For material designation 36K and product specification level 3, the following requirements include:

- Yield strength 0,2 % offset 348 MPa minimum
- Tensile strength 483 MPa minimum
- Elongation in 50 mm 21 % minimum
- Reduction in area No requirement
- Charpy V-notch 20 J minimum average impact value at transverse direction at -46°C
- Brinell hardness 140 HBW minimum².

Requirements are also given to heat treatment procedure, material composition and non-destructive examinations, but nothing specifically addressed to duplex stainless steel.

1.4.5 ISO 13628 Design and operation of subsea production systems

ISO 13628 consists of the following parts:

- Part 1: General requirements and recommendations
- Part 2: Flexible pipe systems for subsea and marine applications
- Part 3: Through flowline systems
- Part 4: Subsea wellhead and tree equipment
- Part 5: Subsea umbilicals
- Part 6: Subsea production control systems
- Part 7: Completion/workover riser systems
- Part 8: Remotely operated vehicle interfaces on subsea production systems
- Part 9: Remotely operated tool intervention systems
- Part 10: Specification for bonded flexible pipe
- Part 11: Flexible pipe systems for subsea and marine applications

² There is no standardized conversion table from Brinell hardness to Vickers or Rockwell hardness for duplex stainless steel. Conversion tables given in ASTM E140 should only be considered valid for the specific materials listed in the standard.

In addition to Part 1, Part 6 is applicable for the Roxar subsea Chemical Injection valve since the valve is designed based on this standard.

ISO 13628-1 General requirements and recommendations

This part of ISO 13628 provides general requirements and overall recommendations for development of complete subsea production systems, from the design phase to decommissioning and abandonment. This part is intended as an umbrella document to govern other parts of ISO 13628 dealing with more detailed requirements for the subsystems which typically form part of a subsea production system [11].

No special requirements or recommendations are given with respect to surface treatment of stainless steel.

ISO 13268-6 Subsea production control systems

This part of ISO 13628 is applicable to design, fabrication, testing, installation and operation of subsea production control systems. It covers surface control system equipment, subsea-installed control system equipment and control fluids. This equipment is utilized for control of subsea production of oil and gas and for subsea water and gas injection services [19].

No special requirements or recommendations are given with respect to surface treatment of stainless steel.

1.4.6 DNV-RP-F112 Design of duplex stainless steel subsea equipment exposed to cathodic protection

This is a recommended practice document which covers all components made from duplex stainless steels that are installed subsea and are exposed to cathodic protection. The objective of this document is to be an industry recommended practice to define the best practice for design of duplex stainless steel components, give detailed recommendations on loads and conditions, to define other parameters affecting the resistance to hydrogen induced stress cracking, to give stress/strain design criteria and manufacturing, fabrication and test recommendations [20]. From the material requirement section, the following recommendations are given:

- Minimum yield strength of 450 MPa (22Cr duplex stainless steel)
- Metallographic characterization of the microstructure like ferrite content, inter-metallic phase precipitation and austenite spacing
- Corrosion test according to ASTM G48
- Impact tests at an appropriate temperature

2 Theory

2.1 Metallurgical principles

Metal alloys involve a broad specter of materials where ferrous alloy represent those of which iron is the prime constituent. A taxonomic classification scheme for the various ferrous alloys is presented in Figure 3 [9].

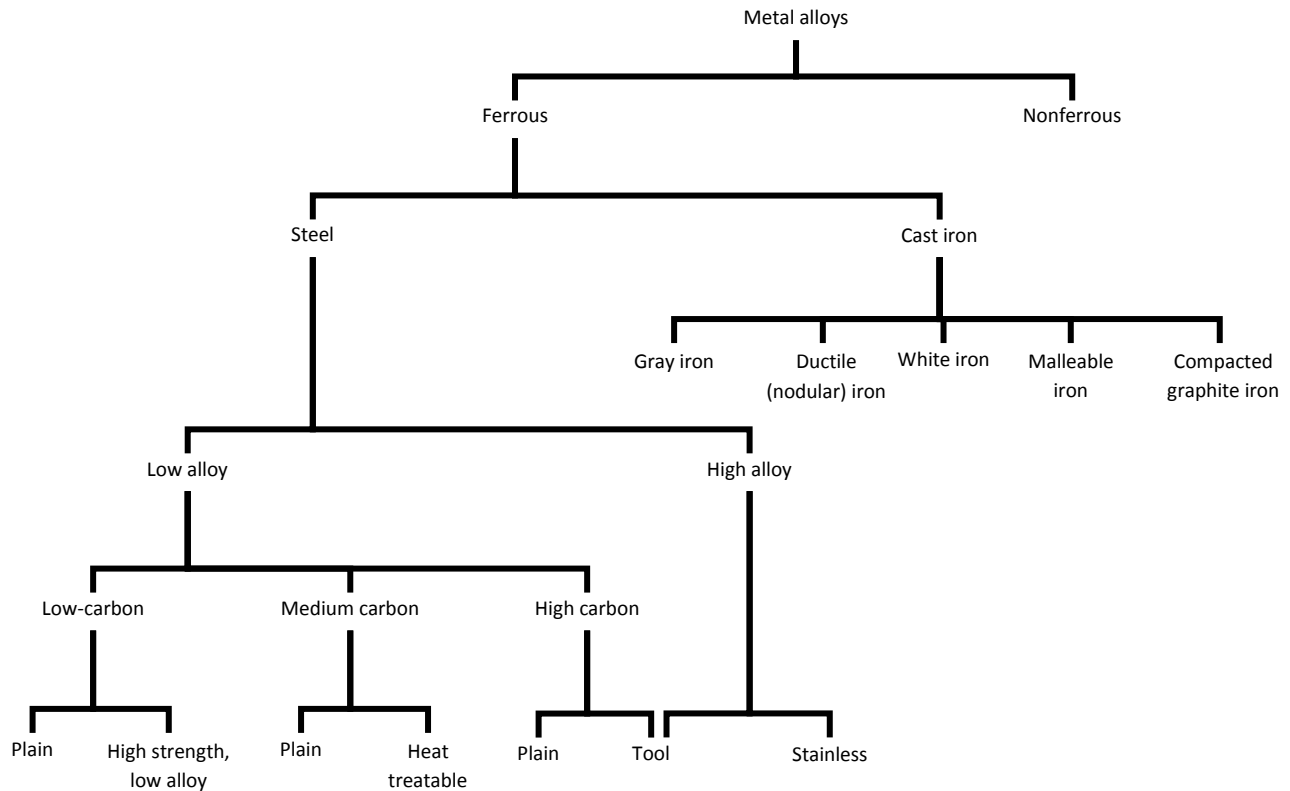


Figure 3. Classification scheme for the various ferrous alloys [9].

Stainless steel is located along with the high alloy steel which is defined as steel with more than 10 % alloying elements and where the chromium content is minimum 10,5 %. This group can again be divided into five main families based on the predominant phase constituent of the microstructure [7]:

- i. Martensitic
- ii. Ferritic
- iii. Austenitic
- iv. Duplex (ferritic-austenitic)
- v. Precipitation hardenable

Transition structures or analytic anomalies give rise to groups that may be placed between or added to the five preceding ones by reason of interest in their properties. There are for example martensitic-ferritic structures and martensitic or austenitic precipitation-hardening structures [21]. The fifth family, the precipitation hardenable alloys, is based on the type of heat treatment used rather than microstructure.

Steel offer a large variety of physical, mechanical and chemical properties. One of the principal reasons for this is that iron has three types of crystal structure between 0 K and its melting point [21]:

1. α -phase with a body centered cubic structure (BCC) from 0 K to 910°C
2. γ -phase with a face centered cubic structure (FCC) from 910°C to 1400°C
3. δ -phase with a body centered cubic structure (BCC) from 1400°C to 1538°C

These crystal structures with respect to temperature and carbon content are illustrated in a phase diagram as shown in Figure 4. However, alloying additions play very different roles on the crystallographic structure of alloys and thereby also on the equilibrium diagrams.

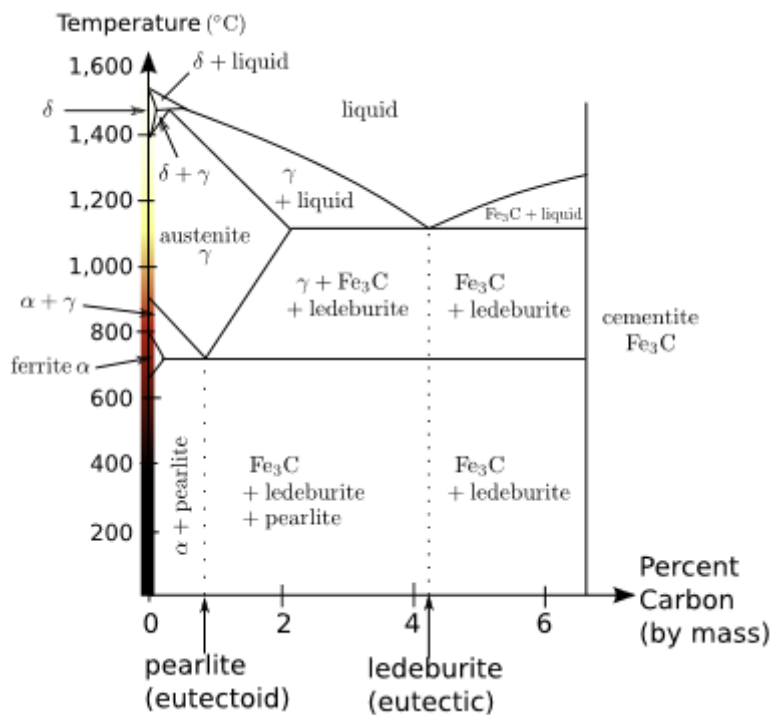


Figure 4. Iron-carbon phase diagram under atmospheric pressure [22].

2.1.1 Alloying additions

Alloying elements are an important part of the material integrity and the effect on some of them in ferrous metal are summarized below with special consideration to duplex stainless steel.

Carbon (C)

Carbon is an austenite (γ) stabilizing element that favors the formation of interstitial solid solutions in the FCC structure. As the carbon content in steel increases, strength increases, but ductility and weldability decrease [7].

The carbon content of most wrought duplex stainless steel is limited to 0,02 % or 0,03 %, primarily to suppress the precipitation of Cr-rich carbides which can act as initiation sites for pitting corrosion and intergranular attack [3].

Chromium (Cr)

Chromium is a medium carbide former and is the most important alloying element in steels. It increases hardenability, corrosion and oxidation resistance of steels, improves high-temperature strength and high-pressure hydrogenation properties and enhances abrasion resistance in high-carbon grades. Chromium carbides are hard and wear-resistant and increase the edge-holding quality. The addition of Cr in steels enhances the impurities like P, Sn, Sb and As segregating to grain boundaries and induces temper embrittlement [7].

Chromium improves the localized corrosion resistance by the formation of a passive chromium-rich oxy-hydroxide film. This is achieved by extending the passive range as shown in the polarization curve in Figure 5.

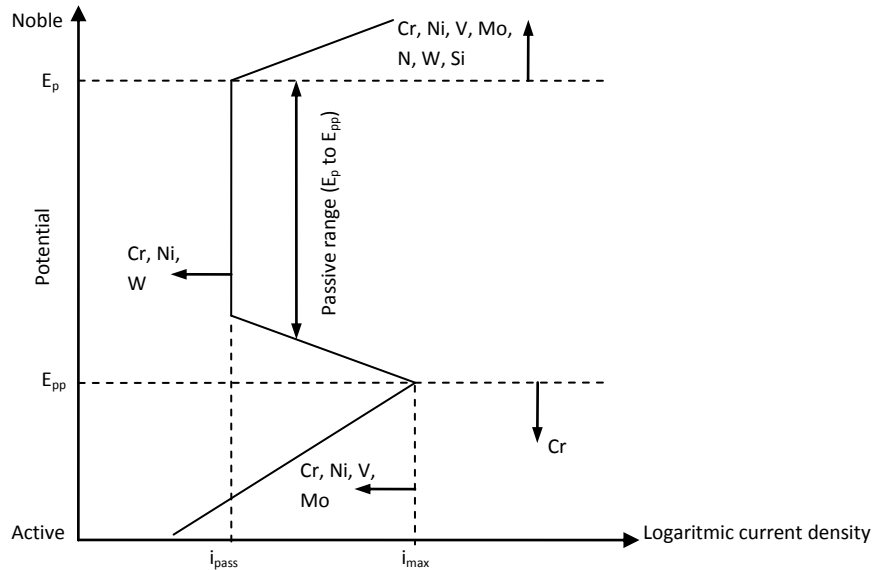


Figure 5. Schematic summary of the effects of alloying elements on the anodic polarization curve [3].

However, there is a limit to the level of chromium that can be added due to enhanced precipitation of intermetallic phases such as σ . This phenomenon is illustrated in Figure 6. These phases often lead to reduction in ductility, toughness and corrosion properties. Chromium stabilize ferrite [3].

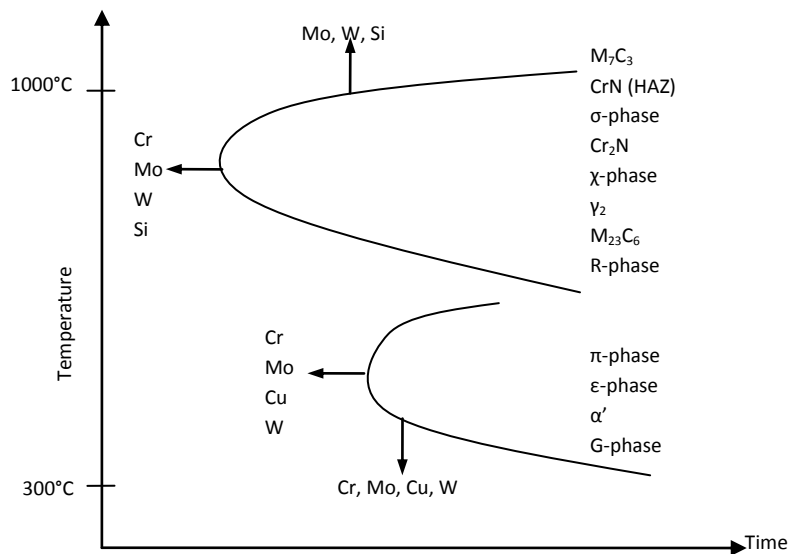


Figure 6. Schematic summary of the effect of alloying elements on the formation of various precipitates [3].

Molybdenum (Mo)

Molybdenum is a pronounced carbide former and stabilizes ferrite. It dissolves slightly in cementite and it forms carbides when the content is high enough. It can induce secondary hardening during tempering of quenched steels and improves the creep strength of low-alloy steels at elevated temperatures. The addition of Mo produces fine-grained steels, increases hardenability and improves fatigue strength. It increases corrosion resistance and is used to a great extent in high-alloy Cr ferritic stainless steels and with Cr-Ni austenitic stainless steels. High Mo content reduces the stainless steel's susceptibility to pitting and crevice corrosion as shown in Figure 5. It has a very strong solid solution strengthening in austenitic alloys at elevated temperatures [7]. Concentrations are limited in duplex steels due to its tendency to promote sigma phase formation [21].

Aluminium (Al)

Aluminium is widely used as a deoxidizer and a grain refiner and is usually an alloying element in nitriding steels since it forms nitrides with nitrogen. It increases scaling resistance and is therefore often added to heat-resistant alloys. In precipitation-hardening stainless steel, aluminium can be used as an alloying element causing precipitation-hardening reaction. Aluminium increases the corrosion resistance in low-carbon corrosion resisting steels and is one of the most effective elements in controlling grain growth prior to quenching. A drawback is the tendency to promote graphitization [7].

Nickel (Ni)

Nickel is a noncarbide-forming element in steels. As a result of the open γ -phase field, Ni is an austenite-forming element. Nickel raises hardenability and in combination with Cr and Mo produces greater impact toughness and fatigue resistance. Nickel raises the corrosion resistance of Cr-Ni austenitic stainless steels in nonoxidizing medium [7]. Larger amounts of nickel increase the risk of sigma formation in duplex steels [21].

Niobium (Nb)

Niobium is a very strong carbide and nitride formers. Small amounts of Nb can form fine nitrides or carbonitrides and refine the grains, therefore increasing the yield strength of steels. Niobium is widely used in micro alloying steels to obtain high strength and good toughness through controlled rolling and controlled cooling practices. Niobium is a stabilizer in Cr-Ni austenitic steels to eliminate intergranular corrosion [7].

Nitrogen (N)

Nitrogen is one of the important elements in expanded γ -field group. It can expand and stabilize the austenitic structure and partly substitute nickel in austenitic steels. Nitrogen can be used as an alloying element in micro alloying steels or austenitic stainless steels, causing precipitation or solid solution strengthening. Nitrogen induces strain aging, quench aging and blue brittleness in low-carbon steels [7].

Nitrogen has a positive effect on the resistance on pitting and crevice corrosion. It has also the ability to stabilize duplex alloys against the precipitation of intermetallic phases such as sigma (σ) and chi (χ) by reducing Cr-partitioning. Nitrogen reduces the risk of nitride formation due to an increase in austenite content and so a reduction in the distance between austenite islands [3].

Manganese (Mn)

Manganese is a weak carbide former only dissolving in cementite. It is an austenite former as a result of the open γ -phase field. Manganese is present in virtually all steels in amounts of 0,30 % or more. It is essentially a deoxidizer and a desulfurizer and has a lesser tendency for macro-segregation than any of the common elements. Manganese favorably affects forgeability and weldability. The addition of Mn in steels enhances the impurities such as P, Sn, Sb and As segregating to grain boundaries and induces temper embrittlement [7].

Manganese additions to stainless steel increase abrasion and wear resistance and tensile properties without loss of ductility. Further, Mn increases the solid solubility of nitrogen and thus allows for increased nitrogen content to be achieved without risk of out-gassing [3].

Copper (Cu)

Copper addition has a moderate tendency to segregate. It increases hardenability and it is detrimental to surface quality and exaggerates the surface defects inherent in resulfurized steels. Cu improves the atmospheric corrosion resistance and tensile properties in alloy and low-alloy steels and reportedly helps the adhesion of paint. In austenitic stainless steels, a Cu above 1 % result in improved resistance to hydrochloric acid and stress corrosion [7]. The addition of Cu to duplex stainless steels is limited to about 2 %, since higher levels reduce hot ductility and can lead to precipitation hardening [3].

Titanium (Ti)

Titanium is a very strong carbide and nitride former. The effects are similar to those of Nb, but titanium carbides and nitrides are more stable. It is widely used in austenitic stainless steels as a carbide former for stabilization to eliminate intergranular corrosion. It increases creep rupture strength through formation of special nitrides and tends significantly to segregation and banding [7].

Tungsten (W)

Tungsten is a strong carbide former and its behavior is very similar to Mo in steels. As the content increases in alloy steels, tungsten forms very hard, abrasion-resistant carbides and can induce secondary hardening during the tempering of quenched steels. It promotes hot strength and red-hardness and thus cutting ability. It prevents grain growth at high temperature [7]. Tungsten addition is added to duplex stainless steel to improve pitting resistance and crevice corrosion resistance [3].

Silicon (Si)

Silicon is a noncarbide former and free from cementite or carbides and is one of the principal deoxidizers used in steelmaking; therefore silicon content also determines the type of steel produced. It dissolves completely in ferrite when content is below 0,30 % increasing its strength without greatly decreasing ductility. If combined with Mn or Mo, silicon may produce greater hardenability of steels. In heat-treated steels, silicon is an important alloy element and increases hardenability, wear resistance, elastic limit and yield strength and scale resistance in heat-resistant steels [7].

Phosphorus (P)

Phosphorus segregates during solidification but to a lesser extent than C and S. It dissolves in ferrite and increases the strength of steels. As the amount of P increases, the ductility and impact toughness of steel decrease. It increases the hardenability [7].

Sulfur (S)

Sulfur has a detrimental effect on transverse ductility, notch impact toughness, weldability and surface quality, but has a slight effect on longitudinal mechanical properties. It has a very strong tendency to segregate at grain boundaries and cause reduction of hot ductility in alloy steels. However, sulfur in the range of 0,08-0,33 % is intentionally added to free-machining steels for increased machinability [7].

2.2 Duplex stainless steel

The melt for a duplex alloy can be produced using either high purity material in a conventional induction furnace, or high alloyed scrap in an electric furnace followed by argon oxygen decarburization (AOD), vacuum oxygen decarburization (VOD) or vacuum argon refinement process (VARP) converters. With this kind of treatment, high quality stainless steel materials are capable by achieving high decarburization rates even at low carbon content. The VARP converter favors lower sulfur content [3].

A duplex alloy is defined as one that contains a two-phase structure and is more often a descriptor of an alloy where both phases are present in significant quantities [3]. A phase may be defined as a homogeneous portion of a system that has uniform physical and chemical characteristics. Every pure material is considered to be a phase; so also is every solid, liquid and gaseous solution. Also, when a substance can exist in two or more polymorphic forms, like having both face-centered cubic crystal (FCC) and body-centered cubic crystal (BCC) structures, each of these structures is a separate phase because their respective physical characteristics differ [9]. For instance, water is a phase and ice is a phase. Ice + water is a two-phase mixture.

The use of the term duplex stainless steel in this document refers to the mixture of ferritic and austenitic crystal structures in a Fe-Cr-Ni alloy, with a range of 30 to 70 % ferrite. Duplex stainless steel are most commonly considered to have roughly equal amounts of ferrite and austenite, with current commercial production just slightly favoring the austenite for best toughness and processing characteristics [23]. Determining the volume fraction of ferrite and austenite structure is dependent on alloying element and thus the chemical composition of the metal. Equations have been derived to quantify the elemental effects of which ferrite and austenite will be stabilized by the so-called chromium and nickel equivalents respectively as shown below [24]:

- Ferrite stabilizer: $Cr_{eq} = \%Cr + 1,5 \%Mo + 2 \%Si + 1,75 \%Nb + 5 \%V + 5,5 \%Al + 1,5 \%Ti + 0,75 \%W$
- Austenite stabilizer: $Ni_{eq} = \%Ni + Co + 30 \%C + 25 \%N + 0,3 \%Cu + 0,5 \%Mn$

An empirical and approximate approach has been made in order to predict the microstructure of stainless steel in room temperature by use of chromium and nickel equivalent in a diagram representing the X- and Y- axes respectively. This diagram is called a Schaeffler diagram and is shown in Figure 7. This method allows a rough evaluation of the microstructure as a function of the steel composition, but it does not take into consideration the influence of the cooling rate and aging heat treatments [7].

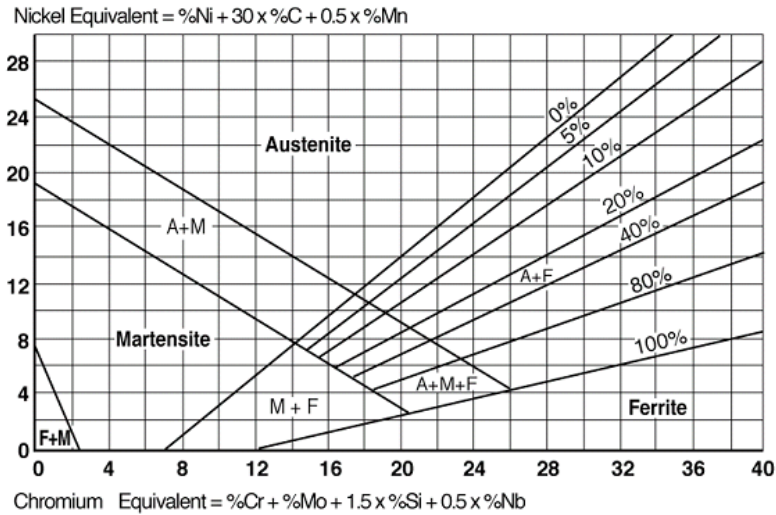


Figure 7. Schaeffler diagram showing the structure of various stainless steels based on chromium and nickel equivalents.

An advantage of having steel with two or more phases in equilibrium at room temperature is somewhat similar to those belonging to composite materials. The duplex structure exhibits properties that take advantage of the better attributes of each of the two phases [25] and its physical properties are between those of the austenitic and ferritic stainless steel. Ferritic stainless steel are composed of the α ferrite BCC phase and the austenitic stainless steels are composed of the γ austenite FCC phase. They have some distinctive difference in mechanical behavior and some of them are listed in Table 4.

Table 4. A general comparison of properties of the ferritic and the austenitic stainless steel [26].

	Ferritic stainless steel	Austenitic stainless steel	Duplex stainless steel
Phase and crystal structure	α ferrite BCC	γ austenite FCC	α ferrite BCC and γ austenite FCC
Ductility	Medium	High	Medium
Strengthening mechanism	Cold work (not heat treatable)	Cold work (not heat treatable)	Cold work (not heat treatable)
Corrosion resistant	Good and immune to stress corrosion.	Good, but susceptible to stress corrosion.	Very good.
Low temperature toughness	Low	High	Medium
Strength	Moderate yield but higher than austenitic	Moderate yield strength and high tensile strength	High yield strength and high tensile strength
Weldability	Bad	Very good	Good
Magnetic	Yes	No	Yes

Combining ferritic and austenitic crystal structure to a duplex stainless steel material provides a material which benefits properties from both structures. Actually, yield strength in duplex stainless steels is more than twice that of the single phase stainless steels of either ferritic or austenitic stainless steel. The high strengths of duplex steels are the result of several simultaneous mechanisms [3]:

- Interstitial solid solution hardening like C and N.
- Substitutional solid solution hardening of elements like Cr, Mo, Ni and more.

- Strengthening by grain refinement due to the presence of two phases.
- Possible hardening due to the formation of γ_2 phase.
- Strengthening due to ferrite since, for a similar composition, this phase is harder than the austenitic structure.
- Strain hardening by differential contraction of the two phases on cooling from annealing temperatures.

Duplex steels have also superior toughness and ductility when compared to the ferritic and martensitic stainless steels, in addition to superior intergranular and stress corrosion resistance compared to the austenitic stainless steel. This favorable combination of properties makes this class of stainless steels widely employed in oil and gas, petrochemical, pulp and paper industries. They are used in aqueous solutions containing chlorides, where they have substituted the austenitic stainless steels that are more susceptible to stress and pitting corrosion [7].

Pitting resistance equivalent number

Pitting corrosion resistance in stainless steels is mainly linked to the chromium, molybdenum and nitrogen contents and related in the form of a pitting resistance equivalent number (PREN) given by:

- $PREN = \%Cr + 3,3 (\%Mo + 0,5 \%W) + 16 \%N$ [17]

This formula is entirely empirical and neglects important residual elements such as sulfur and oxygen, together with the distribution of sulfide, silicate and oxide inclusions [21]. A PRE number greater than 40 is considered satisfactory for long exposure times in chloride-rich environments such as sea water [7], but these are borderline cases and should not be used for mechanical connections without cathodic protection [14]. Alloys containing $PREN > 40$ are known as superduplex. Higher values of PREN provide higher corrosion resistance, however they also lead to increased risk of sigma phase and alpha prime phase formation in the materials ferrite phase during manufacture [17] which is also illustrated in Figure 6.

2.2.1 Structural changes and precipitates

The iron-chromium-nickel ternary phase diagram is a roadmap of the metallurgical behavior of the duplex stainless steels [23] as shown in Figure 8. Duplex steel solidify in a ferritic structure and the austenitic forms in the solid state transformed from δ (α) to γ as the temperature falls to about 1000°C depending on alloy composition. The high temperature form of ferrite is traditionally known as δ rather than α . There is little change in the equilibrium ferrite-austenite balance at lower temperatures. Figure 8 show also the effect of nitrogen additions which stabilize the duplex structure by shifting the γ to δ (α) transformation to higher temperatures.

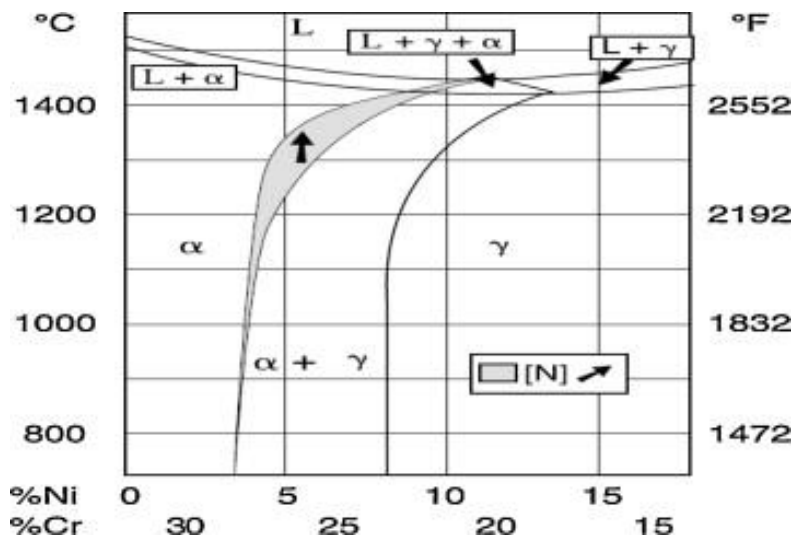


Figure 8. Section of the ternary Fe-Cr-Ni diagram at 68 % iron [23]. The arrow shows the effect of nitrogen additions.

Numerous structural changes can occur in the duplex stainless steels during isothermal or anisothermal heat treatments [21]. Most of these transformations take place in the ferrite, as element diffusion rates are much higher in the BCC ferrite structure than in the FCC austenite structure. The higher diffusion rate in ferrite is due to mainly three concerns [3]:

1. BCC crystal structure has less compact lattice. For instance, the atomic packing factor for BCC is 0,68 versus the atomic packing factor for FCC is 0,74 [9].
2. The ferrite is enriched in chromium and molybdenum which have a strong tendency to promote the formation of intermetallic phases.
3. Element solubility in the ferrite falls with a decrease in temperature, increasing the probability of precipitation during heat treatment.

Structural changes encountered in the duplex alloys can be classified in three groups, depending on whether they occur at temperatures above 1050°C, from 600 to 1050°C or below 600°C [21].

Temperatures above 1050°C

At temperatures above 1050°C, there is a reduction in the partitioning of substitutional elements between the phases and the ferrite content is increased as shown in Figure 8. This is particularly important for duplex grades with less than 0,2 %N on the heat affected zones of welds. An increased level of nitrogen limits ferrite enrichment in the heat affected zones, maintaining volume fractions and compositions similar to those in the base metal [21]. In addition, the ferrite becomes enriched in interstitial elements such as carbon and nitrogen.

Temperatures between 1050 and 600°C

This temperature range has several concerns with respect to structural changes and precipitates. At least three concerns are of importance:

1. Precipitation of carbides and nitrides

The hardening effect of carbide and nitrides is due to the fact that these precipitates work like dispersed phases in what is called dispersion strengthening of a material. This is a strengthening effect that emerges from an analysis of the movement of dislocation around particles showing that the yield stress varies

inversely with the spacing between the particles. This would lead to strengthening, but often they have adverse effect on ductility and toughness [27]. The precipitates nucleate heterogeneous on non-equilibrium defects such as excess vacancies, dislocations, grain boundaries, stacking faults, inclusions and free surfaces, all of which increase the free energy of the material [28].

i. Carbides

In modern duplex grades with less than 0,02 %C, carbides of the form M_7C_3 are rarely seen, but in moderately high carbon levels of about 0,03 %, the carbide $M_{23}C_6$ rapidly precipitates between 650 and 950°C as shown in Figure 9. Precipitation occurs most often where Cr-rich ferrite intersects with C-rich austenite at δ/γ boundaries, but is also found at the δ/δ and γ/γ boundaries and inside the ferrite and austenite grains [21]. Intergranularly precipitated carbides can produce intergranular corrosion and also reduce pitting resistance, primarily as a result of chromium depletion adjacent to the carbide [25]. Chromium carbides precipitation is also responsible for loss in toughness [29].

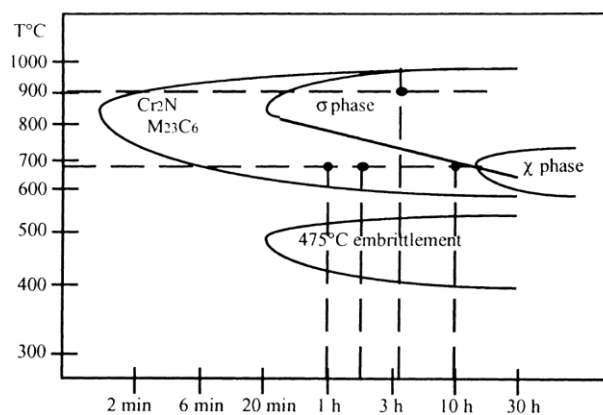


Figure 9. Time-temperature-transformation diagram for duplex stainless steel UNS S31803 [30].

ii. Nitrides

Above the annealing temperature of about 1040°C, the volume fraction of ferrite increases and the nitrogen solubility is high. On cooling, the solubility drops and the ferrite becomes supersaturated in nitrogen, leading to the intergranular precipitation of needle-like Cr_2N [3]. The particles nucleate initially at the α/γ and α/α grain boundaries, but precipitation within grains are also possible [21]. Another nitride, the cubic CrN , may also be formed in the heat affected zone on welds. Nitrides can be deleterious to corrosion resistance and cause loss of toughness. Chromium nitride precipitates are likely to cause chromium-depleted zones and also accommodate substantial amounts of nitrogen, resulting in a great decrease in critical pitting temperature [31].

2. Formation of intermetallic compounds

Depending on the chemical composition, where higher alloy duplex stainless steel are more sensitive, various intermetallic compounds may form in the ferrite:

- i. The sigma (σ) phase is a non-magnetic and intermetallic. The mechanism of precipitation is a eutectoid transformation of ferrite into austenite and sigma phase [32]. It is of most concern and is a hard embrittling precipitate associated with a drastic drop in both impact properties and corrosion resistance. The peak temperature is around 850°C for UNS S31803 as shown in Figure 9 and the σ -formation is especially encouraged by the elements Cr, Mo, Si and Mn. Furthermore, particles such as carbides or inclusions present at grain boundaries accelerate the formation of sigma phase by acting as

nucleation sites [21]. The formation of sigma phase grow from the γ/α boundaries [31] into the ferrite phase due to its faster diffusion rate than in austenite and result in chromium and molybdenum depletion in the surrounding matrix. This is believed to be the cause of reduced corrosion resistance. The reduced impact properties is due to the hard and brittle phase of the sigma [25].

- ii. Chi (χ) may form during a long exposure to relatively low temperatures as shown in Figure 9. Compared to sigma, it forms in much smaller quantities than sigma but has a similar influence on corrosion and toughness properties [21]. The chi phase can be distinguished optically from sigma phase by its more blocky morphology and higher reflectivity [25].
- iii. R, π and τ phases are intermetallic compounds that may appear in the case of long exposures for several hours in the temperature range of typical 550-650°C.

3. Variation of the amount and morphology of austenite

As indicated in Figure 8, the volume fraction of austenite varies with temperature. It is possible to define three type of austenite forming on duplex stainless steels:

- i. γ_1 can be increased by slow cooling.
- ii. γ_2 is a kind of reversion of ferrite to austenite which is identified by three mechanisms:
 - a. In the 700-900°C temperature range, a eutectoid reaction of lamellar $\gamma_2+\sigma$ can form as γ_2 absorbs Ni and, to some extent, rejects Cr and Mo, encouraging Cr, Mo-rich precipitates, such as sigma phase [3].
 - b. “Windmanstätten” precipitates of austenite can form at temperatures between 650 and 800°C. In this temperature range, γ_2 formation involves diffusion as it is enriched in Ni compared to the ferrite matrix. There is some enrichment of nitrogen in γ_2 compared to the ferrite matrix, but both Cr and N content are substantially below that of primary austenite [3].
 - c. A diffusionless, martensite-like reaction can take place below about 650°C and form γ_2 with similar composition to the surrounding ferrite.
- iii. γ_3 formation accompanies the precipitation of carbides, nitrides and/or intermetallic phases due to local depletion in chromium and molybdenum [21].

Temperatures below 600°C

Three structural changes may happen for temperatures below 600°C:

1. An embrittling reaction can occur in the duplex grades at temperatures below 600°C and characterized as 475°C embrittlement or α' as illustrated in Figure 9. It is hardening of the ferrite where α' can be formed by two different mechanisms [21]:
 - i. Ferrite undergoes spinodal decomposition into Fe-rich δ -ferrite and a Cr-rich BCC α' phase.
 - ii. Nucleation and growth at temperatures often around 500°C due to the need for diffusion and the creating of interfaces.

Prolonged exposures above 260 to 340°C, depending on the grade, may initiate embrittlement in duplex stainless steel [33]. The activation energy is similar to Cr-diffusion in ferrite, but Cr-, Mo-, and Cu- content and high ferrite level influence the α' formation as well. Its presence is usually accompanied by increased

hardness, a loss of corrosion resistance and reduced toughness [25]. Nevertheless, a moderate formation of the α' -phase is tolerable and can imply an improvement in the wear resistance [34]. Since α' precipitates have very fine size of few nanometers and have the same crystal structure as the ferrite phase, it is difficult to analyze quantitatively the influence of α' precipitates on various properties by observing them with optical or electron microscopy [35].

2. G-phase may develop at α/α' interfaces between 300 and 400°C after several hours exposure due to enrichment of Ni and Si at these locations [3].
3. Cu-rich epsilon (ϵ) phase may precipitate in alloys containing copper and/or tungsten. This is also a hardening mechanism in the ferrite which may form at lower temperatures after a period of time, typical several hours dependent on the duplex grade.

2.2.2 Heat treatment

The effect of aging temperature on the mechanical properties of a duplex stainless steel is shown in Figure 10. Two ranges stand out where hardening can be seen to occur, something of which is also reflected in Figure 9:

1. 700-900°C with the precipitation of intermetallic phases such as σ and χ .
2. 300-500°C with the formation of α' and ϵ phases.

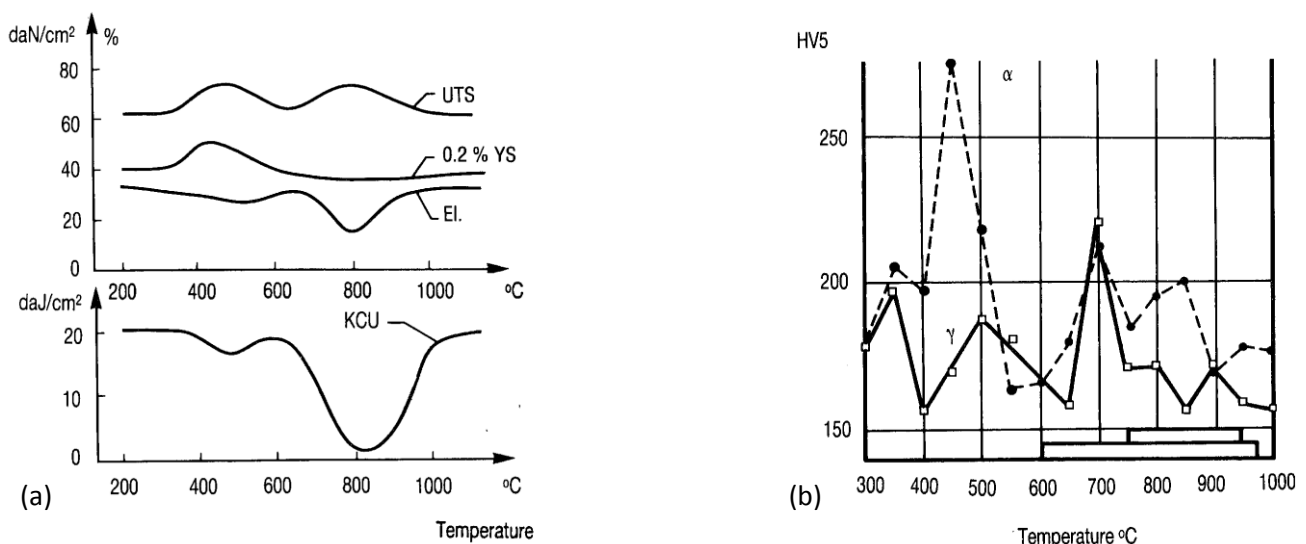


Figure 10. Variation of mechanical properties with heat treatment temperature for UR 50 alloy [21]. (a) Tension characteristics of ultimate tensile strength (UTS), 0.2 % offset yield strength (YS), elongation (El.) and absorbed Charpy U-notch energy (KCU). (b) Vickers hardness (HV) of α and γ phases.

It is important to note that precipitation of intermetallics within the upper temperature hardening range shown in Figure 10 (b) leads to drastic reduction in toughness (KCU) and ductility (El.) as shown in Figure 10 (a). At the lower temperature hardening range, considerable strengthening can be obtained while retaining satisfactory ductility. Heat treatment in the range 700-900°C should therefore be avoided [21].

For most grades however, a prolonged exposure in the lower temperature range may occur to a marked decrease in room temperature toughness, while the ductile to brittle transition is shifted to higher temperatures as shown in Figure 11 (a). Nevertheless, impact toughness may still remain after such exposures. Cold work also increases the ductile to brittle transition temperature and in addition reduces the room temperature impact

strength of duplex steels. The combination of cold work and ageing in the range of 300-400°C leads to an even greater drop in the room temperature impact strength as shown in Figure 11 (b) [3].

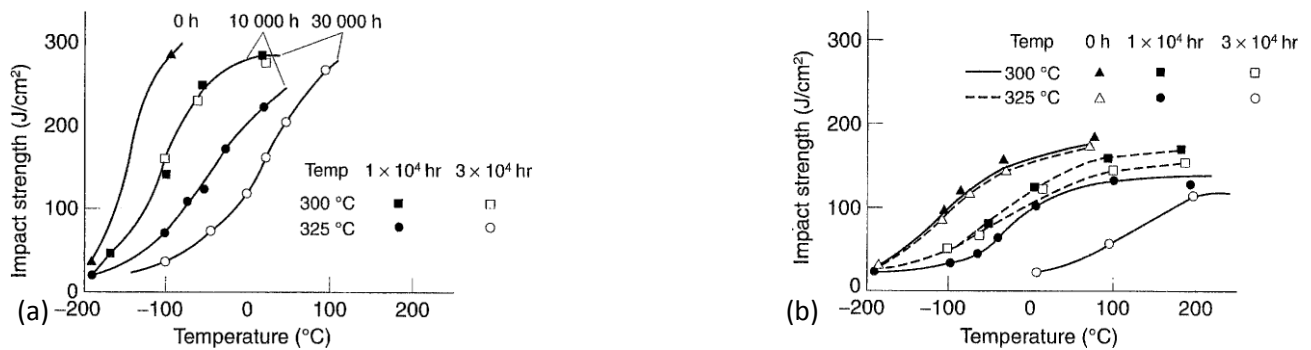


Figure 11. Impact energy curves for alloys aged at 300°C or 325°C: (a) quenched annealed S32750, (b) 45 % cold worked S31803 [3].

Hardening occurs exclusively in the ferrite, leading to transgranular cleavage fracture of this phase during mechanical deformation. Fortunately, because duplex stainless steels contain 50 % austenite, this hardening and embrittling effect is not nearly as detrimental as it is in fully ferritic steels. Because sigma phase precipitates at temperatures below austenite formation from the ferrite on cooling, the goal of avoiding sigma phase is achieved by controlling the annealing temperature and ensuring that the steel is quenched as rapidly as possible from the annealing temperature [23].

In terms of corrosion, intermetallic phases, chromium carbides and nitrides have negative effect. Intermetallic phases lead to depletion of alloying elements such as Cr and Mo which lower the corrosion resistance. Precipitation of carbides and nitrides causes Cr-depleted zones which are selectively attacked in certain corrosive media like in oxidizing and chloride-containing media [3].

The hardening effect with the associated loss of toughness in the duplex steels must be taken into account when defining the maximum service temperature. Various upper temperature limits for duplex stainless steels are defined by different standards and books. For UNS S31803, the following limits are defined:

- ISO 15156-3 Materials for use in H₂S-containing environments 232°C [17]
- 2010 ASME Boiler & Pressure Vessel Code, Section II Materials, Part D Properties 325°C [36]
- Steel heat treatment – metallurgy and technologies 280°C [7]

Solution annealing is a heat treatment to re-dissolve phase transformations such as sigma. The generic term of annealing is a heat treatment in which a material is exposed to an elevated temperature for an extended time period and then slowly cooled [9]. This is primarily done to fulfill one or more of the following goals:

1. Relieve stresses.
2. Increase ductility and toughness.
3. Produce a specific microstructure.

Annealing stainless steels is important in terms of avoiding secondary phase formation, re-solutionizing of precipitates, reduce segregation and avoid potential loss of chromium from surfaces. The annealing temperature range of duplex usually begins above the carbide and sigma solvus temperatures and extends upwards to the temperature that produces a maximum of about 60 % ferrite. Because these grades are not

stabilized with respect to carbon and nitrogen, cooling rates must be rapid enough to avoid sensitization by these elements [25]. Recommended annealing temperatures for UNS S31803 duplex stainless steel is 1020-1100°C with a rapid cooling based on ASM handbook volume 4 [37].

2.3 Tribology

Tribology is defined as friction, lubrication and wears science and technology. It comes from the Greek word “tribos” meaning “to rub”. This topic is indispensable with respect to wear and surface engineering. Material can be removed from a solid surface in only three ways: by melting, by chemical dissolution or by the physical separation of atoms from the surface. Mechanical and chemical processes may operate separately [38].

There is a field agree working in the field of tribology that erosion should be dealt with differently from wear because erosion has fluid motion as a source of the mechanical action on a surface. Basically, erosion and wear may be categorized into the following categories as shown in Figure 12. Further, surface damage may be classified into the idealized types as shown in Table 5.

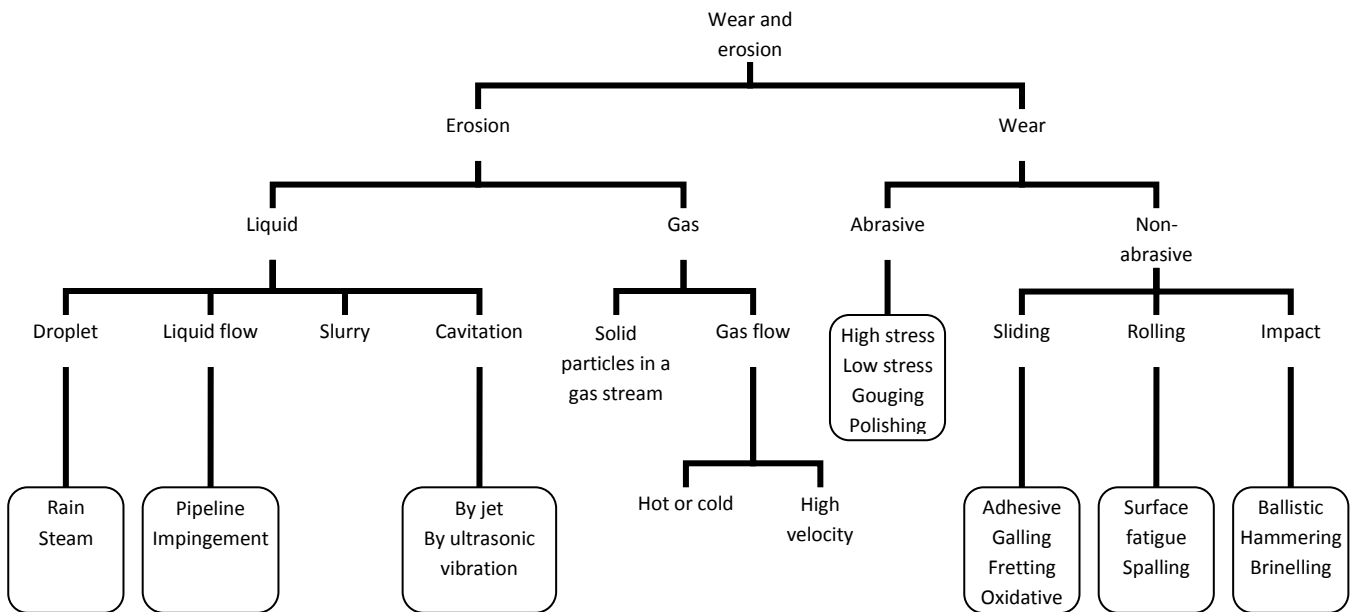
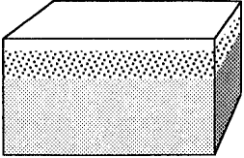
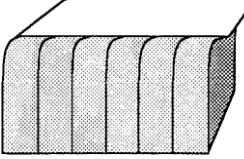
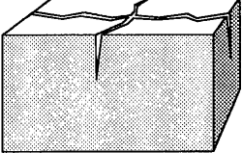
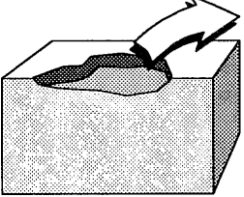
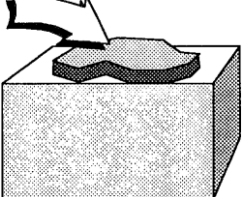



Figure 12. The major categories of erosion and wear and some specific modes in each category [8].

Table 5. Classification of surface damage [38].

1. Surface damage without exchange of material.	Structural change damage such as aging, tempering, phase transformations, recrystallization and so on.	
	Plastic deformation damage characterized by residual deformation of the surface layer, either locally or extensively.	
	Surface cracking damage caused by excessive local contact strains or cyclic variations of thermally or mechanically induced strains.	

<p>2. Surface damage involving loss of material: wear.</p>	<p>Material loss from the surfaces leaves behind wear scars of various shapes and sizes from shear fracture, extrusion, chip formation, tearing, brittle fracture, fatigue fracture, chemical dissolution and diffusion.</p>	
<p>3. Surface damage involving gain of material.</p>	<p>Pickup of loose particles, transfer of material from the counter surface and so on.</p>	
	<p>Corrosion/material degradation by chemical reactions with ambient elements or elements from the counter surface.</p>	

The surface damage involving loss of material, number two in Table 5, is only one type of surface damage, but this type is frequently the most important and will be discussed in more details. This kind of damage may be divided into three groups with subsequent subgroups dependent of what is causing the damage:

1. Wear by particles or fluids
 - a. Abrasive wear
 - b. Polishing wear
 - c. Solid particle erosion
 - d. Cavitation erosion
 - e. Liquid impingement erosion
 - f. Slurry erosion
2. Wear by rolling, sliding or impact
 - a. Sliding and adhesive wear
 - b. Fretting wear
 - c. Rolling contact wear
 - d. Impact wear
3. Chemically assisted wear
 - a. Corrosive wear
 - b. Oxidational wear

Wear may be defined as damage to a solid surface that generally involves progressive loss of material and is due to relative motion between that surface and a contacting substance or substances [38]. Stainless steel is characterized as having relatively poor wear and galling resistance but is often required due to their corrosion resistance. Lubricants and coatings are used to reduce wear [38].

The wear dependencies for various operating conditions may be summarized in a flowchart shown in Figure 13. From this figure, for the purpose of particles involved in a fluid stream, erosive and abrasive wear are found with a possible corrosive effect if a corrosive fluid is present.

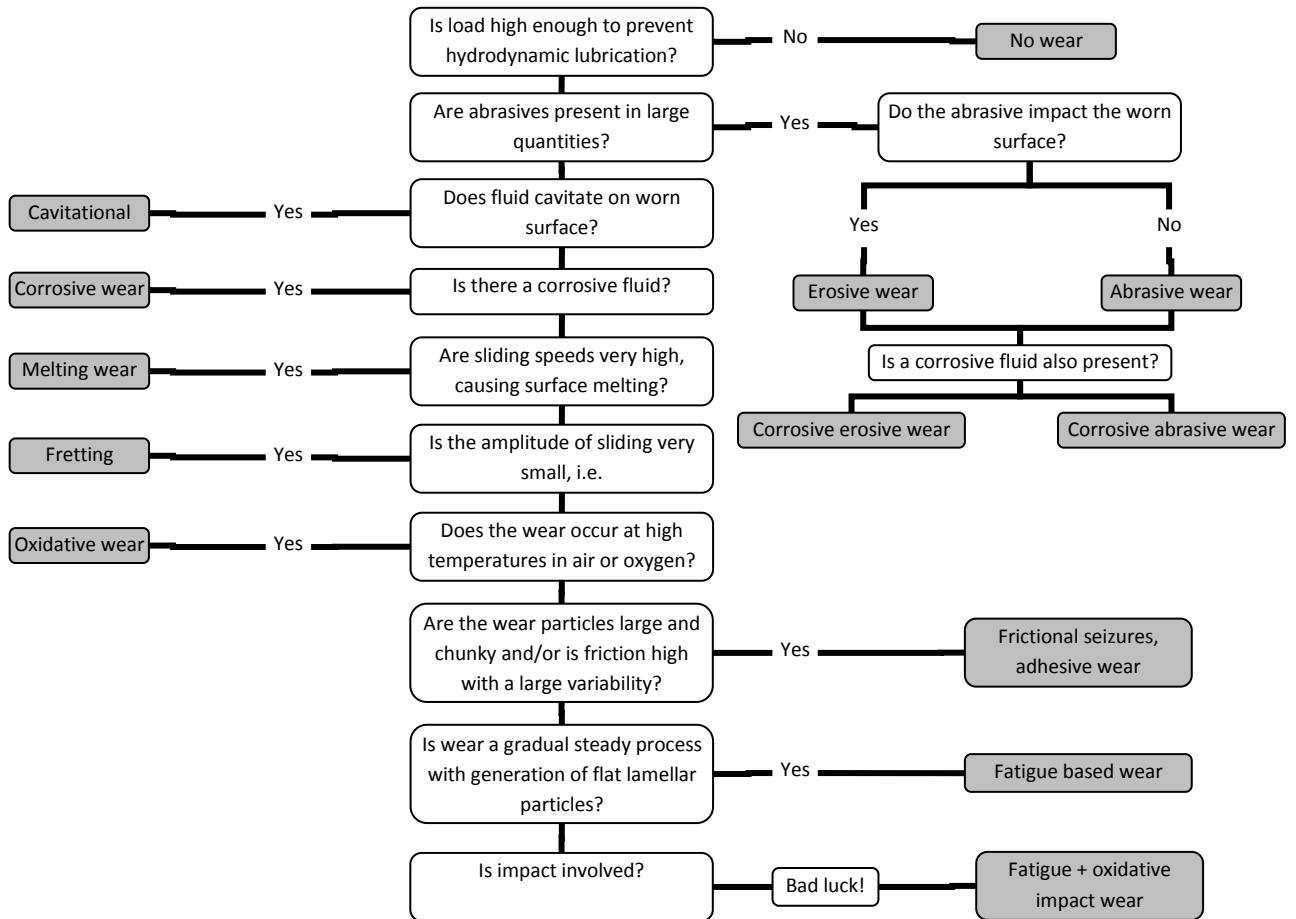


Figure 13. Flowchart illustrating the relationship between operating and type of wear [2].

In general terms, wear can effectively be controlled by selecting materials with specific properties as shown in Table 6. This document will mainly focus on abrasive wear and solid particle erosion and they will be described in more details in the following subsections. However, based on Table 6, hardness, toughness, fatigue resistance and heterogeneous microstructure appear to be the most important factors in order to resist abrasive and erosive wear modes.

Table 6. General materials selection guide for wear control [2].

Critical material property	Wear mechanism							
	Abrasive	Erosive	Cavitation	Corrosive	Fretting	Adhesive	Melting	Fatigue
Hardness	√	√	○	○	○	√	○	○
Toughness	○	√	√	○	○	○	○	√
Fatigue resistance	√	√	√	○	√	○	○	√
Inertness	○	○	○	√	√ ^①	○	○	○
High melting point	○	○	○	○	○	√	√	○
Heterogeneous microstructure	√	○	○	X ^②	○	√	○	○
Non-metallic character	○	○	○	√	○	√	○	○

√ Important

① Fretting in air for metals

○ Marginal

② Homogeneous microstructure inhibits electrochemical corrosion and, with it, most forms of corrosive wear

X Unfavorable

2.3.1 Abrasive wear

Abrasive wear is due to hard particles or hard protuberances that are forced against and moved along a solid surface. When two surfaces contact, wear occurs on both surfaces. Abrasion is typically categorized according to types of contact as well as contact environment [38]. Types of contact include:

1. Two-body abrasive wear.

This type of wear is exemplified by the action of sandpaper on a surface. Hard asperities or rigidly held grits pass over the surface like a cutting tool.

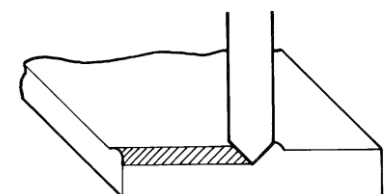
2. Three-body abrasive wear.

This type of wear the grits are free to roll as well as slide over the surface since they are not held rigidly.

Three-body abrasive wear is ten times slower than two-body wear since it has to compete with other mechanisms such as adhesive wear. Property such as hardness of the backing wheel, which forces the grits onto a particular surface, is important for the three-body but not for the two-body abrasive wear. Two-body abrasive wear corresponds closely to the cutting tool model of material removal whereas three-body abrasive wear involves slower mechanisms of material removal [2]. There are also different kinds of processes that are possible when a single abrasive tip traverses a surface. They include [38]:

- Plowing

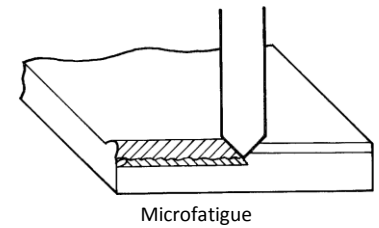
This is a process of displacing material from a groove to the sides. This occurs under light loads and does not result in any real material loss. Damage occurs to the near surface of the material in the form of a buildup of dislocations through cold work.



Plowing

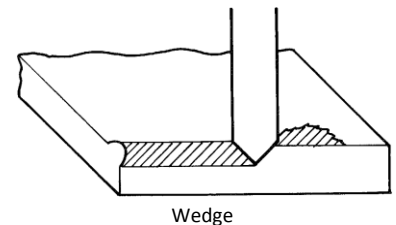
- Microfatigue

This is a process which may occur if the previous cold-worked surface by plowing is scratched, with the result in loss through microfatigue.



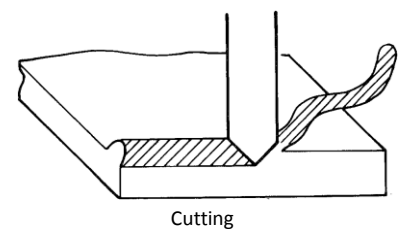
- Wedge

This is a process when a wedge is developed on the front of an abrasive tip when the ratio of shear strength of the contact interface relative to the shear strength of the bulk rises to a high level. In this case, the total amount of material displaced from the groove is greater than the material displaced to the sides.



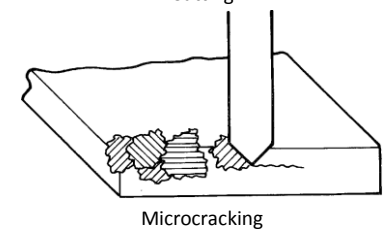
- Cutting

This is a process where an abrasive tip removes a chip, much like a machine tool. This result in removed material, but very little displaced material relative to the size of the groove. For a sharp abrasive particle, a critical angle exists for which a transition from plowing to cutting depending on the material is being abraded.



- Microcracking

This is a process that occur when forces applied by the abrasive grain exceed the fracture toughness of the material. This is special important for brittle materials.



Generally, a material is seriously abraded or scratched only by a particle harder than itself. Abrasive wear is commonly divided into three types:

- Low-stress abrasion

This is wear that occurs due to relatively light rubbing contact. Wear scars usually show scratches and the amount of subsurface deformation is minimal.

- High-stress abrasion

This is wear under a level of stress that is high enough to crush the abrasive. Considerably more strain hardening of the metal surface occurs.

- Gouging abrasion

This is used to describe high-stress abrasion that result in sizable grooves or gouges on the worn surface.

Effect of material properties have been shown to either form a correlation with abrasive wear or have some effect on it. These properties include hardness, elastic modulus, yield strength, melting temperature, crystal structure, microstructure and composition.

- Hardness

It has been shown experimentally and theoretically that the hardness of a material correlates with its abrasion rate. In most instances, the hardness of the material must be greater than 0,8 of the particle hardness for enhanced abrasive wear resistance. Unfortunately this approach finds relatively few applications because most abrasives present in natural minerals are harder than 1000 HB [2].

- Microstructure, crystal structure orientation, second phases and particles
 - Austenite and bainite of equal hardness are more abrasion resistant than ferrite, pearlite or martensite. This is because of the higher strain-hardening capacity, ductility and toughness of austenite [38] and bainite which suppress the more rapid forms of abrasive wear, such as microcutting and brittle fracture. Austenitic steels function by forming a tough, work-hardened layer under conditions of heavy abrasion which can only be removed from the surface with difficulty [2].
 - Cubic metals wear at about twice the rate of hexagonal metals which was attributed to the lower work-hardening rate of hexagonal metals [38].
 - Low-alloy plain carbon steel depends on whether a hyper-eutectoid or hypo-eutectoid steel is selected. For hypo-eutectoid steels, bainite is the most abrasive resistant phase, with tempered martensite and ferrite/pearlite offering successively less wear resistance. For hyper-eutectoid steels, the presence and morphology of cementite, iron carbide, inclusions have dominant influence. With the higher carbon content, the annealed microstructure is superior to hardened, martensitic, hyper-eutectoid steels. The cause of this reversal of wear resistance is the inhibition of abrasion grooves by hard carbide inclusions. The most wear resistant microstructure contains lamellar cementite inclusions of the pearlitic form. When the cementite is present as spherical inclusions, there is less improvement in wear resistance because the spheres do not provide rigid barriers to plastic deformation [2]. The distinction is illustrated in Figure 14.

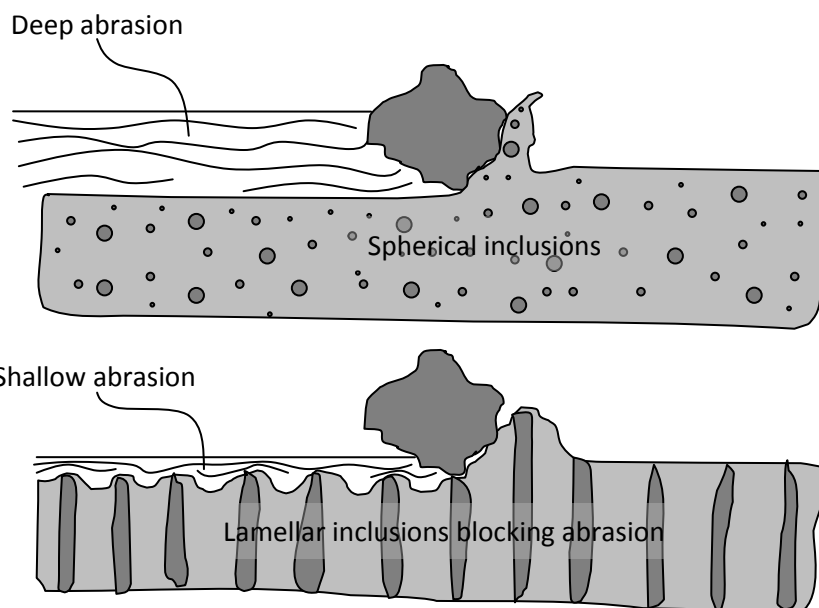


Figure 14. Influence of carbide inclusion morphology on the abrasion process [2].

- Large, hard incoherent precipitates or particles such as carbides can be useful in decreasing abrasive wear. When the incoherent particles are somewhat larger than the abrasive grains abrading the surface, they are generally effective in decreasing the total material wear [38].
- Spherical inclusions of iron carbide can improve abrasive wear resistance of a steel by raising the yield stress of the steel according to the Hall-Petch effect [2].
- If the size of the grits is small compared to the carbide inclusions, there is an additional improvement in wear resistance provided by the direct blockage of abrasion grooves by hard inclusions which is known

as the stand-out effect shown in Figure 15. The stand-out effect becomes significant at approximately 10 % volume fraction of pearlite. For coarse abrasives, the wear resistance rises gradually with increasing pearlite content [2].

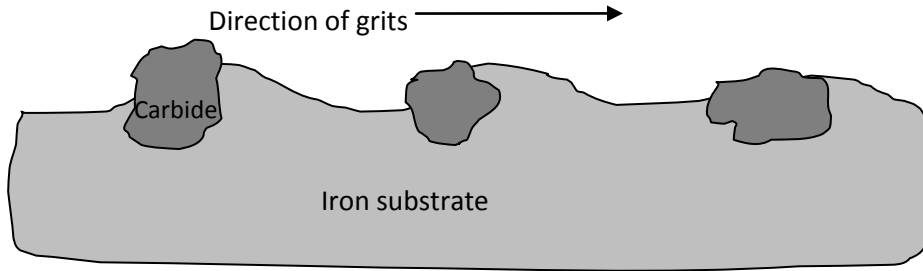


Figure 15. Stand-out effect or inhibition by large carbide inclusions of abrasion by small grits [2].

- The inherently hard martensitic structure is preferable to the softer ferritic and austenitic structure, especially in low-stress abrasion [38].
- Scratching body-centered cubic and face-centered cubic metals with a prepared surface on the (001) plane, showed a wider scratch width, which implies higher wear, along the <100> than the <110> direction [38].
- Fracture toughness
This is especially important for ceramics and to a lesser degree to white cast irons. In general, the wear decrease with the toughness [38].
- Alloying
Increased carbon content, regardless of structure, favors better abrasive wear resistance. Addition of nitrogen and oxygen may also decrease wear for some alloys. Increased volume of carbides also improve abrasive wear resistance as long as their hardness is not exceeded by that of the abrasive medium [38]. A steel containing carbides can possess up to four times the abrasive wear resistance of the corresponding carbide free steel [2].

Effect of environment factors that affect abrasive loss include, but are not limited to: the type of abrasive and its characteristics, temperature, speed of contact, unit load of the abrasive on the material, humidity, lubrication and corrosive effect.

- Abrasive
Changing the abrasive will change the wear rate. Abrasive characteristics are critical angle, hardness, toughness and size. Table 7 gives a summarize of the most important characteristics.

Table 7. Summarize of the most important characteristics of the abrasive particle.

Hardness	Shape	Toughness
As the hardness of the abrasive exceeds that of the wear material, abrasive wear typically becomes much worse. Then it is able to penetrate the surface and cut material without having its cutting edges broken or rounded.	The shape of the abrasive particle is important because it influences the shape of the groove produced in the material. Experiments have confirmed that less wear occurs when materials are abraded by rounded, rather than sharp, particles.	Material loss will increase when the toughness of the abrasive increases.

The brittleness of the abrasive is another constraint. If the grits are too brittle, they may break up into fine particles, thus minimizing wear. If the abrasive is too tough, then the grits may not fracture to provide the new cutting faces necessary to cause rapid wear. The sharp faces of the grits will gradually round-up and the grits will become less efficient abrasive agents than angular particles as illustrated in Figure 16.

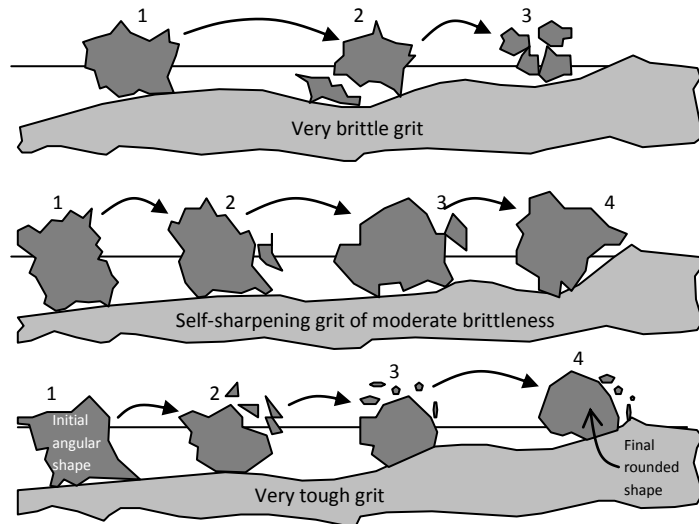


Figure 16. Effect of grit brittleness and toughness on its efficiency to abrade [2].

- **Speed of contact**
The rate of abrasive wear has been found to slightly increase with increasing speed in the range from 0-2,5 m/s. This increase in wear may be attributed to frictional heating, but the effect is small.
- **Load**
Abrasive wear has been shown to be proportional to load. However, this proportional effect breaks down when the load is high enough to fracture the abrasive particles. In that case, new sharp points may be created resulting in an increase of the wear. If the abrasive particles points are rounded, wear will decrease.
- **Lubrication**
Lubrication can encourage cutting by abrasive particles because it offers a smaller ratio of grit penetration to grit diameter than the unlubricated case. This implies that if a grit is rigidly held by being embedded in a soft metal and is drawn under load against a harder metal in the presence of lubricant, then a rapid microcutting form of abrasive wear is more likely to occur than when no lubricant is present [2].
- **Corrosive effect**
Abrasion wear is often enhanced by corrosive conditions, particularly a low pH. The abrasion creates fresh surfaces that rapidly corrode and the normally protective corrosion layer is removed by abrasion.

Based on the description above there are families of materials that have demonstrated better resistance to abrasive wear than other. They are typically hard materials and include ceramics, carbide materials, alloyed white cast irons and hardened alloy steels. In addition, these and other materials can be put, or formed, on the surface of many less-abrasion-resistant materials by welding, plasma spraying, flame spraying, electroplating, diffusion and other techniques. For metals, as a general guide it has been found that the following factors will resist abrasive wear [38]:

- High hardness is the primary requirement.

- Abrasion resistance tends to increase with additions of carbide-forming metals.
- Carbides are useful additions to metals when they are large in relation to the size of the abrasive.

2.3.2 Solid particle erosion

This term is used in the case of loss of material that results from repeated impact of small, solid particles. Solid particle erosion is to be expected whenever hard particles are entrained in a gas or liquid medium impinging on a solid at any significant velocity. In some cases, solid particle erosion is a useful phenomenon as in sandblasting and high-speed abrasive water jet cutting, but it is a serious problem in many engineering systems.

Manifestations of solid particle erosion in service usually include [38]:

- Thinning of components.
- Macroscopic scooping appearance following the gas/particle flow field.
- Surface roughening.
- Lack of the directional grooving characteristic of abrasion.
- Formation of ripple patterns on metals.

The distinction between erosion and abrasion should be clarified, because the term erosion has often been used in connection with situations that might be better classed as abrasion [38]:

- Erosion
Refers to a series of particles striking and rebounding from the surface. The force exerted by the particles on the material is due to their deceleration.
- Abrasion
Results from the sliding of abrasive particles across a surface under the action of an externally applied force which is approximately constant.

In practice, erosion rarely takes place in inert atmosphere or vacuum, but at room temperature the effect of oxidation can generally be ignored and erosion thought of as “pure”. The erosion rate, E , is further on given in terms of mass or volume of material removed per unit mass of erodent impacted. E generally shows power-law velocity dependence as shown in Equation 1,

$$E = K \cdot V^n \quad \text{Equation 1}$$

where K is a constant, V is velocity and n is a velocity exponent that generally depends on material and erosion conditions [38].

Materials are broadly classified as ductile or brittle based on the dependence of their erosion rate on angle of incidence (α). As shown in Figure 17, ductile materials have maximum erosion rate at low angles of incidence, known as ductile mode, while brittle materials have maximum erosion rate at or near 90° known as brittle mode. A variety of curves intermediate between these classical extremes exist, and in some cases the same material exhibits behavior that shifts from one extreme to the other depending on erosion conditions [38].

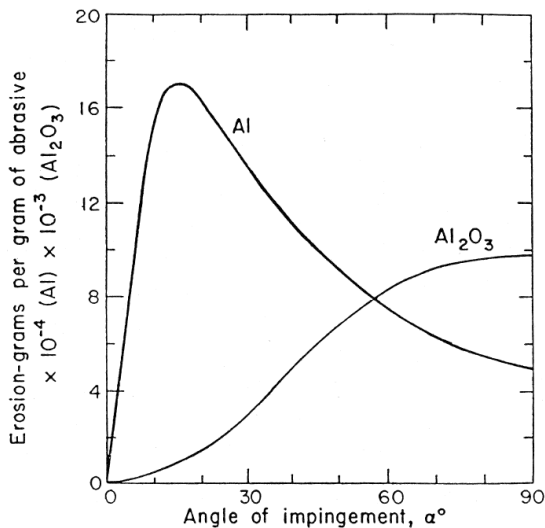


Figure 17. Comparison of erosion behaviors of ductile (Al) and brittle (Al_2O_3) materials along with the angle of impingement [39].

Following, variables affecting pure erosion can be broadly separated into three types:

1. Particles flow; angle of incidence, speed, flux and rotational speed.
 - a. Angle of incidence

A low angle of impingement favors wear processes similar to abrasion because the particles tend to track across the worn surface after impact. A high angle of impingement causes wear mechanism which are typical erosion [2].
 - b. Speed

If the speed is very low, then stresses at impact are insufficient for plastic deformation to occur and wear proceeds by surface fatigue. When the speed is increased it is possible for the eroded material to deform plastically on particle impact. If the eroding particles are blunt or spherical, then thin plates of worn material form on the worn surface as a result of extreme plastic deformation. If the particles are sharp, then cutting or brittle fragmentation is more likely. Brittle material, on the other hand, wears by subsurface cracking. At very high particle speeds, melting of the impacted surface might even occur [2].
 - c. Flux

On impact models, particle flux have no effect on erosion because only one particle is considered, but in general, erosive wear rate is proportional to the flux rate up to a certain limiting value of wear [2]. Nevertheless, it has been demonstrated that because of interference of rebounding particles with incident particles, the surface is effectively shielded. The result is a decrease in erosion exponentially with increasing flux [38].
2. Particles variables; shape, size, hardness and ease of fracture.
 - a. Shape

Relatively blunt, spherical shape particles are unlikely to cause severe erosive wear even if the particles are hard. Sharp particles with flat areas joined by corners with small radii are, on the other hand, much more critical to the process of wear [2].

b. Size

The size of erodent particles has little or no effect on the erosion rate of ductile materials as long as the particles size is above about 100 μm . The erosion rates decreases rapidly with decreasing particle size below 100 μm . This size effect is also found in abrasive wear [38]. This relation is shown in Figure 18 where a 1075 steel is eroded by impingement of increasing the small solid particles in 60 g increments.

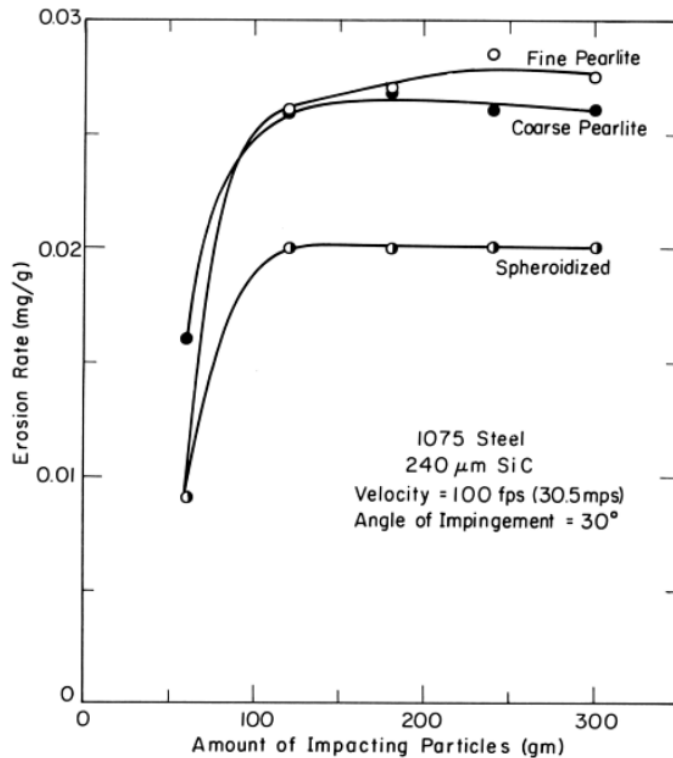


Figure 18. Incremental erosion of 1075 steel to steady-state rate [1].

In general, particle size does affect the wear rate, the mode of erosion and also alters the ranking of hard and ductile material. When the particles are small, the mode of erosion is primarily ductile and the wear rate depends more on the hardness of the material. When the particles are increased in size, the mode of erosion changes from ductile to brittle and the wear rate depends more on the toughness of the material. The change in wear mode is believed to be a consequence of the average spacing of defects. If the impingement particles are very small, only a minority of the impingement site will coincide with a defect. Plastic deformation is the predominant mode of metal removal for small particles. Since repeated plastic deformation is required to remove material, their form of wear is relatively slow. For large eroding particles, a defect is almost always present in the impingement site and material removal by brittle processes is favored [2].

c. Hardness

The hardness of the erodent particles relative to the material being eroded is an important factor in erosion. Erosion rate drops dramatically when particle hardness decreases below that of the material being eroded, just like in the case with abrasive wear. Also, soft erodents favor erosion rates at high angles, while erodents significantly harder than the target favor erosion rates at low angles [38]. In addition, the effect of particle hardness is much more pronounced in brittle mode of erosion than in the ductile mode of erosion [2].

3. Material variables; hardness, work hardening behavior, microstructure and more.

The difficulty with materials optimization for wear is that the characteristics of erosive wear as well as the material characteristics control the wear rate. At the shallow impingement angle, it is evident that the hardness and work-hardening ability of materials suppress a quasi-abrasive process of wear. In this case, materials can be rated according to the hardness of the pure metal. When the impingement angle is 90° , the ranking of materials change significantly. Heat treatment of steel to increase hardness lessens the erosive wear resistance at high impact angles. This mean that changes in material variables cannot be viewed in isolation from the overall system characteristics of erosive wear. There is no general recipe for a high level of erosive wear resistance. Because of the two different erosive wear protection mechanism that can take place, high wear resistance can be achieved by more than one type of material [2].

In some cases the material can be extremely hard and tough so that the impacting particle is unable to make any impression on the surface. This is the approach adapted when developing metallic and ceramic erosion resistant materials and shown illustrative in Figure 19 (a). Alternatively, the material can be tough, but with an extremely low elastic modulus so that the kinetic energy of the particles is harmlessly dissipated as illustrate in Figure 19 (b). The choice of erosion resistant material may also be compromised by other considerations such as operating temperature or material transparency [2].

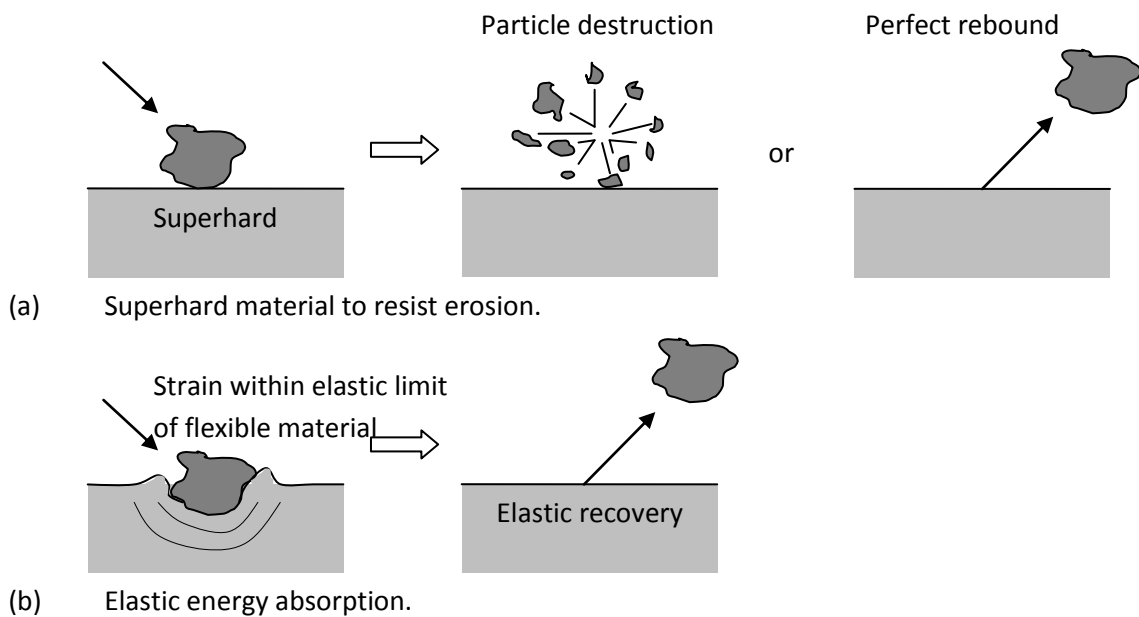


Figure 19. Comparison of the high and low elastic modulus modes of erosive wear protection [2].

The literature available on the effect of steel microstructure on erosive wear rates suggests that ductile steel is the most wear resistant. Hardening of steel to form martensite offers little improvement except at very low impingement angles, and the formation of massive or lamellar carbides reduces erosive wear resistance. The selection of steel for erosive wear minimization is therefore different from the case of abrasive wear. Some considerations for erosive wear resistance of steel are [2]:

- The ferritic phase with sufficient spheroidal carbide inclusions to induce strengthening for low alloy carbon steel is very effective against erosive wear.
- Pearlitic steels show inferior wear resistance to spheroidized steels.

- Erosive wear of steel shows the classical ductile erosion characteristics with subsurface and surface cracking. This suggests that the erosive wear resistance of steels is limited by a lack of ductility.
- For very soft erosive particles, the inclusion of carbides promotes wear resistance slightly.
- Alloying of steels to obtain a microstructure containing a significant amount of retained austenite is an effective means of reducing erosive wear.
- Adding about 2,5 % of silicon to 0,7 % carbon steel results in good erosive wear resistance. The optimum heat treatment of this steel includes a relatively long austempering time where all the martensite is removed and only retained austenite and bainitic ferrite are present.
- As a general rule, ductility rather than hardness should be enhanced in steels for improved erosion resistance.

Most erosive agents are conveyed by a medium of water or air for instance. A mixture of erosive particles and liquid medium is known as slurry. It has been shown that small additions of lubricants to erosive slurries can significantly reduce wear. Further, wear as particle impingement is more likely to occur in turbulent flow than in laminar flow where the medium tends to draw the particles parallel to the surface. An exception is where the laminar flow is directed normally to the surface which is the case when a jet of fluid impinges against a surface [2].

For ductile materials, removal is caused by the micro-cutting and micro-plowing of the solid particles as shown in Figure 20 (a). See also Section 2.3.1 for a more detail description and illustration of the material removal mechanisms. For brittle materials, the energy transfer from solid particles to the surface of the target material induces material deformation, crack initiation and propagation [40] as shown in Figure 20 (b).

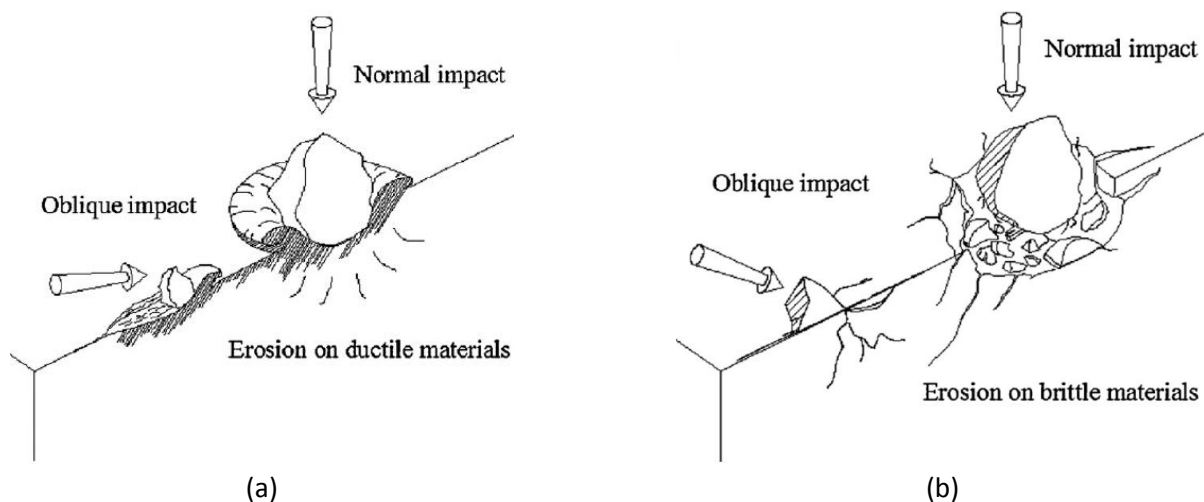


Figure 20. The erosive failure behavior of brittle and ductile materials [40]: (a) erosion on ductile materials and (b) erosion on brittle materials.

Erosion of metals is a result of direct material removal by cutting or micromachining interaction of hard, sharp particles and repeated deformation of material leading to eventual removal of a flake or platelet of material. The distinctions between the cutting mode and the platelet mode are important because cutting models predict an inverse dependence of erosion on hardness, while ductility may be of greater importance for the platelet mechanism because it may affect the ease of platelet removal [38]. Platelet can be shown with low magnification at the region at the edge of a primary erosion region as shown in Figure 21 (a). A classical-shaped

distressed platelet is shown in the center of Figure 21 (b) surrounded by other smaller platelets. It has the appearance of a thin pancake forging with considerable edge cracking and even some internal cracking. It is still attached to the substrate metal by a mushroom-like stem beneath it [1].

Solid particles impacting metals form impact craters and displace material. It has been shown that single impacts of spheres remove no material except above a rather high critical velocity and that single, angular particles impact remove material only for a small fraction of the possible particle orientations. In the great majority of cases, direct material removal does not occur, but a lip of material remains attached at the end of the crater as shown in Figure 21 (c). Such lips are probably vulnerable to later direct removal or to being pushed back into the surface and becoming an extruded platelet that may eventually be removed by ductile fracture or other mechanism. It is also assumed that only a small fraction of the particles cut in the idealized manner, probably because additional impacts are needed to remove the material displaced to the end of the crater [38].

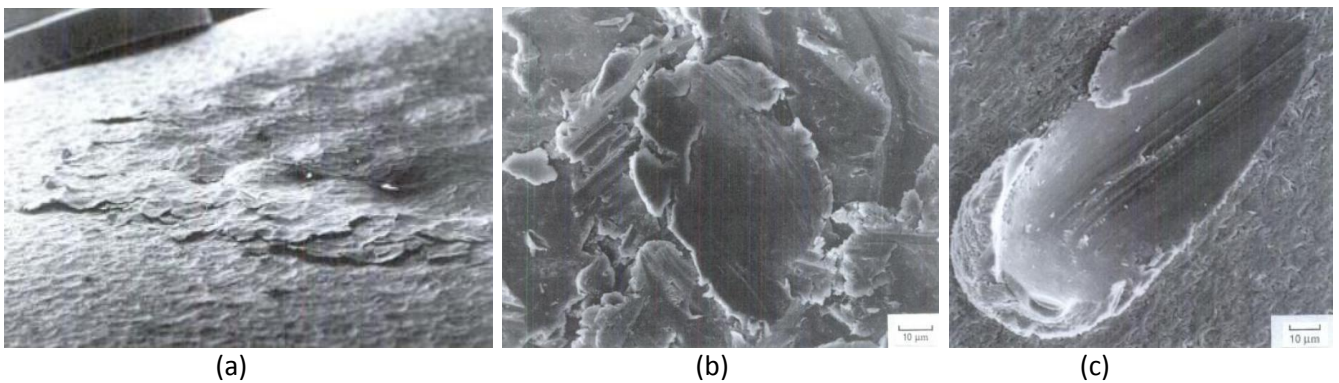


Figure 21. Erosion mechanisms [1] where (a) show platelets at edge of primary erosion zone on 1100-O aluminium, (b) show an erosion platelet on a 7075-T6 aluminium and (c) show a single particle impact crater in a 1100-O aluminium.

2.4 Surface hardening

A surface can be defined as the outer boundary of an object and is subjected to degradation by corrosion and wear. Rather than by manufacturing the whole item from a wear-resistant material, which might not give the overall properties required or which would be very expensive, a localized surface treatment could be a good solution. Such local treatment may take form of surface alloying and/or heat treatment, or the application of a surface coating [41].

Surface hardening is a process which includes a wide variety of techniques used to improve the wear resistance of parts without affecting the more soft and tough interior of a part. The hard surface resist wear and the tough interior resist impact. Further, surface hardening of steel has an advantage over through hardening because less expensive low-carbon and medium-carbon steels can be surface hardened without the problems of distortions and cracking associated with the through hardening of thick sections [37].

There are two approaches to the problem of wear; (1) production of hard surface and (2) application of soft lubricating films. Below are listed the two approaches with subsequent related techniques.

1. Produce hard surfaces:
 - a. Method that involve surface and subsurface modification without any intentional buildup or increase in part dimensions by surface alloying and heat treatment:

- i. Diffusion methods:
 - Carburizing
 - Nitriding
 - Low temperature nitriding/carburizing
 - Solution nitriding
 - Carbonitriding
 - Nitrocarburizing
 - Boriding
 - Titanium-carbon diffusion
 - ii. Selective hardening methods:
 - Flame hardening
 - Induction hardening
 - Laser hardening
 - Electron beam hardening
 - Ion implantation
 - Selective carburizing and nitriding
 - Use of arc lamps
 - iii. Plastic flow processes:
 - Burnishing
 - Peening
 - Skin pass rolling
- b. Method that involve an intentional buildup or addition of a new layer by hard facing and coatings:
- i. Thermal spray coatings:
 - Flame spray
 - Electric arc spray
 - Plasma spray
 - High-velocity oxygen fuel spray
 - Detonation gun
 - ii. Fusion hardfacing (welded overlay)
 - iii. Electrochemical plating
 - iv. Vapor deposition processes:
 - Physical vapor deposition (PVD).
 - Chemical vapor deposition (CVD).
 - Physical-chemical vapor deposition
 - v. Thermoreactive deposition/diffusion process (TRD)
2. Apply soft lubricating films.
- This relates to the application of such materials as PTFE, molybdenum disulphide, graphite, lead and indium in such a way as to produce a surface film on the material which reduces the friction coefficient and/or which will embed particles and reduce abrasive wear [41].

For wear and abrasion resistance, the general rule is that a harder surface is better than a less hard surface. Thus, for the most economical approach, one would select heat-treated carbon or alloy steels. For prevention of galling and seizure, microstructure is as important as hardness. Materials containing large carbides, such as hardfacing alloys, can be considered for applications where this is a factor. The microstructure, the surface finish, the residual stresses, the porosity and depth of hard coating or soft coating can be significant factors for wear resistance [38].

This document will mainly focus on surface treatments applicable according to the test matrix in Table 1, i.e. Expanite, Kolsterising, high velocity oxygen fuel and Sursulf. These surface treatments include conventional nitriding and low temperature nitriding/carburizing and thermal spray coating. The two former belong into the category called diffusion methods of surface hardening and the last method belong into the category that involve an intentional buildup of a new layer. An additional diffusion method is added called solution nitriding which is affected by the high temperature Expanite process.

2.4.1 Diffusion methods of surface hardening

Surface hardening by diffusion methods involves the chemical modification of a surface. This is done most effective if the solute element dissolves interstitially when penetrating on the surface. Once dissolved, the elements increase the hardness of the surface by forming interstitial compounds-carbides, nitrides or borides [42].

A thermochemical process is needed because some heat is needed to enhance the diffusion of hardening species into the surface. Process methods for exposure involve the handling of hardening species in forms such as gas, liquid or ions which they all produce difference in typical case depth and hardness. A comparison of various diffusion surface hardening techniques is shown in Figure 22.

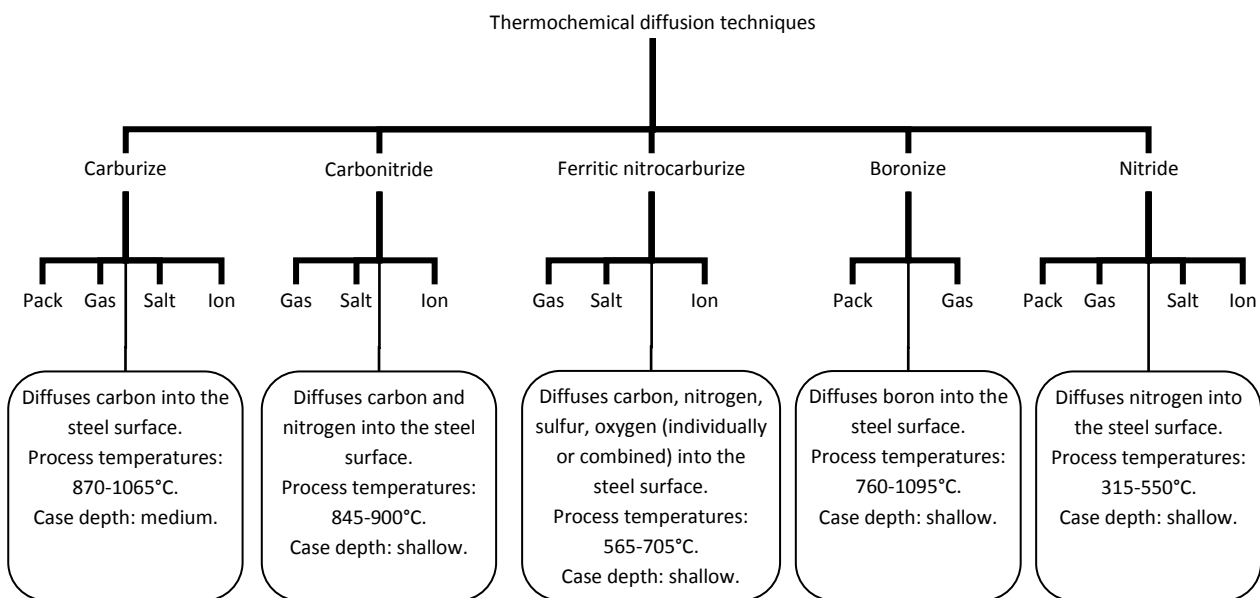


Figure 22. Comparison of various diffusion surface hardening techniques [7].

Surface hardening is possible by transfer of mass from the reactions that take place in the interface between a phase like gas, liquid or solid and the component surface. The mass transfer is possible by diffusion which is basically material transport by atomic motion from lattice site to lattice site [9] in the microstructure. The rate of which the mass transfer occurs is expressed as diffusion flux designated J and with unity [$\text{kg}/\text{m}^2\cdot\text{s}$] or

[atoms/m²·s]. For a steady-state diffusion in a single direction, i.e. diffusion flux does not change with time, Fick's first law apply and is shown in Equation 2,

$$J = -D \frac{\partial c}{\partial x} \quad \text{Equation 2}$$

where D is called diffusion coefficient [cm²/s], c is concentration and x is distance from surface. For nonsteady state diffusion, i.e. when diffusion causes change in the concentration gradient and thus becomes dependent in time and location [7], Fick's second law apply and is shown in Equation 3.

$$\frac{\partial c}{\partial t} = -\frac{\partial}{\partial x} D \frac{\partial c}{\partial x} \quad \text{Equation 3}$$

In the case of a semi-infinite system, that is when the diffusion flow does not reach the end of the specimen as is the case in thermomechanical surface treatments [7], Fick's second law yields the solution as shown in Equation 4,

$$c(x,t) - c_0 = (c_s - c_0) \left(1 - \operatorname{erf} \left[\frac{x}{2\sqrt{Dt}} \right] \right) \quad \text{Equation 4}$$

where	$c(x,t)$	concentration c at a distance x from surface after a certain diffusion time t
	c_0	initial concentration
	c_s	surface concentration
	erf	Gaussian error function

Equation 4 leads to the empirical rule that to get double the depth of penetration it is necessary to quadruple the diffusion time [7]. Further, the diffusion coefficient, D, is given by Equation 5,

$$D = D_0 \exp \left(-\frac{Q}{RT} \right) \quad \text{Equation 5}$$

where	D_0	element dependent and temperature independent constant [m ² /s]
	Q	activation energy for diffusion [J/mol]
	R	the gas constant [J/mol·K]
	T	absolute temperature [K]

This mean that temperature, time, diffusing species and concentration gradient are factors influencing the diffusion of atoms to a specific depth into the surface. This theory applies for the process of surface hardening by diffusion methods.

Nitriding

Nitriding is a surface-hardening heat treatment that introduces nitrogen into the surface of steel, normally not to duplex stainless steel, at a temperature range while it is in the ferritic condition, generally between 500 and 550°C. This is based on plain carbon steel and the crystallographic structure is shown in Figure 4 with respect to temperature and carbon content.

Nitriding can be accomplished with a minimum of distortion and with excellent dimensional control [37]. Hardness will then depend on the formation of hard nitrides and high surface hardness is only obtained when

using special alloy steels containing aluminium, chromium, molybdenum or vanadium which are all elements that can form hard and stable nitrides as soon as they come into contact with nitrogen atoms [42].

Nitrogen has partial solubility in iron and based on Figure 23 the following phases can form [7]:

- α -iron (BCC), which dissolves less than 0,0001 % at 20°C and up to 0,115 % nitrogen at 590°C.
- γ' -nitride (FCC), Fe_4N , which can dissolve 5,7-6,1 % nitrogen.
- ϵ -nitride (hexahedral), $Fe_{2,3}N$, which exists in the range of 8-11 % nitrogen.
- ζ -nitride (orthorhombic), Fe_2N , which forms at temperatures below about 500°C and nitrogen contents exceeding 11 %, This phase condition is not used in technical practice.
- γ -iron (FCC), forms at temperatures above 590°C and may dissolve a maximum of 2,8 % nitrogen at 650°C.

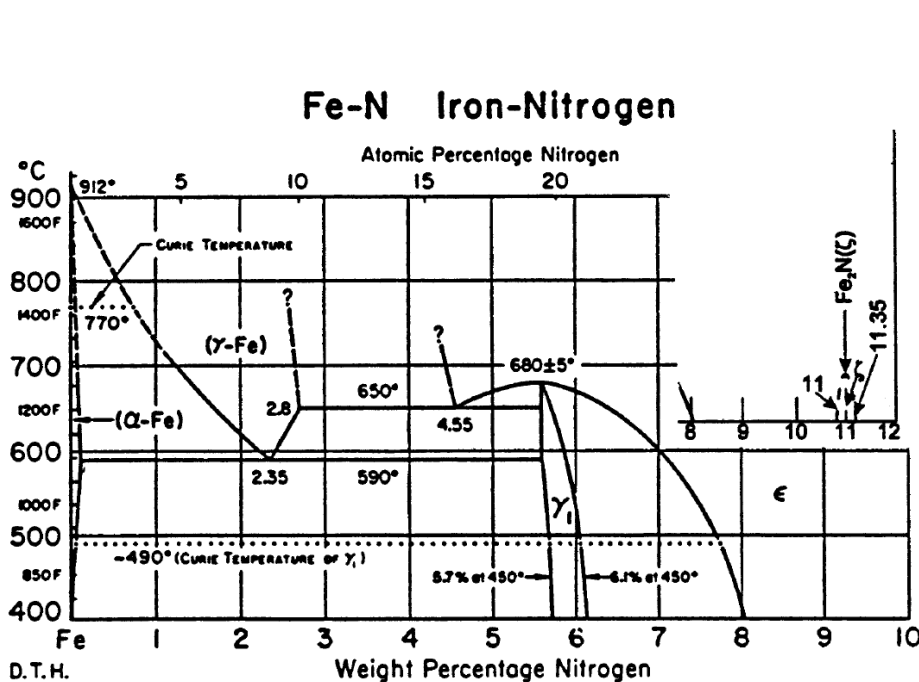


Figure 23. Fe-N phase diagram. The δ phase shown on the insert exist from 11,0 to 11,35 % N below about 500°C [43].

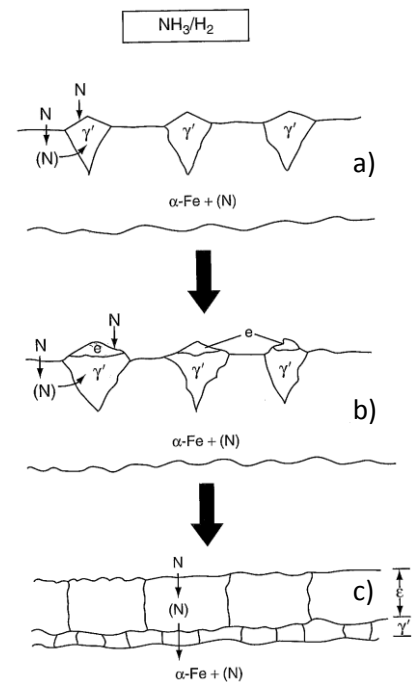


Figure 24. Scheme of nucleation of γ' - and ϵ -nitrides on iron [7].

Nitrided cases are stratified and develop as follows, see Figure 24 for illustration [7]:

- Nitrides develop by γ' -nucleation at the interface between nitriding atmosphere and the substrate.
- Subsequent nucleation of ϵ -nitrides at the interface between the atmosphere and the already formed γ' -nitrides.
- Build-up of a complete layer of γ' -nitride toward the substrate and of ϵ -nitride towards the surface which is called the compound layer.
- Below the two surfaces above is some solid solution strengthening from the nitrogen in the solid solution. This layer is called diffusion layer composed of nitrogen in interstitial solution in the ferritic matrix in combination with nitride dispersions. The soluted nitrogen in α -iron segregates during cooling in correspondence with the decreasing of solubility in α -iron as coarse-shaped α'' -nitrides, Fe_8N . In

quenched microstructures, nitrogen remains in supersaturated solution and subsequent aging leads to more uniformly dispersed finer α'' -nitrides [7].

In the outer areas of the compound layer a porous zone can be found. The percentage of γ' and ϵ - nitride depends on the carbon content of the steel: higher carbon content promotes the formation of ϵ -nitrides, lower carbon content forms more γ' iron nitride. The composition of the compound layer, also called the white layer, is also affected by the nitriding atmosphere. Higher temperatures or a longer nitriding time produce increased growth of the compound layer. The structure of the diffusion layer can be affected by the nitriding temperature, the cooling rate from nitriding temperature to room temperature, low-temperature annealing after cooling to room temperature and the type of steel being nitrided [38]:

- High nitriding temperature promotes the formation of large, coarse distributed nitrides. Low temperatures promote the formation of finely dispersed nitrides.
- Slow cooling rates from nitriding temperature to room temperature, annealing treatments or heating by stressing the parts favors dissolution, growth and change in nitride structure.
- The nitriding depth can be increased either by increasing the process temperature or by increasing the nitriding time.
- Increasing the content of nitride-forming elements in the material increases the hardness of the surface layer and decreases the nitriding depth.

Nitriding of plain carbon steels produce a case of only moderate hardness because nitrogen diffuses fairly quickly beneath the surface forming nitrides dispersed at greater depths. Aluminium, and to a lesser extent chromium, vanadium and molybdenum, has a higher affinity for nitrogen and prevents diffusion to a greater depth. Instead they form very hard and stable nitrides as shown in Figure 25 (a) near the surface up to 1,0 mm in depth which is illustrated in Figure 25 (b). On the other hand, this depletion of especially Cr and Mo reduces the corrosion resistance on stainless steels. Chromium nitrides should be avoided in order to keep the corrosion resistance high [34]. This is one of the problems associated with nitriding stainless steels which lead us the next section of low temperature nitriding/carburizing.

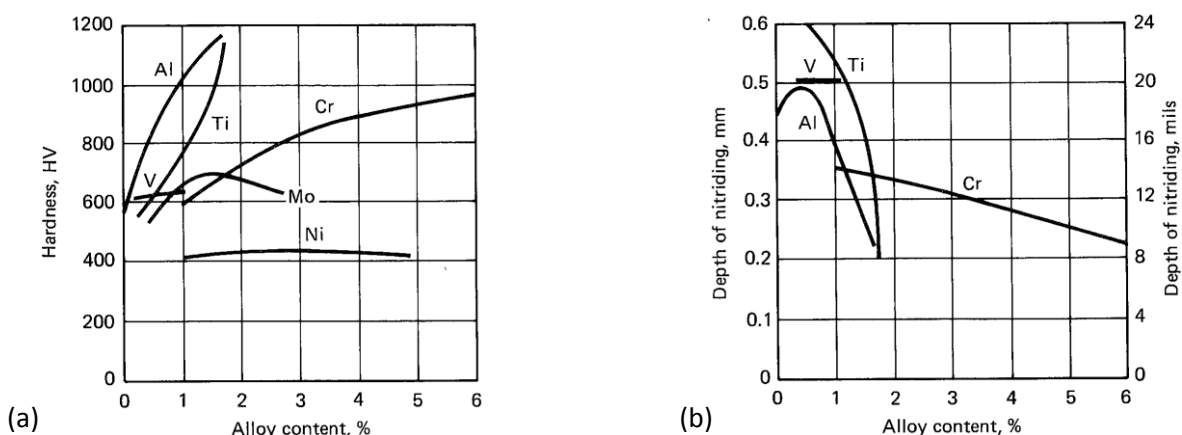


Figure 25. Influence of alloying elements on (a) hardness after nitriding and (b) depth of nitriding measured at 400 HV [37]. HV=Vickers hardness.

Low temperature nitriding/carburizing

In recent years nitriding processes were developed that led to a higher hardness of the case and thus better wear resistance of Cr- and Cr-Ni-alloyed stainless steel without diminishing their corrosion resistance. The processes can be distinguished by their low nitriding temperatures of between 250 and 450°C. A layer of usually 6-20 μm thickness is produced in which around 8-12 % nitrogen are soluted [7]. Structurally, the low temperature nitride layer is free from chromium nitride precipitation. This precipitation free nitride layer is commonly named the S phase or expanded austenite, which has a crystal structure similar to that of the face centered austenite, but with tetragonal distortion and lattice expansion due to the dissolution of nitrogen. A similar phenomenon is also observed during low temperature carburizing where a carbon S phase layer can be formed on austenitic stainless steels which is precipitation free [44]. The S layers are characterized by their supersaturation with the respective interstitial, nitrogen and carbon, and designated γ_N and γ_C respectively.

Low temperature carburizing is normally carried out at temperatures between 400 and 500°C, a little higher than low temperature nitriding. This make it possible to produce a much thicker hardened and corrosion resistant layer as schematically illustrated in Figure 26 (a). Although the hardness of the carburized layer is lower than that of the nitride, its distribution is of the diffuse type towards the layer-core interface, which is in contrast to the abrupt hardness drop at the layer-core interface for the nitride process. The resultant is a gradually decreased hardness gradient of the carburized layer which ensures good toughness and high load bearing capacity in contrary to the thin nitride layer with lower load bearing capacity. Also, the extremely high hardness and the abrupt drop in hardness at the interface for the nitride layer lead to poorer toughness. However, due to the nitride layer harder surface, the sliding wear resistance is higher than for the carburized layer [44].

The maximum allowable temperature for the low temperature nitriding and the low temperature carburizing are both time dependent and material dependent and decrease with increasing treatment time as shown by the temperature-time threshold curve in Figure 26 (b). An increase in processing temperature or time above the threshold value will lead to the formation of chromium nitride precipitates or carbide precipitation in the layer, deteriorating its corrosion resistance [44].

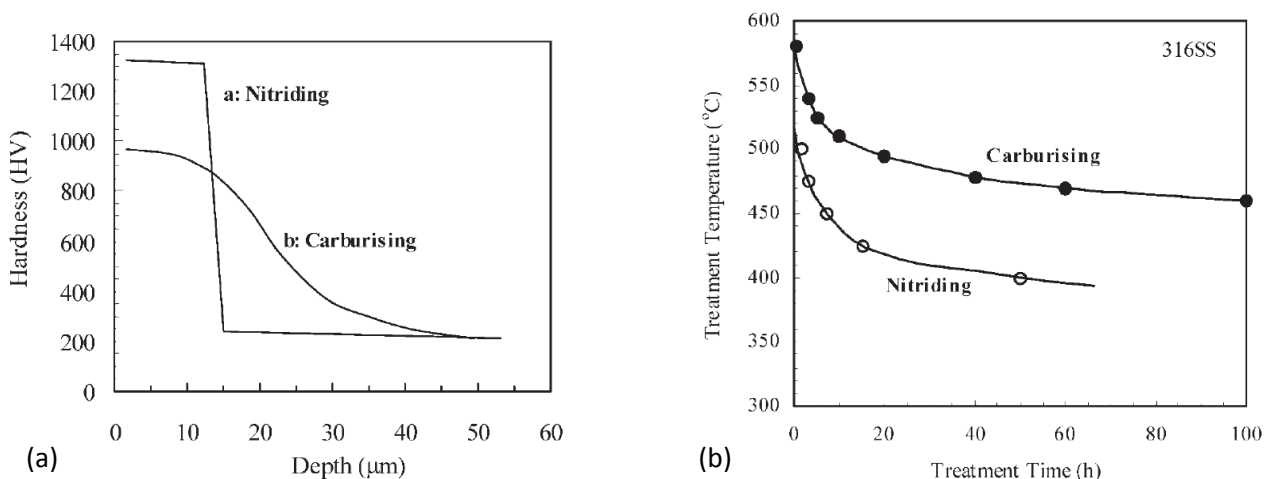


Figure 26. Characteristics of low temperature nitriding and low temperature carburizing in terms of [44] (a) hardness with respect to depth of austenitic stainless steels and (b) threshold temperature-time curves of 316SS stainless steel.

A hybrid process alloying both nitrogen and carbon simultaneously into the surfaces of austenitic stainless steel is possible and in many cases advantageous. Such a process forms a dual layered structure characterized of both nitriding and carburizing process with a nitrogen S phase layer on top of a carbon S phase layer as shown in Figure 27 (a). Note that the lower part of the nitrogen enriched layer is nearly free from carbon, while quite a large amount of carbon is incorporated in the outer part of the nitrogen enriched layer. This carbon incorporation leads to a further lattice expansion of the nitrogen S phase and contributes to the extremely high hardness up to 2000 HV measured for the hybrid treated surface as compared to the individually nitride and carburized surfaces. This also indicates that is possible to form a hybrid S phase with both nitrogen and carbon incorporation [44].

The thickness of the nitrogen S phase layer, carbon S phase layer and total alloyed zone increase with temperature. The increase in thickness with temperature is more significant for the nitrogen S phase layer than for the carbon S phase layer. A good linear relationship is found for the nitrogen S phase layer when using square root of time which indicate diffusion controlled growth as shown Figure 27 (b). However, the underlying carbon S phase layer does not follow a linear relationship. The decreasing behavior after 12 hours treatment can be explained by the fact that the active carbon atoms has to diffuse through the nitrogen S phase layer to provide the necessary carbon supply for the growth of the carbon S phase. As the thickness of the nitrogen S phase layer is increased, the carbon has to diffuse through a longer path before it reaches the carbon S phase layer, thus slowing down the rate of carbon supply [44].

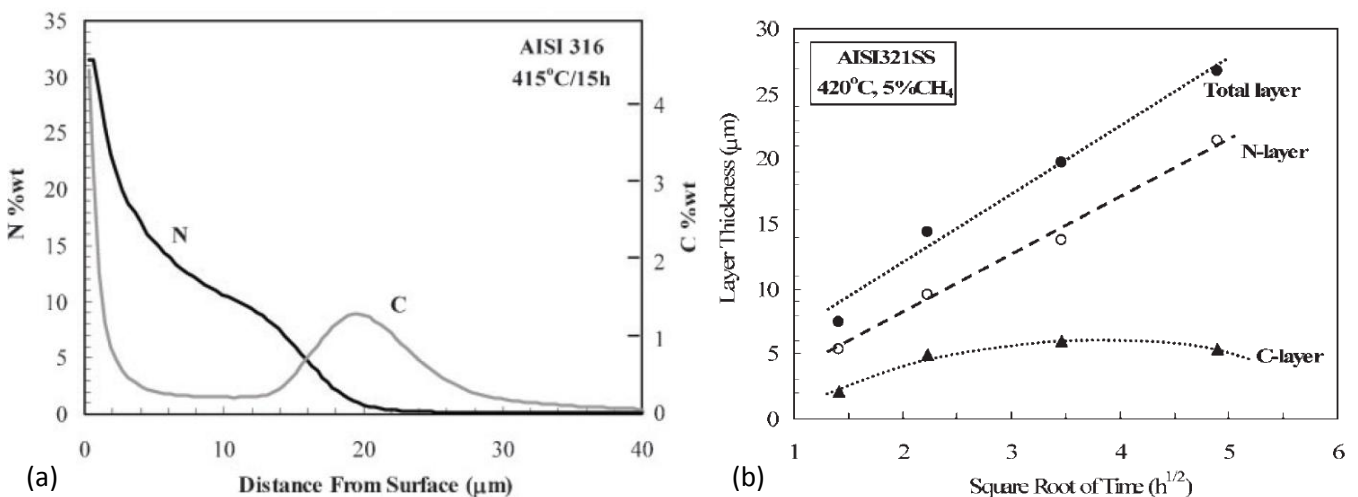


Figure 27. Hybrid low temperature nitriding/carburizing where [44] (a) show the nitrogen and carbon concentration profiles across alloyed zone while (b) show the hybrid layer thickness as function of square root of processing time.

Performing low temperature nitriding and low temperature carburizing on duplex stainless steel, the S phase will be formed on both the austenitic phase and the ferritic phase and some nitrided layers will be formed on the ferritic phase [13]. The major structural and property features of the three processes described above are summarized in Table 8.

Table 8. Main features of low temperature S phase technological processes [44].

Features	Process		
	Nitriding	Carburizing	Hybrid
Temperature [°C]	300-450	350-520	300-450
Layer thickness [µm]	2-20	5-45	5-35
Layer uniformity	Poor	Good	Very good
Layer structure	Nitrogen S phase	Carbon S phase	Nitrogen S phase + carbon S phase
Surface appearance	Silver grey, clean	Carbon sooty, black	Silver grey, clean
Surface hardness	1300-1500 HV	900-1100 HV	1500-2000 HV
Hardness gradient	Abrupt	Gradual	Graded
Load bearing capacity	Low	High	Very high
Toughness	Poor	Very good	Good

Solution nitriding

Solution nitriding is a high temperature nitriding which anneals stainless steel in a N₂-containing gas atmosphere in the range 1000-1200°C. In this high temperature gas nitriding treatment, atomic nitrogen is absorbed at the near surface of the steel and then diffuses into the near surface region. Case-depths from 0,5 to 2,0 mm and nitrogen contents in solid solution at the surface from 0,5-1,0 % can be obtained. This process successfully improve the surface properties of martensitic, austenitic, ferritic-austenitic and martensitic-ferritic stainless steel [45]. This treatment leads to the dissolution of nitrogen in austenite and is quite different from the conventional nitriding at 500 to 580°C, which entails the precipitation of a nitride layer, and the low temperature nitriding at approximately 400°C which also keep the nitrogen in solution but yields a much thinner case depth of less than 20 µm. A high strength yet ductile austenitic case is produced on austenitic and duplex stainless steels while a hard martensitic one is brought about on a martensitic-ferritic grade [46].

2.4.2 Thermal spray coating

Thermal spray is a generic term for a group of processes in which metallic, ceramic, cermet and some polymeric materials in the form of powder, wire or rod are fed to a torch or gun with which they are heated to near or somewhat above their melting point. The resulting molten or nearly molten droplets of material are accelerated in a gas stream and projected against the surface to be coated. On impact, the droplets flow into thin lamellar and interlocking as they solidify [47].

The thermal spray coating methods can only coat what the torch or gun can “see”, a so called line-of-sight nature. There are also limitations prohibiting the coating of small, deep cavities into which a torch or gun will not fit. Advantages are on the other hand several:

- Any material that melts without decomposition can be used.
- Ability to apply a coating to a substrate without significantly heating it.
- Ability to strip and recoat worn or damaged coatings without changing the properties or dimensions of the part.

One of the methods for applying a new layer of coating by thermal spraying is by a so-called high velocity oxygen fuel spray system described in more details below.

High velocity oxygen fuel (HVOF)

Fuel, usually propane, propylene, methylacetylene propadiene (MAPP) or hydrogen is mixed with oxygen and burned in a chamber as shown in Figure 28. The products of the combustion are allowed to expand through a nozzle where the gas velocities may become supersonic. Powder is introduced, usually axially, in the nozzle and is heated and accelerated. The powder is usually fully or partially melted and achieves velocities of up to about 550 m/s [47]. The powder particles flatten plastically upon impact with the substrate which eventually cools and solidifies to form the coating [48]. A wide variety of coating materials are possible.

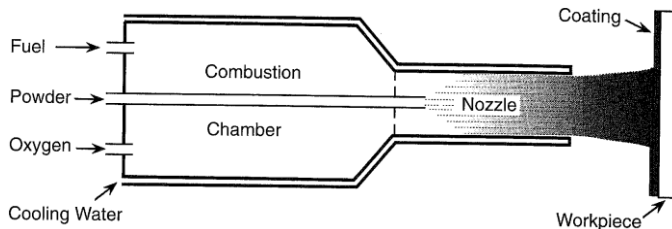


Figure 28. High-velocity oxyfuel process [47].

2.5 Applicable surface treatment methods

2.5.1 Expanite

Expanite is a Danish company established in 2010 based on ongoing research since 2000 by Thomas Christiansen, Marcel Somers and Thomas Strabo Hummelshøj. Expanite is a term used for the expansion of the host lattice through the dissolution of carbon or nitrogen in austenite in low temperature treatment less than 500°C, also known as expanded martensite, expanded austenite or S-phase. The tailoring processes of Expanite are the so-called ExpaniteHigh-T, ExpaniteLow-T and SuperExpanite.

The principle of the ExpaniteLow-T process is the dissolution of carbon and nitrogen atoms in the surface region with a typical thickness layer in the range of 20-35 µm. Nitrogen adds increased peak surface hardness up to 1800 HV while carbon bridges the gap to the relatively soft base material. The consequence is a smooth transition in compressive stresses from the hardened zone to the base material [49]. An additional benefit of nitrogen is the significantly improved electrochemical properties, resulting in an improved pitting corrosion resistance.

The principle of the ExpaniteHigh-T process is the dissolution of nitrogen in solid solution in the austenite phase similar to the process of solution nitriding described in Section 2.4.1. To avoid nitrides, a special Argon quench or high pressure N₂ quench is applied. The result is a surface layer of austenite with nitrogen, which is a strengthener and an austenite stabilizer, in solid solution for austenitic and duplex stainless steel.

The process for stainless steels can combine ExpaniteLow-T with the ExpaniteHigh-T that can supply a recrystallized substrate with improved hardness. This process is called Superexpanite [50]. This combination utilize the high hardness of low temperature nitriding and the case depth of the high temperature nitriding resulting in a surface with high load bearing capacity, superior corrosion properties, improved low temperature treatment response and high erosion-corrosion and cavitation resistance. The hardness-case depth profile for the SuperExpanite process will look something like shown in Figure 29

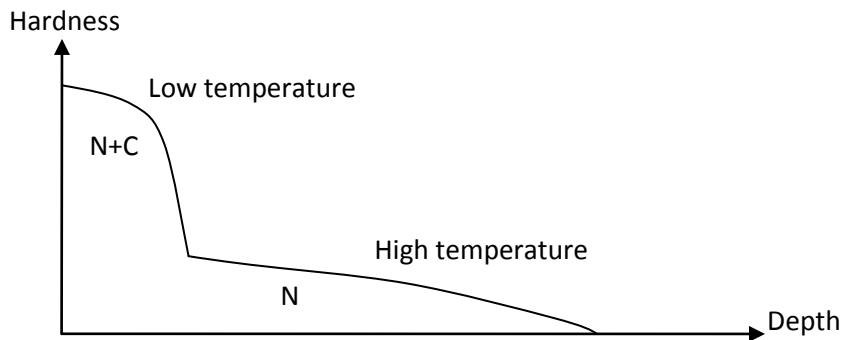


Figure 29 SuperExpanite hardness-depth profile utilizing both ExpaniteLow-T and ExpaniteHigh-T.

Procedure of the ExpaniteLow-T process

The process of which the parts will be subjected to is not available in details. The information available is the following:

1. Parts are subjected to a nitrogen atmosphere at high temperature above 1100°C for a relatively short time of period.
2. Subsequently the parts are nitrocarburised at low temperature for a short period of time below 470°C.

Due to the risk of 475°C embrittlement for the duplex stainless steel material, both high temperature and low temperature process variants are not standard.

2.5.2 Bodycote Kolsterising

Bodycote Kolsterising is a unique process only available within the Bodycote Group. Kolsterising process was developed by Professor Ben Kolster in the Netherlands in the early 1980s. At that time a company named Hardiff BV was formed and later on joined Bodycote Group in 1998. Their processing services are comprised of a number of core technologies, which include heat treatments, metal joining, hot isostatic pressing and surface technology [51].

Among heat treatments Bodycote offer is the so-called Specialty Stainless Steel Processes (S³P) featuring Kolsterising and Nivox. These heat treatments are surface hardening solutions for all stainless steel as well as nickel-based alloys and cobalt-chromium alloys producing increased mechanical and wear properties without adversely affecting corrosion resistance. S³P treatments involve low temperature diffusion of large quantities of carbon and/or nitrogen into the surface without the formation of chromium precipitations. No additional chemical elements that were not already present prior to the treatment are introduced during the process. There is no risk of delamination because S³P processes neither add a coating nor introduce brittle phases in the material [52].

Kolsterising is a low temperature diffusion process which adds carbon to the outer surface of a component. A carbon increase of up to 4 % dissolved in the steel matrix increases hardness and induces compressive stresses in the surfaces. This is possible due to the interstitially dissolved carbon in the austenitic phase which causes residual stresses by the expanded austenite, also called S phase. The effective diffusion depth varies between 20 and 40 μm, depending on the base material and the heat treatment selection. As carbide formation is suppressed, the corrosion resistance of the base material can be fully maintained. This process enhances in general the wear resistance of stainless steel and have the following characteristics [53]:

- No change in shape or size.
- No change in surface roughness.
- No change in color.
- Increased surface hardness to 1000-1200 Hv_{0,05}.
- No elements are added which were not already present prior to treatment.
- The non-magnetic behavior of austenitic materials is not altered.
- Highly resistant to galling.
- Superior resistance to cavitation and erosion wear.
- Uniform hardening of sharp edges, inside bores, cavities and gaps measuring only few microns.
- Corrosion resistance is unchanged or even improved in stainless materials containing molybdenum or steels.

Procedure of the Kolsterising process

The Kolsterising process is a protected and restrictive process of Bodycote not available in details. The Kolsterising process includes a carbon-rich gas process pressurized in a furnace in a temperature of approximately 400°C for 5-6 day and night.

2.5.3 High velocity oxygen fuel

High velocity oxygen fuel (HVOF) is a thermal spray process developed during the 1980s [54]. This process is used to improve or restore the surface properties or dimensions of a component. This is done by spraying molten or semi-molten materials onto the surface by means of high temperature, high velocity gas stream, producing a dense coating which can be ground to a very high surface finish. This process is a well known technology used among several companies around the world.

Trio OilTech Services is a company offering a wide variety of repair, rebuilding, wear facing and production technologies for various components using advanced welding and coating technologies where HVOF is one of them. Trio OilTech Services was founded in 1999 and became part of the Castolin Eutectic Group in 2007. Castolin Eutectic is a worldwide leader of application solutions in maintenance, repair and wear protection and was founded in Switzerland in 1906 [55].

Trio OilTech Services offer thermal spraying with high velocity oxyfuel by use of their JP-8000 HVOF spray system completed with an ABB robot as shown in Figure 30. This system is a Praxair model system that incorporates features like programmable logic controller (PLC)-based closed-loop mass flow controls, intuitive touch screen interface and constant process monitoring.



Figure 30. The JP-8000 HVOF spray system at Trio OilTec facilities.

The heart of this system is the Model 5220 Gun shown schematically in Figure 31, a kerosene-fueled HVOF gun that produces particles velocities of 1005-1190 m/s and gas velocities up to 2195 m/s. Coating thickness up to 12,7 mm is possible. A number of powders are available, from pure metals and metal alloy powder such as aluminium, cobalt, copper, iron, molybdenum and nickel, to ceramic powders such as aluminium oxide, chromium oxide and zirconium oxide to carbide powders such as chromium carbide, advanced powder technology (APT) and tungsten carbide.

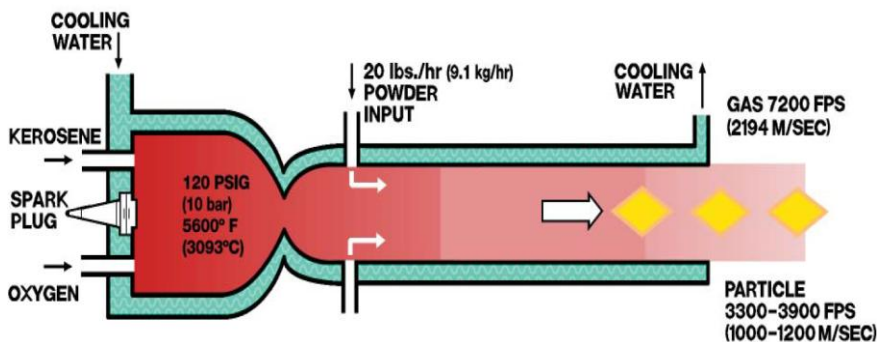


Figure 31. Schematic illustration of Model 5220 Gun used on JP-8000 HVOF spray system [56].

Procedure of the HVOF process

The HVOF process consists of the following steps:

1. Surface preparation
 - a. Degreasing for removal of oil and grease.
 - b. Preheat to 40°C to 80°C.
 - c. Grit blast with an abrasive media until all surfaces is uniformly roughened.
2. Spraying of tungsten carbide with binder consisting of 10 % Cobalt and 4 % Chromium. The component surface temperature shall not exceed 150°C.
3. Cooling of parts in normal room temperature down to 40°C.
4. Sealing of the hard-coating with special sealer by spraying, brushing or pouring.

2.5.4 Sursulf

Sursulf is a salt bath nitriding process used by Br. Bauer Nilsen AS within Techniques Surfaces Ltd. which is the principal subsidiary division of the French company HEF Group [57]. HEF Group is a worldwide company in the field of tribology and surface engineering. Their focus is on technical expertise, liquid nitriding, physical vapor deposition technologies and bushings and joints for severe applications and jobbing services [58].

Sursulf utilizes sulphur activated non-polluting salts operating at 570°C. Sursulf effectively resolves problems associated with wear, fatigue and seizure in both steels and cast irons. The process produces a hard compact layer at the surface of the treated components with fine surface porosity. This eliminates the potential for adhesive and abrasive wear, whilst introducing high residual compressive stress at the surface considerably improves fatigue resistance. In addition, the morphology and composition of the surface microlayer provide retention which considerably reduces the instability threshold of lubrication film breakdown [57].

Sursulf is carried out in a molten salt bath which consists of alkaline cyanates and carbonates and is stabilized by the addition of lithium compounds. The bath is therefore free from cyanides when made up and also specifically contains very small additions of sulphur compounds [59]. Typical Sursulf layer is 1) a compound zone of an approximately thickness of 20 μm consisting of a porous and a compact zone layer and 2) a nitrogen diffusion zone with an approximately thickness of 500 μm .

Procedure of the Sursulf process

The Sursulf procedure is described below and photos of the equipment is shown in Figure 32:

1. Place parts in furnace and pre-heat to 300°C. This in order to evaporate waste products for cleaning purposes and pre-heat the parts for the higher temperature nitriding bath.
2. Place parts in nitriding bath which has a temperature of 565°C. The temperature of the nitriding bath will cool due to the cooler parts being submerged.
3. Leave the parts for 180 minutes once the nitriding bath has reached 565°C.
4. Place the parts in oil bath for cooling.
5. Place the parts in water bath for cleaning.
6. Clean and remove all grit, scale and salt.

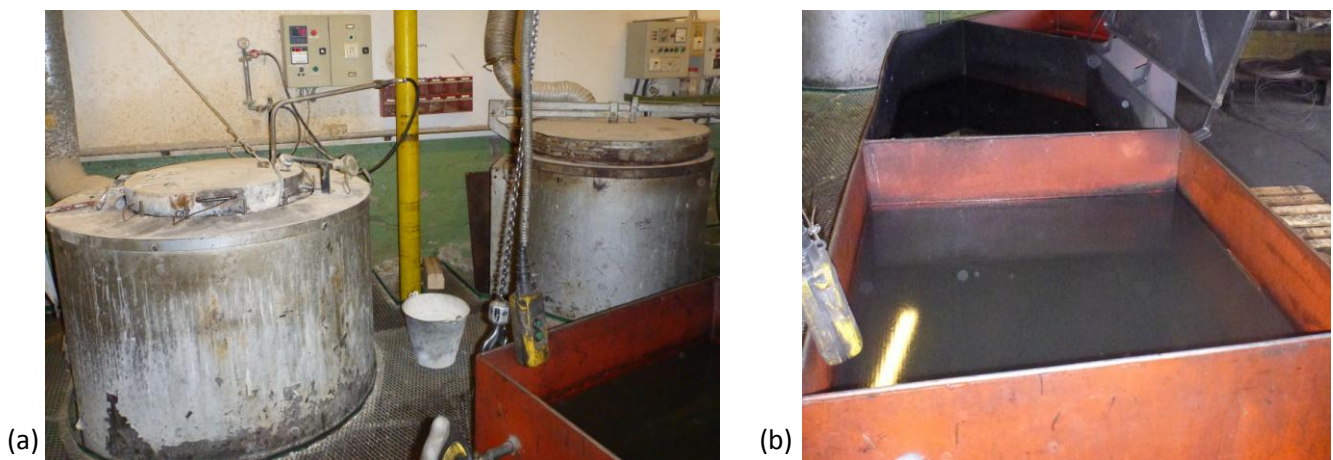


Figure 32. The Sursulf process where (a) is showing the pre-heat furnace to the right and the salt bath container to the left and (b) is showing the oil cooling bath behind and water bath for cleaning in front.

3 Experiments

According to oil and gas standards, different mechanical tests are required in order to use a particular material. Mechanical tests are used to determine properties required in the product specifications. Variations in testing methods are to be avoided and standard methods of testing are to be followed to obtain reproducible and comparable results [60]. Here are a summary of some of the requirements given in the following standards:

- Norsok M-630 MDS D47
Impact test, tensile test, hardness test and microstructural examination to be performed.
- ISO 10423
Material qualification testing depends on the equipment considering, but for bodies, bonnets and end and outlet connections it contains requirements in terms of tensile strength, yield strength, hardness, impact strength, elongation and reduction of area and chemical composition.
- ISO 15156-3
Hardness test to be performed.
- DNV-RP-F112
Metallographic characterization of the microstructure, corrosion testing according to ASTM G48 and impact test. Testing and requirements as specified in DNV-OS-F101 and Norsok M-630 are acceptable. DNV-OS-F101 describe that the following material characteristics shall be considered for material selection: mechanical properties, hardness, fracture toughness, fatigue resistance, weldability and corrosion resistance.

Based on the test requirements given above, the experiments stated in Table 2, i.e. tension test, Charpy impact test, hardness test, corrosion test and metallographic examination, are performed and described in more details in the following subsections. These tests are selected in order to verify whether the surface heat treatment affects the base material. Erosion test is the main test in order to test the wear resistance of the surface layer with reference to the wear mechanism involved for the Roxar subsea Chemical Injection valve described in Section 1.2 Challenge on the receptacle assembly. More experiments could be added, like an abrasion test or a scratch test, but for the purpose of this Master thesis, a finish line must also be set.

3.1 Material details

All material used in this document are bar shaped solid UNS S31803 duplex stainless steel obtained from Scana Steel Stavanger. The material was delivered in the solution annealed and water quenched condition according to the requirements given in Norsok M-630 and DNV-RP-F112. The material was delivered in the form of rectangular (10x20) cm plates with a thickness of 2 cm and marked with their respective heat number listed in Table 9. The first page of the material certificates is available in Attachment A: Material certificates.

The plates were additionally punch marked with the numbers from 1 to 5 in order to have traceability of the base material heat number when processing the test specimens. Ideally, all test pieces should be made of the same heat number in order to attain equal conditions for all pieces. Due to the limited size of the plates, the production of test pieces had to be made depending on the size of the specimen and the size of the plate. An overview of the test pieces divided among the plates, or heat number, is also shown in Table 9.

Table 9. Overview of available material obtained from Scana Steel Stavanger with information about material grade, heat treatment and produced test pieces.

#	Heat no.	Grade	Heat treatment	Charge no.	Specimen/test piece
1	T12688	Norsok MDS D47, rev.4 A479 UNS S31803	Solution annealed 1060°C, 1,5 hrs; water	A22306	<ul style="list-style-type: none"> ▪ Tension test pieces (5 each)
2	T12694	Norsok MDS D47, last revision UNS S31803	Solution annealed 1060°C, 1,5 hrs; water	A22352	<ul style="list-style-type: none"> ▪ Tension test pieces (5 each) ▪ Charpy specimens (3 each)
3	T12704	A276 UNS S31803	Solution annealed 1060°C, 5 hrs; water	A22440	<ul style="list-style-type: none"> ▪ Charpy specimens (12 each)
4	T12706	A479 UNS S31803	Solution annealed 1060°C, 3 hrs; water	A22440	<ul style="list-style-type: none"> ▪ G48 corrosion (2 each) ▪ Erosion specimens (30 each)
5	T12659	Norsok MDS D47, rev.4 A479 UNS S31803	Solution annealed 1060°C, 3 hrs; water	A22328	<ul style="list-style-type: none"> ▪ G48 corrosion (8 each)

The ASTM A479 standard gives the requirements for the chemical and mechanical properties for UNS S31803 duplex stainless steel. The chemical requirements and the mechanical property requirements are reproduced in Table 10 and Table 11 respectively.

The chemical requirements given in Table 10 can be compared to the chemical requirements given by ISO 15156-3, materials for use in H₂S-containing environments in oil and gas production, as shown in Table 3. It is obvious that the requirements are exactly the same. In addition, due to the fact that the Roxar subsea Chemical Injection valve will be subjected to cathodic protection, an additional document is applicable, namely DNV-RP-F112, design of duplex stainless steel subsea equipment exposed to cathodic protection [20]. This document, which is also linked to DNV-OS-F101, submarine pipeline systems [61], has the same requirements as those described in Table 10 and Table 11, with the only exception of the nitrogen content to be within 0,14-0,20 %. This nitrogen requirement is also specified by Norsok M-630 MDS D47 [15].

Table 10. Chemical requirements of UNS S31083 duplex stainless steel based on ASTM A479 [62]. Maximum percentage (%) composition is designated unless range is indicated.

Carbon C	Manganese Mn	Phosphorus P	Sulfur S	Silicon Si	Chromium Cr	Nickel Ni	Nitrogen N	Molybdenum Mo
0,030	2,00	0,030	0,020	1,00	21,0-23,0	4,5-6,5	0,08-0,20	2,5-3,5

Table 11. Mechanical property requirements of UNS S31083 duplex stainless steel based on ASTM A479 [62].

Condition	Yield strength min.	Tensile strength min.	Elongation in 50 mm or 4D min.	Brinell hardness max.
Annealed	450 MPa	620 MPa	25 %	290

Examination of the material certificates given in Attachment A: Material certificates reveal that:

- The chemical requirements shown in Table 10 are satisfied for all heat numbers in addition to the 0,14-0,20 % nitrogen window specified specifically in DNV-OS-F101 and Norsok MDS D47.

- The mechanical requirements from all material certificates, summarized in Table 12, are in accordance with the requirements stated in Table 11. It is worth noting the difference in the property data depending on the direction of which the mechanical tests have been performed, either longitudinal or transverse the orientation of the original material bar shape. See Figure 47 for more details regarding longitudinal and transverse orientation definition.

Table 12. Mechanical properties of the material given by Scana Steel Stavanger. T=transverse and L=longitudinal.

#	Test direction [L/T]	Yield strength [N/mm ²]	Tensile strength [N/mm ²]	Elongation [%]	Impact value @ -46°C [KV]	Hardness [HB]
1	L	541	707	39	110	223
		532	710	38	114	223
	T	520	722	35	67	217
		543	730	35	67	217
2	L	537	712	39	74	217
	T	514	726	37	49	217
3	L	537	719	40	121	217
4	L	549	716	39	238	217
5	L	598	753	35	138	229
		574	735	38	123	223
	T	548	740	35	67	223
		557	747	34	60	217

3.2 Material preparation

An overview showing the allocation of which test pieces to be used for which heat treatment is shown in Table 13. This table is necessary in order to have traceability of the individual test piece to the specific material certificate. Unfortunately, the control of whether the test pieces have been made in the longitudinal or transverse direction has not been maintained. The process of making the test pieces has been strictly restricted based on the original shape of the material plates and the geometry of the specific test piece. For instance, the production of tensile test pieces could only be made in one direction on the material plates due to their length. Anyway, microstructural examinations reveals to which direction the test pieces have been made. Further, the longitudinal or transverse direction of material is only critical for the tensile test and the Charpy impact test and to a less degree for the hardness test.

Table 13. Overview of which material certificate the test pieces were made, see Table 9, related to the specific surface treatment they were made for.

	A: Tension	B: Charpy	C: Hardness	D: Corrosion G48	E: Erosion
0: Untreated	1	3	①	5	4
1: Expanite	2	3	①	5	4
2: Kolsterising	1 and 2	3	①	5	4
3: HVOF	2	3	①	5	4
4: Sursulf	1	2	①	4	4

① Hardness to be performed on one or more of the other test pieces.

The test pieces for the various experiments have all been made from the plates given by Scana Steel Stavanger. In order to obtain the correct geometric shape and size, the following equipment has been used:

- Manual band saw machine – Pilous ARG 220 Plus shown in Figure 33 (a).
This machine is used for small size solid and metal profiles with cooling fluid applied to the band saw blade and profile. The manual band saw was used to cut the plates into smaller pieces for the process of making tensile specimens, Charpy test pieces and erosion test pieces.
- Manual cut-off machine – Stuers Labotom-3 shown in Figure 33 (b).
Labotom-3 is a compact table-top model for abrasive wet cutting. The machine is able to cut more precisely and with improved cutting surface compared to the manual band saw machine. This was used to cut the pre-machined $\varnothing 25$ mm erosion test specimens into smaller thickness and cutting the corrosion G48 test pieces from the original plate.
- Centre punch shown in Figure 33 (d).
Centre punch is used to mark the centre of a point in order to prevent wander of a drill bit for instance. This tool was used to mark the centre of the tensile specimens.
- Center drill with countersink shown in Figure 33 (e).
The main purpose of this drill is to drill a countersunk hole in a part to accommodate the live center on a lathe. This was done for the tensile specimens in order to perform the lathing process.
- Gear head drill – Ibarmia AX-35 shown in Figure 33 (i).
Ibarmia AX-35 is a drill machine with geared transmission and with the possibility of automatic feed by a mechanical clutch. This machine was used to make the countersunk hole in the center of the tensile test pieces.
- Lathe machine manual – Luna Swing 430N (17") shown in Figure 33 (c).
The lathe machine rotates the work piece on its axis to perform operations such as cutting, sanding, knurling, drilling, or deformation, facing, turning, with tools that are applied to the work piece to create an object which has symmetry about an axis of rotation [63]. This machine was used to make the circular shape of the tensile specimens and erosion test specimens. It was also used to make the facing of the erosion test specimens.
- Lathe machine CNC – Okuma LB9 shown in Figure 33 (g).
Okuma LB9 is a computer numerically controlled (CNC) horizontal turning machine with 2 axis. This machine was used to make the confined area of the tensile test piece in order to achieve high tolerance and good repetitive tensile test pieces.
- Milling machine – Somatec STF-5000V shown in Figure 33 (h).
Milling is the machining process of using rotary cutters to remove material from a work piece feeding in a direction at an angle with the axis of the tool. Somatec STF-5000V is a vertical mill where the spindle axis is vertically oriented. Milling cutters are held in the spindle and rotate on its axis. This machine has been used to make the flat faces of the Charpy test specimens and the corrosion G48 specimens.
- Charpy notch machine - Blacks CNB-31 [64] shown in Figure 33 (f).
This fixed speed motorized Charpy notch machine is specially designed for cutting Charpy and Izod V- and U notches in pre-machined standard 10 mm square, subsize and 0,45" diameter specimens. This machine made the V notches for the Charpy specimens.

- Grinding and polishing machine – Knuth-Rotor 2 shown in Figure 33 (j).
Knuth-Rotor 2 is a wet grinder machine with two rotating discs in order to perform grinding and polishing processes on an object. This machine was used to grind the surfaces of the erosion- and corrosion test specimens with a 120 grit SiC-paper.
- Slide caliper shown in Figure 33 (k).
This is a device to measure the distance between two opposite sides of an object. The slide caliper is necessary in order to ensure that all the specimens have their correct size.
- Letter and number stamps shown in Figure 33 (l).
Letter and number stamps are used in order to mark the respective test piece with traceability to the material heat number. The letters and/or numbers are punched into an insignificant area on the test piece with a hammer.



(a) Band saw



(b) Cut-off machine



(c) Lathe machine



(d) Centre punch



(e) Center drill



(f) Charpy notch machine



(g) Lathe machine CNC



(h) Milling machine



(i) Gear head drill



(j) Grinding machine



(k) Slide caliper



(l) Letter stamps

Figure 33. Equipment used for material preparation of the test specimens.

The material specimens

Overview of the machined test pieces in terms of shape and size is shown in Figure 34. Five sets of test specimens have been produced for each of the surface treatment listed in Table 1, namely Expanite, Kolsterising, HVOF and Sursulf in addition to the untreated duplex.

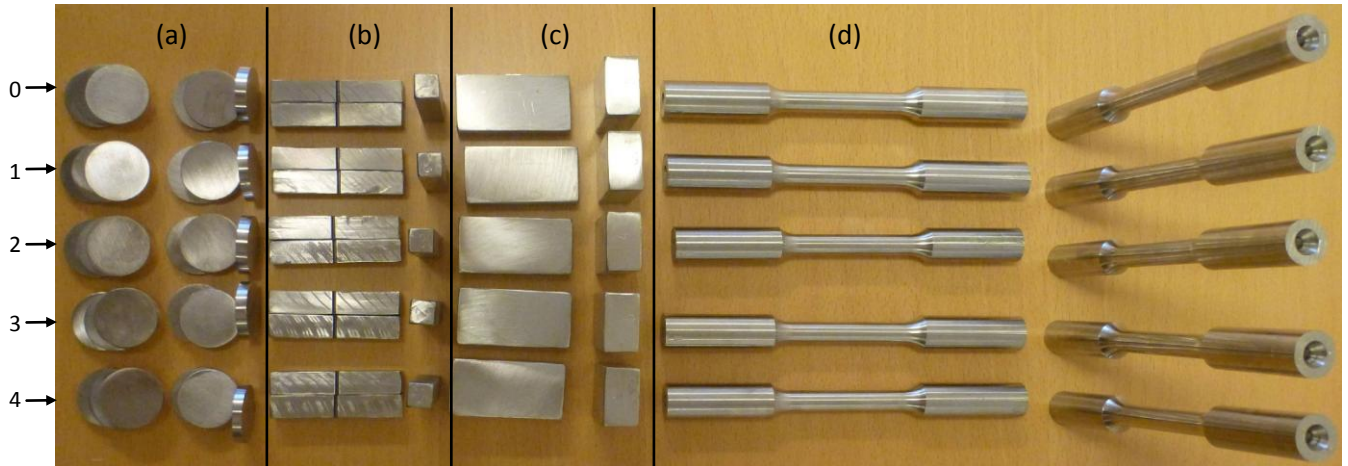


Figure 34. Overview of produced test pieces for experimental tests. 5 sets was produced for each test sample; (a) Erosion test specimens 6 each, (b) Charpy test pieces 3 each, (c) Corrosion G48 2 each, (d) Tensile test pieces 2 each.

The next step of the finished test specimen shown in Figure 34 is the surface treatments to be performed at their respective companies and locations shown in Table 14. This part of the process was arranged directly with the company in question in terms of arranging the necessary logistics. More details regarding the company and the surface treatment are given in Section 2.5 Applicable surface treatment methods.

Table 14. Overview of the companies performing the surface treatments and their location.

Treatment	Company	Location
Expanite	Expanite A/S	Hillerød, Denmark
Kolsterising	Bodycote	Hardiff, Netherlands
High velocity oxygen fuel	Trio OilTec Services	Tananger, Norway
Sursulf	Bauer Hydraulic motors	Haugesund, Norway

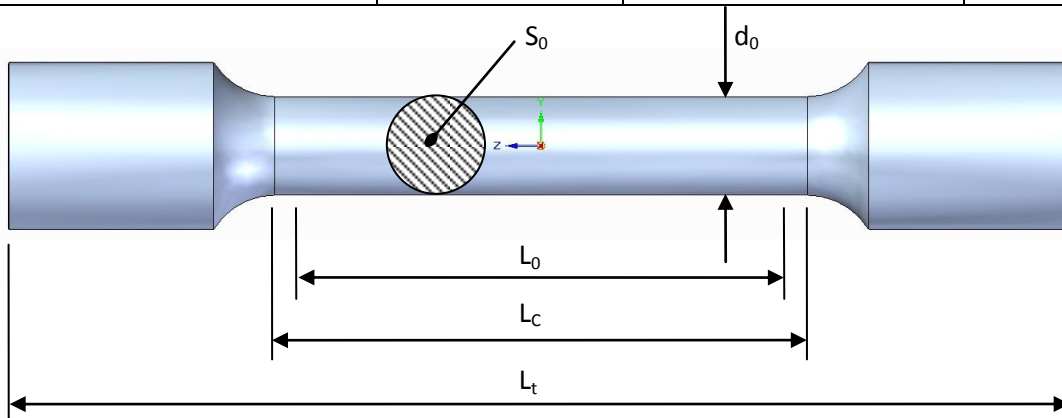
3.3 Tensile test

Objective of the test

Tensile test involves straining a test piece by tensile force, generally to fracture, for the determination of one or more of the mechanical properties of the tested material and to obtain the engineering stress-engineering strain curve [65]. A typical test piece have a circular cross-sectional shape with a diameter of $\varnothing 10$ mm and a gauge length of 50 mm, but other shapes and dimensions are also permitted according to ISO 6892-1 Tensile testing. Preferred test pieces have a direct relationship between the original gauge length, L_0 , and the original cross-sectional area, S_0 , expressed by the equation $L_0 = 5\sqrt{S_0}$, where k is the coefficient of proportionality with an internationally adopted value of 5,65. Using a diameter of 10 mm, the shape and size of the test piece will be as shown in Table 15 and Figure 35. The total length, L_t , shall be sufficient in order to ensure proper gripping of the test piece and in order to perform the tension test safely and reliable.

Table 15. Dimension of circular cross-section test pieces. Minimum parallel length, L_c , shall be at least equal to $L_0+(d_0/2)$.

Coefficient of proportionality k	Diameter d_0	Original gauge length $L_0 = 5\sqrt{S_0}$	Minimum parallel length L_c
5,65	10 mm	50 mm	55 mm

**Figure 35 Sketch of circular cross-section test piece for tensile test.**

Typical recommendations and requirements based on ISO 6892-1 include:

1. Original cross sectional area to be obtained from an average of three cross-section measurements.
2. Each end of the original length, L_0 , shall be marked by means of fine marks or scribed lines, but not by notches which could result in premature fracture.

Equipment

Equipment needed for performing the tension test:

- A tensile testing machine together with a strain-indicating device as shown in Figure 36.
- A vernier caliper as shown in Figure 33.

**Figure 36. The tensile testing machine, Schütz+Licht Prüftechnik GmbH – Wolpert U60, to be used on the tensile test at Quality lab. facility in Forsand.**

Experimental procedure

1. Make the two marks for the original length (L_0) and measure the diameter of the test specimen and record it.
2. Secure the ends of the test specimen in the grips of the testing machine.
3. Mount the strain-indicating device.
4. Apply the load slowly to insure that it is quasi-static. Take strain readings and record the upper and lower yield loads.
5. Remove the strain-indicating device after yield point and before necking to avoid breaking it. Proceed with the test to obtain the maximum load and the fracture load.
6. Remove the fractured test specimen from the grips and measure the final gage length and the diameter of the specimen at the fracture neck.

3.4 Charpy test

Objective of the test

Charpy test involves an impact fracture on a square cross section specimen in order to determine fracture properties of the tested material. Typical size of specimen is (10x10x55) mm and a 2 mm deep V-notch is introduced in the middle on the specimen as shown in Figure 37. The results of the impact tests are qualitative and its main interest is to compare tests done on different materials and/or temperatures. Absolute values are of less significance [9].

The result of the Charpy test is a measure of the absorbed impact energy of the V-notch specimen designated as KCV. The energy required to break the sample is determined from an indicator that measures how high the pendulum swings after breaking the sample. The energy absorption of the specimen is therefore an expression of the impact toughness of the material.

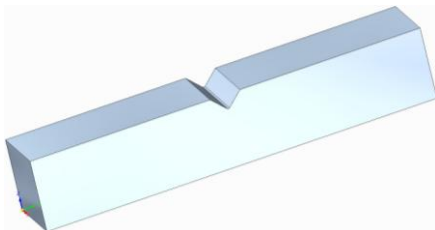


Figure 37. Typical Charpy specimen.

Equipment

The following devices are necessary for performing Charpy impact test:

1. Charpy impact tester as shown in Figure 38 (a).
2. Temperature test chamber (freezer) as shown in Figure 38 (b).

In addition, a plier must be used for moving the test specimens from temperature chamber to the impact tester.

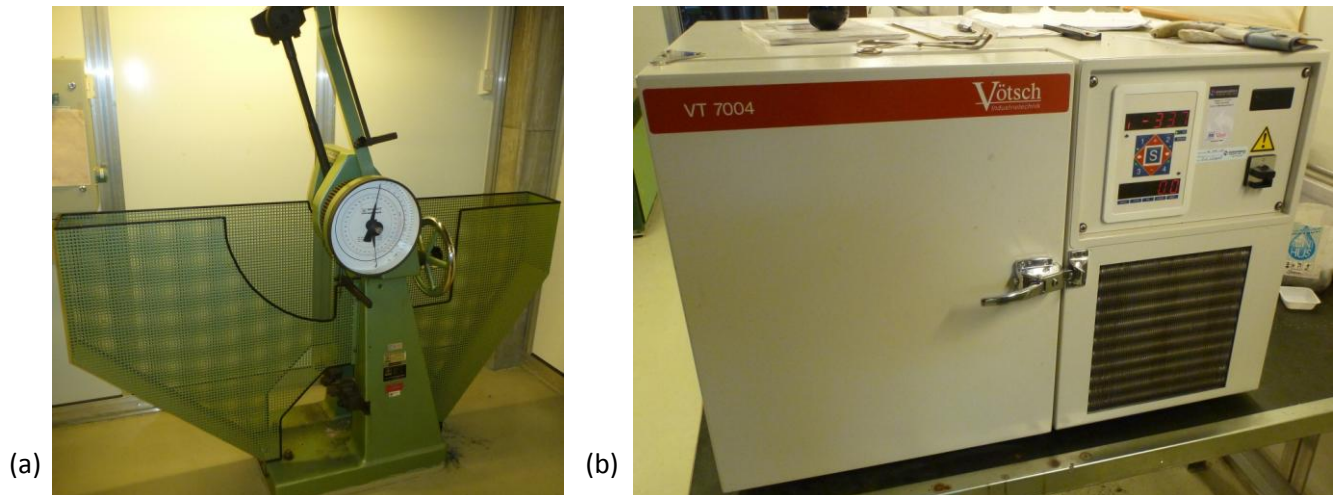


Figure 38. The two devices necessary for performing Charpy impact test; (a) Impact tester from Otto Wolpert-Werke GMBH PW30/15 and (b) Vötsch VT7004 temperature test chamber.

Experimental procedure

The temperature of which the Charpy test will be performed is by Norsok M-630 MDS D47 defined to be -46°C . The test shall be performed according to ASTM A370 which describes, among other, the following [60]:

1. The test shall consist of three specimens.
2. Specimen shall be held at the specified temperature for at least 5 minutes in liquid coolants and 60 minutes in gaseous environments. Since gaseous environment is used, 60 minutes is required.
3. Specimen shall be inserted in the machine and broken within 5 seconds.
4. Read and record the energy absorbed.

3.5 Hardness test

Objective of the test

Hardness is a mechanical property which is a measure of a material's resistance to localized plastic deformation [9]. It can be defined as the resistance of a material to scratching, abrasion or penetration and it is a manifestation of the combined effect of several related properties which may include the yield point, ultimate tensile strength, malleability, work hardening characteristics, wear-resistance properties and more [66]. The influence of hardness may be related to the strength of the metal and, thus, indirectly to its ductility, where a higher hardness is related to a stronger metal but also a lower ductility [5]. Various techniques are available, but basically a small indenter is forced into the surface of a material under controlled conditions of load and rate of application. The depth or size of the resulting indentation is measured, which in turn is related to a hardness number.

Two hardness test methods are used and described in more details below:

- Rockwell hardness test
Hardness number is determined by the difference in depth of a penetration resulting from the application on an initial minor load followed by a larger load. The utilization of a minor load enhances test accuracy since it establishes a reference position for the depth measurement and penetrates through any surface

scale or foreign particles. Intenders include spherical and hardened steel balls and a conical diamond intender [9]. Various combinations of intender and load are applied to accommodate a wide range of materials which include in the two types of Rockwell testing; regular Rockwell and superficial Rockwell. The latter uses smaller forces and causes smaller indentations [67] and are used for testing very thin steel or thin surface layers [60]. Each scale is represented by a letter corresponding to an intender and a specific load represented by Table 16.

Based on this table, scale symbol A, C and D are possible test methods for the purpose of tungsten carbide coating and thin case hardened steel. Also scale B might be applicable depending on the material's hardness. Scales E to V are not applicable for the duplex material but added for reference and overview purpose only. The Rockwell test is standardized by ASTM E18.

Table 16. Rockwell hardness scales [4].

Scale symbol	Intender	Total test force [kgf]	Typical applications of scales
A	Diamond	60	Cement carbides, this steels and shallow case-hardened steel.
B	1/16" ball	100	Copper alloys, soft steels, aluminium alloys, malleable iron etc.
C	Diamond	150	Steel, hard cast irons, pearlitic malleable iron, titanium, deep case hardened steel and other materials harder than B100.
D	Diamond	100	Thin steel and medium case hardened steel and pearlitic malleable iron.
E	1/8" ball	100	Cast irons, aluminium and magnesium alloys, bearing metals.
F	1/16" ball	60	Annealed copper alloys, thin soft sheet metals.
G	1/16" ball	150	Malleable irons, copper-nickel-zinc and cupro-nickel alloys. Upper limit G92 to avoid possible flattening of ball.
H	1/8" ball	60	Aluminium, zinc, lead.
K	1/8" ball	150	Bearing metals and other very soft of thin materials. Use smallest ball and heaviest load that does not give anvil effect.
L	1/4" ball	60	
M	1/4" ball	100	
P	1/4" ball	150	
R	1/2" ball	60	
S	1/2" ball	100	
V	1/2" ball	150	

Different equations are used in order to calculate the Rockwell hardness as shown in Equation 6 and Equation 7 for diamond sphero-conical intender and ball intender respectively. The scale for diamond intenders are therefore maximum 100 and for ball intenders maximum 130. Nevertheless, reading above 100 is not recommended since the sensitivity of most scales is poor in this region for ball intender, and because diamond intenders are not calibrated below values of 20, they should not be used when readings fall below this level [5].

$$\text{Rockwell hardness}_{\text{diamond}} = 100 - \frac{h}{0,002} \quad \text{Equation 6}$$

$$\text{Rockwell hardness}_{\text{ball}} = 130 - \frac{h}{0,002} \quad \text{Equation 7}$$

- Vickers microindentation

Hardness is determined based on the formation of a very small indentation by application of a relative low force in comparison to ordinary indentation hardness test. This is a method standardized by ASTM E384. A highly polished, pointed, square-based pyramidal diamond with face angles of 136° is pressed into the test specimen surface under an applied force in the range of 1-1000 gf. The size of the indentation is measured using a light microscope equipped with a filar type eyepiece or other type of measuring device. The Vickers hardness number is based upon the force divided by the surface area of the indentation. Microindentation tests allow specific phases or constituents and regions or gradients too small for macroindentation testing to be evaluated. For optimum accuracy of measurement, the test should be performed on a flat specimen with a polished or otherwise suitable prepared surface but should not be etched before making an indentation. However, when determining the microindentation hardness of an isolated phase or constituent, a light etch can be used to delineate the object of interest [68].

In general, the larger the indent is, the better the precision will be. ASTM E384 recommends that the operator should try to keep indents larger than $20\ \mu\text{m}$. The intender must be perpendicular to the test piece.

Equipment

- Rockwell hardness tester

The Rockwell hardness test is performed with a diamond intender or a ball intender dependent of the scale used and a total test force between 60 and 150 kgf. The test is performed at Roxar facilities on a Wolpert Wilson universal hardness tester as shown in Figure 39 (a).

- Micro hardness tester

The micro hardness tester is performed according to Vickers hardness-testing technique capable of applying loads ranging between 10 and 1000 g. The test is performed at the laboratory facilities at University of Stavanger on a Matsuzawa DMH-1 tester as shown in Figure 39 (b).



Figure 39. Hardness testers: (a) Wolpert Wilson universal hardness tester, model 930, used for Rockwell hardness testing. (b) Matsuzawa DMH-1 micro hardness tester used for Vickers hardness testing.

Experimental procedure

▪ Rockwell hardness test

The Wolpert Wilson hardness tester shown in Figure 39 (a) is an automated test which adds the minor load and the larger load without any manual influence. The hardness test procedure to be run in accordance with ASTM A370 and ASTM E18 as follows:

1. Make sure the test pieces are free from grease, impurities, dust and more which may affect the testing and the test results.
2. Perform a verification test of the test machine with a test block.
3. Perform at least three indentations on each test piece. For each test piece, bring the indenter into contact with the test surface and press start. The test machine will then perform a test cycle in accordance with the schematic illustration shown in Figure 40.

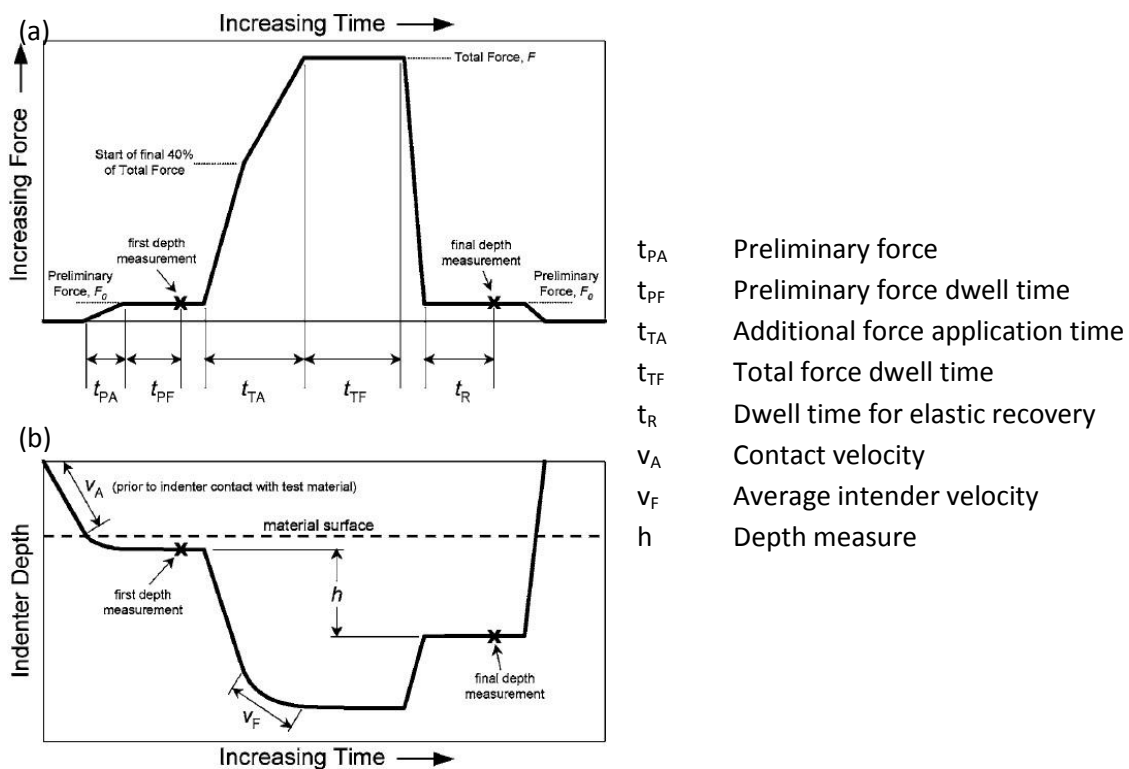


Figure 40. Schematic of (a) force-time plot and (b) indenter depth-time plot of an HRC test illustrating the test cycle parts [4].

▪ Vickers micro hardness test

The hardness procedure include:

1. Selection of applied load.
2. Place and secure the test specimen on grips.
3. Observation and placement of indenter at desired position on specimen.
4. Measurement of the impression in two directions which is automatically converted into hardness number by the testing machine.

3.6 Erosion test

Objective of the test

As defined earlier, erosion is defined as a series of particles striking and rebounding from the surface with the result of material loss. In order to test a material's resistance to an erosive action, some kind of laboratory equipment involving a gas blast system to accelerate a stream of particles towards a test sample is required. The sample must be held at a defined distance and angle with respect to the gas and particle outlet stream. Important parameters, apart from the working distance and angle of impact, is the particle velocity, because the wear increases in line with a power law relationship with velocity [69]. Such a gas blast erosion system is standardized in the ASTM G76; standard test method for conducting erosion tests by solid particle impingement using gas jets. However, an erosion test system has also been developed by Det Norske Veritas at their test facilities at Høvik, Oslo. This is a test rig with similar structure as the ASTM G76 test. The test rig applies air from the in-house air supply system and the sand particles are injected into the air stream at the inlet of a 2 m long pipe as shown in Figure 41. The specimen holder is positioned at a distance of 20 mm from the pipe exit [70].

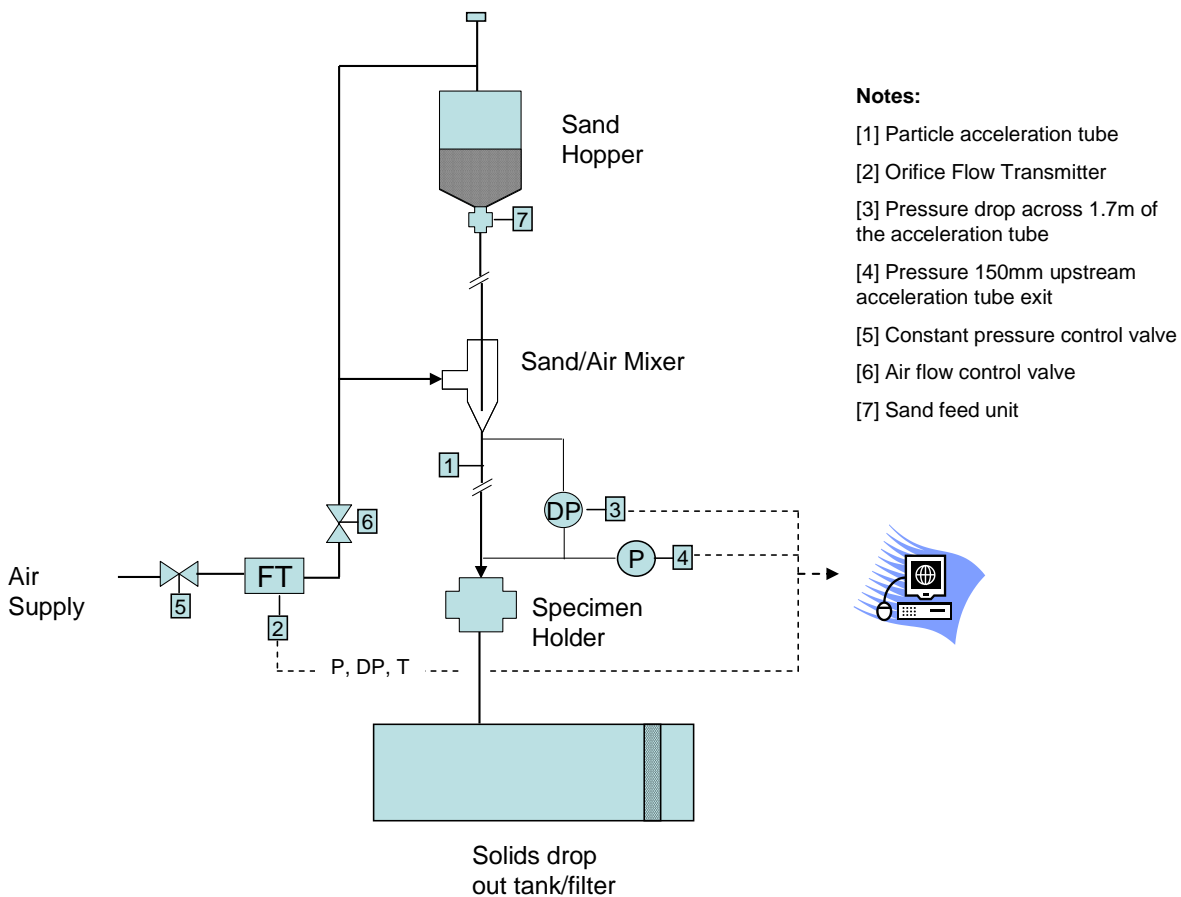


Figure 41. Erosion test facility developed and built by DNV Høvik. Sketch is made and given by DNV Høvik.

The experimental test, as presented in Figure 41, will make it possible to establish a ranking of the erosion resistance, rather than obtaining absolute erosion rates, for the duplex stainless steel candidates represented in Table 13. I.e. the main purpose of the erosion test in this document is to compare the material candidates against each other. This is only possible by testing the various surface treated specimens with the same test conditions. The ranking will be obtained by comparing the weight losses and/or volume losses combined with

some inspection of the eroded surface with microscopy. Generally, the correlations for determination of erosion rates are given in the form shown in Equation 8 which is also illustrated in Figure 42,

$$E = M_p \cdot K \cdot V_p^n \cdot F(\alpha)$$

Equation 8

where	E	weight loss of target material [kg]
	M_p	mass of sand hitting the target material [kg]
	V_p	particle impact velocity [m/s]
	α	particle impact angle
	K	material constant [(s/m) ⁿ]
	F(α)	function of particle impact angle
	n	velocity exponent

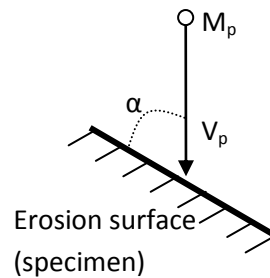


Figure 42. Parameters characterizing erosion impact on a surface with reference to Equation 8.

K, F(α) and n are the parameters which characterize the erosion behavior of the various materials or surface treatments. The function F(α) characterizes the ductility of the material with typically two extremes representing ductile and brittle materials as shown in Figure 17. The velocity exponent n usually falls in the range of 2 to 2,5 for metals and 2,5 to 3 for ceramics, although observations exist outside these ranges [38].

Equipment

The equipment necessary for performing this test is:

1. The test setup as shown in Figure 41 with power supply to the sand feeder unit.
2. Standard weight balance for measuring mass of sand accelerated against the metal surface as shown in Figure 43 (a).
3. Analytic weight balance with readability of 0,1 mg or better for weighing mass loss of the test specimens as shown in Figure 43 (b).
4. Metallographic microscope shown in Figure 44 (b).
5. Scanning electron microscope (SEM) shown in Figure 44 (c).



(a)



(b)

Figure 43. Balance scale for (a) standard weight purpose measuring sand mass (Precisa 18000D) and (b) analytic weight purpose measuring mass loss after one erosion test (Mettler AE100).

Experimental procedure

The test procedure proceeds as follows:

1. Marking of all specimens with a unique serial number and with head and tail in order to be able to perform two test conditions for each test specimen (one on each side).
2. Weight loss to be recorded by weighing the test specimen before and after the tests including a dummy element for weighing reference for minimizing uncertainties. The weight scale to be of 0,1 mg accuracy.
3. The tests for one individual test condition to be repeated until a stable erosion rate has been obtained, typically 3-5 tests.
4. Surface inspection by metallographic microscope and scanning electron microscope.

Test conditions:

- Sand
Quartz sand with maximum diameter of 250 μm , characterized as angular particles, is applied with a feed rate kept below 100 parts per million volume (ppmV) in order to avoid the influence of sand feed on the resulting erosion rate. Reference is made to Table 7 and also to the description of particle variables in Section 2.3.2 regarding the effect of particle shape and flux on wear. The sand is not recycled due to the possible fracturing and blunting of the sand particles. I.e. recycled sand would not give representative testing. $100 \text{ ppmV} = 100 \cdot 10^{-6} \text{ m}^3 \text{ sand per m}^3 \text{ air}$.
- Particle velocity (V_p)
At least two particle velocities are necessary in order to calculate the unknown parameters from Equation 8. The particle velocity is estimated by applying fluid mechanical models coupled with equation for calculation of particle motion developed by DNV Høvik. By controlling gas flow rate, the pressure 150 mm upstream of the pipe exit and the pressure drop across 1,7 m of the acceleration tube, give an estimation of particle velocity. This pressure monitoring ensures equal test conditions for all test specimens. The particle velocities have been estimated by taking drag, added mass, pressures and gravity forces into account for particle with a diameter of 250 μm . The selected particle velocities, which in turn define the pressure drop, DP, to be monitored as shown in Table 17, are based on the following factors:
 - Estimated fluid velocity along the sleeve of the Roxar subsea Chemical Injection valve. Fluid velocity is estimated based on maximum fluid flow through the valve and the dimension of the sleeve by the law of continuity; $\text{velocity} = \text{volume flow} / \text{area}$.
 - Low particle velocities require very long erosion time testing due to mainly two reasons:
 - 1) Erosion rates are low, which mean that more sand must be sent through the system to achieve measurable weight loss. This also magnifies reason number two.
 - 2) Gas velocity is low and therefore also gas flow. This involves a very low sand feed per minute to maintain the requirement of 100 ppmV.

Due to the factors above, high particle velocity testing favor the time related issue because erosion rates are higher and more sand can be fed per minute. However, estimated fluid velocity is limited for the purpose of the Roxar subsea Chemical Injection valve. The resulting velocities and pressure drop are therefore a compromise between these two factors and shown in Table 17.

Table 17. Calculated gas velocity at exit and pressure drop across 1,7 m in order to obtain desired particle velocity.

Particle velocity, V_p	Gas velocity, V_g	Pressure drop, DP
30 m/s	38 m/s	62,5 mbar
52 m/s	70 m/s	172,5 mbar

An uncertainty is applied to the particle impact velocity in the order of 15-20 % due to the interaction between particles and the pipe wall, interaction between individual particles, the particle size distribution and gas velocity profile. The relative erosion resistance between the different surface treatments will, however, be determined with a better accuracy since the tests are performed with the same test conditions [70].

- Impact angle (α)

As with the particle velocity, a minimum of two particle impact angles are necessary in order to calculate the unknown parameters from Equation 8. Angles typically maximizing erosion rate for ductile and brittle materials, see Figure 17, are chosen with 30° and 90° respectively. An additional low angle impingement of 15° is applied, if time permits, since this is a condition relevant based on the flow regime along the sleeve of the Roxar subsea Chemical Injection valve. The flow regime through the receptacle and sleeve, shown in Figure 2, is estimated to have a somewhat circular behavior before entering the retrievable valve assembly shown in Figure 1. This circulation movement of the fluid along the inner surface of the sleeve represents a low angle impingement and thus giving the 15° particle impact angle relevant. Anyway, an impact angle less than 10-15° is not recommended since this would give an increased uncertainty to whether the particles will hit the erosion surface or not.

3.7 G48 corrosion test

Objective of the test

G48 corrosion test cover testing methods for the determination of the resistance of stainless steels and related alloys to pitting and crevice corrosion when exposed to oxidizing chloride environments [71]. For duplex stainless steel, this test is further applicable to confirm that there is a sound microstructure after manufacturing and fabrication [61]. The following procedures are described and identified in ASTM G48:

- Method A Ferric chloride pitting test
- Method B Ferric chloride crevice test
- Method C Critical pitting temperature test for nickel-base and chromium-bearing alloys.
- Method D Critical crevice temperature test for nickel-base and chromium alloys.
- Method E Critical pitting temperature test for stainless steels.
- Method F Critical crevice temperature test for stainless steels.

According to DNV-OS-F101, corrosion test according to ASTM G48 is recommended as general requirements for duplex stainless steel materials. More specifically, pitting corrosion test shall be carried out according to test method A of ASTM G48 with a maximum allowable weight loss of 4 g/m². This method is designed to determine the relative pitting resistance of stainless steels so that the weight loss and the formation of pits on the surfaces make it possible to compare and rank them up against each other.

Pitting is a localized corrosion which selectively attacks areas of a metal surface where there is (1) a surface scratch or mechanically induced break in an otherwise protective or passive film, (2) an emerging dislocation or slip step caused by applied or residual tensile stresses or (3) a compositional heterogeneity such as an inclusion, segregate or precipitate [72]. ASTM G48 is designed to accelerate the time to initiate localized corrosion relative to most natural environments. Requirements or recommendations given in method A include:

1. Bath temperature to be $22 \pm 2^\circ\text{C}$ or $50 \pm 2^\circ\text{C}$. Although the temperature will be 25°C for the purpose of this test due to Roxar specific requirement.
2. Dissolve 100 g of reagent grade ferric chloride, $\text{FeCl}_3 \cdot 6\text{H}_2\text{O}$, in 600 ml of Type IV reagent water according to specification ASTM D1193 (about 6 % FeCl_3 by mass). Type IV reagent water may be prepared by distillation, ion exchange, continuous electrodeionization reverse osmoses, electrodialysis or a combination thereof [73].
3. Test specimen standard size to be 25 by 50 mm. This recommendation is also given by DNV-OS-F101.
4. All surfaces of the specimen should be polished to a uniform finish where a 120-grit abrasive paper has been found to provide a satisfactory finish.
5. Measure the dimension of the specimen and calculate the total exposed area of interest.

Equipment

This test requires the following equipment:

- Weight scale for dissolving precise amount of ferric chloride in reagent water.
- Glassware; test beaker, cradle and covers.
- Temperature controlled water bath.
- Analytic balance with readability of 1 mg or better for weighing mass loss of the test specimens similar to the one shown in Figure 43 (b).
- A low-magnification device for examination of specimen faces after test.

Experimental procedure

G48 method A test to be performed as follows [71]:

1. Pour 600 mL of the ferric chloride test solution into the 1000 mL test beaker. Provide a solution of at least 5 mL/cm^2 of specimen surface area. Transfer the test beaker to a constant temperature bath and allow the test solution to come to the equilibrium temperature of $25 \pm 2^\circ\text{C}$.
2. Place specimen in a glass cradle and immerse in the test solution after reaching the desired temperature.
3. Cover the test vessel with a watch glass. A reasonable test period is 72 hours, although the test period for this test will be 24 hours due to Roxar specific requirements.
4. Remove the specimens, rinse with water and scrub with a nylon bristle brush under running water to remove corrosion products, dip in acetone or methanol and air-dry. Ultrasonic cleaning may be used as a substitute method in cases in which it is difficult to remove corrosion products from deep pits.
5. Weigh each specimen to 0,001 g or better.
6. Perform a visual examination and photographic reproduction of specimen surfaces. Count the number of pits on the specimen faces under low-power magnification to determine pit density.

3.8 Metallographic examination

Objective of the test

Metallography is basically the study of the structures and constitution of metals and alloys. The metallographic examination is carried out by means of standard optical microscope and/or scanning electron microscope techniques. These tests require careful sectioning of the applicable sample avoiding heating or excessive cold working and a successive planing, grinding and polishing of the specimen. After polishing, a subsequent etching by chemical or electrochemical means are often included to bring out different microstructural features like [21]:

- Grain boundaries and general microstructure
- Ferrite and austenite
- Sigma and other intermetallic phases
- Carbides and nitrides

Microstructures in stainless steel can be quite complex and a wide range of second-phase constituents can be observed like carbides ($M_{23}C_6$, M_6C , M_7C_3 and MC), nitrides (MN and M_2N), sigma (σ), chi (χ) and laves (η). Precipitation of $M_{23}C_6$ carbides occurs as a result of heating solution-annealed grades to 500 to 950°C and occurs first at austenite/ δ -ferrite phase boundaries followed by precipitation at other noncoherent interfaces and finally by precipitation at coherent twin boundaries. It may also precipitate at inclusion/matrix-phase boundaries. Sigma is an intermetallic phase observable at temperatures below approximately 595°C which is a very potent embrittler [74].

In the case of the scanning electron microscope, the production of images by the use of secondary electrons remains the most used technique for the observation of the structure of bulk specimens. Back scattered electrons is the best method for obtaining grain contrast and the intensity of these electrons are sensitive to the crystallographic orientation of the specimen and to the “perfection of the crystal lattice” at the point of the incident beam [21].

The perfection of crystal lattice may be explained by the theory of diffraction contrast [75]: A perfect crystal lattice will appear more “open” in certain crystallographic directions than others. This will result in a deeper penetration of the incident beam electrons into the surface so that the probability of the electrons to reflect from the specimen are limited compared to a incident beam hitting the surface at another, less “open” crystallographic direction. I.e. the backscattered coefficient, meaning the number of electrons detected by the backscatter detector from that spot, differs from one crystallographic orientation to another orientation.

Equipment

The following equipment to be used:

- Cut-off machine for sectioning as shown in Figure 33 (b).
- Baking templates/holders.
- Grinding machine as shown in Figure 33 (j).
- Polishing machine as shown in Figure 44 (a).

- Etching equipment with a local power supply and the following chemicals:
 - Sodium Hydroxide pellets. Molecular formula: NaOH. Molar weight: 40 g/mol.
 - Oxalic acid dehydrate. Molecular formula: C₂H₂O₄·2H₂O. Molar weight: 126,07 g/mol.
- Metallographic microscope as shown in Figure 44 (b).
- Scanning electron microscope as shown in Figure 44 (c).

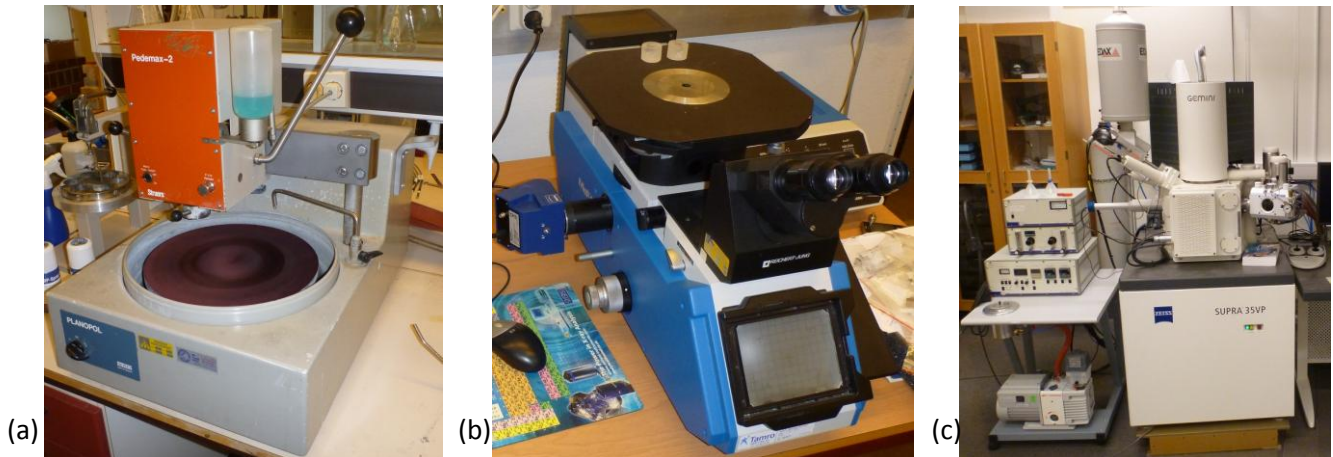


Figure 44. Equipment used for metallographic examination: (a) Polishing machine Struers Planopol, (b) Metallographic microscope Reichert Jung MeF3 and (c) Scanning Electron Microscope Zeiss Supra 35VP.

Experimental procedure

The following procedure is based on the materials science and engineering lab manual book [66]:

1. Sectioning

Sectioning will be done on the excessive $\varnothing 25$ mm test pieces originally made for the erosion test. Cut the $\varnothing 25$ mm test piece by means of a hacksaw, a band saw or an abrasive cut-off wheel to a relatively small piece. Care must be taken to avoid alteration of the microstructure by excessive heating or work hardening. Remove any burrs by filing or any other appropriate means and carefully wash the sample.

2. Baking

Mount the sample in a matrix of phenolformaldehyde resin, bakelite, plexiglass or any other appropriate thermoplastic or thermosetting polymer. Use either the compression mounting method or the cold mounting method.

3. Coarse grinding

Grind the mounted sample until all the polymeric resin is removed from the entire surface of the metallurgical sample. Frequently change the direction of the sample.

4. Fine grinding

Fine grinding gradually decreases the thickness of the distorted cold-work layer as the particle size of the abrasive decreases. Perform grinding involving a series of emery paper with grit sizes, starting from 240, 320, 400, 600, 1000, 2400 and 4000. The grinding to be performed wet on a flat surface. Hold the sample so that the scratch marks caused by the strip of emery paper are at 90° to those formed by the preceding strip. Wash the specimen and your hands after each grinding step.

5. Polishing

Polishing to be done in three stages on rotating wheels covered with napless cloth that is charged with 6, 3 and 1 micron abrasives of aluminium oxide.

6. Etching if applicable

Etching is necessary in order to make visible the many structural characteristics of the metal that are not revealed by the microscopic examination of the as-polished specimen. The etching operation involves subjecting the surface to the chemical action of an appropriate reagent under carefully controlled conditions. Chemical reagent etch at different rates and leads to preferential attack and/or staining of one or more of the metal's phases. This in turn establishes the structural contrast that enables different phases of a microstructure to be identifiable under the metallurgical microscope. Etching is conducted by immersing it into a small vessel partly filled with the reagent.

The following etchants to be used:

- a. Electrolytic with 10 % aqueous oxalic acid dihydrate: 5,5 V, 10 second.
To reveal grain boundaries, grain size and carbide precipitation [76].
- b. Electrolytic with 20% aqueous sodium hydroxide (NaOH): 3 V, 8 seconds.
To reveal the duplex structure and sigma phase [77].

7. Metallurgical examination using optical and/or scanning electron microscope.

Micro examination of duplex stainless steel shall, according to standards like DNV-OS-F101, be performed and documented at a minimum magnification of 400X.

The following to be examined and compared within the surface treatments:

- a. Grain boundaries and general structure
- b. Possible precipitation(s)
- c. Surface layer(s)
- d. Ferrite content to be determined according to ASTM E562

4 Experimental results

4.1 Tensile test

Tensile test were performed at Quality Lab AS facilities and the test results are presented in Table 18. Yield strength ($R_{0,2}$) and tensile strength (R_m) are obtained directly from the stress-strain curve from each test while elongation (e_f) and reduction (q) are obtained from Equation 9 and Equation 10 respectively. Modulus of Elasticity is basically obtained from the slope of the initial linear portion of the stress-strain curve. However, these stress-strain curves are not shown and the Modulus of Elasticity could not be read at this time due to some calibration problem at the time of testing.

$$e_f = \frac{L_f - L_0}{L_0} \quad \text{Equation 9}$$

$$q = \frac{S_0 - S_f}{S_0} \quad \text{Equation 10}$$

Table 18. Tensile test results.

Material	Dimension d_0 [mm]	Area S_0 [mm ²]	Temp. T [°C]	Yield strength $R_{0,2}$ [MPa]	Tensile strength R_m [MPa]	Elongation e_f [%]	Reduction q [%]
Untreated	10,05	79,33	20	517	734	38,0	77
	10,03	79,01	20	586	746	35,5	79
Expanite	10,05	79,33	20	580	785	34,3	71
	10,03	79,01	20	592	783	30,7	73
Kolsterising	10,06	79,49	20	611	775	35,2	74
	10,05	79,33	20	536	751	39,4	74
HVOF	10,31	83,48	20	521	681	27,0	79
	10,31	83,48	20	517	688	28,2	78
Sursulf	10,06	79,49	20	555	739	39,1	73
	10,05	79,33	20	540	728	38,5	77

Note:

- The first test on the untreated duplex was adjusted with some mistakes with respect to the strain-indicative device and may have influenced the yield strength.
- The gauge length for HVOF could not be placed on the original 50 mm length (see L_0 in Figure 35). The gauge length used for calculating elongation is based on the edges of the necking due to the fact that the coating on these specimens crumbled away during tension testing as shown in Figure 45 (a). The original gauge length markings (L_0) disappeared.
- Pre and post diameter of the HVOF specimen are accurate but involve a degree of uncertainty to the results. This is due to the crumbled coating, causing the diameter (see d_0 in Figure 35) measured before and after the test to be done with and without the coating layer.
- All treated duplex, i.e. Expanite, Kolsterising, HVOF and Sursulf, showed a ductile fracture appearance with a “cup and cone” surface as shown in Figure 45 (b) for untreated duplex.

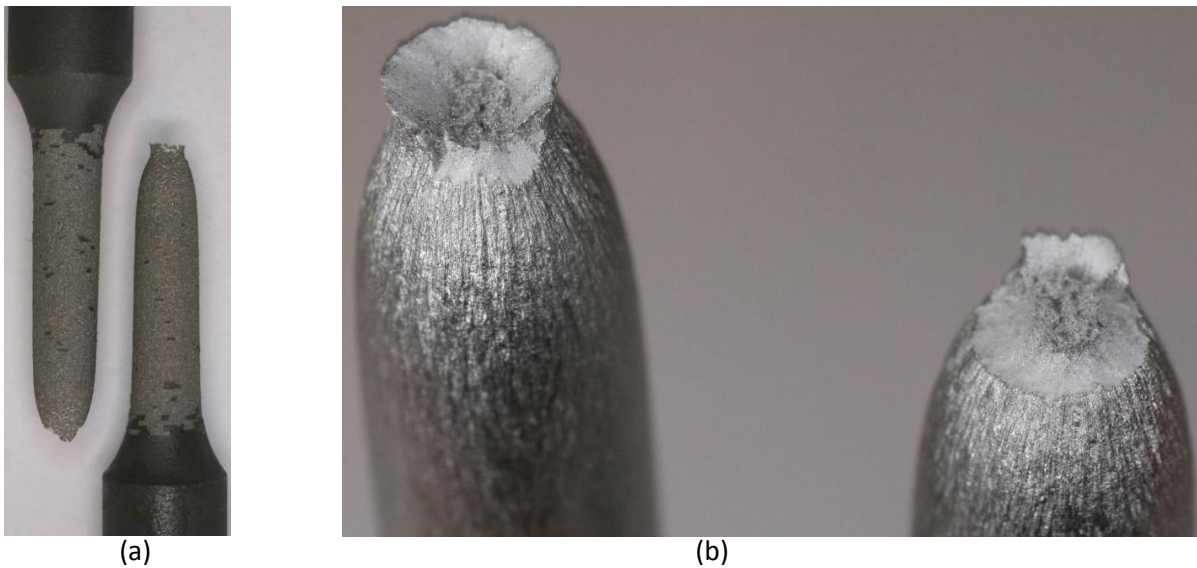


Figure 45. Photos of (a) the fractured HVOF tensile test specimen showing the crumbled tungsten carbide coating along the gauge length and (b) the fractured untreated duplex “cup and cone” surface of the tensile test specimens. The typical appearance of “cup and cone” as shown in (b) was present in all test specimens.

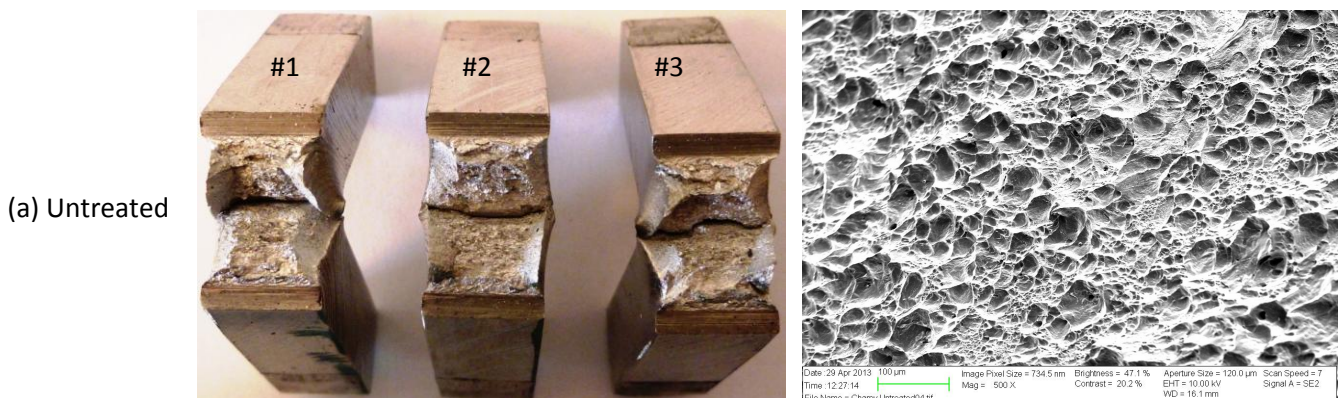
4.2 Charpy test

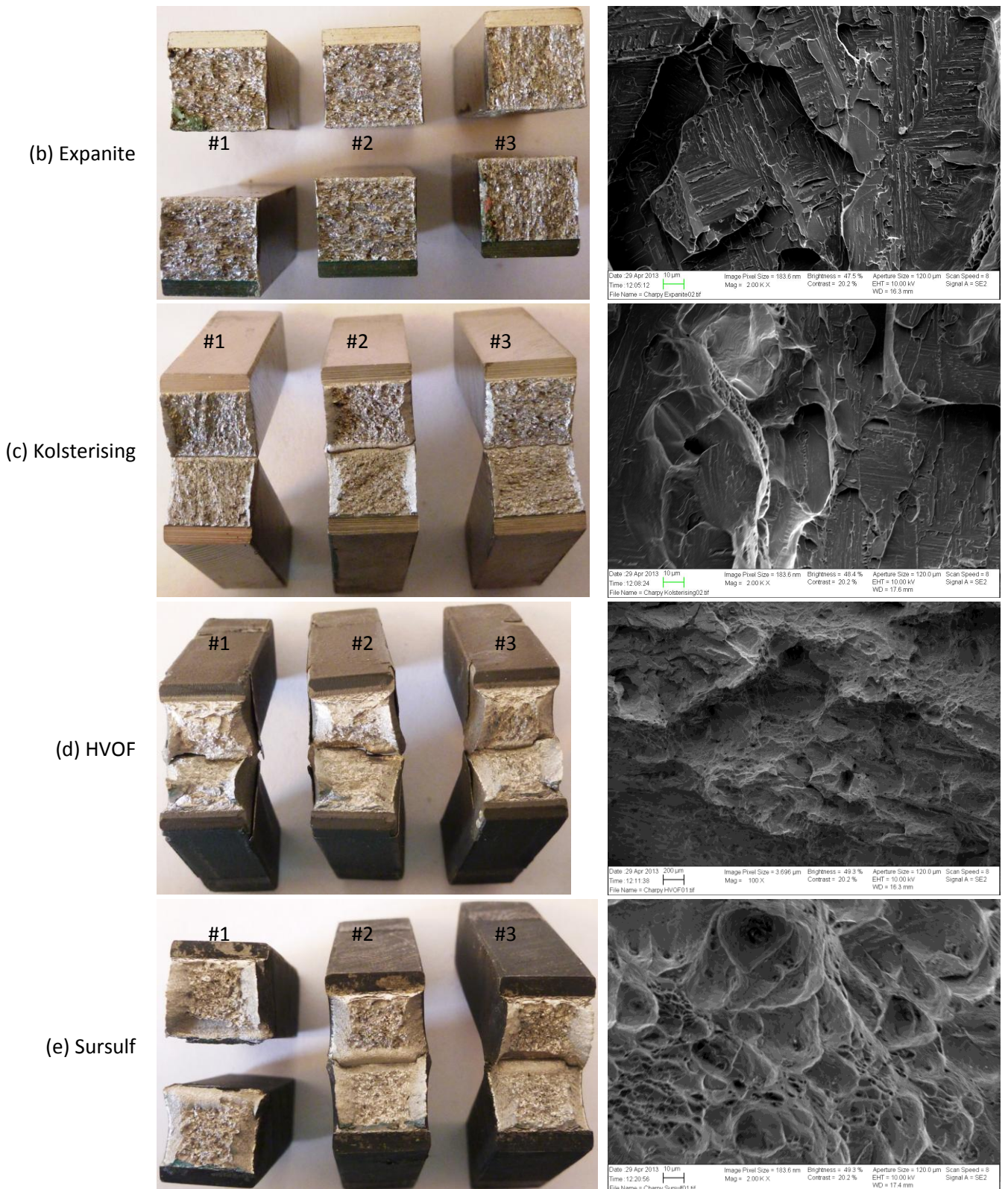
Charpy impact test were performed at UiS facilities and the results are presented in Table 19. Photographs and scanning electron microscope images of the fractured specimens and surfaces are shown in Figure 46.

Table 19. Charpy impact test results performed on test specimens at -46°C. L= longitudinal and T=transverse are obtained from images in Table 20. Related impact values from material certificate is also shown in bold on the right hand side.

Test piece	Test #1	Test #2	Test #3	Average
Untreated:	215,5 J (T)	163,0 J (T)	251,0 J (T)	209,8 J (T)
Expanite:	14,5 J (T)	14,5 J (T)	12,1 J (T)	13,7 J (T)
Kolsterising:	19,0 J (T)	50,0 J (L)	24,3 J (T)	21,6 J* (T)
HVOF:	202,0 J (T)	214,5 J (T)	200,0 J (T)	205,5 J (T)
Sursulf duplex:	132,0 J (L)	121,0 J (L)	115,0 J (L)	122,7 J (L)

* Average impact value for Kolsterising is based on the two transverse tests only.



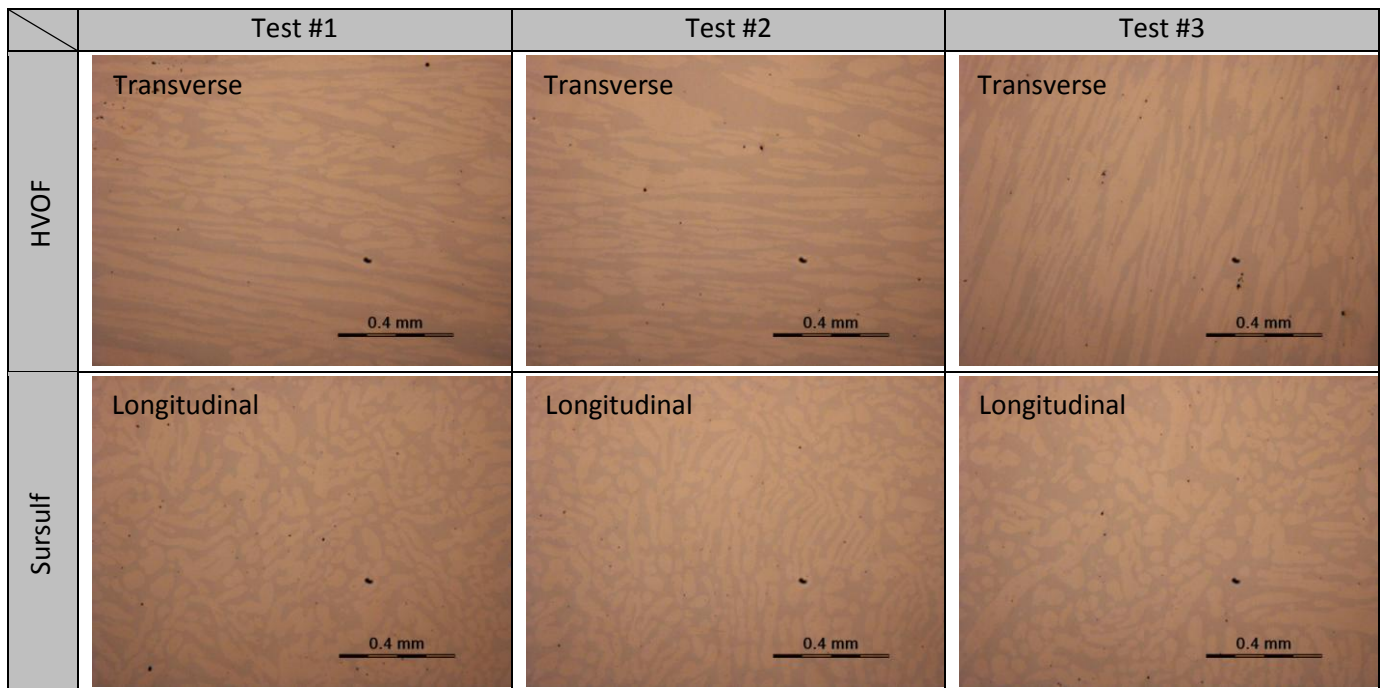


The SEM images in Figure 46 are taken from a typical site on the fractured surface. Except for Expanite and Kolsterising, all samples show both a ductile and a cleavage fracture features. The images show clearly the typical void appearance of ductile fracture for untreated duplex, HVOF and Sursulf. In the case of Expanite and Kolsterising, the fracture surfaces are approximately fully brittle with the appearance shown in the SEM images in Figure 46 with no sign of void creation.

In order to verify to which structural direction the test specimens were made, a metallographic examination is performed and shown in Table 20. This is done by cutting the end of each Charpy test specimen and preparing each sample according to the experimental procedure described in Section 3.8. This examination is important since the microstructural orientation influence the impact toughness of the material, whereas longitudinal direction normally absorb more energy than transverse orientation. This is also reflected by the higher absorption energy requirements for Charpy test performed in longitudinal direction by DNV-OS-F101.

Table 20. Overview of the microstructural orientation of the Charpy test specimens by optical microscope (200X). The Charpy notch is located along lower end of each image (not shown).

	Test #1	Test #2	Test #3
Untreated			
Expanite			
Kolsterising			



Definition of longitudinal and transverse orientation is based on the direction of the greatest extension of the steel during rolling or forging [60]. For an ASTM A479 bar, the greatest extension is along the bar as shown in the schematic drawing of Figure 47. The greatest extension defines the longitudinal direction shown with the longitudinal microstructural lines in figure below.

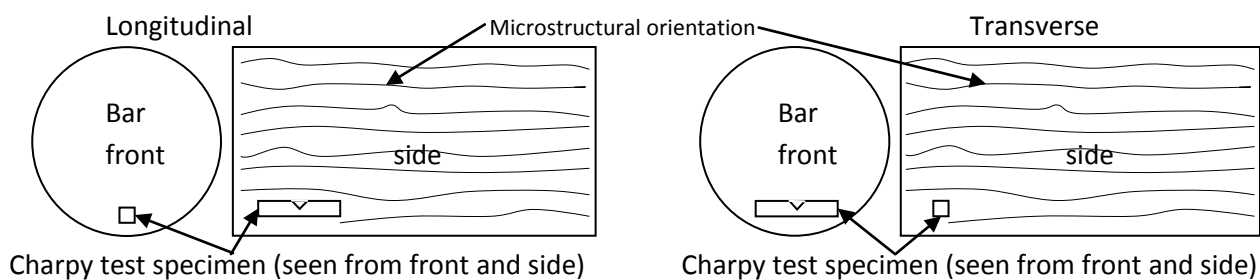


Figure 47. Definition of longitudinal and transverse orientation with reference to a bar material. Left hand side show a Charpy test specimen cut out in a longitudinal orientation whereas right hand side shows a transverse orientation.

4.3 Hardness test

Rockwell hardness scale B and C

Surface hardness tests were performed on the excessive $\varnothing 25$ mm test pieces originally made for the erosion test which are all marked with unique serial numbers. Rockwell hardness test according to scale C and Rockwell hardness test according to scale B were performed. Both scales were performed because the Rockwell hardness test according to scale C gave some values below 20 which are outside the calibration area of the tester. An additional hardness test using scale B was therefore performed on each and all of the test specimens. A verification test of the hardness machine was first performed on a test block to check the precision and calibration of the tester. The tests results are presented in Table 21. This table shows that the surface treated duplex, except Sursulf, have experienced an increased hardness even with test load of 100 kg and 150 kg by Rockwell B and C method respectively.

Table 21. Rockwell scale C and B test results of the surface on the $\varnothing 25$ mm erosion test pieces.

Test piece material and serial number	Rockwell C				Rockwell B			
	Test #1	Test #2	Test #3	Average	Test #1	Test #2	Test #3	Average
Untreated: 06T	18,05	18,49	18,41	18,3	96,90	96,28	96,61	96,6
Expanite: 16T	23,62	23,11	23,65	23,5	99,44	99,61	99,92	99,7
Kolsterising: 26T	23,75	25,15	24,24	24,4	100,68	100,02	100,22	100,3
HVOF: 36T	26,87	25,40	27,49	26,6	107,80	109,10	105,74	107,5
Sursulf: 46T	16,44	17,48	16,82	16,9	95,01	95,54	96,56	95,7

Vickers micro hardness

Vickers micro hardness test has been performed directly on the surface and on the cross section of the erosion test specimens:

- Surface hardness

The surface treated duplex have a hardened surface layer in the order of microns in thickness. This means that hardness tests involving test loads in the order of kilograms, as with Rockwell B and C, would penetrate through this layer. In order to measure the actual surface layer hardness, test loads in the order of grams must be applied. The test results performed with Vickers micro hardness tester and a test load of 25 g are presented in Table 22.

Table 22. Surface Vickers hardness values with 25 g test load.

Surface treatment	Vickers hardness	Comments
Untreated duplex	258 HV _{0,025}	
Expanite	861 HV _{0,025}	3,3X relative hardness value of untreated duplex
Kolsterising	988 HV _{0,025}	3,8X relative hardness value of untreated duplex
Sursulf	751 HV _{0,025}	3,7X relative hardness value of untreated duplex

Test result of the HVOF test specimen is not included since the impression was not readable due to the roughness of the surface. In fact, the test results overall are quite uncertain due to a relatively rough surface finish in terms of performing micro hardness testing, but they do at least represent approximately and relative values. The hardness values show that the surface hardness have increased with a factor in the range of 3,3-3,8 for Expanite, Kolsterising and Sursulf with respect to untreated duplex.

- Cross section hardness

Cross section hardness is useful to see the hardness with respect to depth in order to obtain a hardness profile. Micro Vickers hardness test method is used with a light load to be able to measure small areas like the surface layer and individual grains. The hardness tests were performed on non etched cross sections.

Basically, the accuracy of micro hardness testers are more accurate the larger the impression is, i.e. higher load. Due to the thin surface layers to be measured, the load was selected to be 10 g which is the minimum capacity of the tester. First of all, some comparable measurements were performed to check the accuracy of the 10 g impressions against higher loads of 100 g and 1000 g. Overall, the 10 g hardness value were measured to be half the hardness value performed with 100 g and 1000 g. Typical hardness value at the center of the cross sections were approximately 230 HV_{1/0,1} and 115 HV_{0,01} for 1000 g, 100 g and 10 g respectively. By multiplying the 10 g hardness value with a factor two, a hardness value of 230 HV is

achieved as shown in Equation 11. This modification will be designated with an asterisk, *, attached to the hardness value where this is performed.

$$115HV_{0,01} \times 2 = 230HV_{0,01}^* = 230HV_{0,1/1} \quad \text{Equation 11}$$

The hardness values presented in Table 23 are the results from the micro hardness with respect to distance from free surface with a factor of 2 added to the original $HV_{0,01}$ values. This table shows that there is a hardness profile with the highest hardness measured close to the surface and decreasingly hardness values towards the center of material.

Table 23. Vickers micro hardness value performed with 10 g load. $HV_{0,01}^* = 2 \times HV_{0,01}$ as shown in Equation 11.

Expanite		Kolsterising		HVOF		Sursulf	
Distance [μm]	$HV_{0,01}^*$	Distance [μm]	$HV_{0,01}^*$	Distance [μm]	$HV_{0,01}^*$	Distance [μm]	$HV_{0,01}^*$
5	298	4	626	64	973	5	522
14	236	8	471	114	1073	18	599
23	241	16	278	190	315	25	263
35	214	29	281	221	271	27	244
48	232	39	271	280	219	37	235
-	-	52	234	-	-	54	202
Center	230	Center	227	Center	222	Center	225

4.4 Erosion test

The original test matrix shown in Table 1 is expanded slightly for the erosion test only. Sursulf carbon is added to the test matrix based on an inquiry from Bauer Hydraulic Motors AS. Sursulf carbon is basically carbon steel subjected to the same treatment as Sursulf duplex. The carbon steel specimens was made by Bauer Hydraulic Motor AS and treated along with the duplex parts. The results from testing the Sursulf carbon are added along with the duplex stainless steel parts for comparison and general for attaining more information.

Erosion rate

Erosion rate may be given in terms of mass or volume of material removed per unit mass of erodent impacted on test surface. The results obtained below are given in terms of mass of material removed since this is more accurate than volume of material removed due to an unknown density of the surface.

The ranking of the surface treatments is obtained by comparing the weight losses at the various test conditions. The untreated duplex is used as reference material and the relative erosion resistance (REF) will be calculated as stated in Equation 12.

$$REF = \frac{\text{Weight loss test material}}{\text{Weight loss untreated material}} \quad \text{Equation 12}$$

The relative erosion resistance equation implies that when:

- REF > 1 Surface treated duplex will be more exposed to erosion than untreated duplex at that specific condition.
- REF < 1 Surface treated duplex will be less exposed to erosion than untreated duplex at that specific condition.

The test is done at Det Norske Veritas facilities in Høvik and the test results are presented in Table 24 and Table 25 showing the recorded weight losses and the relative erosion rate respectively.

Table 24. Weight loss [mg/kg] as function of particle impact velocity and impact angle.

Particle velocity, V_p :	30 m/s			52 m/s		
Angle, α :	90°	30°	15°	90°	30°	15°
Untreated: 0	1,05	1,72	1,75	6,78	12,87	7,20
Expanite: 1	1,08	1,03	0,92	7,02	8,37	4,72
Kolsterising: 2	1,44	1,46	1,06	9,00	8,83	5,80
HVOF: 3	2,24	1,68	No data	4,67	4,00	No data
Sursulf duplex: 4	1,96	2,53	No data	7,27	6,47	No data
Sursulf carbon: 5	7,21	4,72	No data	22,87	13,07	No data

Table 25. Relative erosion resistance (REF) with untreated duplex as reference material.

Particle velocity, V_p :	30 m/s			52 m/s		
Angle, α :	90°	30°	15°	90°	30°	15°
Untreated: 0	1	1	1	1	1	1
Expanite: 1	1,03	0,60	0,52	1,04	0,65	0,66
Kolsterising: 2	1,38	0,85	0,60	1,33	0,69	0,81
HVOF: 3	2,14	0,98	No data	0,69	0,31	No data
Sursulf duplex: 4	1,88	1,47	No data	1,07	0,50	No data
Sursulf carbon: 5	6,88	2,75	No data	3,37	1,02	No data

Table 24 shows that there is a remarkable increase in weight loss when increasing the particle velocity from 30 m/s to 52 m/s. However, the increased weight loss seems to be higher for untreated duplex, Expanite and Kolsterising than HVOF, Sursulf duplex and Sursulf carbon. Table 25 shows that untreated duplex has relatively good erosion resistance for impact angle of 90° both at low and high velocities. Overall, Expanite and Kolsterising show good results compared to untreated duplex both at low velocity and high velocity. Generally, HVOF, Sursulf duplex and Sursulf carbon show relatively bad erosion resistance at low velocity compared to untreated duplex but relatively good erosion resistance at high velocity, especially for impact angles less than 90°.

Transient behavior

Transient behavior is the behavior of the surface of which an incubation or maturation period is experienced for most of the metals. Generally, it is the initial stage of the erosion process where the surface structure of the materials may change significantly. This effect gives rise to a transient behavior in the erosion characteristics of each material and causes the erosion test to be repeated until stationary conditions are obtained [78].

Note that the test results shown in Table 24 are average weight loss after a relatively stationary erosion rate has been obtained for each test condition. This mean when the weight loss of each test specimen per kg sand impact has become constant. A typical stationary erosion rate will show a linear gradient on a weight loss to mass of sand diagram. However, a transient behavior at the start of each test condition occurs for most of the materials and is typically shown with another gradient on a weight loss to mass of sand diagram. This behavior was especially clear for the high velocity oxygen fuel coated duplex and the Sursulf treated materials as shown in Figure 48. This figure shows basically all tests performed on each test piece marked with a solid square for

untreated duplex, Expanite, Kolsterising, HVOF, Sursulf duplex and Sursulf carbon. For most cases, the transient behavior is a result of changes in the surface Vp structure or surface conditions due to the erosion attacks [70].

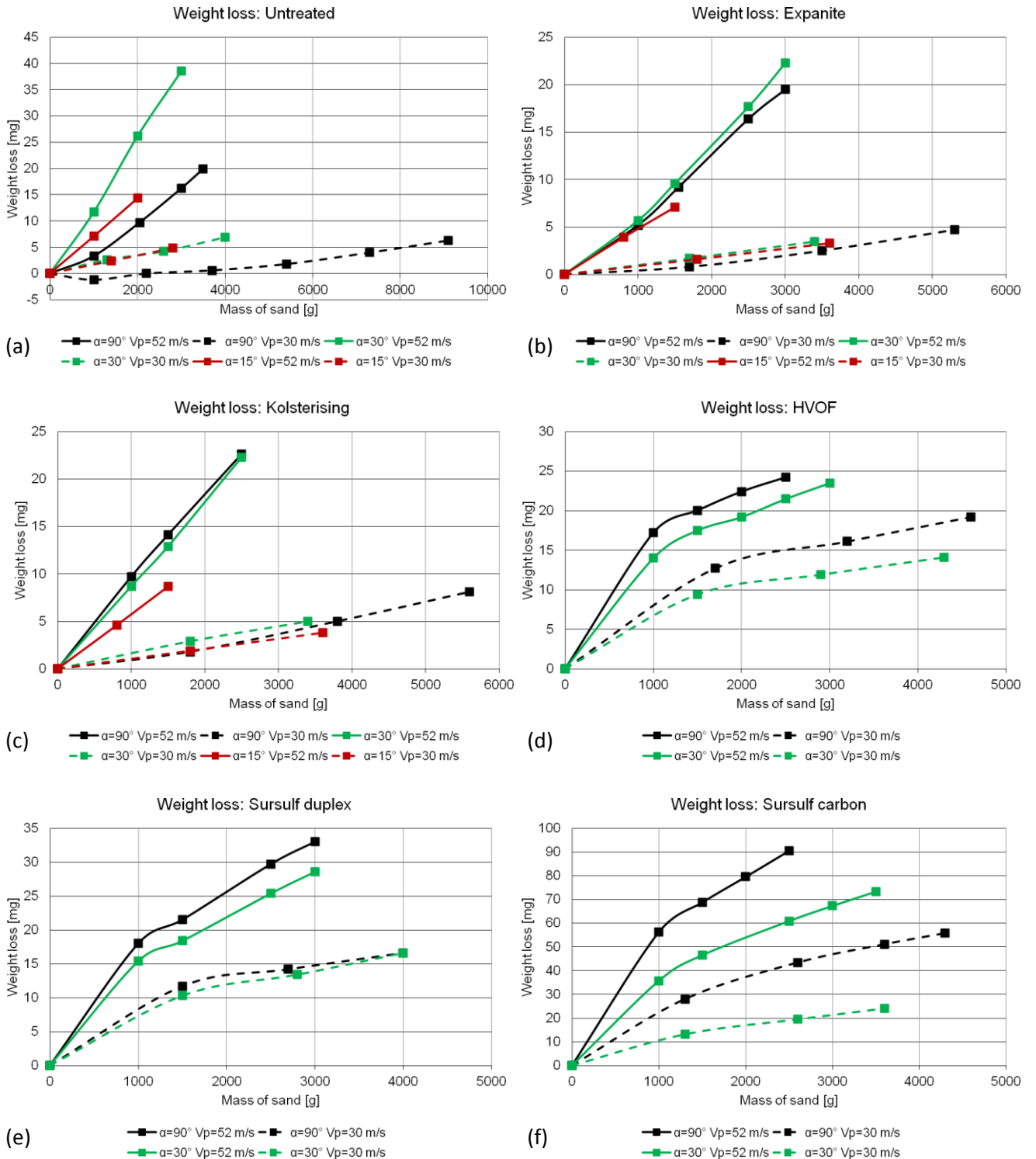


Figure 48. Diagram showing weight loss with respect to mass of impacted sand of all tests performed on all materials where a linear gradient reflects a stationary erosion rate. A transient behavior is typically at the start of the test. Black, green and red line represent impact angle of 90°, 30° and 15° respectively. Solid and dashed line represents particle velocity of 52 m/s and 30 m/s respectively. (a) Untreated (b) Expanite (c) Kolsterising (d) HVOF (e) Sursulf duplex (f) Sursulf carbon.

Scanning electron microscope examination

In order to evaluate material loss mechanisms, microscope examination by use of a scanning electron microscope has been performed. SEM images have been taken of all eroded surfaces, except Sursulf carbon, in addition to the respective non eroded surfaces for comparison as shown in Figure 49 to Figure 54. Optical photographs have been attached for reference only.

In order to limit the amount of images, only the high particle velocity images with 5000X magnification are shown for each impact angle the surface is subjected. Additional images with 1000X magnification are shown in Attachment B: SEM images of erosion surfaces, except for Sursulf carbon. The 1000X magnification images show a larger area of the surface and thus a better overview of the eroded surface. The images are important in order to evaluate erosion mechanisms involved on the surfaces.

The backscatter detector has been used in Figure 53 in order to show atomic number contrast for the purpose of the HVOF tungsten carbide coating. The other SEM images have used the detector using secondary electrons, the so-called Everhart-Thornley detector, in order to examine the eroded surfaces. All eroded images show signs of erosion primarily due to the modification of the non eroded surface shown as reference for all tests in Figure 49 to Figure 54. The erosion mechanisms involved and more detail description of the eroded surfaces is given in Section 5.4.

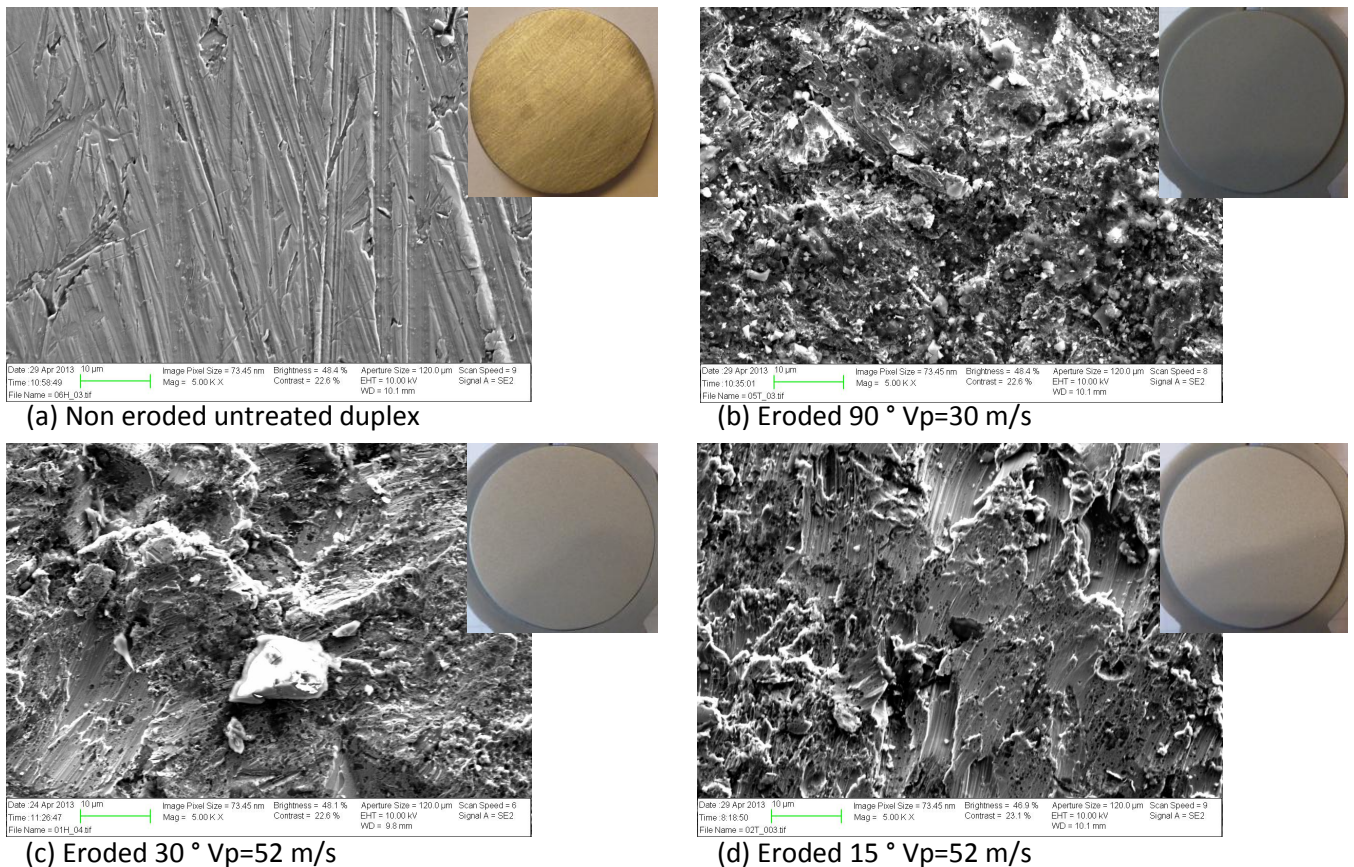
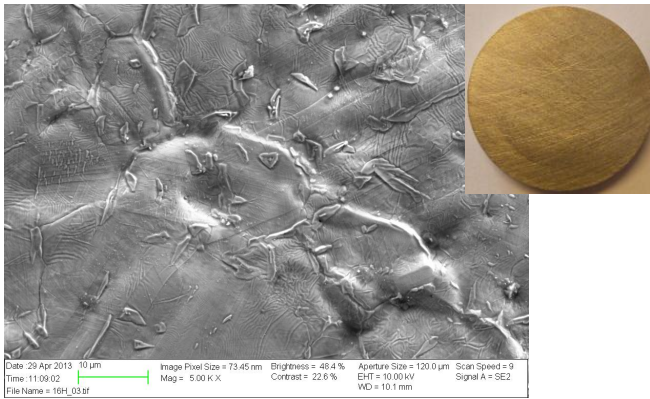
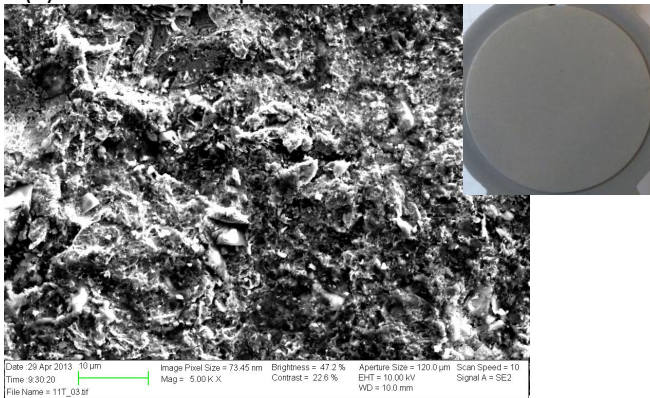


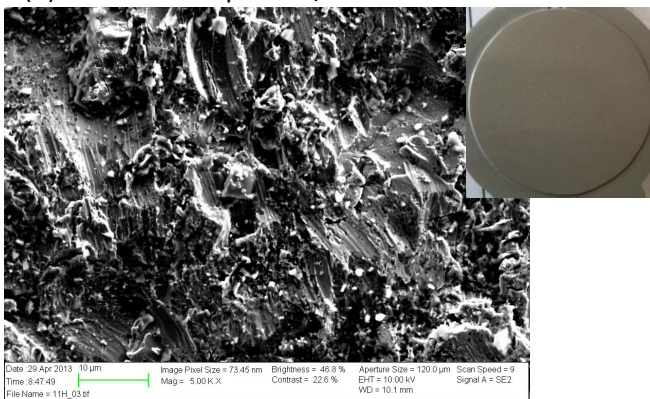
Figure 49. SEM images of untreated duplex (5000X) with a particle velocity of 52 m/s.



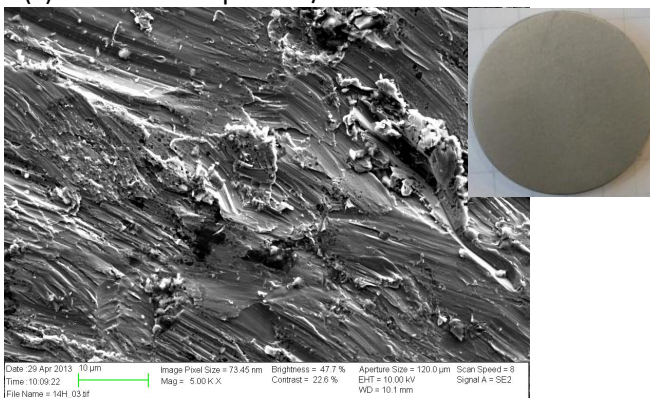
(a) Non eroded Expanite



(b) Eroded 90 ° Vp=52 m/s

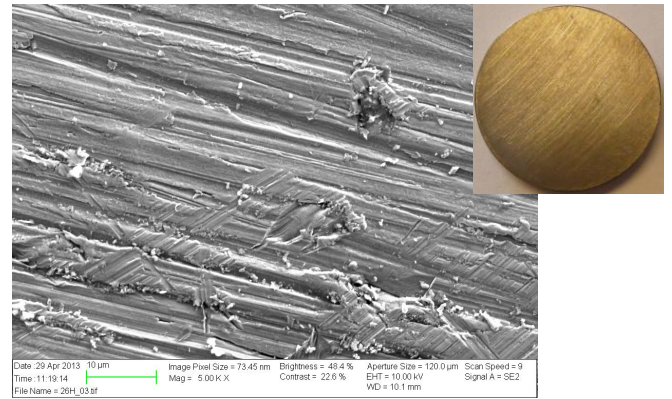


(c) Eroded 30 ° Vp=52 m/s

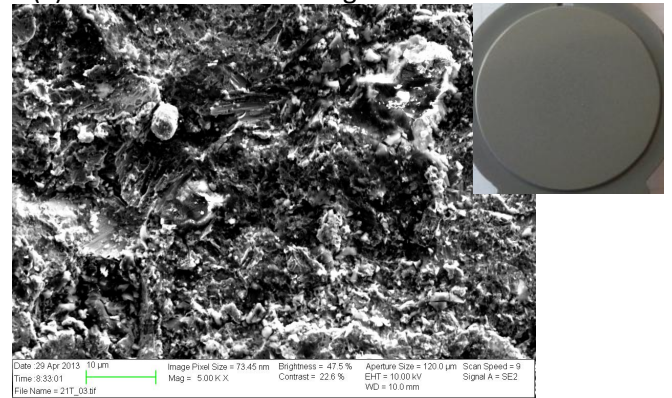


(d) Eroded 15 ° Vp=52 m/s

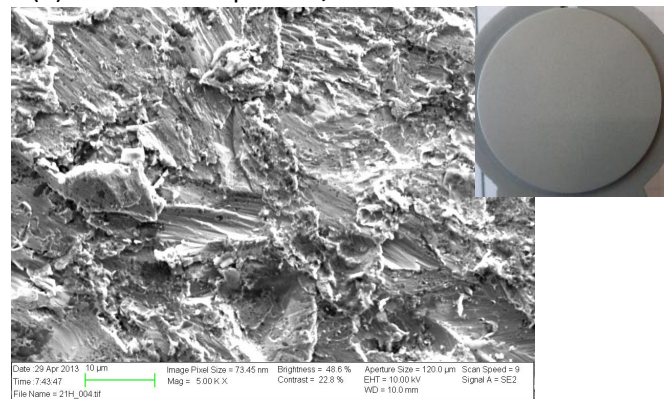
Figure 50. SEM images of Expanite treated duplex (5000X) with particle velocity of 52 m/s.



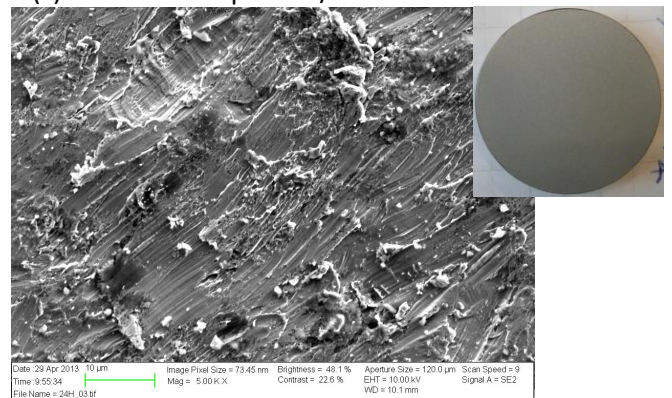
(a) Non eroded Kolsterising



(b) Eroded 90 ° Vp=52 m/s

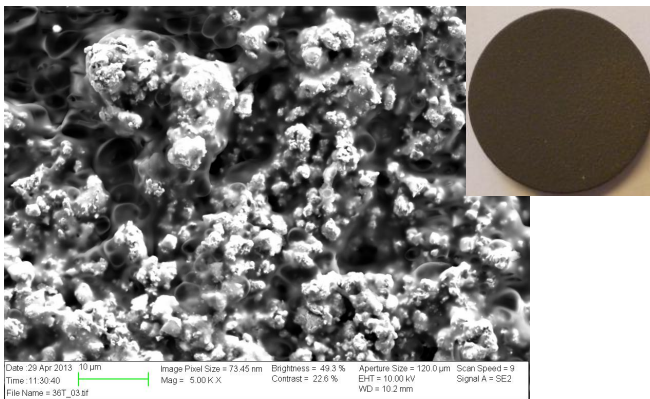


(c) Eroded 30 ° Vp=52 m/s

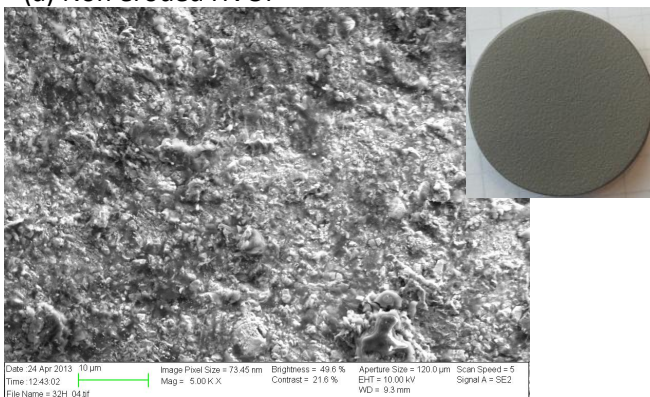


(d) Eroded 15 ° Vp=52 m/s

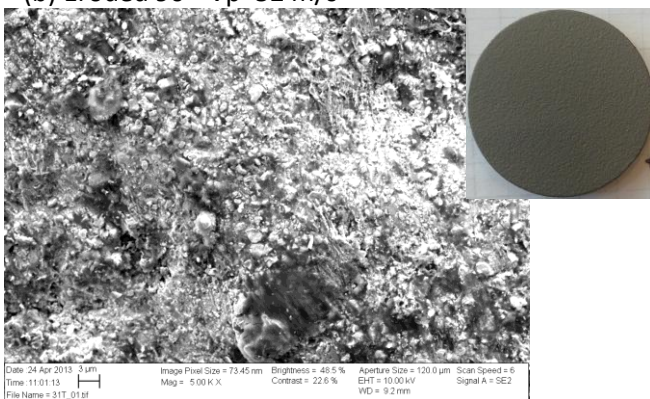
Figure 51. SEM images of Kolsterising duplex (5000X) with a particle velocity of 52 m/s.



(a) Non eroded HVOF

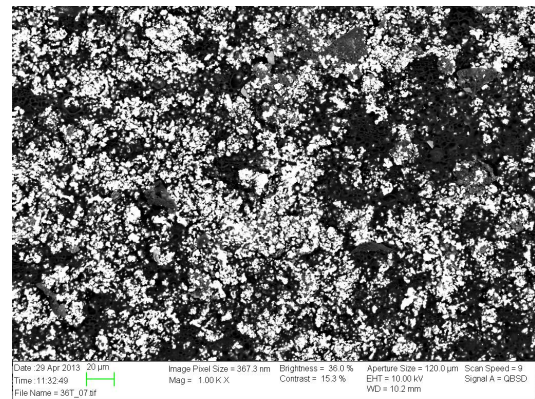


(b) Eroded 90 ° Vp=52 m/s

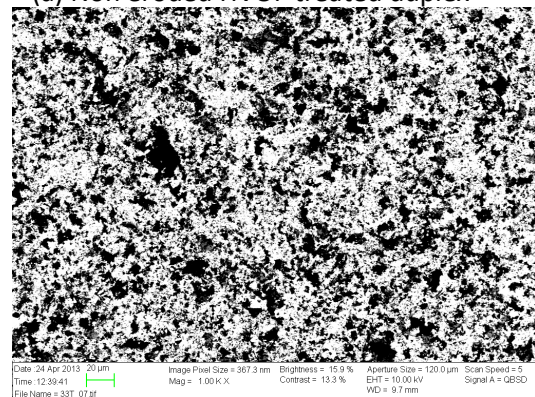


(c) Eroded 30 ° Vp=52 m/s

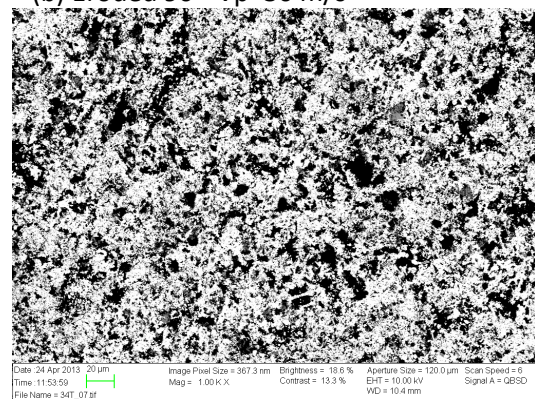
Figure 52. SEM images of HVOF treated duplex (5000X) with a particle velocity of 52 m/s.



(a) Non eroded HVOF treated duplex

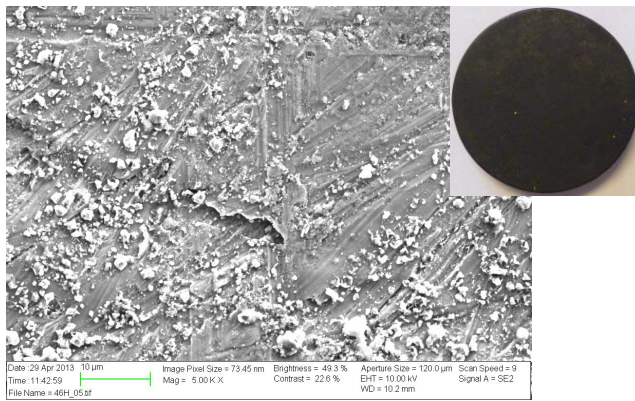


(b) Eroded 90 ° Vp=30 m/s

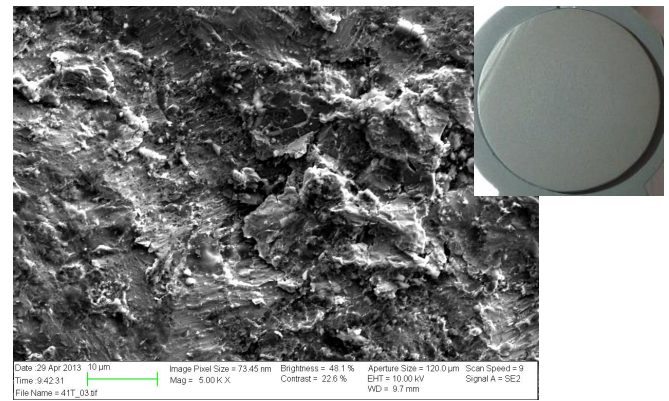


(c) Eroded 30 ° Vp=30 m/s

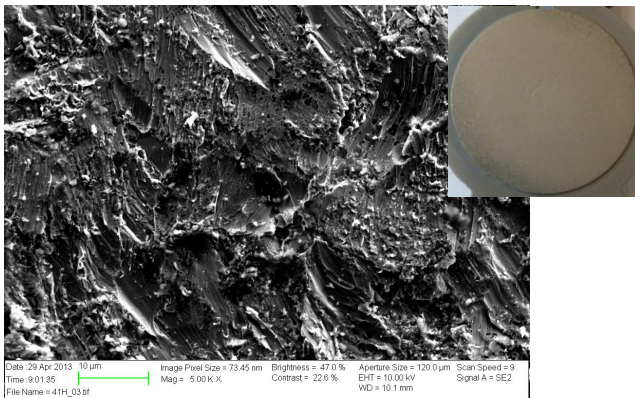
Figure 53. SEM images of HVOF by use of the backscatter electron detector for atomic number contrast. Dark area represent binder and bright area represent tungsten carbides. The eroded surfaces are generally brighter, i.e. contain less binder, than the non eroded surface.



(a) Non eroded Sursulf



(b) Eroded 90 ° Vp=52 m/s



(c) Eroded 30 ° Vp=52 m/s

Figure 54. SEM images of Sursulf treated duplex (5000X) with a particle velocity of 52 m/s.

4.5 Corrosion G48

The corrosion test setup used for performing ASTM G48 method A is shown in Figure 55. The glassware submerged in the temperature controlled water bath is partly shown above the balls covering the entire surface for insulation purpose and to reduce evaporation.



Figure 55. Test setup of the corrosion G48 test showing the temperature controlled water bath with submerged glassware. One glass container for each treated duplex; untreated duplex, Expanite, Kolsterising, HVOF and Sursulf. The water bath and the FeCl_3 solution are covered by balls for insulation and evaporation purposes.

The temperature control unit was set to 25°C and left for 24 hours. However, it turned out that the temperature control unit was not trustworthy. The temperature control unit was not able to maintain a temperature of 25°C, instead the temperature have been increased and maintained something around 70-75°C! This has, obviously, a big impact on the creation of pittings and total weight loss and the test has therefore not been performed according to ASTM G48 standard.

Before the test, a precise measurement of the specimen size and weight according to standard were performed with the following results:

- Untreated: #1 (4,980x2,495x1,495)cm and 144,233 g
#2 (4,980x2,495x1,490)cm and 143,690 g
- Expanite: #1 (4,985x2,500x1,495)cm and 144,233 g
#2 (4,980x2,495x1,495)cm and 143,928 g
- Kolsterising: #1 (4,980x2,495x1,495)cm and 144,242 g
#2 (4,985x2,495x1,490)cm and 144,417 g
- HVOF: #1 (4,985x2,520x1,545)cm and 152,340 g
#2 (5,000x2,525x1,540)cm and 152,380 g
- Sursulf: #1 (4,995x2,495x1,490)cm and 144,411 g
#2 (4,985x2,500x1,495)cm and 144,352 g

The corrosion test was performed at UiS facilities and the test results are presented in Table 26. Note that the number of pits are manual counted on the two (5x2,5) cm faces for each material without magnification to exclude the infinite number of small pits presented on most of the test specimen. I.e. only pits above a certain dimension were counted for. Normally this would have been done with a low magnification with the result of none or just a few pits like the results from the material certificates (not shown in Attachment A: Material certificates).

Table 26. Corrosion test results from ASTM G48 method A. The solution temperature has been approximately 70-75°C!

Material	#	Total area [cm ²]	Pre weight [g]	Duration [hours]	Post weight [g]	Loss [g]	Loss [g/m ²]	Number of pits* [pits]	Pit density [pits/cm ²]
Untreated	1	32,31	144,233	24	142,601	1,633	505	42	3,4
	2	32,29	143,690	24	141,956	1,734	537	65	5,2
Expanite	1	32,40	144,233	24	141,381	2,852	880	6	0,5
	2	32,31	143,928	24	140,762	3,165	980	16	1,3
Kolsterising	1	32,31	144,242	24	141,062	3,180	984	115	9,3
	2	32,34	144,417	24	141,684	2,733	845	104	8,4
HVOF	1	32,91	152,340	24	149,584	2,756	837	1	0,1
	2	33,03	152,380	24	150,621	1,759	533	0	0,0
Sursulf	1	32,36	144,411	24	140,783	3,627	1121	131	10,5
	2	32,40	144,352	24	142,122	2,230	688	122	9,8

* Number of pits is approximate based on manual counting without magnification.

Table 26 does not present the presence of large, “oversized” pits on the subjected surfaces. Photographs of the worst side of the test specimens subjected to pitting corrosion are shown in Figure 56.



(a) Untreated #1



(b) Untreated #2



(c) Expanite #1



(d) Expanite #2



(e) Kolsterising #1



(f) Kolsterising #2



(g) HVOF #1



(h) HVOF #2



(i) Sursulf #1



(j) Sursulf #2

Figure 56. Appearance of the worst side of each of the test specimens after corrosion G48 A test.

Table 26 shows that a remarkable weight loss have occurred on all test specimens in the range of 1,6-3,6 g and 500-1100 g/m². This is well above the acceptance criteria of 4 g/m² applicable for corrosion tests performed at a temperature of 25°C. Due to the high temperature of which the test specimens were subjected, the acceptance criteria cannot be used as intended and the overall value of the test is reduced. However, a relative comparison of the test specimens is possible in terms of weight loss, formation of pits and appearance of the surfaces.

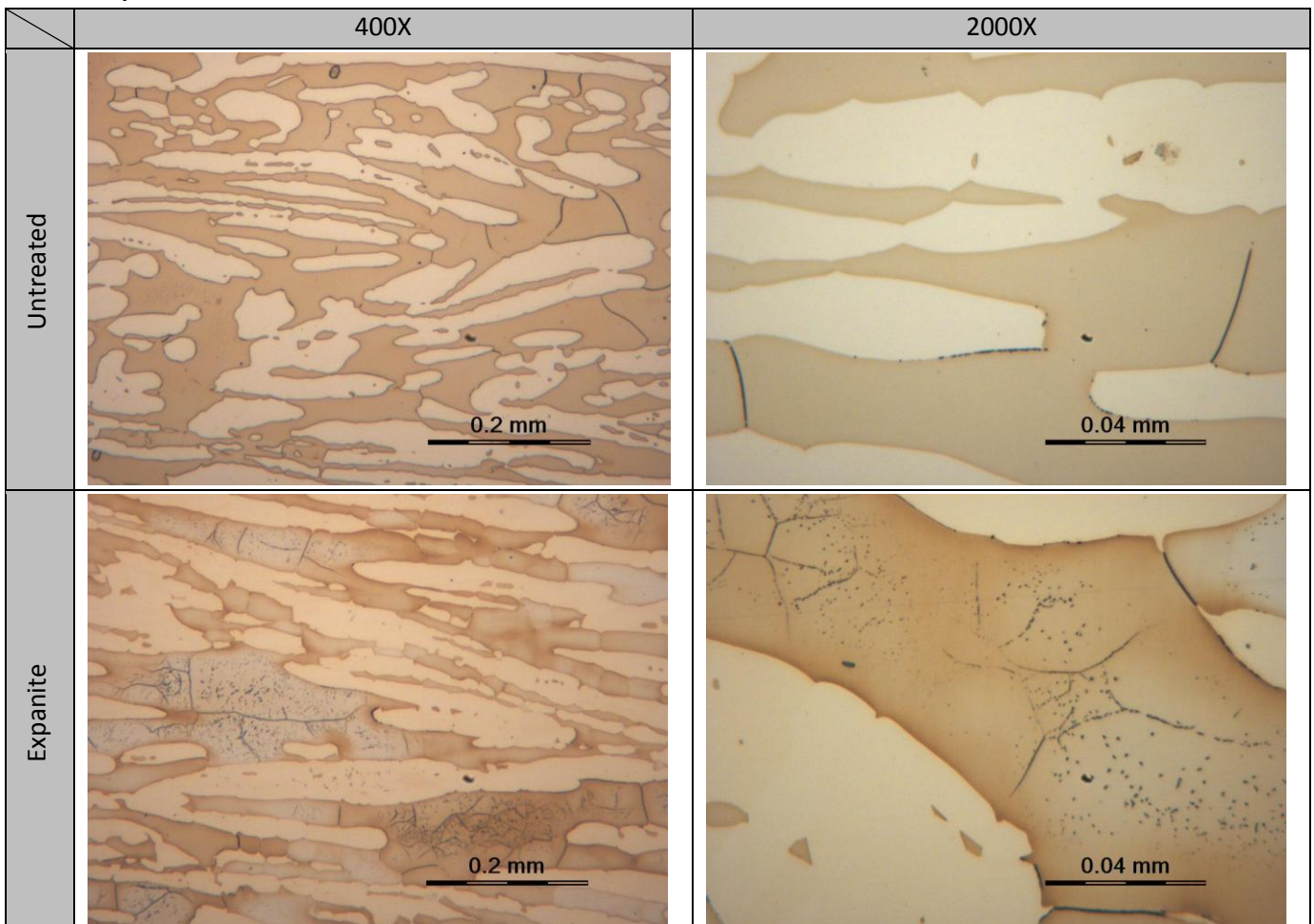
Figure 56 shows that untreated duplex and Kolsterising have suffered from severe pitting corrosion with the creation of a few, large pits. Sursulf have also suffered from the formation of a number of small pits which is also reflected in Table 26. Expanite shows only a few pits while HVOF have no pits. However, Table 26 reveals remarkable weight losses even for Expanite and HVOF. Details and discussions regarding these test results are given in Section 5.5.

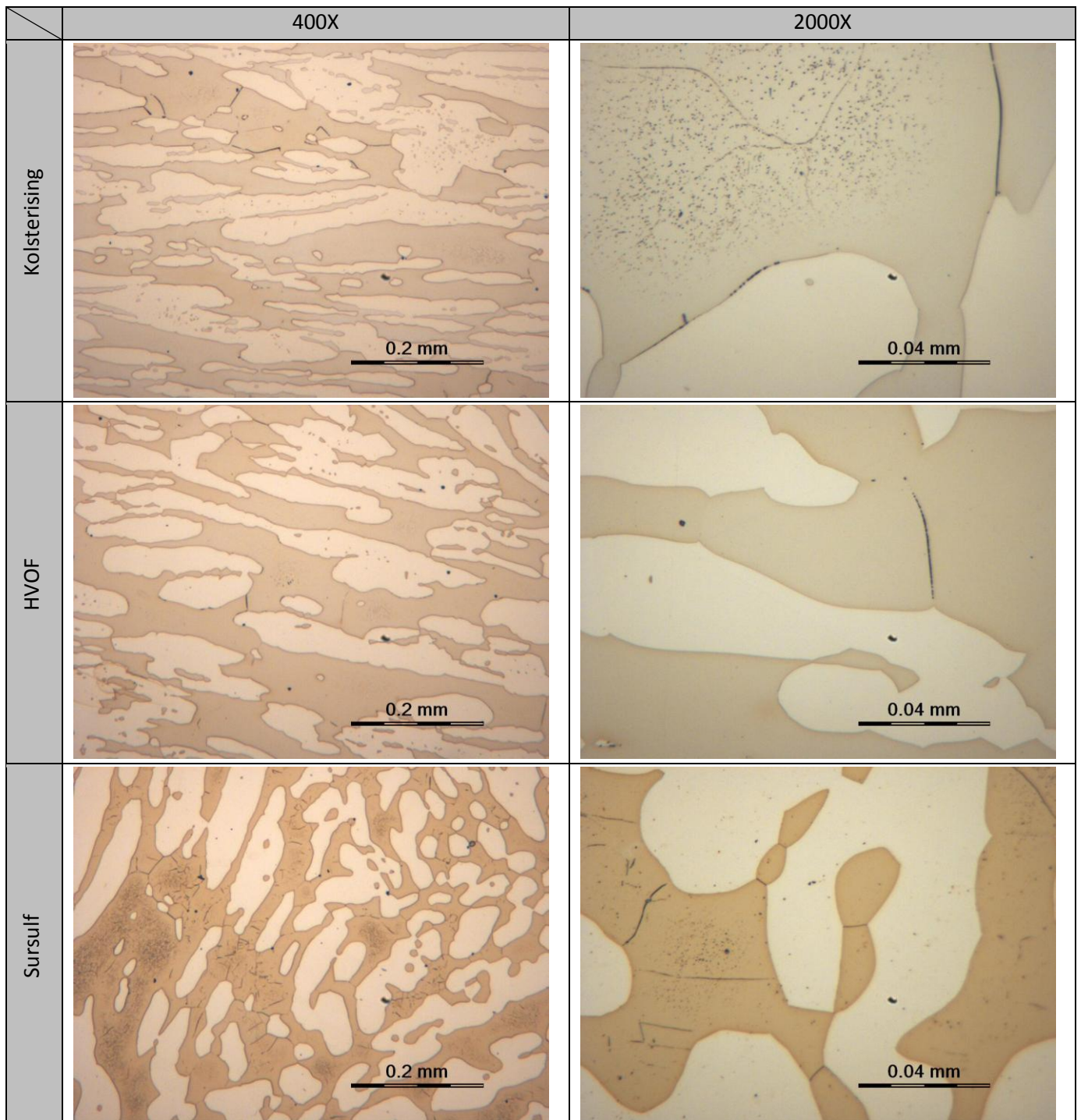
4.6 Metallographic examination

General structure of bulk material

The metallographic examination of the surface treated duplex approximately in the middle of the specimen is shown in Table 27. The images are taken in 400X and 2000X magnification from etched Charpy test specimens subjected to oxalic acid dihydrate and sodium hydroxide.

Table 27. Metallographic images in two different amplifications (400X and 2000X) based on the Charpy test specimens "far" away from the free surface.






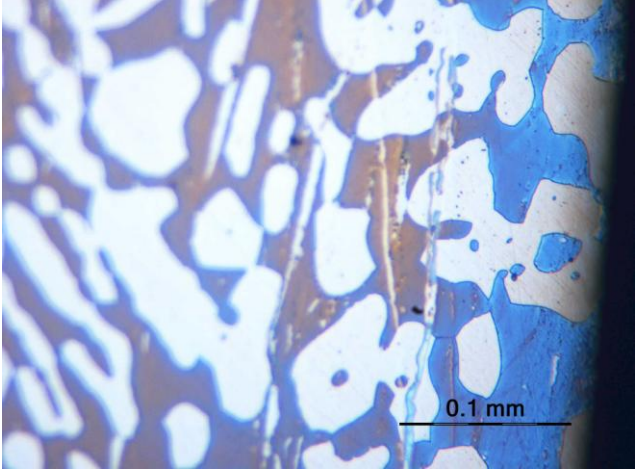

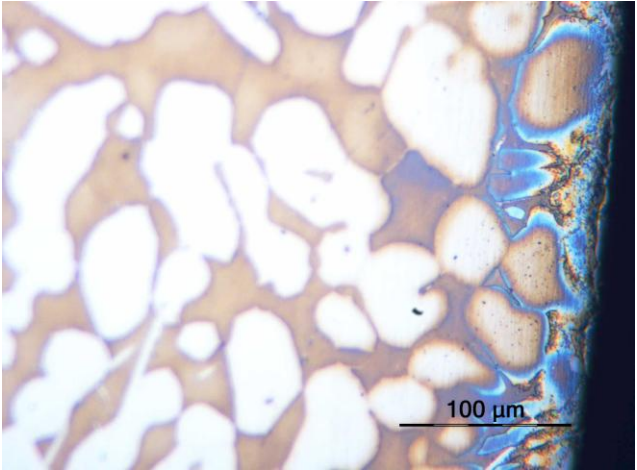
The black lines at grain boundaries and the black spots inside the grains in the metallographic images in Table 27 are most likely precipitates in the form of carbides and/or nitrides. The precipitates are most prominent for Expanite, Kolsterising and Sursulf. Also untreated duplex and HVOF shows some traces of precipitates at grain boundaries, but the difference are small so that the HVOF treatment have probably not introduced any changes in the microstructure. Also note that the areas next to the ferrite/austenite grain boundaries, especially clear for the 2000X image of Kolsterising, are free from precipitates. See Section 5.6 for more details.

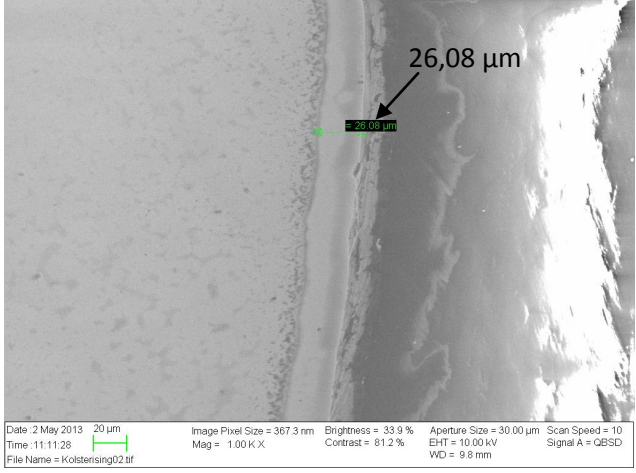
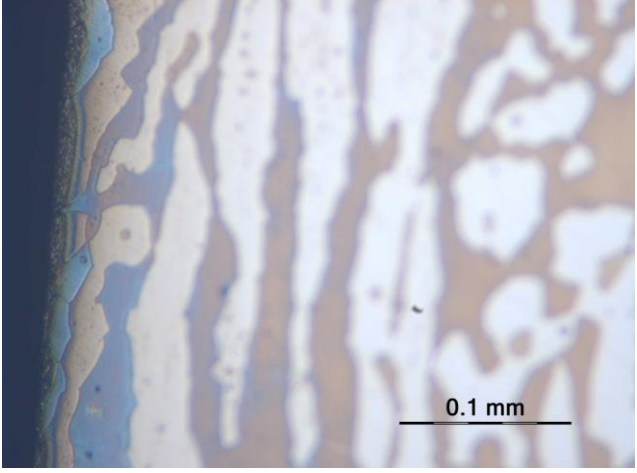
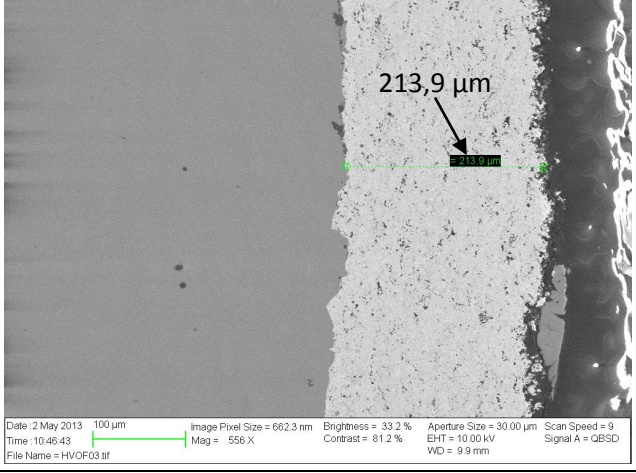
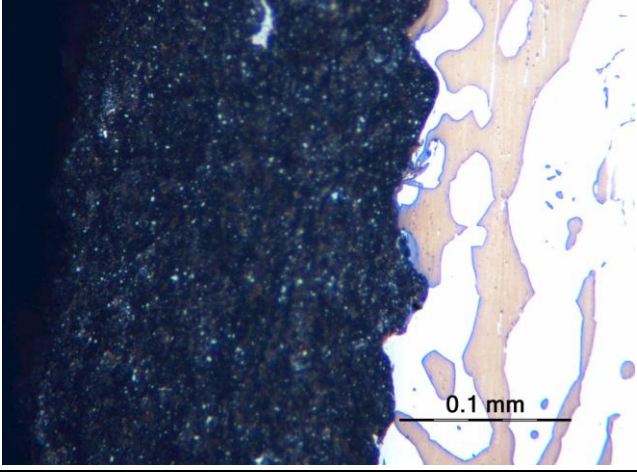
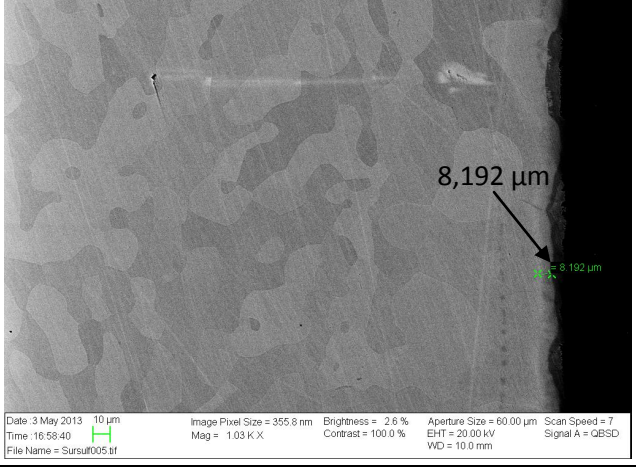
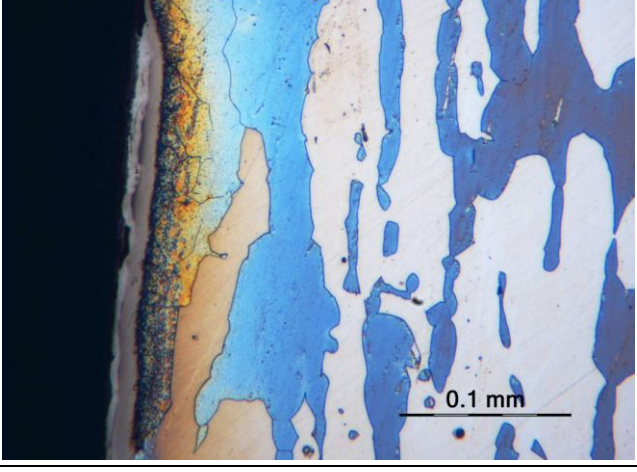
Surface layer(s)

The examination of surface layer(s) on the surface treated duplex is of interest in order to verify that the surface treatment have been accomplished correctly with the result of a surface layer in accordance with expected thickness and appearance. Depending of the origin of the treatment, the surface layer(s) should be visible by use of optical microscopy and/or use of electron microscopy. For some cases, etching is advisable to improve the visibility of the layer(s).

Surface layer images are taken by the use of the backscatter electron detector of a scanning electron microscope and by the use of a metallographic optical microscope on test specimens cut from the erosion specimens. For the SEM images, the cross sections are not etched in order to maintain the surface as plane and realistic as possible. For the metallographic microscope images, the test specimens are etched for 8 seconds in a 3 V electrolyte consisting of 20 % Sodium Hydroxide. The resulting images are shown in Table 28.

Table 28. Surface layer images by scanning electron microscope using backscatter electron detector and optical microscope with 400X magnification for each of the surface treated duplex material. The inspection samples for the SEM images are not etched, while they are etched with 20 % Sodium Hydroxide for the optical images.

	SEM	Optical microscope (400X)
Untreated	 <p> <small>Date: 3 May 2013 10 µm Time: 17:41:49 File Name: Untreated001.tif</small> </p> <p> <small>Image Pixel Size = 278.8 nm Mag = 1.32 K X</small> </p> <p> <small>Brightness = 6.6 % Contrast = 100.0 %</small> </p> <p> <small>Aperture Size = 60.00 µm EHT = 20.00 kV WD = 10.6 mm</small> </p> <p> <small>Scan Speed = 6 Signal A = QBSD</small> </p>	 <p>0.1 mm</p>
Expanite	 <p> <small>Date: 3 May 2013 10 µm Time: 16:38:25 File Name: Expanite02.tif</small> </p> <p> <small>Image Pixel Size = 216.2 nm Mag = 1.70 K X</small> </p> <p> <small>Brightness = 1.9 % Contrast = 100.0 %</small> </p> <p> <small>Aperture Size = 60.00 µm EHT = 20.00 kV WD = 9.6 mm</small> </p> <p> <small>Scan Speed = 6 Signal A = QBSD</small> </p>	 <p>100 µm</p>

	SEM	Optical microscope (400X)
Kolsterising	 <p>26,08 µm</p> <p>Date: 2 May 2013 20 µm Image Pixel Size = 367.3 nm Brightness = 33.9 % Aperture Size = 30.00 µm Scan Speed = 10 Time: 11:11:28 Mag = 1.00 K.X Contrast = 81.2 % EHT = 10.00 kV Signal A = QBSD File Name = Kolsterising02.tif WD = 9.8 mm</p>	 <p>0.1 mm</p>
HVOF	 <p>213,9 µm</p> <p>Date: 2 May 2013 100 µm Image Pixel Size = 662.3 nm Brightness = 33.2 % Aperture Size = 30.00 µm Scan Speed = 9 Time: 10:46:43 Mag = 556 X Contrast = 81.2 % EHT = 10.00 kV Signal A = QBSD File Name = HVOF03.tif WD = 9.9 mm</p>	 <p>0.1 mm</p>
Sursif	 <p>8,192 µm</p> <p>Date: 3 May 2013 10 µm Image Pixel Size = 355.8 nm Brightness = 2.6 % Aperture Size = 60.00 µm Scan Speed = 7 Time: 16:58:40 Mag = 1.03 K.X Contrast = 100.0 % EHT = 20.00 kV Signal A = QBSD File Name = Sursu005.tif WD = 10.0 mm</p>	 <p>0.1 mm</p>

The austenite and ferrite grains are visible on some of the SEM images in Table 28 by the property of atomic number contrast of the backscatter electron detector. This was only obtainable when the acceleration voltage was set to 20 kV and preferably with high current mode. Since the specimens were embedded in epoxy, grounding of the specimen could only be accomplished by carbon tape. This feature limited the amount of electrons being sent against the surface of specimen without the creation of a flashy, non usable and unreadable image. This relation was especially prominent in combination with low scan speed and high magnification. Kolsterising and HVOF, which clearly show a surface layer as a consequence of the surface

treatment, do therefore not show the grains since these images are only subjected to 10 kV acceleration voltage.

The images in Table 28 show that all surface treated duplex have been subjected to some kind of modification relative the untreated duplex which has no sign of a modified surface layer. Both the SEM image and the optical microscope image of HVOF show very clearly the tungsten carbide coating on top of the duplex material with a thickness of approximately 0,2 mm. SEM image of Kolsterising shows a very defined surface layer which must be the result from the Kolsterising treatment. The SEM image of Expanite, however, does not show a clear surface layer, but the optical image shows that a modification has occurred. The surface layer is also seen best by the optical image for Sursulf, while it is less prominent for the Kolsterising process.

The layer thickness is, based on the images in Table 28, estimated to be approximately as follows:

- Expanite: Color change in optical image penetrates as far as approximately 50 μm from surface.
- Kolsterising: SEM image reveals a surface layer of approximately 26 μm from surface.
- HVOF: SEM and optical image reveal a coating thickness of approximately 210 μm .
- Sursulf: Color change in optical image penetrates as far as approximately 60 μm from surface.

Ferrite content in accordance with ASTM E562

Phase balance is of interest in order to verify whether the ferrite content has, due to the surface heat treatment of the specimen, increased, decreased or is approximately equal compared to untreated duplex or compared to material certificates. Ferrite content versus austenite content is important in terms of impact toughness and precipitation of minor phases in the matrix. More description regarding ferrite content will be given in Section 5 Discussion where applicable.

A manual point count for determining volume fraction of the two phases in duplex steel is performed according to ASTM E562. This test method describes a systematic manual point counting procedure for statistically estimating the volume fraction of an identifiable constituent or phase from section through the microstructure by means of a point grid [79]. The result from this point count is presented in Table 29. A total number of 30 fields were counted with a 16 points test grid.

Table 29. Phase constituent of ferrite in the base material of duplex stainless steel from the Charpy test specimens. Information regarding microstructural orientation, standard deviation, 95 % confidence interval and % relative accuracy is also given according to ASTM E562.

Material:	Untreated		Expanite		Kolsterising		HVOF		Sursulf	
Test number:	#2	#3	#1	#3	#1	#2	#1	#3	#2	#3
Orientation:	L	L	L	L	L	T	L	L	T	T
Phase constituent (α):	49,5	50,9	53,5	53,9	47,8	51,3	45,4	47,6	44,3	47,7
Standard deviation:	10,9	12,1	14,4	10,1	13,8	12,1	11,4	11,5	9,5	10,2
95 % confidence interval:	4,1	4,5	5,4	3,8	5,1	4,5	4,3	4,3	3,6	3,8
% relative accuracy:	8,2	8,8	10,0	7,0	10,8	8,8	9,4	9,0	8,1	8,0

Table 29 shows that only Expanite has resulted in a slight increase in ferrite content with respect to untreated duplex. Kolsterising, HVOF and Sursulf have a tendency of ferrite reduction compared to untreated duplex.

5 Discussion

5.1 Tensile test

Table 18 shows the test results from the tensile testing for each surface treatment method and Table 30 shows the average test results based on the two test specimens for each of the treated duplex material. Note that Expanite and Kolsterising treatments have resulted in a slight increase in yield ($R_{0,2}$) and tensile (R_m) strength whereas reduction (q) is reduced.

For the HVOF coated duplex, the coating itself is most likely responsible for the differences of yield strength, tensile strength, elongation and reduction values shown in Table 30 due to the increase in cross sectional area S_0 . See Figure 35 for overview in the use of applicable notations. The original diameter, d_0 , on the tensile specimen gauge length is 10,05 mm. The tungsten carbide coating results in an increase in gauge length diameter to 10,35 mm. This gives an increased cross sectional area, S_0 , from 79,33 mm² to 84,13 mm².

Tungsten carbide coatings are very brittle and do not have the same capacity for strain before fracture. Steel and tungsten carbide have a typical elasticity of modulus of approximately 200 GPa and 400 GPa respectively [9]. This means that tungsten carbide is very stiff relative to steel and will soon fracture when the tensile test specimen is elongated. Due to the fact that the tungsten carbide coating is very thin relative the duplex base material, the coating will contribute very little to the yield strength and tensile strength. This will result in an artificial low value of yield strength and tensile strength of the duplex base material because these parameters are based on the cross sectional area (S_0) of 84,13 mm² and not 79,33 mm². Therefore, in order to compare the surface treatments directly, this effect must be taken into consideration. True stress of the HVOF tensile test specimen, which takes the constantly cross section area reduction into account, is probably similar to the true stress obtained for the untreated duplex.

The tungsten carbide coating layer, which actually did fracture over the whole gauge length, L_0 , during the tensile test as shown in Figure 45 (a), has also impact on the reduction in area, q , to a higher value as shown in Equation 13. This equation is based on a diameter reduction from $d_0=10,0$ mm to a fracture diameter $d_f=4,8$ mm using two different cross sectional areas, S_0 , with and without tungsten carbide coating.

Percent elongation, e_f , of HVOF may neither be related directly to the other tests since this is based on a longer gauge length (L_0) and fracture length (L_f) due to the difficulties in marking original gauge length on the tungsten carbide coating that disappears during tension test. The accuracy is thus lower and longer gauge length force the percent elongation to lower values since the denominator in Equation 9 is higher. This is shown in the example below where the elongation is assumed the same, i.e. $L_f-L_0=19$ mm, but the gauge length is increased from 50 mm to 70 mm as shown in Equation 14.

$$q = \frac{S_0 - S_f}{S_0} \quad \begin{array}{l} S_0 = 79 \Rightarrow q = 1 - \frac{18}{79} = 0,77 = 77\% \\ S_0 = 84 \Rightarrow q = 1 - \frac{18}{84} = 0,79 = 79\% \end{array} \quad \text{Equation 13}$$

$$e_f = \frac{L_f - L_0}{L_0} \quad \begin{array}{l} L_0 = 50 \Rightarrow e_f = \frac{19}{50} = 0,38 = 38\% \\ L_0 = 70 \Rightarrow e_f = \frac{19}{70} = 0,27 = 27\% \end{array} \quad \text{Equation 14}$$

Table 30. Average engineering tensile test results based on two successive tests for each surface treated duplex.

Material	Yield strength $R_{0,2}$ [MPa]	Tensile strength R_m [MPa]	Elongation e_f [%]	Reduction q [%]
Untreated	552	740	37	78
Expanite	586	784	33	72
Kolsterising	574	763	37	74
HVOF	519 ¹	685 ¹	28 ²	79 ¹
Sursulf	548	734	39	75

¹ HVOF test specimen have an increased cross sectional area due to the tungsten carbide coating which have influence on yield strength, tensile strength and reduction.

² Gauge lengths are longer than original with the result of an artificial lower elongation value.

Test results relative to material certificate and ASTM A479

The test results shown in the table above have been compared to the test results obtained on the material certificates and with respect to minimum mechanical properties of ASTM A479. This comparison is shown in Figure 57. The minimum mechanical properties of ASTM A479 and the mechanical properties from the material certificates are shown for reference in Table 11 and Table 12 respectively. Compared to ASTM A479, all test results are well above minimum requirements. Compared to material certificates, there is a tendency that yield strength and tensile strength have increased slightly whereas elongation has a tendency of reduction.

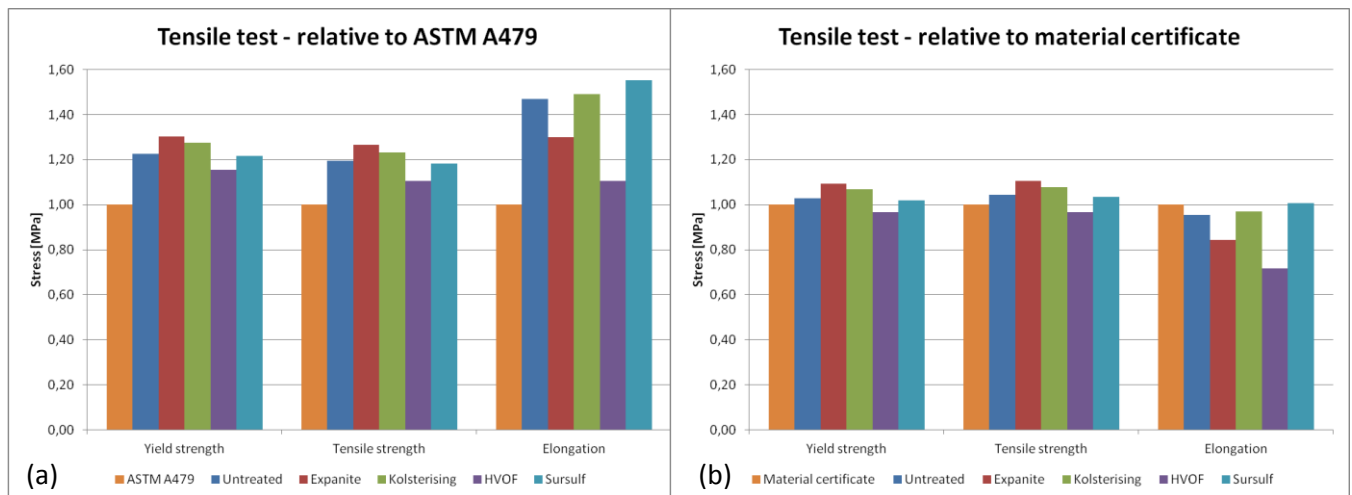


Figure 57. Tensile test results of the surface treated duplex relative to (a) ASTM A479 and (b) material certificates.

Ductility

Ductility is a measure of the degree of plastic deformation that has been sustained at fracture. It may be expressed quantitatively as either percent elongation (e_f) or percent reduction in area (q) as shown in Equation 9 and Equation 10 [9]. High percentage of elongation and reduction of area are typical indicators of ductile materials. For instance, duplex stainless steel with percent elongation of approximately 35 % is ductile with respect to cast iron UNS F33800 with a percentage elongation of 6 % [80]. The elongation values given in Table 30 may in such terms define the surface treated duplex as ductile.

Other common fracture mechanisms in metals and alloys, other than ductile fracture, are cleavage and intergranular fracture shown schematically in Figure 58. Ductile materials usually fail as a result of nucleation,

growth and coalescence of microscopic voids that initiate at inclusions and second-phase particles. Cleavage fracture involves separation along specific crystallographic planes and the fracture path is transgranular. Intergranular fracture occurs when the grain boundaries are the preferred fracture path in materials [6].

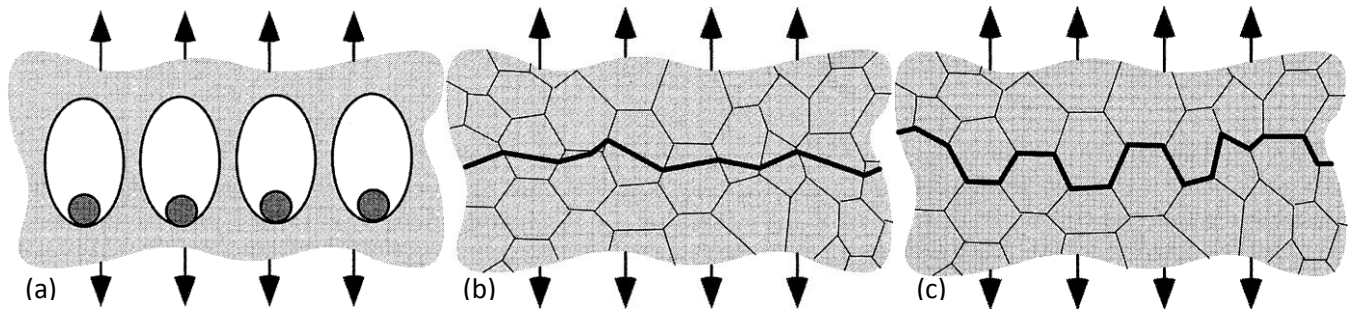


Figure 58. Three micromechanisms of fracture in metals [6]: (a) ductile fracture, (b) cleavage and (c) intergranular fracture.

Based on the pictures from Figure 45, all test specimens showed a “cup and cone” fracture surface. The neck produced a triaxial stress state in the center of the specimen. This state promotes void nucleation and growth in the larger particles. Upon further strain, the voids coalesce, resulting in a penny-shaped flaw. The outer ring of the specimen contains relatively few voids, because the hydrostatic stress is lower than in the center. The penny-shaped flaw produces deformation bands at 45° from the tensile axis [6].

5.2 Charpy test

An overview of the average Charpy test results compared to the Charpy test results from the related material certificates and minimum Charpy requirements in accordance with Norsok M-630 are given in Table 31. The Charpy test results are presented in Table 19 for reference. It is obvious that the impact toughness at -46°C have changed quite noticeable to both higher and lower energy levels. Most critical is the results from the Expanite and Kolsterising process which reduces the impact toughness below the requirements given by Norsok M-630. These surface treatments show a reduction in impact toughness compared to the material certificate with a factor of 0,1 and 0,2 respectively. The remaining surface treatments, including the untreated duplex, show an increase in impact toughness with a factor of approximately 1,7 without concerning the transverse or longitudinal difference.

Table 31. Comparison of the Charpy impact average test results performed at -46°C from Table 19 to related impact values from material certificate and Norsok M-630 minimum requirements.

Test piece	Average	Factor ²	Material certificate average		Norsok M-630
Untreated:	209,8 J (T)	1,7	#3	121 J (L)	Minimum 45 J average and 35 J single
Expanite:	13,7 J (T)	0,1	#3	121 J (L)	
Kolsterising:	21,6 J ¹ (T)	0,2	#3	121 J (L)	
HVOF:	205,5 J (T)	1,7	#3	121 J (L)	
Sursulf duplex:	122,7 J (L)	1,7	#2	74 J (L) 49 J (T)	

¹ Average impact value for Kolsterising is based on the two transverse tests only.

² Factor is based on the average Charpy impact values with respect to respective material certificate average.

Disregarding the comparison against material certificate and Norsok M-630, the fact that the same material have been used for making all test specimens, except Sursulf treatment, and that all test specimens have gone through the same testing condition, the internal difference are great. These differences indicate the influence

each surface treatment, i.e. temperature, has on the material and thus the impact toughness. The following comments to be highlighted:

- Expanite and Kolsterising have a strong, negative influence on impact toughness and not acceptable in accordance with acceptance criteria defined by Norsok M-630.
- HVOF have little or no effect on impact toughness.
- Sursulf duplex have a notably, negative influence on impact toughness but is still within acceptance criteria.

Determination of percent shear fracture

Another way of presenting the results from the impact testing is by use of the fracture appearance method. This is done by carefully measuring the dimensions of the brittle cleavage exhibited on the specimens fracture surface as shown schematically in Figure 59. The brittle cleavage dimensions are then compared and used as input to standardized tables in ASTM A370. These tables give information about percentage of shear whereas minimum acceptable criteria is 50 % [5].

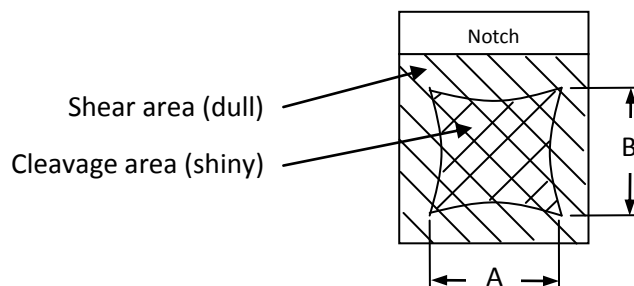


Figure 59. Sketch of a fractured impact test specimen. The method used in calculating percent shear involves measuring average dimensions A and B to the nearest 0,5 mm [5].

The resulting overview of the estimated percent shear from each test specimen is presented in Table 32. From this table it is clear that the Expanite and the Kolsterising process have been subjected to brittle fracture by cleavage. The resulting materials have a little over 50 % shear fracture and are thus accepted. This is in accordance with the absorbed energy values presented in Table 19.

Table 32. Overview of percent shear from each of the test specimen based on A and B measurements [mm] and standardized tables for resulting shear from ASTM A370.

Test piece	Test #1			Test #2			Test #3		
	A	B	Shear	A	B	Shear	A	B	Shear
Untreated	6,0	5,5	59 %	7,0	5,5	52 %	6,5	5,5	55 %
Expanite	10	8,0	0 %	10	8,0	0 %	10	8,0	0 %
Kolsterising	8,5	7,5	20 %	8,5	7,5	20 %	8,5	7,5	20 %
HVOF	6,5	5,5	55 %	6,5	5,5	55 %	6,5	6,0	51 %
Sursulf	6,0	6,0	55 %	6,0	6,0	55 %	6,5	6,0	51 %

Microstructure influence on impact toughness

The negative change in impact toughness is an indication that some microstructural changes have occurred. The changes may have happened due to different mechanisms, such as: precipitation of secondary phases like nitrides, formation of 475°C embrittlement, change in grain size and/or change in the phase balance between ferrite and austenite. As indicated in Table 4, ferrite, with BCC crystal structure, have a low temperature

toughness compared to austenite with FCC crystal structure. The characteristic ductile-to-brittle transition for BCC steels is dependent on temperature and it is sensitive to both alloy composition and microstructure. For instance, decreasing the average grain size would result in a lowering of the transition temperature while increasing carbon content would raise the transition temperature. In terms of phase balance between ferrite and austenite, an increase or decrease of ferrite content due to heat treatment would change the transition temperature due to its higher temperature dependence. For instance, a fast cooling rate from relatively high temperature favors retention of ferrite since austenite is forming from the ferrite as shown in Figure 8. Regardless of reason, an increase in ferrite content would have negative consequences on impact toughness at low temperature due to its brittle behavior.

A phase balance determination is performed and shown in Table 29. Based on this table, there is one material showing an increase in ferrite content. Expanite has for some reason an increased phase constituent of ferrite of approximately 53,5 % compared to the untreated of approximately 50 %. From Attachment A: Material certificates #2 and #3, the phase balance is reported to be between 47 % and 49 %. This emphasizes the tendency of an increased amount of ferrite in the material, something which may partly explain the brittle fracture of Expanite. Factors that may affect the ferrite/austenite phase balance in the microstructure can be predicted by the Schaeffler diagram shown in Figure 7. This diagram is based on the chromium equivalent equation (Cr_{eq}) and the nickel equivalent equation (Ni_{eq}) described in Section 2.2. In addition, heat treatment, i.e. temperature, has also an impact on the phase balance as shown in Equation 15.

$$\% Ferrite = -20,93 + 4,01Cr_{eq} - 5,6Ni_{eq} + 0,016T \quad [23] \quad \text{Equation 15}$$

T is the annealing temperature ranging from 1050-1150°C. Also, since the cooling rate determines the amount of ferrite that can transform to austenite, see Figure 8 for reference, cooling rates following high temperature exposures influence the phase balance. Fast cooling rates favor retention of ferrite and thus make it possible to have more than the equilibrium amount of ferrite [23].

Based on the metallographic images in Table 27, there are also some quite visible precipitates of what seems to be nitrides, but it could also be carbides, inside the ferrite grains and at ferrite/ferrite and ferrite/austenite grain boundaries. The most vulnerable precipitates are those at ferrite/austenite boundaries which are present in both Expanite and Kolsterising images. This is because at a temperature of -46°C, the most important phase for impact toughness is austenite. Precipitates influencing the austenite grains will therefore have the greatest impact on low temperature toughness. Based on other work, chromium nitride and carbide precipitation on duplex stainless steel certainly causes loss of toughness [29]. Other precipitates which also will affect the impact toughness are sigma phase and α' (475°C embrittlement) as reported in the following references for instance: [31], [32], [35], [81]. More detail regarding this is given in Section 5.6 Metallographic examination.

5.3 Hardness test

Surface hardness

Hardness test of the surface should ideally be accomplished without penetrating the surface layer but still with a sufficient load in order to get a hardness value with satisfactory accuracy. The hardness testing using Rockwell B and C method uses a test load too high so that the indenter penetrates in the range of 0,05-0,07 mm and 0,15-0,17 mm respectively. This is too deep with respect to the approximately 0,02-0,05 mm surface layer of Expanite, Kolsterising and Sursulf. With respect to HVOF, which has a coating thickness of approximately 0,2 mm, Rockwell B and C are even here not ideally due to the tungsten carbide content of the surface to be

measured. The surface of tungsten carbide may fracture during impingement and the diamond life will be reduced considerably. The Rockwell A scale is probably the best method for this surface layer since this method is intended for cemented carbides and shallow case-hardened steel as recommended in Table 16 [5].

Anyway, the hardness value presented in Table 21 does represent the hardness tendency of the surface with respect to untreated duplex. When the indenter penetrates through the surface layer, the hardness value will be a function of both the surface layer and the core material. In terms of converting the Rockwell hardness values to Vickers hardness value for comparison, a best fit equation has been developed in order to perform a conversion from HRC to HV as shown in Equation 16.

$$HV = \frac{HRC + 2,4}{0,091} \quad [3] \quad \text{Equation 16}$$

Based on the average HRC values in Table 21 and conversion Equation 16, the following Vickers hardness values are obtained:

- Untreated duplex: 18,3 HRC = 228 HV
- Expanite: 23,5 HRC = 284 HV
- Kolsterising: 24,4 HRC = 294 HV
- HVOF: 26,6 HRC = 319 HV
- Sursulf: 16,9 HRC = 212 HV

The results from Table 21 and the conversion from HRC to HV above tell us that all treatments, except Sursulf, show an increased hardness with respect to untreated duplex when applying a relatively high load.

In terms of applying a light load, the actual surface hardness can be measured more accurate without the influence of the core material. The test results presented in Table 22 are measured by using a 25 g load on a Vickers micro hardness tester. The hardness values are associated with a degree of uncertainty due to the relative rough surface of the test specimen. Basically, the finish of the specimen must be smooth enough to permit the ends of the diagonals to be clearly defined so that the length can be measured with high precision [5]. This diagonal measurement could not be done with sufficient accuracy, so the presented hardness values are not absolute. Nevertheless, a clear indication of hardness increase is easily observed with hardness values in the range of 800-1200 HV_{0,025} as shown in Figure 60. Hardness increase in the range of 3,3X to 3,8X is found relative untreated duplex for the Expanite, Kolsterising and Sursulf surface treatment. Reference hardness value of untreated duplex is approximately 258 HV_{0,025}, something which is relatively close to the original hardness value in the range of 217-230 HB³ shown in Attachment A: Material certificates.

Note that the surface hardness of HVOF, which consist tungsten carbide, could not be performed with only 25 g test load due to a surface finish too rough making the measurement of diagonals impossible. Anyway, tungsten carbide is relatively stable with a typical hardness in the range of 1100-1400 HV, see reference [82] and [83]. Measured hardness with 500 g test load was performed with the result of a hardness of approximately 1050 HV_{0,5}.

³ According to ASTM E140 Standard hardness conversion tables, 217-230 HB = 217-230 HV. However, there is no standardized conversion between these two scales for duplex stainless steel, so the conversion for carbon steel is invoked.

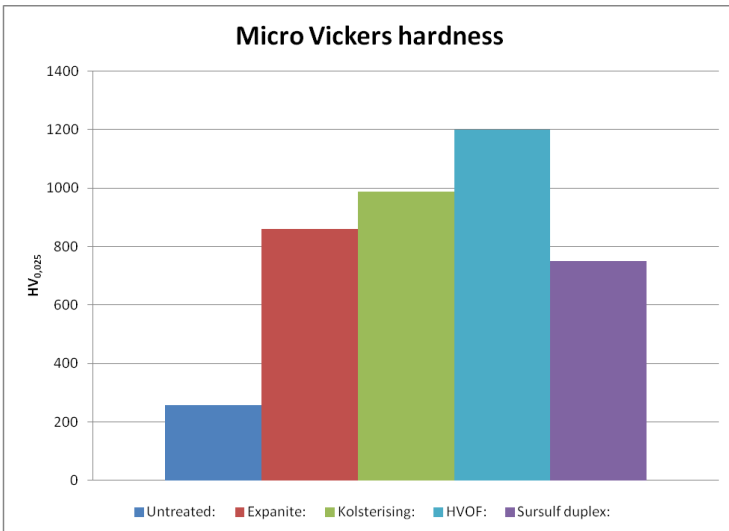
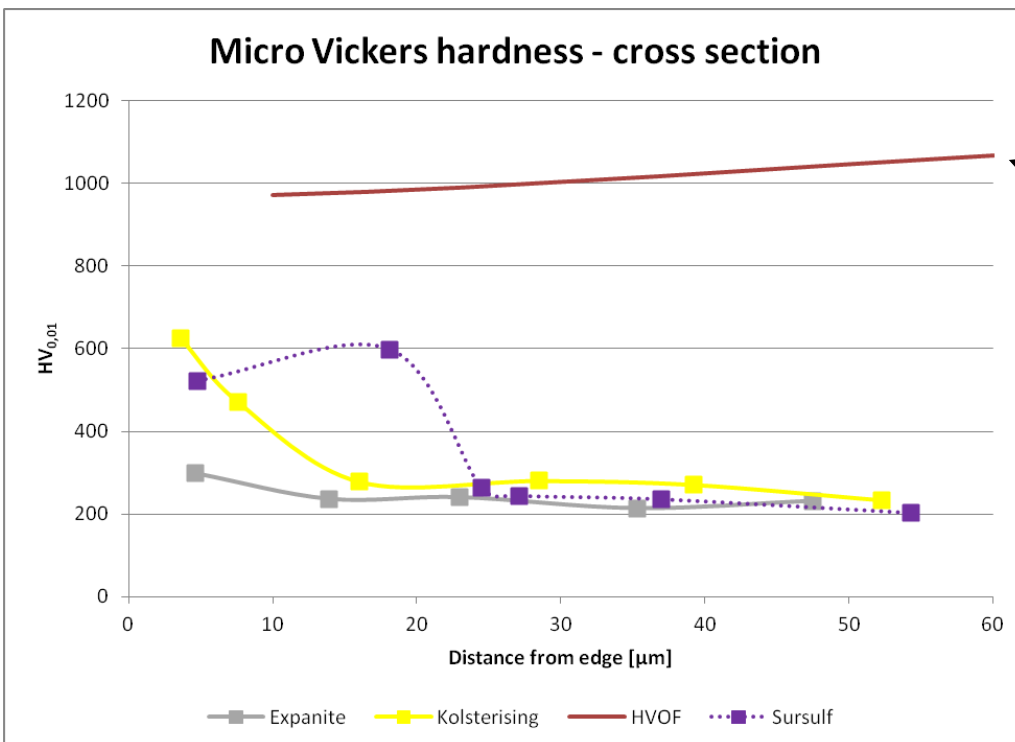


Figure 60. Surface layer micro Vickers hardness values using 25 g test load. Hardness values are obtained from Table 22. Hardness value of tungsten carbide by HVOF is not measured but estimated to be 1200 HV based on [82] and [83].

Cross section hardness

There are uncertainties related to the hardness close to the free surface due to lack of sharp edge and difficulties determining which grains are ferrite and which are austenite. There is a tendency of the edge to be slightly rounded which produces inaccuracy to the reading. In addition, the 10 g load resulted in hardness values which seemed to be the half of the realistic value as described in Section 4.3. All these factors made it difficult to obtain absolute hardness values on the cross sections. Despite of this, a hardness profile is made based on Table 23 and shown in Figure 61. HVOF hardness profile is approximately constant across the coating thickness and due to its high thickness compared to Expanite, Kolsterising and Sursulf is not shown entirely in the figure.



Approximately constant hardness across coating layer (200 μm).

Figure 61. Micro Vickers hardness values as a function of distance from edge. HVOF hardness values of approximately 1000 HV continues throughout the coating thickness of 200 μm.

Due to the uncertainties related to the hardness value shown in Figure 61, some additional tests were performed using 25 g test load on Sodium Hydroxide etched specimens. These tests were performed to confirm the hardness profile tendency shown in Figure 61. Based on these tests, the results shown in Table 33 were obtained. This table confirms that the core hardness of the ferrite grains is not far from the hardness values obtained by 10 g test load and the hardness values shown in Attachment A: Material certificates of 215-230 HB. As stated earlier, 215-230 HB is equivalent to 215-230 HV according to ASTM E140. This conversion is strictly not valid for duplex stainless steel but invoked for reference purpose. See footnote earlier in this subsection.

The austenite grains are a little bit softer than ferrite with hardness just below 200 HV_{0,025} for austenite and approximately 220 HV_{0,025} for ferrite. The maximum hardness measured as close to the surface as possible, typical around 10 µm without introducing errors too large, were shown to be a little higher for Expanite and Sursulf using 25 g test load than when performed with 10 g test load. Nevertheless, most of the reading in the range of 10-20 µm from surface showed hardness values in the range of 350-250 HV for Expanite and Kolsterising where Kolsterising showed a tendency of being slightly harder than Expanite. Sursulf, however, showed a noticeable higher hardness than 10 g test load with hardness values in the range of 400-650 HV as shown in Table 33.

Table 33. Additional cross section micro Vickers hardness tests performed with 25 g test load on etched specimens.

	Untreated	Expanite	Kolsterising	HVOF	Sursulf
Austenite grain far from edge	184	163	184	203	196
Ferrite grain far from edge	212	219	217	219	225
Maximum hardness measured close to edge	-	408	401	1220 ¹	698
Typical hardness measured at 15±5 µm from edge	-	250-350	300-350	-	400-650
Expected based on similar material and treatment ²	-	1400	1000	1200	700

¹ Maximum hardness on HVOF test specimen measured with 300 g test load.

² Expanite; [84] and [85]. Kolsterising; [86]. HVOF; [82] and [83]. Sursulf; [87].

The cross sectional hardness profile shown in Figure 61 and Table 33 are considered to be markedly below the expected and probably real hardness profile present in the surface treated duplex specimens. This is based on measured surface hardness shown in Figure 60 and based on previous work performed on similar materials and similar surface treatments as shown in the references in Table 33 (table footnote 2).

5.4 Erosion test

Weight loss

The results from Table 24 may be illustrated in terms of weight loss and relative erosion resistance (REF) as shown in Figure 62 and Figure 63 respectively. This will give a better description of the ductile versus brittle mode of the solid particle erosion behavior shown in Figure 17 and the relative erosion resistance described in Equation 12.

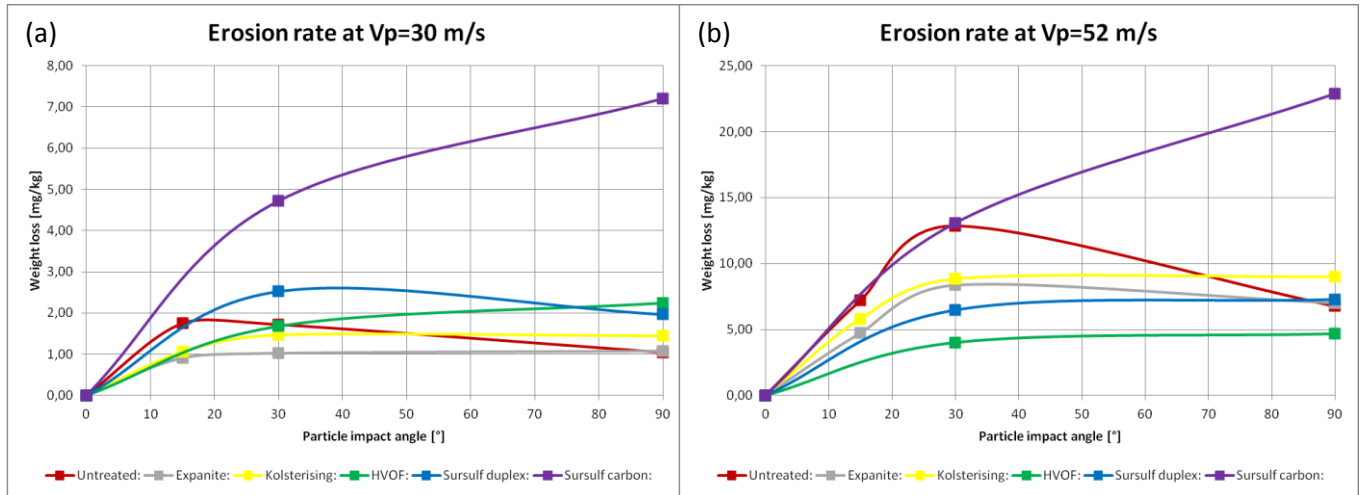


Figure 62. Weight loss with respect to particle angle at (a) low velocity $V_p=30$ m/s and (b) high velocity $V_p=52$ m/s. Note that except from 0° with 0 weight loss, data from only two angles are used for HVOF, Sursulf duplex and Sursulf carbon, while data from three angles are used for untreated duplex, Expanite and Kolsterising.

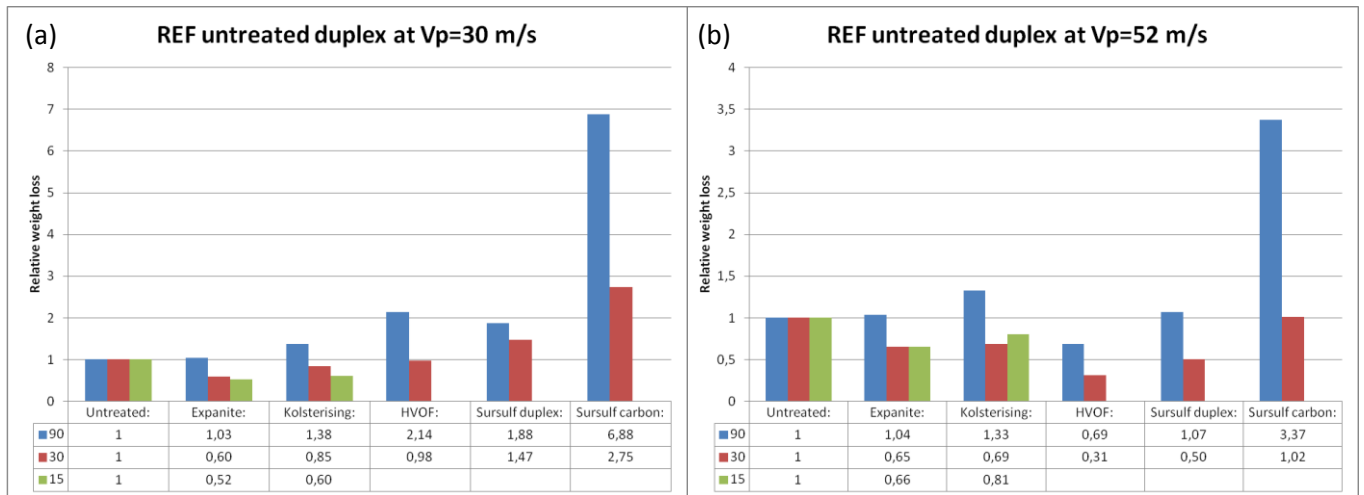


Figure 63. Relative erosion resistance (REF) with respect to untreated duplex at (a) low velocity and (b) high velocity. 90, 30 and 15 represent the particle impact angles (α) of which the surfaces have been subjected.

Based on the curves in Figure 62 and columns in Figure 63, the following relations may be given:

- The untreated duplex behaves in a ductile manner where maximum erosion rate is obtained at impact angles in the range of 15-30°.
- The Sursulf carbon behaves in a brittle manner where maximum erosion attack is obtained at impact angles of 90°.
- The remaining treatments of duplex stainless steel behave in a manner combined of ductile mode and brittle mode and prominent features is summarized below:
 - Expanite behave more in a ductile manner at high velocity than low velocity.
 - For Sursulf duplex, ductile mode is more prominent at low velocity than high velocity.
 - HVOF is the treatment with highest level of brittle mode except of Sursulf carbon, especially at low velocity. However, the differences to the other treatments are small.

- A relatively constant weight loss over a wide range of impact angles from approximately 30-90° is common for all treatments, except Sursulf carbon and untreated duplex as shown in Figure 62.
- The increased level of weight loss from low velocity to high velocity is quite constant for Expanite and Kolsterising treatments relative untreated duplex as shown in Figure 63. The weight loss has increased also for HVOF, Sursulf duplex and Sursulf carbon but to a much less degree compared to the other treatments. While untreated duplex, Expanite and Kolsterising have increased a factor of approximately 6-8 without considering impact angle, HVOF, Sursulf duplex and Sursulf carbon have increased a factor of approximately 2-3,5. I.e. HVOF, Sursulf duplex and Sursulf carbon are less prone to erosion at increased particle impact velocity relative to untreated duplex, Expanite and Kolsterising.
- The relative angle dependencies from low velocity to high velocity are approximately constant for untreated duplex, Kolsterising, HVOF and Sursulf carbon but it has decreased slightly for Expanite and increased slightly for Sursulf duplex at high impact angle as shown in Figure 62.

Angle dependencies

The general equation for erosion shown previously in Equation 8 may be revised so that the unit becomes [kg/kg] instead of only [kg]. The mass of sand hitting the target material, M_p , is removed from Equation 8 and take form as shown in Equation 17.

$$E = K \cdot V_p^n \cdot F(\alpha)$$

Equation 17

For a given particle impact velocity, V_p , and by defining the function of particle impact angle, $F(\alpha)$, having a maximum value of 1, an angle dependency chart may be developed as shown in Figure 64 (a) and (b) for low and high velocity respectively. The general function $F(\alpha)$ for steel grades is given by the relation given in Equation 18 derived from DNV document Erosion Wear in Piping systems, DNV RP0501 [88]. The result is a function $F(\alpha)$ shown in Figure 64 named as DNV RP0501 drawn with a black color. This curve is shown as reference to the other curves from testing the surface treated duplex stainless steel.

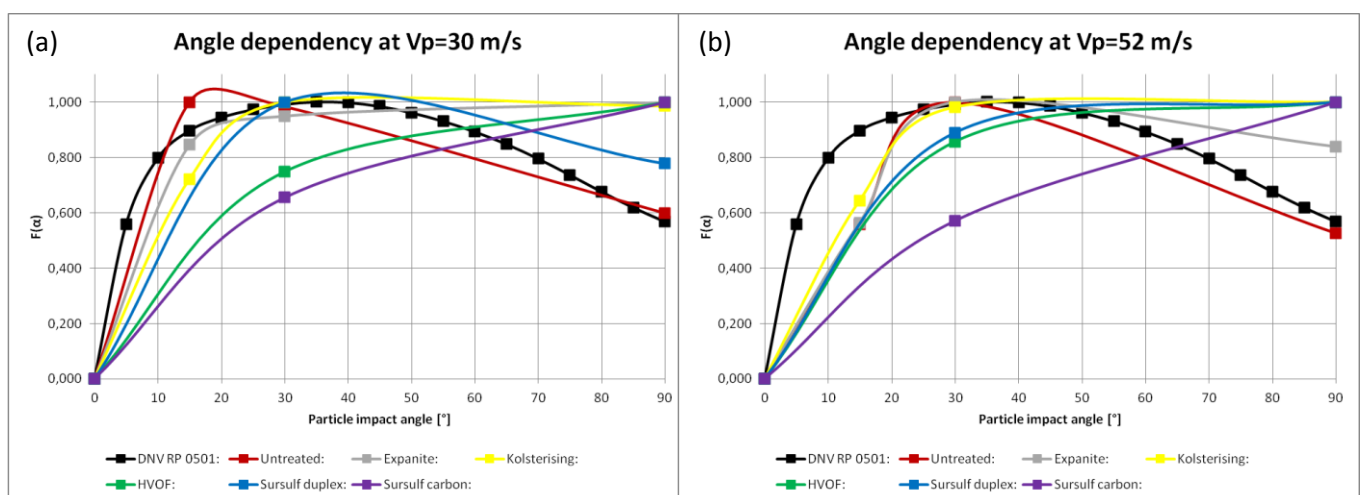


Figure 64. Function of particle impact angle dependency at (a) low velocity and (b) high velocity. The black curve is based on a relation given in a document from DNV called Erosive Wear in Piping systems (DNV RP 0501).

Figure 64 gives a clear indication of the erosion resistance the various surface treatments have with respect to angle and thus to what degree it behaves like a ductile or brittle manner. Compared to the DNV RP0501 curve, the treated duplex materials do not have the downward slope for angles greater than 30° which is typical for

ductile materials. Untreated duplex behave in a ductile manner both at low velocity and at high velocity. Besides that, only Sursulf duplex has a ductile mode at low velocity and only Expanite has a ductile mode at high velocity. All other tests intend to behave more like a brittle material by their higher erosion rate at increasingly higher impact angle (α). This brittle mode behavior is reasonable due to the fact that the surface treatments have introduced a hard surface layer which would make it less ductile. A composite with a hard case and a soft core is more brittle than a nonhardened microstructure [7].

$$F(\alpha) = \sum (-1)^{i+1} A_i \left(\frac{\alpha \cdot \pi}{180} \right)^i \quad \text{Equation 18}$$

A_i is given in Table 34.

Table 34. Constants to be used in Equation 18 based on DNV RP 0501 [88].

A_1	A_2	A_3	A_4	A_5	A_6	A_7	A_8
9,370	42,295	110,864	175,804	170,137	98,398	31,211	4,170

Material constants and velocity exponents

The material constant, K, and the velocity exponent, n, have to be determined by experimental investigation by using more data than what is available from the erosion testing. The values would not be accurate. However, a short introduction will be given but the actual values of K and n will not be calculated for the surface treatments referenced in this document.

The velocity exponent is derived by converting Equation 17 with respect to n and using results from erosion values based on two velocities as shown in Equation 19.

$$\begin{aligned} E_1 &= K \cdot V_{P,1}^n \\ E_2 &= K \cdot V_{P,2}^n \end{aligned} \Rightarrow \frac{V_{P,1}^n}{E_1} = \frac{V_{P,2}^n}{E_2} \Rightarrow \left(\frac{V_{P,1}}{V_{P,2}} \right)^n = \frac{E_1}{E_2} \Rightarrow n \cdot \ln \left[\frac{V_{P,1}}{V_{P,2}} \right] = \ln \left[\frac{E_1}{E_2} \right] \Rightarrow n = \frac{\ln \left[\frac{E_1}{E_2} \right]}{\ln \left[\frac{V_{P,1}}{V_{P,2}} \right]} \quad \text{Equation 19}$$

Further, the material constant K may be calculated by simple conversion of Equation 17 as shown in Equation 20.

$$E = K \cdot V_p^n \Rightarrow K = \frac{E}{V_p^n} \quad \text{Equation 20}$$

Recommended values of the n and K coefficients for steel grades are by DNV given to be [70]/[88]:

- n: 2,6
- K: $2,0 \cdot 10^{-9} \text{ (m/s)}^{-n}$

Scanning electron microscope examination

Scanning electron microscope examinations of the eroded surfaces were carried out in order to determine details of the erosion mechanisms. Images are taken both before and after erosion test for all test conditions applied, but only 1000X and 5000X magnification images with high particle velocity, $V_p=52 \text{ m/s}$, are shown with a few exceptions among untreated duplex and HVOF specimens due better quality of image. The images are

shown in Figure 49 to Figure 54 for the 5000X magnification images and in Attachment B: SEM images of erosion surfaces for the 1000X magnification images.

Modes of erosion of metals is subdivided into five types, namely cutting, fatigue, shear localization, adiabatic shear-induced spalling and delamination [89]. There are several models and theories developed for the explanation of the erosion mechanisms involved due to impingement of solid particles against a surface:

- a) The classical micro-cutting which assumes that metal removal involves cuts similar to that found in machining with chip-like debris [89].
- b) Plowing mechanism is dominant in soft metals which causes extrusion of a lip at the exit side of the crater. Successive impacts of multiple erodent particles are required in order to detach the lip debris from the surface. A critical threshold erodent velocity is required in order to introduce plowing [89].
- c) Platelet is the phenomena-logical model combining forging-extrusion mechanism which produces highly-distressed platelets of target material that are knocked off from the surface by succeeding impacts. As with plowing, successive impacts of multiple erodent particles are required in order to detach the platelet debris from the surface [89].

A combination of plate-like debris formation and micro-machining is reported for erosion of stainless steel by aluminium oxide, whereby the plate-like debris was prominently formed at higher angles of incidence. Wear debris are either detached lips from craters formed through plowing or platelets detached from the rims of "smear" craters. For 90° impingement angle on a low carbon steel, 60 % of the wear debris covered the platelet model, whereas micro-machining played a negligible role [89].

With reference to the images in Figure 46 to Figure 54 and the images in Attachment B: SEM images of erosion surfaces, the following observation and comments are made:

- Untreated duplex

The images in Figure 49 and Figure 70 show the surface of non eroded and eroded test specimen at 5000X and 1000X magnification respectively. The non eroded surface is seen to have marks resulting from the machining and grinding of the test specimen. The eroded surface, especially for the impact angle of 30° and 15°, show that erosion attacks have resulted in an uniform surface structure where the impact of the individual particles can be seen to have traversed the material by a combination of cutting and plowing and repeatedly deformed the material. A typical scenario might be that the deformed material have led to a lip of material attached to the end of the crater that eventually have been pushed back into the surface and becoming an extruded platelet that again have been removed by ductile fracture or other mechanism. This can be seen by the craters created by the particles, where the typical lip attached to the end of the crater is removed some places and still attached on other places as shown on the right hand side of Figure 49 (d) for instance.

The 90° eroded surface does not show the micromachining or plowing path of the individual particles, but similar mechanism have probably occurred as shown in the sketch in Figure 20 (a). Normal impact has introduced material deformation on the surface and thereby introduced the production of platelets which are subsequently knocked off with the result of material loss. This mechanism is, however, not easy to identify from the SEM images, but the surface show characteristics of surface roughening, lack of directional grooving characteristics of abrasion and lack on the formation of ripple pattern. Traces of the preparation process of the test specimen, porosities and other inhomogenities are removed. These

processes, converting the non eroded surface into a uniform surface structure, give evident for the transient behavior of the erosion rates observed and shown in Figure 48 (a).

- Expanite, Kolsterising and Sursulf duplex

The 5000X images in Figure 50, Figure 51 and Figure 54 and the 1000X images in Figure 71, Figure 72 and Figure 74 show the surface of the non eroded test specimens and how they are eroded with respect to impact angle. The differences in surface appearances between them are not huge, such that the erosion mechanisms involved for each of these surface treatments are similar and therefore described in common. In fact, the erosion mechanisms involved are probably quite similar to the mechanisms described for untreated duplex, especially when comparing impact angles of 30° and 90° images. The biggest difference is found for impact angle of 15°, where the remaining surface have less excessive or surviving flakes from material lips being produced by the transverse motion of the particles. There is a less tendency of deep plowing which is seen from a relatively even surface on Expanite and Kolsterising compared to untreated duplex. The erosion mechanism is probably favoring the classical micro-cutting more than the plowing mechanism and the platelet phenomena. Another factor showing the relatively plane surface of Expanite and Kolsterising at 15° impact angle is probably due to the combination of an increased surface hardness and the fact that the impact angle is sharp. These factors give the particles a higher tendency to rebound from the material surface more than on less sharp impact angle. This mechanism is described and shown schematically in Figure 19 (a).

- HVOF

The duplex stainless steel being coated with tungsten carbide by use of high velocity oxygen fuel stand out compared to the heat treated diffusion methods in terms of surface appearance and in fact that this duplex material is coated and not subjected to surface modification like Expanite, Kolsterising and Sursulf. Both 5000X magnification SEM images by use of the detector for secondary electrons and by use of the backscatter detector have been taken and shown in Figure 52 and Figure 53 respectively. Additional 1000X magnification images by use of the detector for secondary electrons are shown in Figure 73. The backscatter detector has the advantage of showing atomic number contrast where the tungsten carbide particles, having higher density and atom number, are represented as bright and the binder material as dark.

The non eroded test specimen show the tungsten carbide particles of different size distributed in the binder. The eroded surface in Figure 52 show a general smoother surface where the outstanding tungsten carbide particles have been removed, something which may explain the transient behavior of the erosion rates observed as shown in Figure 48 (d). This is also reflected in Figure 53 where the eroded surfaces at 90° and 30° are distinctly brighter. The higher amount of bright area means that a larger fracture of the surface is binder material, i.e. the carbides are removed. The erosion rates are associated with fracture of the carbide particles and erosion/fracturing of the binder material resulting in that the carbide particles are falling out from the matrix. The literature has proposed an abrasive wear mechanism for tungsten coating as follows: (i) extrusion of the binder phase and removal by plastic deformation and fatigue, (ii) undermining of the particles and subsequent particle pull-out, (iii) micro-cutting, (iv) carbide grain fracture and (v) delamination of the coating [83]. These wear mechanisms are probably similar to those happened on the erosion testing. There is no prominent formation of ripple pattern like seen on the other treated duplex since the carbides function like barriers for the cutting or plowing motion of the erodent particles at angles less than 90°. This behavior is partly described and shown in Figure 15.

5.5 Corrosion G48

As described in the test result section, the corrosion test according ASTM G48 method A was not completed with a temperature stable at $25\pm 2^\circ\text{C}$, but closer to a temperature around $70\text{--}75^\circ\text{C}$. This was confirmed by a contact thermometer made available. Ideally, the temperature should be set to 25°C for 24 hours whereby a more precise description and relation to other similar tests in the industry would be possible. This temperature failure also eliminates the possibility to relate the weight loss against acceptance criteria formulated by DNV-OS-F101 of 4 g/m^2 . Anyway, even though an absolute weight loss against acceptance criteria cannot be performed, a relative corrosion resistance against pitting corrosion at elevated temperature may be documented. This is possible since all test specimens have gone through same preparation procedures and subjected to the corrosion test at the same time involving equal test conditions.

The test results shown in Table 26 are more illustrative on column charts showing the weight loss with respect to exposed area and the formation of pits. These column charts are shown in Figure 65 (a) and (b) respectively.

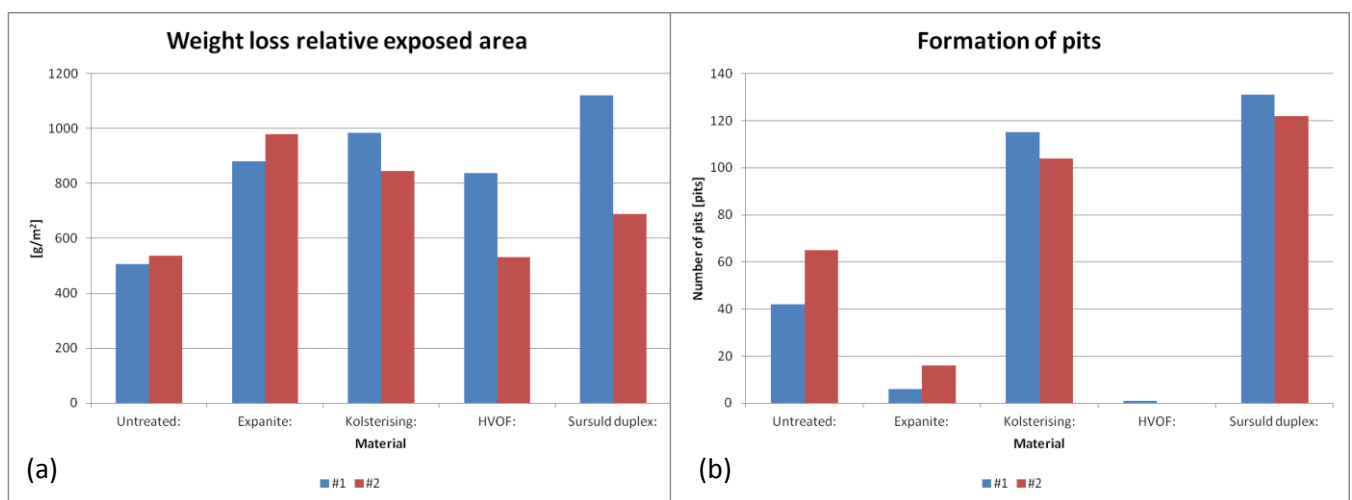


Figure 65. Charts from the corrosion test showing (a) weight loss relative exposed area and (b) formation of pits. #1 and #2 notation is added for separation of the test specimens (2 specimens for each treated duplex material).

Note the following important considerations and evaluations made to the column charts in Figure 65 and to the images shown in Figure 56:

- For the HVOF corrosion specimen, tungsten addition generally improve pitting resistance and crevice corrosion resistance [3]. This is also reflected in the HVOF photographs which show approximately no tendency to pit formation on the (5x2,5) cm faces. Even though, the weight loss is quite noticeable. There are mainly two reasons for this:
 - 1) Practically all pitting corrosion has occurred on the (2,5x1,5) cm faces which are not coated as shown in Figure 66.
 - 2) Corrosion has occurred on the binder phase and/or the hard phase itself. Corrosion of cemented carbides is generally based on the surface depletion of the binder phase [90] such that at the surface region only a carbide skeleton remains [91]. In the literature, the corrosion mechanisms of tungsten carbide powders and WC-Co-Cr thermal spray coatings have been discussed and it has been shown that a sequence of corrosion reactions occurring on the metal binder, at the interface between the binder and the ceramic hard phase and on the hard phase itself, which all contribute to the corrosion degradation [92]. The open circuit potential difference between WC particles and binder materials

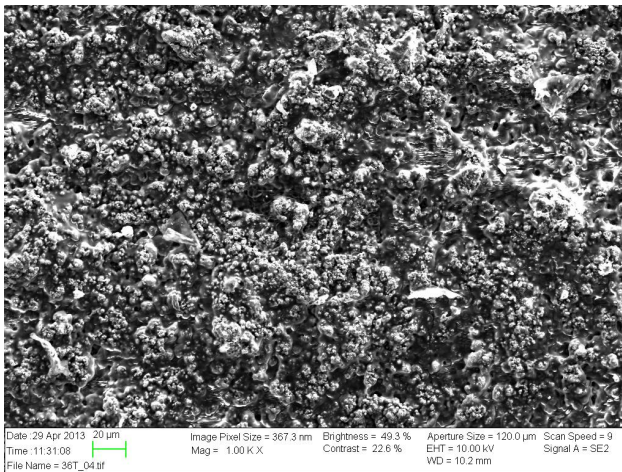
causes a microgalvanic corrosion between the two in an acidic environment. The WC becomes cathodic and the binder material becomes anodic, resulting in corrosion of anodic binder materials [90].

Figure 66 show a photograph of the typical pitting appearance from one of the HVOF corrosion specimen (2,5x1,5) cm face. These pits have occurred on the non coated faces of the specimen with the result of material removal and are part of the reason of the weight loss registered for HVOF specimens.

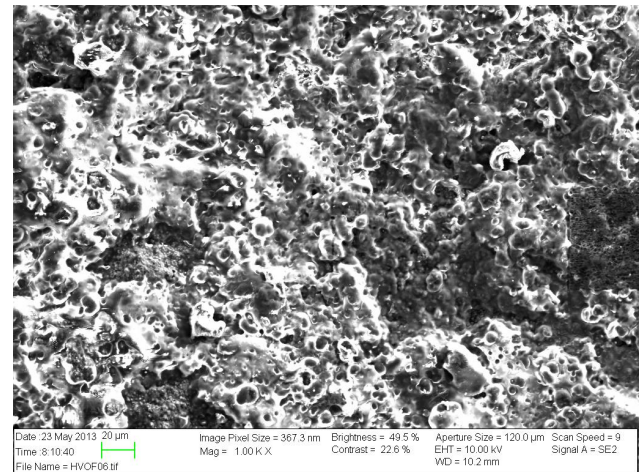
Figure 67 shows how the ferric chloride solution has attacked the coating probably at the carbide/binder interfaces and is also the reason for the pitting of the CoCr binder as reported in other similar work as well [90]. Dissolution of the tungsten carbide phase is probably involved and there is a potential for a loss of integrity from loss of hard phase through dissolution [92]. Based on the SEM image in Figure 67, the ferric solution has attacked the coating leaving a lot of pits or voids on the binder surface. This has probably led to the detachment of the outermost tungsten carbides. Moreover, the loss of one unit volume of tungsten carbide has quite an impact on weight loss relative duplex stainless steel. This is because the density of tungsten carbide is higher than duplex, i.e. 13000 kg/m^3 for WC [93] versus 8030 kg/m^3 for high alloy steels [36] representing the duplex stainless steel. More SEM images of the HVOF surface by use of secondary electron detector and backscatter detector are shown in Attachment C: SEM images of HVOF surface – corrosion G48, which emphasizes these mechanisms.



Figure 66. Approximately all pitting corrosion has occurred on one of the (2,5x1,5) cm face on the HVOF test specimens.



(a)



(b)

Figure 67. HVOF surface SEM images (a) before and (b) after corrosion G48 test. The ferric chloride solution has attacked the binder such that the surface consists of a lot of voids in the binder and the tungsten carbide detaches.

- Untreated and Kolsterising have both some large, “oversized” pits as shown in Figure 56, but Kolsterising have a lot more small pit formations than untreated duplex.

- Sursulf test specimens have no oversized pit formation like untreated duplex and Kolsterising. They only contain a lot of small pits slightly more than Kolsterising.
- Before weighing of the test specimens prior corrosion test, all test specimens were rinsed with water and scrubbed with a nylon bristle brush, dipped in methanol and air-dried. After corrosion test the same cleaning procedure were performed in addition to an ultrasonic cleaning. The ultrasonic cleaning was added in accordance with ASTM G48 in order to remove corrosion products from deep pits. The ultrasonic cleaner has probably lead to an excessive cleaning of especially the HVOF and Sursulf specimens with the result of measuring a higher weight loss than realistic for the corrosion test alone. This theory is based on the fact that these test specimens consists a thin surface layer which is partly removed during ultrasonic cleaning but not during normal scrubbing with brush and water. The images in Figure 56 (i) and (j) reveal some of this theory for the Sursulf test specimens where a remarkable portion of the black color is removed. This uncertainty would have been eliminated if ultrasonic cleaning would have been performed before the corrosion test as well.
- Expanite have only a few visual pits but still a remarkable weight loss. The reason for this is not known exactly, but it may be related to one or more of the following:
 - 1) The ultrasonic cleaning described above.
 - 2) A uniform corrosion has occurred on the surfaces with the result of material removal.
 - 3) A more detailed investigation was performed on the Expanite corrosion specimen with the use of a scanning electron microscope. This revealed that the surfaces contain a lot of micro pits in the range of 20-30 μm in diameter as shown in Figure 68. The penetration depth may be larger than the pits indicate from outside inspection and all these pits together may have led to a noticeable weight loss. Untreated duplex specimens did not have all these micro pits on the surfaces except those being visible without magnification. If such micro pits would be found, one would than expect that the weight loss for untreated duplex would be far greater than for Expanite since these specimens have the existence of the large, "oversized" pits in addition.

The reason for the formation of all the tiny pits may be the non homogeneous layer of Expanite on the surface, creating so-called holidays, i.e. micropeaks or small spots that are poorly or not covered by the Expanite treatment. This non homogeneity is described in more details in Section 5.6 Surface layer(s) with reference to Figure 69. This non-homogeneous distribution of charge across the electrified solid/liquid interface give rise to variation in the electrochemical potential over tiny areas within the whole [72]. The result is the creation of local anodes and cathodes and may be designated as galvanic corrosion or at least the result of a galvanic effect. Another corrosion mechanism that may have contributed to the initiation of pits is a sort of selective attack due to the presence of precipitates typical at grain boundaries. Grain boundaries are often the preferred sites for the precipitation and segregation processes observed in many alloys [72].

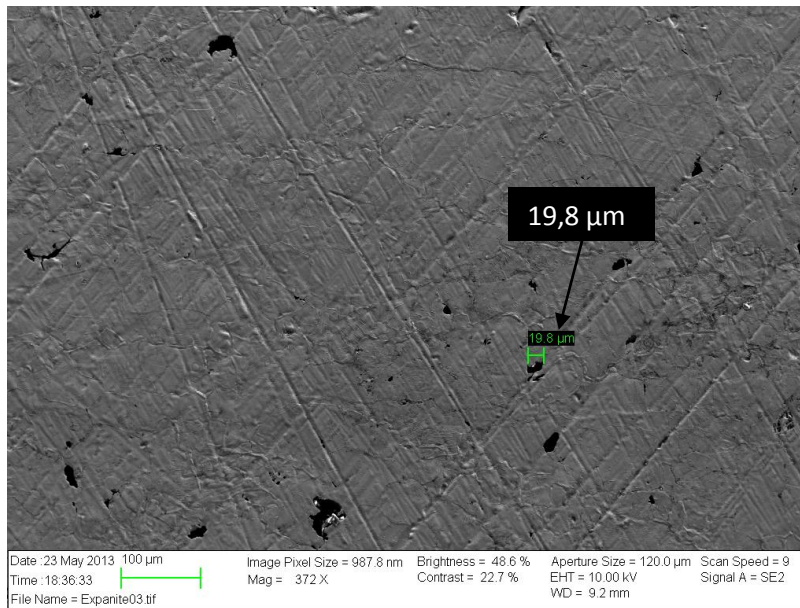


Figure 68. Scanning electron microscope image by the use of secondary electron detector (372X) on the Expanite corrosion test specimen surface showing a selection of micro pits.

- The few, large pits on untreated duplex have not resulted in higher weight loss than the remaining materials. In fact, only HVOF can match untreated duplex in terms of weight loss, especially if including the (25x15) cm face effect on HVOF which were not coated and was the reason for some of the weight loss for this material.
- A depletion of chromium in the surface layer due to the formation of chromium nitrides and/or carbides could be responsible for the lower corrosion resistance of the Kolsterising and the Sursulf surfaces [34]. The driving force for iron and chromium nitride precipitation is the high nitrogen saturation on the austenitic matrix [94]. The chromium depleted areas become the anodes in a cell and the remaining oxide-coated metal forms the cathode [72].
- Nitrogen addition in solid solution added to the surface improves the pitting resistance, something which is also reflected in the pitting resistance equivalent number equation given as:

$$\text{PREN} = \%Cr + 3,3 (\%Mo + 0,5 \%W) + 16 \%N$$
[17]. This may be the reason for the increased pitting corrosion resistance for the Expanite treatment compared to the untreated duplex in terms of macro pits. This is also effecting Kolsterising and Sursulf treatments, but these test specimens have probably been subjected to some chromium depleted areas more than Expanite due to precipitation of nitrides and/or carbides which is vulnerable to pitting corrosion. For instance, nitride in the form of Cr_2N is poorer in chromium than carbide in the form of Cr_{23}C_6 . I.e. formation of carbide versus nitride would cause a higher depletion of chromium in the vicinity of the grain boundaries, something which lessen the resistance to localized corrosion like pitting or intergranular corrosion [21].

Final remark

Due to the exaggerated temperature to which the corrosion test specimen where subjected, realistic and scientific relations are difficult to make unless a throughout examination is performed. Expected results from a standard 24 hours test at temperature of $25 \pm 2^\circ\text{C}$ would be zero weight loss and hopefully the presence of zero pits. This is at least the result from similar corrosion G48 test performed for the duplex material received from Scana Steel Stavanger according to the material certificates (not shown in Attachment A: Material certificates).

5.6 Metallographic examination

General structure

The metallographic images in Table 27 show quite clearly some kind of precipitates inside the ferrite grains and at grain boundaries. In fact, all treated and non treated duplex stainless steel samples show this tendency to a certain extent. Generally, only HVOF could match microstructural similarity with respect to untreated duplex. This is reasonable since this surface treatment method did not involve heat treatment or significant high temperatures of the material above the recommended temperature limits for duplex steel of around 280°C [7].

Untreated duplex and HVOF show some traces of precipitates at grain boundaries. On the other hand, Expanite, Kolsterising and Sursulf show a significant amount of precipitates at grain boundaries and within the ferrite grains. This means that the microstructure has been susceptible to some kind of changes in one way or another as a consequence of the heat treatments:

- As the carbon content is low in duplex stainless steel, approximately 0,02 % as shown in Attachment A: Material certificates, the precipitates are more likely to be nitrides rather than carbides [31]. At least higher volumetric fraction of nitrides are expected compared to carbides [29]. Based on other work, [29], [95], [94], [30] and [34], chromium nitrides and carbides are often precipitated as the result of heat treatment even at temperatures in the range of 400-600°C. These kind of precipitates are related to loss of toughness, sigma phase formation [29] and lower resistance to pitting corrosion and critical pitting temperature [31].
- As shown in Figure 23, nitrogen has very low solubility in ferrite at room temperature but the solubility increases as the temperature increase and it reaches a maximum of approximately 0,1 % at 590°C. The solubility of nitrogen in austenite is on the other hand much higher, approximately 2,35 % at 590°C [27]. This means that a heat treatment at high temperature would result in a more even distributed nitrogen throughout the material. A rapid quench would consequently result in ferrite supersaturated with nitrogen with the effect of precipitation of chromium nitrides. This is because the nitrogen atoms would not be able to diffuse fast enough from ferrite to austenite except the nitrogen located at a short distance from the austenite grains. Consequently, some of the nitrogen in the ferrite grains is trapped to form nitrides as the temperature lowers from high temperature to room temperature. These nitrides would preferentially form at the α/α subgrain boundaries and further spread to γ/α phase boundaries and within the α phase [31].

The description above is also applicable for carbon to form carbides due to the low solubility of carbon in ferrite compared to austenite. The metallographic examination techniques used in this document cannot distinguish whether the precipitates shown in Table 27 are nitrides or carbides. Based on previous work on duplex stainless steel, [29] and [31], one can only anticipate that the nitrides and carbides present are in the form of Cr_2N and M_{23}C_6 respectively. Anyway, the presence of nitride and/or carbide is quite clear based on the images in Table 27, especially for Expanite, Kolsterising and Sursulf.

- Ferrite and austenite phase balance determination by manual point count in accordance with ASTM E562 is important in terms of ferrite content before and after a heat treatment. A possible increase in ferrite content would give good condition for precipitation of nitrides due to the mechanisms described above. Based on the actual phase balance determination shown in Table 29, only Expanite demonstrated a substantial increase in ferrite content relative to material certificates and untreated duplex. This effect can also partly explain the precipitation of nitrides.

- Heat treatment within the temperature range of 700-900°C can lead to precipitation of secondary austenite (γ_2) within the ferrite grains. This decomposition of ferrite can occur even at lower temperatures so that the austenite particles become increasingly small and more difficult to detect. These secondary austenite particles are enriched in nitrogen compared to the ferrite matrix but rejects chromium and molybdenum. Precipitation of nitrides may therefore be accompanied by the formation of secondary austenite. There is however no evident of secondary austenite present at the images shown in Table 27, but as they might be very fine they cannot be excluded.

Based on the results from the Charpy impact test, two other mechanisms should be evaluated in order to highlight possible factors for the embrittling behavior of at least Expanite, Kolsterising and also Sursulf to some degree, namely precipitation of σ -phase and 475°C embrittlement:

- Formation of intermetallic compound like sigma (σ) normally take place at temperature above 650°C after some time dependent on the temperature as shown in Figure 9. The sigma phase occurs after chromium nitrides and carbides precipitation [29]. Incident of sigma phase will have detrimental effect on ductility, impact strength and corrosion [30]. There is however no sign of the formation of sigma phase on the samples shown in Table 27 and there is no reason for this to be present either. One exception is Expanite which have been subjected to temperature above 1100°C, but, according to discussion with Expanite AS, the cooling rate has been fast in order to prevent formation of sigma.

The presence of no sigma is more clear and easier to see on specimens etched with only sodium hydroxide (NaOH). Possible sigma phase should then be visible as orange-brown fields [77]. In order to verify that there is no sigma present on the specimens, sodium hydroxide etching is performed and shown in Attachment D: Optical micrographs of NaOH etched specimens. These images show only the ferrite/austenite grain structure with no sign of sigma phase formation.

- 475°C embrittlement is caused by the presence of the α' in the range of 300-550°C temperature range [7]. Aging at this temperature range would cause the spinodial decomposition of the ferrite into chromium-depleted α'' and chromium-rich α' regions [31]. Hardness, yield and tensile strength are increased while elongation and impact resistance are decreased. The alpha prime has a BCC structure, they are coherent with ferrite and they are very small. Since these precipitates contain essentially chromium and iron which show very similar atomic sizes, combined with the small precipitate size, their direct observation is difficult even using transmission electron microscopy [7]. This kind of embrittlement might therefore be part of the reason for the low impact resistance of Expanite and Kolsterising even though they cannot be proven to be present based on the images in Table 27. Further, the hardening effect of precipitates and low impact resistance may be related to the fact that Expanite and Kolsterising did experience a slight increase in yield strength and tensile strength and a small reduction in percent reduction in area based on the tensile test as shown in Figure 57. The surface treatment may have led to a hardening effect which are normally correlated to an increased tensile strength [9] and also a reduction in toughness.

Surface layer(s)

Regarding the surface layer images in Table 28, the untreated duplex shows no indication of an external surface layer. The austenite and ferrite grains can be seen vaguely on the SEM images due to the atomic number contrast property of the backscatter electron detector of the scanning electron microscope. Expanite, Kolsterising, HVOF and Sursulf images show more or less an expected surface layer and may be summarized as follows:

- Expanite

The SEM image from the cross-section analysis of the surface show no clear layer as would be expected from this treatment. A color change is visible and may be the presence of the Expanite layer, but the layer is not approximately 20 μm thick as would be expected [85]. This was also confirmed by the attempt of measuring the hardness profile. Due to uncertainties related to thickness, Expanite AS was contacted for discussions and received a test specimen in order to perform a cross section analysis themselves. This investigation cleared that the Expanite layer is narrow, only 5-10 μm thick, and not perfectly homogeneous as shown in Figure 69. Such thin layer makes it difficult in characterizing the Expanite layer. The reason that the Expanite layer is not as expected might be due to the following:

- Insufficient cleaning of the parts.
- The high and low temperature Expanite processes of which the test samples were subjected were not performed according to normal procedure/standard according to Expanite AS due to 475°C embrittlement problem of duplex stainless steels.

The optical microscope image in Table 28 shows, however, that the surface has been modified due to the Expanite process. The surface layer characterized by the color change penetrates as far as 50 μm from free surface.

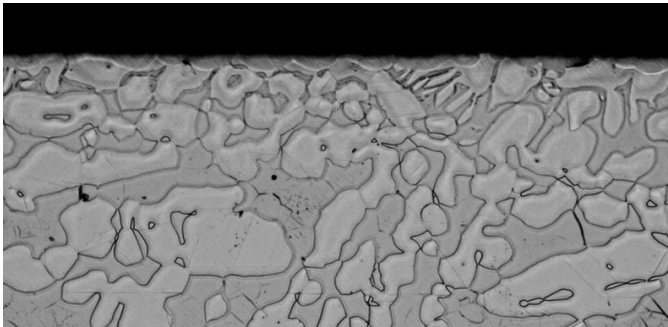


Figure 69. Cross sectional microscope image of the Expanite treated specimen. The image is given by Expanite AS based on the specimen that was sent back to Expanite AS for further examination. The shaded area visible along the surface is not continuous, something which reveals a non homogeneous Expanite layer on the surface.

- Kolsterising

The SEM image shows a clear layer of approximately 26 μm of a carburized layer, something of which is expected based on earlier work [86]. The optical image also show a thin surface layer which has to be the result from the Kolsterising process.

- HVOF

Measurements of the surface layer based on the SEM image is approximately 0,21 mm, something which correspond well to the desired thickness. This is also clearly shown in the optical image. Hardfacing by thermal spraying of tungsten carbide is described in Norsok M-630 by element data sheet NHF2. The coating thickness shall be in the range of 0,15-0,25 mm after grinding and lapping whereas the process shall be of type high velocity oxygen fuel or equivalent [15].

- Sursulf

This method shows a visible nitride layer up to 10 μm deep according to the SEM image and some kind of surface modification as deep as 60 μm from free surface according to the optical image. Based on available Sursulf literature obtained from Br. Bauer Nilsen AS [59], the nitriding procedure should give an effective depth of 0,05-0,1 mm for an austenitic stainless steel. This includes the compound zone and the nitrogen diffusion zone.

6 Conclusion

There are relative big amount of data and results to emphasize with respect to the examination and the comparative evaluation of the different heat treatment techniques applied on the duplex stainless steel. Erosion testing at DNV Høvik, being the mean wear test method in this document, did not point out a surface treatment that was superior to the others when exposed to different angles and velocities. Nevertheless, Expanite and Kolsterising gave remarkable good, average results over the whole spectrum of angles and velocities. HVOF and Sursulf had some longer transient time before a stationary erosion rate was established, but even though the erosion rates were higher at low velocity, the erosion rates increased less than the other treatments at high velocity. HVOF actually achieved the best erosion rates at high velocities and Sursulf had erosion rates similar to Expanite and Kolsterising.

Charpy test, tensile test, hardness test, corrosion test and metallographic examination are all included in order to evaluate the possible degree of change in base material properties and specification of the surface layer. Tensile test and Charpy impact test of the surface treated duplex were not expected to expose changes on mechanical properties relative to the untreated duplex.

Surprisingly maybe, the Charpy impact test revealed a rather important weakness among the Expanite and Kolsterising treatments with the result of a brittle fracture and low capacity to absorb impact energy. The other surface treatments did not have this weakness and were within the acceptance criteria stated in Norsok M-630.

Tensile test did not result in any major surprises and all specimens demonstrated tensile properties within the acceptance criteria stated in ASTM A479. HVOF showed some differences with respect to the other treatments mainly due to the increased cross sectional area of specimens influencing the yield strength and tensile strength to lower values and percent area reduction to higher values. Longer gauge length for the HVOF specimens also produced lower value of elongation relative to the other treatments. The only surface treatments to highlight, except HVOF, are Expanite and Kolsterising which resulted in slightly higher yield strength and tensile strength and a small reduction in percent area reduction. These results, combined with the low impact toughness for Expanite and Kolsterising, may be related to the relative large amount of precipitates of carbides and/or nitrides revealed on the metallographic examination images and possible precipitation of α' -phase, i.e. 475°C embrittlement, in the ferrite phase. Sursulf is also affected by these factors but in less degree than Expanite and Kolsterising. HVOF is the only surface treatment technique with similar base material properties as the untreated duplex. Hardfacing by thermal spraying of tungsten carbide is also the only surface treatment specified in Norsok M-630. Based on ISO 15156-3, however, other surface treatment techniques like nitriding are allowed as long as the permitted case depth is less than 0,15 mm and the surface treatment is conducted at a temperature below the lower critical temperature of the alloy being treated.

Hardness test, combined with the metallographic examination of the cross sectional analysis, shall confirm the existence and the characterization of the surface layer according to surface treatment. Micro hardness of the surface for all treated duplex showed an increased hardness of approximately 3,5X for Expanite, Kolsterising and Sursulf and approximately 4,5X for HVOF relative to untreated duplex. The hardness as a function of distance from surface was more difficult to measure and more difficult to relate to other, similar work obtained for the surface treatment in question. However, it was possible to detect a noticeable hardness increase as deep as approximately 25 μm from free surface for Expanite, Kolsterising and Sursulf, but the hardness was somewhat lower than expected. Further, metallographic examination images of the cross sections revealed that the surface treatment have resulted in a surface modification penetrating as deep as 20-25 μm for Expanite and

Kolsterising and up to 60 μm for Sursulf. Cross sectional analysis of HVOF gave reasonable results with a hardness value of approximately 1200 $\text{HV}_{0,3}$ of the tungsten carbide coating with a thickness of approximately 0,2 mm.

The G48 corrosion test was not performed as intended due to some problem with the temperature control unit. Nevertheless, a comparative evaluation between the surface treatments revealed some differences in the resistance against pitting corrosion. Whilst HVOF clearly had the least formation of pits, this treatment is particularly subjected to corrosion reactions occurring on the metal binder and at the interface between the binder and the hard phase. Also, the tungsten carbide can contribute to the overall corrosion degradation by dissolution. These effects must be considered for this treatment, but basically HVOF showed good resistance against pitting corrosion with low weight loss compared to the other surface treatments. Kolsterising and Sursulf are superior in terms of the number of visual pits formed without magnification, but they are also subjected to a relative high weight loss. Expanite have far less visual pit formations when examined without magnification compared to Kolsterising, Sursulf and untreated duplex and Expanite have neither the formation of large pits. Even though, this surface treatment is subjected to a higher weight loss than untreated duplex for instance. Further investigation, however, revealed that the Expanite corrosion specimens have led to the formation of a lot of micro pits visual under high magnification using scanning electron microscope. This is probably the main cause that the weight loss matches the weight loss of Kolsterising and Sursulf. Untreated duplex has actually least average weight loss, even less than HVOF, but also untreated duplex is subjected to a few, very large pits like Kolsterising.

Summa summarum, there is no clear and easy choice of selecting the most appropriate surface treatment method evaluated in this documented on a duplex stainless steel material. In fact, none of the selected surface treatments can be used without further research in terms of improving wear resistance on duplex stainless steel without affecting base material properties. Based on the results and analysis presented in this document, thermal spraying of tungsten carbide by HVOF stand out to fulfill the original objective of this thesis in a reasonable good manner. Expanite and Kolsterising are also interesting techniques due to the potential of these treatments, but further investigations are required concerning heat treatment and precipitation of intermetallic phases and embrittlement. Future research is highly recommended within at least the following areas:

- Coating duplex stainless steel with ceramic material. Reference to similar work: [96], [97], [98], [99], [100].
- Wear testing to include abrasion test.
- Duplex stainless steel involves difficulties in terms of unwanted precipitations and danger of 475°C embrittlement during heat treatment. Surface treatments like Expanite and Kolsterising on nickel alloys are of current interest and possible alternatives to the duplex stainless steel.
- More detail and supplementary work could be done on the erosion testing by using higher particle velocities and more impact particle angles.
- Corrosion G48 test should be done according to standard in order to withdraw relevant and useful information. The current corrosion G48 test presented in this document can not give absolute and trustworthy results.
- A deeper understanding of the brittle behavior of Expanite and Kolsterising is of interest. A full metallographic examination of the Expanite and Kolsterising specimens by including transmission electron microscope and X-ray microanalysis for chemical analysis would give valuable information about present precipitates and to which elements they consists of.

7 References

1. Levy, A.V., *Solid particle erosion and erosion-corrosion of materials*. 1995, United States of America: ASM International.
2. Stachowiak, G. and A.W. Batchelor, *Engineering Tribology*. 2011, Oxford: Elsevier Science. 1 online resource (831 s.).
3. Gunn, R.N., *Duplex stainless steels : microstructure, properties and applications*. 1997, Cambridge: Abington. xii, 204 s. : ill.
4. ASTM, *Standard test methods for Rockwell hardness of metallic materials*, in *E18*. 2008, ASTM. p. 37.
5. *Mechanical testing and evaluation*. Vol. 8. 2000, Materials Park, OH: ASM International. XIV, 998 s.
6. Anderson, T.L., *Fracture mechanics: fundamentals and applications*. 2005, Boca Raton, Fla.: Taylor & Francis. 621 s. : ill.
7. (edited), G.E.T., *Steel heat treatment : metallurgy and technologies*. 2. ed. 2007, Boca Raton, Fla.: CRC/Taylor & Francis. 833 s.
8. Budinski, K.G., *Guide to Friction, Wear, and Erosion Testing: (MNL 56)*. ASTM International.
9. Callister, W.D. and D.G. Rethwisch, *Materials science and engineering : an introduction*. 7th ed. 2007, New York: Wiley. XXV, 721, [82] s. : ill.
10. Roxar. *Roxar - about us*. [cited 2013 10.01.2013]; Available from: <http://www2.emersonprocess.com/en-US/brands/roxar/aboutus/Pages/AboutRoxar.aspx>.
11. ISO, *ISO 13628-1 Petroleum and natural gas industries - Design and operation of subsea production systems*, in *Part 1: General requirements and recommendations*. 2005, International Standard Organization.
12. Veritas, D.N., *Technical Report - Joining methods - Technological summaries*. 2005: Høvik, Norway. p. 38.
13. Nagatsuka, K., A. Nishimoto, and K. Akamatsu, *Surface hardening of duplex stainless steel by low temperature active screen plasma nitriding*. *Surface and Coatings Technology*, 2010. **205, Supplement 1(0)**: p. S295-S299.
14. Standard, N., *M-001*, in *Material selection*. 2004, Standards Norway.
15. Standard, N., *M-630*, in *Material data sheets and element data sheets for piping*. 2010, Standards Norway.
16. ISO, *ISO 15156-1 Petroleum and natural gas industries - Materials for use in H2S-containing environments in oil and gas production*, in *Part 1: General principles for selection of cracking-resistant materials*. 2009, International Standard Organization.
17. ISO, *ISO 15156-3 Petroleum and natural gas industries - Materials for use in H2S-containing environments in oil and gas production*, in *Part 3: Cracking-resistant CRAs (corrosion-resistant alloys) and other alloys*. 2009, International Standard Organization.
18. ISO, *ISO 10423 Petroleum and natural gas industries - Drilling and production equipment - Wellhead and christmas tree equipment*. 2009, International Standard Organization.
19. ISO, *ISO 13628-6 Petroleum and natural gas industries - Design and operation of subsea production systems*, in *Part 6: Subsea production control systems*. 2006, International Standard Organization.
20. DNV, *Design of duplex stainless steel subsea equipment exposed to cathodic protection*, in *DNV-RP-F112*. 2008, Det Norske Veritas.
21. Lacombe, P., B. Baroux, and G. Béranger, *Stainless steels*. 1993, Les Ulis: Les éditions de physique. XX, 978 s. : ill.
22. Wikipedia, *Steel phase diagram, Iron-carbon phase diagram under atmospheric pressure*, S. pd.svg, Editor.: Wikipedia.
23. (IMOA), I.m.a., *Practical Guidelines for the Fabrication of Duplex Stainless Steel*. 2009, International Molybdenum Association (IMOA): London, UK.
24. Martin, J.W., *Materials for engineering*. Vol. B0756. 2002, London: The Institute. X, 244 s. : ill.
25. Kovach, C.W., *High-performance stainless steels*, I. Technical Marketing Resources, Editor., Nickel Development Institute: Pittsburgh, PA, USA.

26. department, A.s.t., *Atlas steels technical handbook of stainless steels*, A. steels, Editor. 2010, Atlas steels.
27. Bhadeshia, H.K.D.H. and R.W.K. Honeycombe, *Steels: microstructure and properties*. 2006, Amsterdam: Elsevier. XI, 344 s. : ill.
28. Porter, D.A. and K.E. Easterling, *Phase transformations in metals and alloys*. 1981, New York: Van Nostrand Reinhold. xii, 446 s. : ill.
29. Zucato, I., et al., *Microstructural characterization and the effect of phase transformations on toughness of the UNS S31803 duplex stainless steel aged treated at 850 deg C*. Mikrostrukturcharakterisierung und der Effekt der Phenumwandlung auf die Zähigkeit eines bei 850 Grad C gealtertem UNS S31803 nichtrostendem Duplex-Stahl, 2002(3): p. 385.
30. Lopez, N., M. Cid, and M. Puiggali, *Influence of σ -phase on mechanical properties and corrosion resistance of duplex stainless steels*. Corrosion Science, 1999. **41**(8): p. 1615-1631.
31. Deng, B., et al., *Effect of thermal cycles on the corrosion and mechanical properties of UNS S31803 duplex stainless steel*. Corrosion Science, 2009. **51**(12): p. 2969-2975.
32. Michael, P., S. Oliver, and G. Thomas, *Effect of intermetallic precipitations on the properties of duplex stainless steel*. Materials Characterization. **58**: p. 65-71.
33. API, *Use of Duplex Stainless Steels in the Oil Refining Industry*, in API 938-C. 2011, American Petroleum Institute: Washington. p. 11.
34. Kliauga, A.M. and M. Pohl, *Effect of plasma nitriding on wear and pitting corrosion resistance of X2 CrNiMoN 22 5 3 duplex stainless steel*. Surface and Coatings Technology, 1998. **98**(1-3): p. 1205-1210.
35. Chandra, K., et al., *Low temperature embrittlement of duplex stainless steel: Correlation between mechanical and electrochemical behavior*. Materials Science & Engineering A. **527**: p. 3904-3912.
36. ASME, *ASME Boiler & Pressure Vessel Code*, in Section II MATERIALS Part D: Properties. 2010, The American Society of Mechanical Engineers: New York.
37. *Heat treating*. Vol. 4. 1991, Materials Park, OH: ASM International. xiii, 1012 s.
38. *Friction, lubrication, and wear technology*. Vol. 18. 1992, Materials Park, OH: ASM International. xiii, 942 s.
39. Zhao, H.X., et al., *Slurry erosion properties of ceramic coatings*. Wear, 1999. **233–235**(0): p. 608-614.
40. Wang, Y.-F. and Z.-G. Yang, *Finite element model of erosive wear on ductile and brittle materials*. Wear, 2008. **265**(5–6): p. 871-878.
41. Charles, J.A. and A.A.A. Crane, *Selection and use of engineering materials*. 1989, London: Butterworths. VII, 336 s. : ill.
42. Higgins, R.A., *Engineering metallurgy Part 1: Applied physical metallurgy*. 6. ed. 1993: Edward Arnold. 550.
43. Malaczynski, G.W., et al., *Characterization of surface modified α -iron by nitrogen plasma immersion ion implantation: a microstructural study*. Materials Science and Engineering: A, 1999. **262**(1–2): p. 289-299.
44. Sun, Y., *Production of nitrogen and carbon S phases in austenitic stainless steels by hybrid plasma surface alloying*. Surface Engineering, 2010. **26**(1/2): p. 114-122.
45. Garzón, C.M. and A.P. Tschiptschin, *New high temperature gas nitriding cycle that enhances the wear resistance of duplex stainless steels*. Journal of Materials Science, 2004. **39**(23): p. 7101-7105.
46. Berns, H., et al., *Solution Nitriding of Stainless Steels for Process Engineering*. Materialwissenschaft und Werkstofftechnik, 2000. **31**(2): p. 152-161.
47. *Surface engineering*. Vol. 5. 1994, Materials Park, OH: ASM International. XIV, 1039 s.
48. *High Velocity Oxy-fuel (HVOF) solutions*. 2012, Sulzer Metco: www.sulzer.com.
49. *Expanite*. [cited 2013 28.02]; Available from: <http://www.expanite.com/index.php>.
50. Thomas Kreuzaler, T.S., *New plug-and-play installation technology for surface hardening of stainless steel*. Seco/Warwick.
51. *Bodycote*. [cited 2013 27.02]; Bodycote Group home]. Available from: <http://www.bodycote.com/en.aspx>.
52. *Bodycote Specialty Stainless Steel Processes (S³P)*. [cited 2013 27.02]; Available from: <http://www.bodycote.com/en/services/heat-treatment/specialty-stainless-steel-processes.aspx>.

53. *Bodycote Kolsterising*. [cited 2013 27.02]; Available from: <http://internet.bodycote.org/kolsterising/en/company-profile.html>.
54. *Thermal spraying*. [cited 2013 27.02]; Available from: http://en.wikipedia.org/wiki/Thermal_spraying#High_velocity_oxygen_fuel_spraying_.28HVOF.29.
55. *Castolin Eutectic*. [cited 2013 27.02]; Available from: <http://www.castolin.com/content/about-castolin-eutectic>.
56. *Praxair HP/HVOF Equipment solutions*. 2009, Praxair Surface Technologies, Inc. and TAFE Incorporated: United States of America.
57. *Techniques surfaces Ltd*. [cited 2013 27.02]; Available from: <http://www.techniques-surfaces.uk.com/frameset.htm>.
58. *HEF Group*. [cited 2013 27.02]; Available from: <http://www.hef-group.com/>.
59. *Sursulf nitriding procedure*. 2006, Br. Bauer Nilsen AS: Norway.
60. ASTM, *Standard test method and definitions for mechanical testing of steel products*, in ASTM A370. ASTM.
61. DNV, *Submarine pipeline systems*, in DNV-OS-F101. 2012, Det Norske Veritas.
62. ASTM, *Standard Specification for Stainless Steel Bars and Shapes for Use in Boilers and Other Pressure Vessels*, in A479. 2012, ASTM. p. 8.
63. *Lathe*. [cited 2013 08.03]; Available from: <http://en.wikipedia.org/wiki/Lathe>.
64. *Blacks charpy cutting machines*. [cited 2013 08.03]; Available from: <http://www.blackscharpy.com/index.htm>.
65. ISO, *ISO 6892-1 Metallic materials - Tensile testing*, in *Method of test at room temperature*. 2009, International Standard Organization.
66. El Wakil, S.D., *Materials science and engineering lab manual*. 1994, Boston: PWS Publ. Co. IX, 78 s. : ill.
67. Dowling, N.E., *Mechanical behavior of materials : engineering methods for deformation, fracture, and fatigue*. 1999, Upper Saddle River, N.J.: Prentice Hall. XVIII, 830 s. : ill.
68. ASTM, *Standard test methods for microindentation hardness materials*, in E384. 2005, ASTM. p. 33.
69. Gee, M.J.N.a.M., *Guide to wear problems and testing for industry*. 2001, USA: William Andrew Publishing, LLC.
70. K. Haugen, O.K., R. Sandberg and H. Trandem, *Erosion resistance of materials exposed to sand particle impact*, in DNV-92-3444. 1992, Det Norske Veritas: Høvik. p. 64.
71. ASTM, *Standard test methods for pitting and crevice corrosion resistance of stainless steels and related alloys by use of ferric chloride solution*, in G48. 2011, ASTM. p. 11.
72. Trethewey, K.R. and J. Chamberlain, *Corrosion for science and engineering*. 1995, London: Longman. XIV, 466 s. : ill.
73. ASTM, *Standard specification for reagent water*, in D1193. 1999, ASTM. p. 3.
74. *Metallography and microstructures*. Vol. 9. 1985, Metals Park, Ohio: American Society for Metals. XV, 775 s.
75. Hjelen, J., *Scanning elektron-mikroskopi*. 1989, Trondheim: SINTEF. 106 s. : ill.
76. Small, K.B., D.A. Englehart, and T.A. Christman, *Guide to etching specialty alloys*, in *Advanced materials & processes*. 2008, www.asminternational.org; Wyomissing, Pennsylvania. p. 6.
77. Voort, G.V. *Identification of phases in stainless steel by etching-1*. [cited 2013 04.06]; Available from: <http://www.georgevandervoort.com/metallography-articles/1061-identification-of-phases-in-stainless-steels-by-etching.html>.
78. Haugen, K., et al., *Sand erosion of wear-resistant materials: Erosion in choke valves*. *Wear*, 1995. **186-187**(PART 1): p. 179-188.
79. ASTM, *Standard test method for determining volume fraction by systematic manual point count*, in E562. 2002, ASTM. p. 7.
80. *UNS F33800 Cast iron*. [cited 2013 03.06]; Available from: <http://www.matweb.com/search/datasheet.aspx?matguid=418fd58104504cecb2d9a4df657e1507&ckk=1>.

81. Weng, K.L., H.R. Chen, and J.R. Yang, *The low-temperature aging embrittlement in a 2205 duplex stainless steel*. Materials Science & Engineering A. **379**: p. 119-132.
82. Xie, M., S. Zhang, and M. Li, *Comparative investigation on HVOF sprayed carbide-based coatings*. Applied Surface Science, 2013. **273**(0): p. 799-805.
83. Wang, Q., et al., *Wear and corrosion performance of WC-10Co4Cr coatings deposited by different HVOF and HVAF spraying processes*. Surface and Coatings Technology, 2013. **218**(0): p. 127-136.
84. Hummelshøj, T.S., T.L. Christiansen, and M.A.J. Somers, *Low temperature thermochemical treatment of stainless steel; bridging from science to technology*.
85. Hummelshøj, T.S., T.L. Christiansen, and M.A.J. Somers, *Towards commercialization of fast gaseous nitrocarburising stainless steel*. Materialer-fra grundforskning til anvendelse, 2010: p. 105-110.
86. Faccoli, M., et al., *Effect of Kolsterising treatment on surface properties of a duplex stainless steel*. La Metallurgia Italiana, 2012(4/2012): p. 13-18.
87. *Sursulf; a nitriding treatment in a non-polluting salt bath accelerated with sulphur*. Centre stephanois de recherches mecaniques hydromecanique et frottement, n.d.: France.
88. DNV, *Erosion Wear in Piping systems*, in *DNV-RP 0501*. 2007, Det Norske Veritas.
89. Momber, A.W. and Y.C. Wong, *Geometrical features of wear debris. Part I Erosion of ductile by solid particle impingement*. Geometrische Aspekte von Verschleißstrümmern. Teil I Erosion von duktilem Stahl durch Aufprall von festen Partikeln, 2005(13): p. 3517.
90. Cho, J.E., S.Y. Hwang, and K.Y. Kim, *Corrosion behavior of thermal sprayed WC cermet coatings having various metallic binders in strong acidic environment*. Surface and Coatings Technology, 2006. **200**(8): p. 2653-2662.
91. *Handbook of corrosion data*. 2nd. ed. 1995: ASM international.
92. Souza, V.A.D. and A. Neville, *Corrosion and synergy in a WCCoCr HVOF thermal spray coating—understanding their role in erosion–corrosion degradation*. Wear. **259**: p. 171-180.
93. *Stelcar Jet Kote 120H Technical data*, K. Stellite, Editor. 2013: www.kennametal.com/stellite.
94. Mingolo, N., A.P. Tschiptschin, and C.E. Pinedo, *Structure and properties of expanded austenite formed during low temperature plasma nitriding of an AISI 316L austenitic stainless steel*. 2006.
95. Bielawski, J. and J. Baranowska, *Formation of nitrided layers on duplex steel - influence of multiphase substrate*.
96. Adraider, Y., et al., *Structure characterisation and mechanical properties of crystalline alumina coatings on stainless steel fabricated via sol–gel technology and fibre laser processing*. Journal of the European Ceramic Society, 2012. **32**(16): p. 4229-4240.
97. Monticelli, C., A. Balbo, and F. Zucchi, *Corrosion and tribocorrosion behaviour of thermally sprayed ceramic coatings on steel*. Surface and Coatings Technology, 2011. **205**(12): p. 3683-3691.
98. Habib, K.A., et al., *Comparison of flame sprayed Al₂O₃/TiO₂ coatings: Their microstructure, mechanical properties and tribology behavior*. Surface & Coatings Technology. **201**: p. 1436-1443.
99. Vargas, F., et al., *Mechanical and tribological performance of Al₂O₃-TiO₂ coatings elaborated by flame and plasma spraying*. Surface and Coatings Technology, 2010. **205**(4): p. 1132-1136.
100. Bolelli, G., et al., *Wear behaviour of thermally sprayed ceramic oxide coatings*. Wear, 2006. **261**(11–12): p. 1298-1315.

Attachment A: Material certificates




#1

INSPECTION CERTIFICATE/ INSPEKTION ZERTIFIKAT

4100 Jørpeland, Norway
Country of origin: Norway

EN 10204 - 3.2

Customer / <i>Bestiller</i> Aarbakke AS Postboks 108 4341 Bryne	Date / <i>Datum</i> 23.10.2012	Cert.no / <i>Zeugnis Nr.</i> C1633/12
	Our order no. / <i>Unsere Auftrags- Nr.</i> 30884.100	Our work-order no. / 1068427
	Customer order no. / <i>Bestellungs- Nr.</i> 113715	
Specification / <i>Spezifikation:</i> Certified goods / <i>Gegenstand</i> Ø340 mm i fallende lengde Leveringsmål Ø340/121 x ca 5500 mm		
Marking / <i>Kennzeichnung:</i> A22306 T12688 8427  STG2012-371 Grade / <i>Werkstoff- Nr.</i> Norsok M-630 D47, rev.4 ASTM A479 UNS S31803 ISO15156/NACE 0175, DNV RP-F112 Spec 109697/C, LIWAN 3-1, LIW-S-SP-SU-1218 rev.1 Aarbakke spec. Duplex Meter body rev.2		

CERTIFIED GOODS / ZERTIFIKERTES GUT

Test no. / <i>Probe Nr.</i>	Number / <i>Stück</i>	Weight / <i>Gewicht (kg)</i>	Dimension	Heat treatment / <i>Wärmebehandlung</i>	Process / <i>Erschmelzungsart</i>	Reduction grade / <i>Verschmiedungsgra- d.</i>	Charge no. / <i>Schmelze</i>
T12688	2	3310 3546	340 x 5600 341 x 5700	Solution annealed 1080°C, 1,5hrs, Water	Forged E/ AOD	4,26:1	A22306

CHEMICAL COMPOSITION / CHEMISCHE ANALYSE

C	Si	Mn	S	P	Cr	Ni	W	V	Mo	Cu	Al	Ti	Nb	N	B	Pb	PRE	SSA Quality name: 26C0 58490
0,023	0,67	1,12	0,001	0,023	22,21	5,67	0,06	0,07	3,13	0,25	0,011	0,001	0,008	0,175	0,0017	0,0001	35,34	

MECHANICAL PROPERTIES (L=Longitudinal, T=Transverse) MECHANISCHE EIGENSCHAFTEN (L=längs, T=Quer)

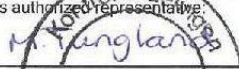
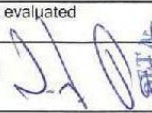
Test L/T <i>Probe L/T</i>	Temp. °C	Yield Strength / <i>Streckgrenze</i>		Tensile Strength / <i>Zugfestig- keit</i>		Elongation / <i>Dehnung</i>	Red. of areal / <i>Lin- schrumpung</i>	Impact values / <i>Kerbschlagarbeit</i> Kv				Temp. °C	Hardness / <i>Härte</i>
		Rp0.2 N/mm2	Rp1.0 N/mm2	Rm N/mm2	Rp/Rm			J	J	J	Avg.		
A1	-	-	-	-	-	-	-	72	73	57	67	-46	-
C1	20	520	-	722	-	35	73	-	-	-	-	-	217
A2	-	-	-	-	-	-	-	86	58	58	67	-46	-
C2	20	543	-	730	-	35	73	-	-	-	-	-	217
F1	-	-	-	-	-	-	-	112	125	95	110	-46	-
E1	20	541	-	707	-	39	73	-	-	-	-	-	223
F2	-	-	-	-	-	-	-	115	99	128	114	-46	-
E2	20	532	-	710	-	38	75	-	-	-	-	-	223

RESULTS OF OTHER TESTS / ERGEBNIS ANDERER PROBEN.

Sample-taking : A1: Charpy-V, transverse 1/4T A2: Charpy-V, transverse 1/2T
 C1: Tensile, transverse 1/4T C2: Tensile, transverse 1/2T
 E1: Tensile, longitudinal, 1/4T E2: Tensile, longitudinal, 1/2T
 F1: Charpy-V, longitudinal 1/4T F2: Charpy-V, longitudinal 1/2T
 D3: Micro, subsurface D2: Micro, 1/2T
 D1: Micro, 1/4T
 B1: Corrosion, longitudinal 1/4T B2: Corrosion, longitudinal 1/2T

PT + UT - accepted. Report attached
 Microstructure examination-accepted. Reports attached
 Austenit spacing carried out. Reports attached
 Corrosion testing-accepted. Report attached.

Heat treated dimension Ø370mm Heat treatment graph-Report attached

We hereby declare that the product supplied are in compliance with the order in which test results are supplied.	Fitness for purpose not evaluated
Manufacturer's authorized representative: 	3. party representative: Magne Puntervold 





#2

**INSPECTION CERTIFICATE/
INSPEKTION ZERTIFIKAT**

4100 Jørpeland, Norway

Country of origin: Norway

EN 10204 - 3.2

Customer / <i>Besteller</i> Aarbakke AS Postboks 108 4341 Bryne	Date / <i>Datum</i> 01.11.2012	Cert.no. / <i>Zeugnis Nr.</i> C1632/12 rev.1
	Our order no. / <i>Unsere Auftrags- Nr.</i> 30956.100	Our work-order no. / 1068681
	Customer order no. / <i>Bestellungs- Nr.</i> 113846	
Specification / <i>Spezifikation:</i>		Certified goods / <i>Gegenstand</i> Ø340 mm fallende lengder 5,2 m leveringsmål Ø340/121 x ca. 5,2 meter
Marking / <i>Kennzeichnung:</i> A22352 T12694 8681 STG2012-370		Grade / <i>Werkstoff Nr.</i> Norsok M-630 D47 siste versjon, ISO15156/NACE 0175, ISO 104323/API 6A PSL 3, DNV RP-F112 og etter LIWAN 3-1, LIW-S-SP-SU-1218 rev.1, samt Spec 109697/C. Scana MS no: S8490-022, rev.0

CERTIFIED GOODS / ZERTIFIKERTES GUT

Test no. / <i>Probe Nr.</i>	Number / <i>Stück</i>	Weight / <i>Gewicht (kg)</i>	Dimension	Heat treatment / <i>Wärmebehandlung</i>	Process / <i>Erschmelzungsart</i>	Reduction grade / <i>Verschleißungsgrada.</i>	Charge no. / <i>Schmelze</i>
T12694	1	3370	339,7 x 5671	Solution annealed 1360°C, 1,5hrs, Water	Forged E/ AOD	3,78:1	A22352

CHEMICAL COMPOSITION / CHEMISCHE ANALYSE

SSA Quality name: 26C0 S8490

C	Si	Mn	S	P	Cr	Ni	W	V	Mo	Cu	Al	Ti	Nb	N	B	Pb	PRE
0,016	0,53	1,22	0,001	0,028	22,26	5,82	0,10	0,06	3,22	0,28	0,004	0,001	0,005	0,182	0,0018	0,0001	35,80

MECHANICAL PROPERTIES (L=Longitudinal, T=Transverse) MECHANISCHE EIGENSCHAFTEN (L=längs, T=Quer)

Test L/T <i>Probe L/T</i>	Temp. <i>°C</i>	Yield Strength / <i>Streckgrenze</i>		Tensile Strength / <i>Zugfestigkeit</i>		Elongation / <i>Dehnung</i>	Red. of area / <i>Ein-schnürung</i>	Impact values / <i>Kerbschlagarbeit</i>				Temp. <i>°C</i>	Hardness / <i>Härte</i>
		Rp0.2 <i>N/mm2</i>	Rp1.0 <i>N/mm2</i>	Rm <i>N/mm2</i>	Rp/Rm			J	J	J	Avg.		
F1	-	-	-	-	-	-	-	74	70	78	74	-46	-
E1	20	537	-	712	-	39	77	-	-	-	-	-	217
A1	-	-	-	-	-	-	-	57	38	52	49	-46	-
C1	20	514	-	726	-	37	76	-	-	-	-	-	217

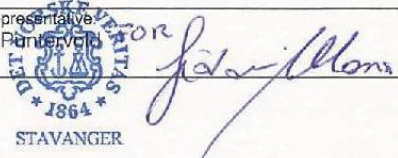
RESULTS OF OTHER TESTS / ERGEBNIS ANDERER PROBEN.

Sample-taking : A1: Charpy-V, transverse 1/4T C1: Tensile, transverse 1/4T
 E1: Tensile, longitudinal, 1/4T F1: Charpy-V, longitudinal 1/4T
 D3: Micro, subsurface D2: Micro, 1/2T
 D1: Micro, 1/4T
 B1: Corrosion, longitudinal 1/4T B2: Corrosion, longitudinal 1/2T

PT + UT carried out and accepted. Report attached
 Microstructure examination carried out. Reports attached
 Austenit spacing carried out. Reports attached
 Corrosion testing carried out and accepted. Reports attached.

Heat treated dimension Ø393mm Heat treatment graph-Report attached

We hereby declare that the product supplied are in compliance with the order in which test results are supplied.	Fitness for purpose not evaluated
Manufacturer's authorized representative:	3. party representative: Magne Penterveg





#3

**INSPECTION CERTIFICATE/
INSPEKTION ZERTIFIKAT**

4100 Jørpeland, Norway

Country of origin: Norway

EN 10204 - 3.1

Customer / <i>Besteller</i> Highland International Co Ltd 4/F Kaneda bldg. 2-15-1 Koenjikota Suginamiku 166-0002 Tokyo Japan	Date / <i>Datum</i> 13.12.2012	Cert.no. / <i>Zeugnis Nr.</i> C1913/12 rev.1
	Our order no. / <i>Unsere Auftrags- Nr.</i> 31209.100	Our work-order no. / 1068964
	Customer order no / <i>Bestellungs- Nr.</i> PO 2-09-04 (EBARA)	
Specification / <i>Spezifikation:</i> No. MPS -4V146E Rev.1	Certified goods / <i>Gegenstand</i> Ø185 x 3200 mm Forged and rough machined to above dimension.	
Marking / <i>Kennzeichnung:</i> A22440 T12704 UNS S31803 8964 R110231118 B01 12X16X21-3STBHSB 8017	Grade / <i>Werkstoff. Nr.</i> ASTM A276 UNS S31803	

CERTIFIED GOODS / ZERTIFIKERTES GUT

Test no. / <i>Probe Nr.</i>	Number / <i>Stück</i>	Weight / <i>Gewicht (kg)</i>	Dimension	Heat treatment / <i>Wärmebehandlung</i>	Process / <i>Erschmelzungsart</i>	Reduction grade / <i>Varschmiedungsgrad.</i>	Charge no. / <i>Schmelze</i>
T12704	1		Ø185 x 3200	Solution annealed 1060°C;5hrs. Waterquenched.(Cooling <12°C)	Forged E/ AOD	4.01:1	A22440

CHEMICAL COMPOSITION / CHEMISCHE ANALYSE

SSA Quality name: 26C0 S8490

C	Si	Mn	S	P	Cr	Ni	W	V	Mo	Cu	Al	Ti	Nb	N	B	Pb	PRE			
0,021	0,58	1,18	0,001	0,025	22,21	5,87	0,03	0,06	3,15	0,18	0,006	0,001	0,008	0,178	0,0020	0,0001	35,46			

MECHANICAL PROPERTIES (L=Longitudinal, T=Transverse) MECHANISCHE EIGENSCHAFTEN (L=längs, T=Quer)

Test L/T <i>Probe L/T</i>	Temp. °C	Yield Strength / <i>Streckgrenze</i>		Tensile Strength / <i>Zugfestigkeit</i>		Elongation / <i>Dehnung</i>	Red. of area / <i>Ein-schnürung</i>	Impact values / <i>Kerbschlagarbeit</i>				Temp. °C	Hardness / <i>Härte</i>
		Rp0.2 N/mm2	Rp1.0 N/mm2	Rm N/mm2	Rp/Rm			J	J	J	Avg.		
L	20	537		719		40	75	108	130	124	121	-46	217

RESULTS OF OTHER TESTS / ERGEBNIS ANDERER PROBEN.

UT and PT - accepted. Reports attached.
 Microstructure examination-accepted. Reports attached.
 Heat Treatment report attached.
 Dimension inspection carried out and accepted. Report attached.

We hereby declare that the product supplied are in compliance with the order in which test results are supplied.	
Manufacturer's authorized representative:	3.party representative:





#4

**INSPECTION CERTIFICATE/
INSPEKTION ZERTIFIKAT**

4100 Jørpeland, Norway

EN 10204 - 3.2

Country of origin: Norway

Customer / <i>Bestiller</i> Aarbakke AS Postboks 108 4341 Bryne	Date / <i>Datum</i> 13.11.2012	Cert.no. / <i>Zeugnis Nr.</i> C1831/12
	Our order no. / <i>Unsere Auftrags- Nr.</i> 31116.100	Our work-order no. / 1068776
Customer order no. / <i>Bestellungs- Nr.</i> 114154		
Specification / <i>Spezifikation</i> : Norsk M-630 MDS D-47 rev.4	Certified goods / <i>Gegenstand</i> 2 stk. Ø180 x ca. 4 m/stk. grov maskinert utførelse i fallende lengder	
Marking / <i>Kennzeichnung</i> : A22440 T12706 8776 STG2012-486	Grade / <i>Werkstoff. Nr.</i> ASTM A479, UNS S31803	

CERTIFIED GOODS / ZERTIFIKERTES GUT

Test no. / <i>Probe Nr.</i>	Number / <i>Stück</i>	Weight / <i>Gewicht (kg)</i>	Dimension	Heat treatment / <i>Wärmebehandlung</i>	Process / <i>Erschmelzungsart</i>	Reduction grade / <i>Verschmiedungsgrad</i>	Charge no. / <i>Schmelze</i>
T12706	2	814 824	Ø180 x 4115 Ø180,5 x 4111	Solution annealed 1060°C, 3hrs; Water	Forged E/ AOD	4,09:1	A22440

CHEMICAL COMPOSITION / CHEMISCHE ANALYSE

SSA Quality name: 26C0 S8490

C	Si	Mn	S	P	Cr	Ni	W	V	Mo	Cu	Al	Ti	Nb	N	B	Pb	PRE
0,021	0,56	1,18	0,001	0,025	22,21	5,67	0,03	0,03	3,15	0,18	0,006	0,001	0,008	0,178	0,0020	0,0001	35,46

MECHANICAL PROPERTIES (L=Longitudinal, T=Transverse) MECHANISCHE EIGENSCHAFTEN (L=längs, T=Quer)

Test L/T Probe L/T	Temp. °C	Yield Strength / <i>Streckgrenze</i>		Tensile Strength / <i>Zugfestigkeit</i>		Elongation / <i>Dehnung</i>	Red. of area / <i>Ein- schränkung</i>	Impact values / <i>Kerbschlagarbeit</i>				Temp. °C	Hardness / <i>Härte</i>
		Rp0.2 N/mm2	Rp1.0 N/mm2	Rm N/mm2	Rp/Rm			J	J	J	Avg.		
L	20	549		716		39	77	230	234	249	238	-46	217

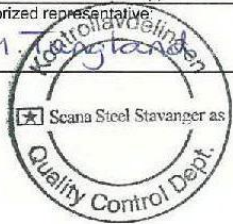
RESULTS OF OTHER TESTS / ERGEBNIS ANDERER PROBEN.

Sample-taking : Charpy-V; longitudinal 1/4T, Tensile; longitudinal 1/4T
Micro; 1/4T Corrosion; 1/4T

PT + UT carried out and accepted. Report attached
Microstructure examination carried out. Report attached
Corrosion testing carried out and accepted. Report attached.

Heat treated dimension Ø198mm Heat treatment graph-Report attached

We hereby declare that the product supplied are in compliance with the order in which test results are supplied.	Fitness for purpose not evaluated
Manufacturer's authorized representative: 	3.party representative: Magne Puntervold






#5

**INSPECTION CERTIFICATE/
INSPEKTION ZERTIFIKAT**

4100 Jørpeland, Norway
Country of origin: Norway

EN 10204 - 3.2

Customer / Bestiller Aarbakke AS Postboks 108 4341 Bryne	Date / Datum 16.10.2012	Cert.no./Zeugnis Nr. C1586/12
	Our order no./ Unsere Auftrags-Nr. 30884.100	Our work-order no./ 1068428
	Customer order no./ Bestellungs-Nr. 113715	
Specification / Spezifikation: Certified goods / Gegenstand 3 stk Ø340 mm i fallende lengde Leveringsmål Ø340/70 x ca 5500 mm		
Marking / Kennzeichnung: A22328 T12659 8428 STG2012-320  Grade / Werkstoff Nr. Norsk M-630 D47, rev.4 ASTM A479 UNS S31803 ISO15156/NACE 0175, DNV RP-F112 Spec 109697/C, LIWAN 3-1, LIW-S-SP-SU-1218 rev.1 Aarbakke spec.Duplex Meter body rev.2		

CERTIFIED GOODS / ZERTIFIKERTES GUT

Test no./ Probe Nr.	Number / Stück	Weight / Gewicht (kg)	Dimension	Heat treatment / Wärmebehandlung	Process / Erschmelzungsart	Reduction grade / Verschleißungsgrad	Charge no. / Schmelze
T12659	1	8638	Ø341 x 5620	Solution annealed 1080°C,3hrs;Water	Forged E/ AOD	4,26:1	A22328

CHEMICAL COMPOSITION / CHEMISCHE ANALYSE

C	Si	Mn	S	P	Cr	Ni	W	V	Mo	Cu	Al	Ti	Nb	N	B	PRE	SSA Quality name: 26C0 S8490
0,026	0,62	1,23	0,001	0,027	22,18	5,60	0,17	0,07	3,19	0,24	0,006	0,001	0,007	0,188	0,0021	35,74	

MECHANICAL PROPERTIES (L=Longitudinal, T=Transverse) MECHANISCHE EIGENSCHAFTEN (L=längs, T=Quer)

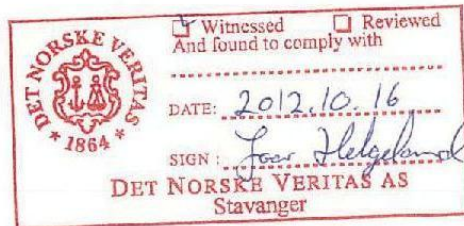
Test L/T Probe L/T	Temp. ° C	Yield Strength / Streckgrenze		Tensile Strength / Zugfestigkeit		Elongation / Dehnung A %	Red. of area / Einschnürung z %	Impact values / Kerbschlagarbeit Kv				Temp. ° C	Hardness / Härte HB
		Rp0.2 N/mm2	Rp1.0 N/mm2	Rm N/mm2	Rp/Rm			J	J	J	Avg.		
A1	-	-	-	-	-	35	68	72	52	77	67	-46	-
C1	20	548	-	740	-	-	-	-	-	-	-	-	223
A2	-	-	-	-	-	-	-	68	45	68	60	-46	-
C2	20	557	-	747	-	34	70	-	-	-	-	-	217
E1	-	-	-	-	-	-	-	111	137	167	138	-46	-
F1	20	598	-	753	-	35	71	-	-	-	-	-	229
E2	-	-	-	-	-	-	-	101	132	137	123	-46	-
F2	20	574	-	735	-	38	72	-	-	-	-	-	223

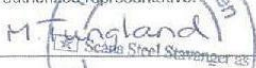
RESULTS OF OTHER TESTS / ERGEBNIS ANDERER PROBEN.

Sample-taking : A1: Charpy-V, transverse 1/4T A2: Charpy-V, transverse 1/2T
 C1: Tensile, transverse 1/4T C2: Tensile, transverse 1/2T
 E1: Tensile, longitudinal, 1/4T E2: Tensile, longitudinal, 1/2T
 F1: Charpy-V, longitudinal 1/4T F2: Charpy-V, longitudinal 1/2T
 D3: Micro, subsurface D2: Micro, 1/2T
 D1: Micro, 1/4T
 B1: Corrosion, longitudinal 1/4T B2: Corrosion, longitudinal 1/2T

PT + UT - accepted. Report attached
 Microstructure examination-accepted. Reports attached
 Austenit spacing carried out. Reports attached
 Corrosion testing-accepted. Report attached.

Heat treated dimension Ø370mm Heat treatment graph-Report attached



We hereby declare that the product supplied are in compliance with the order in which test results are supplied.	Fitness for purpose not evaluated
Manufacturer's authorized representative:  M. Fungland Scana Steel Stavanger AS	3.party representative: Joar Helgeland



Attachment B: SEM images of erosion surfaces

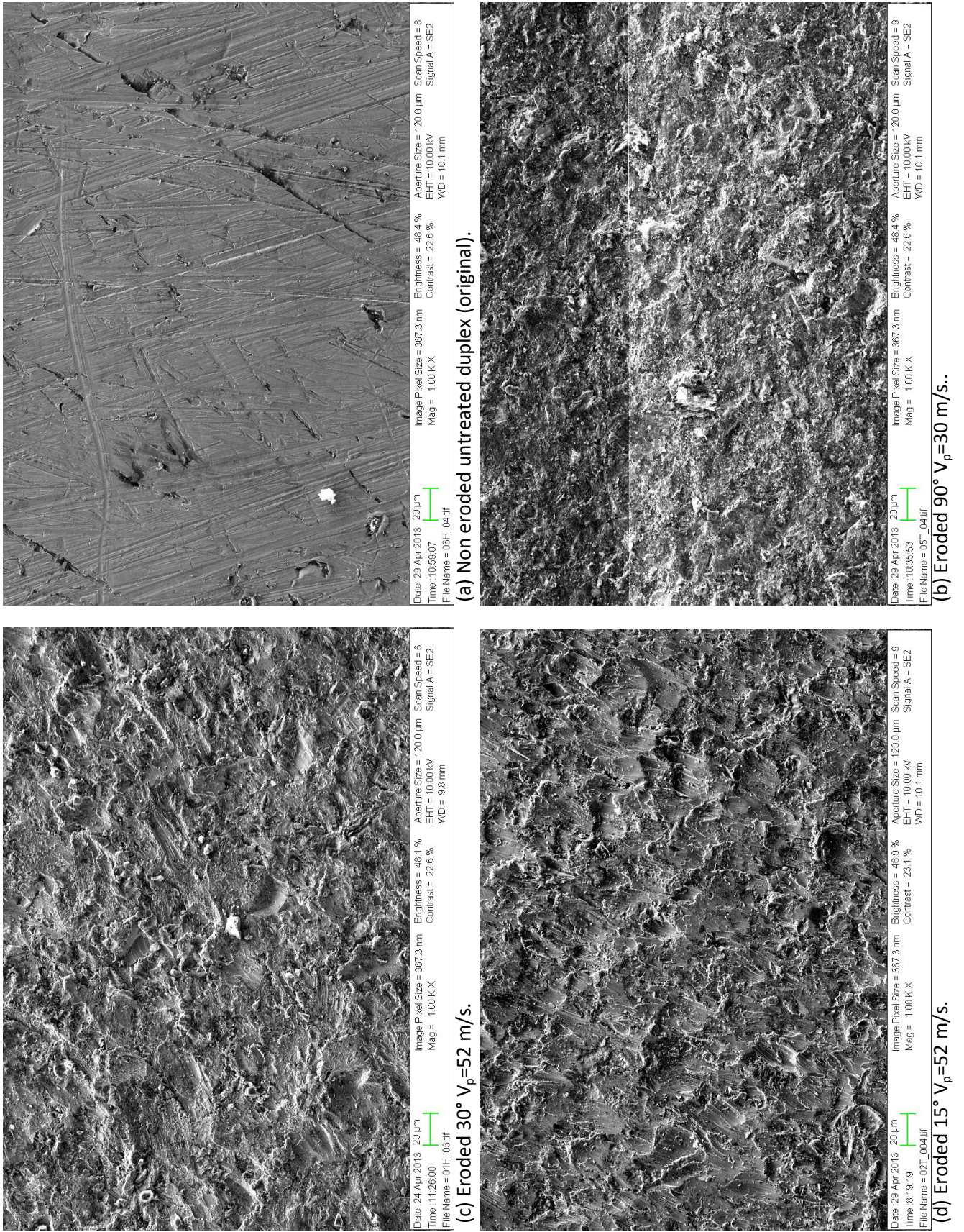
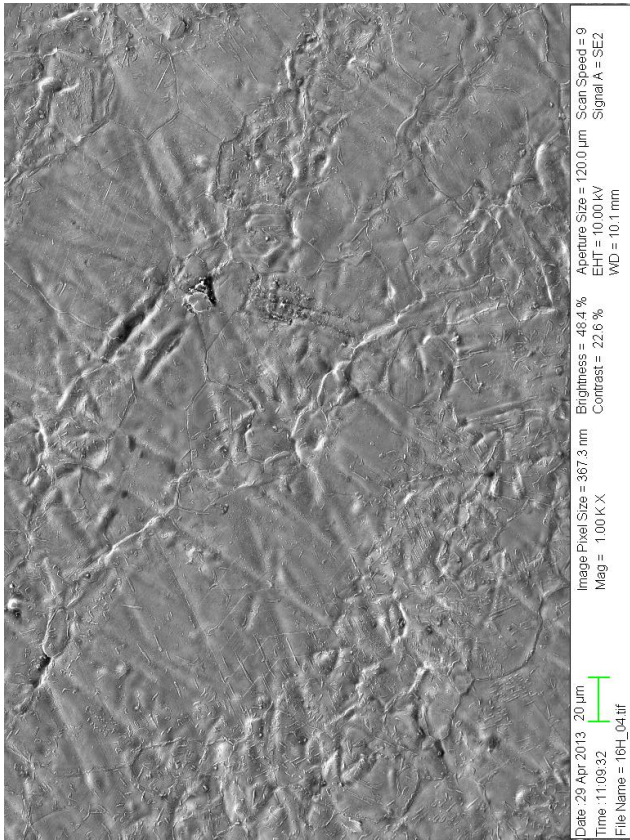
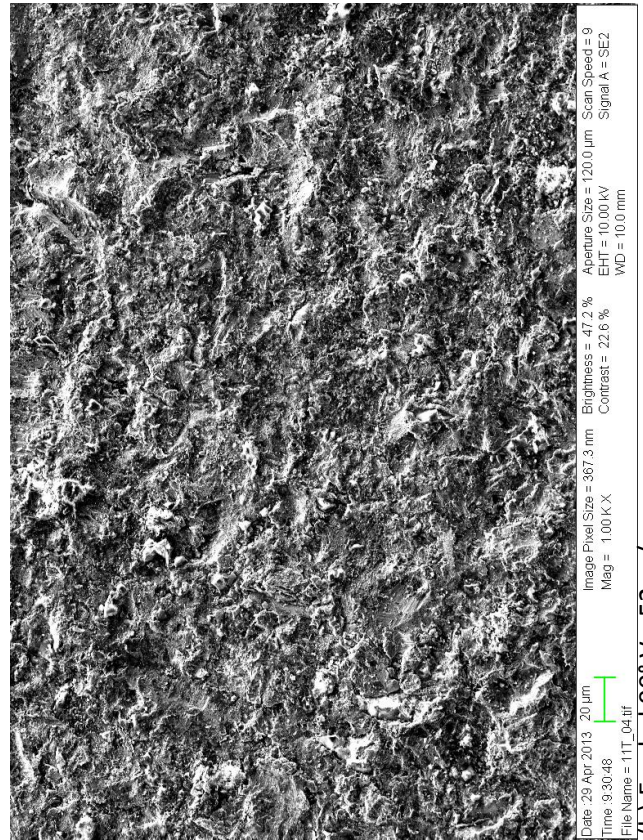


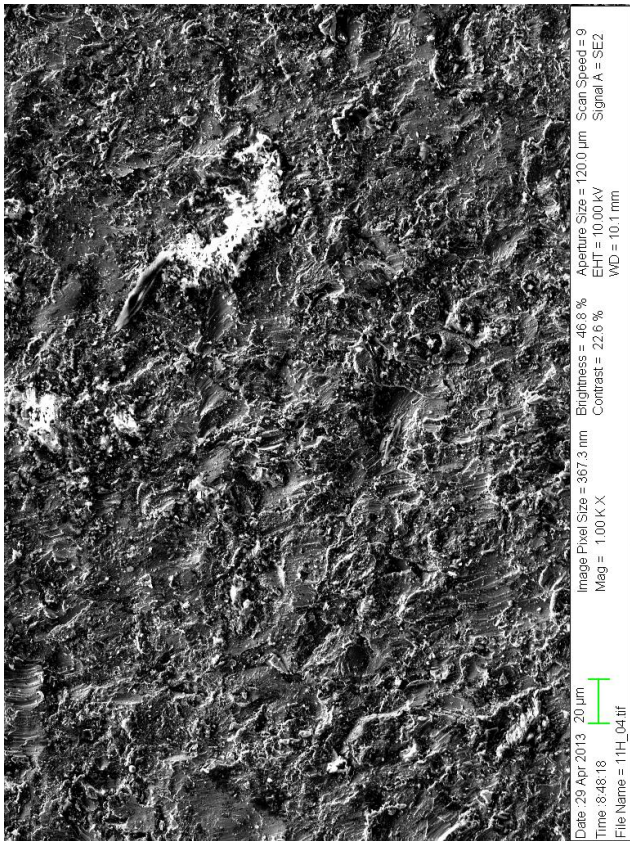
Figure 70. SEM images of untreated duplex (1000X) with a particle velocity of 52 m/s except of (b) with $V_p=30$ m/s.



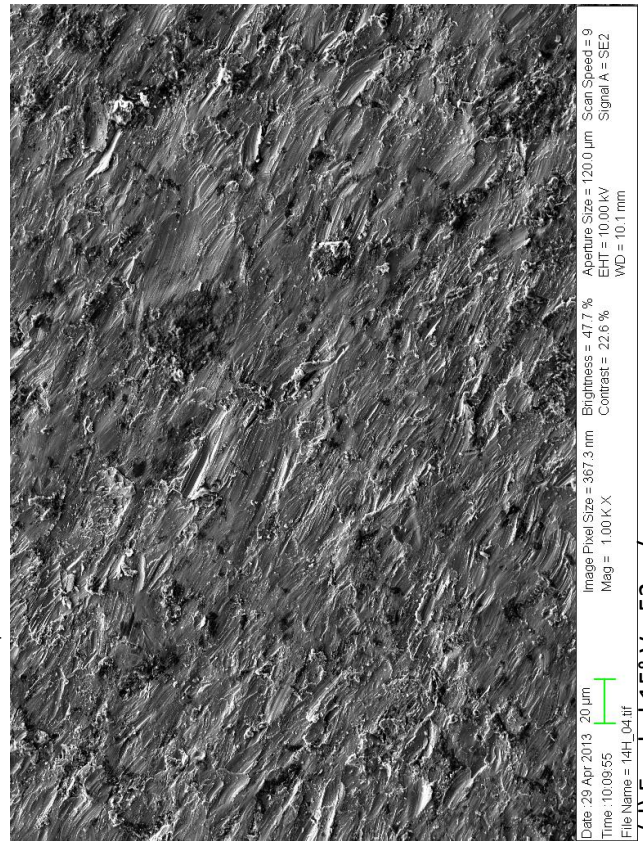
(a) Non eroded Expanite (original).



(b) Eroded 90° $V_p=52$ m/s.

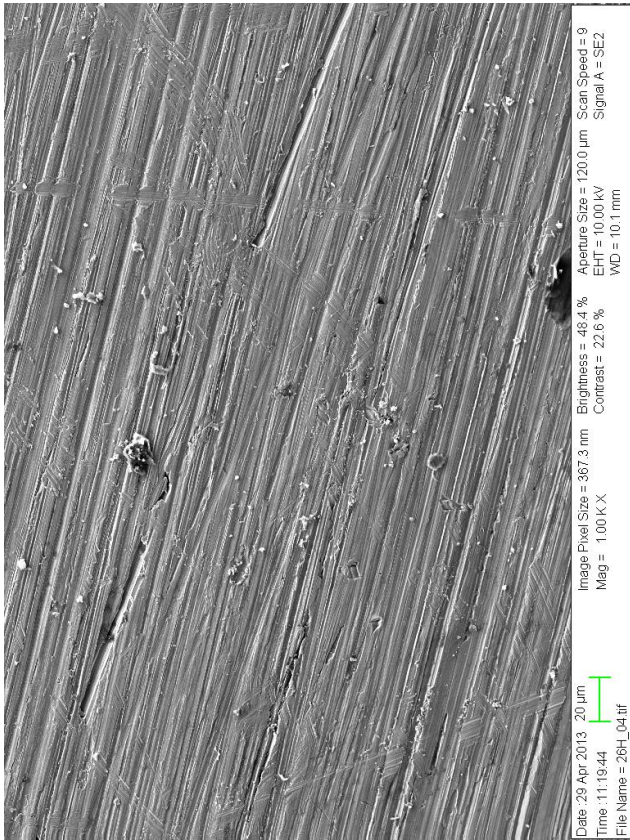


(c) Eroded 30° $V_p=52$ m/s.

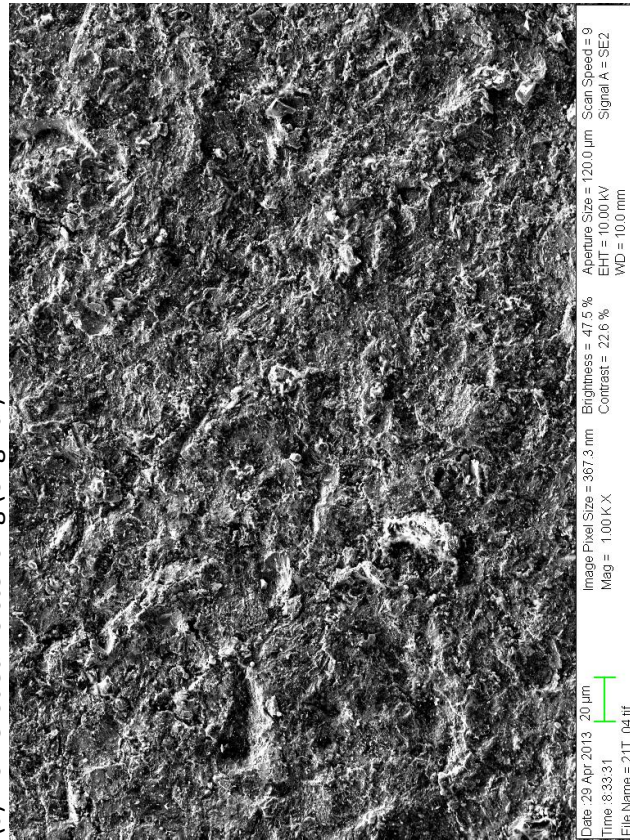


(d) Eroded 15° $V_p=52$ m/s.

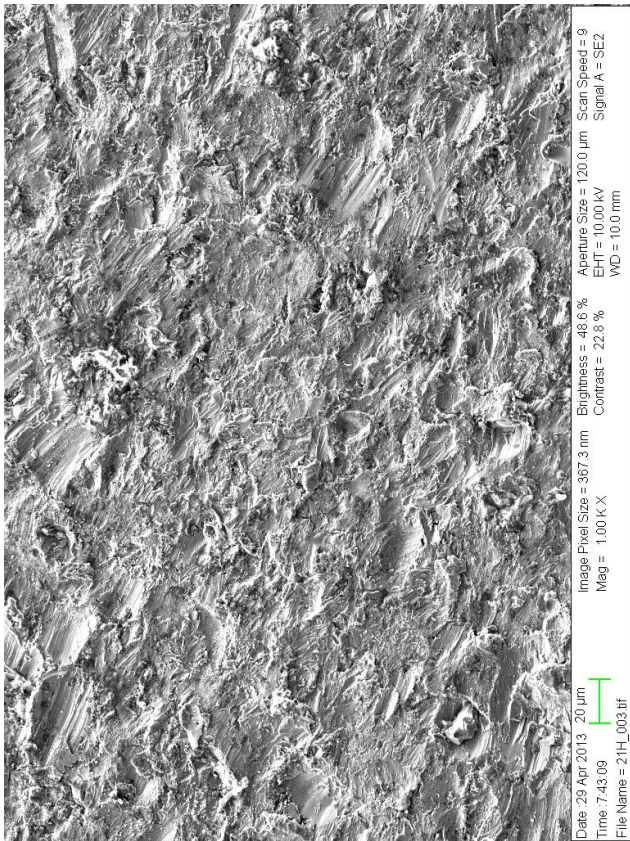
Figure 71. SEM images of Expanite (1000X) with a particle velocity of 52 m/s.



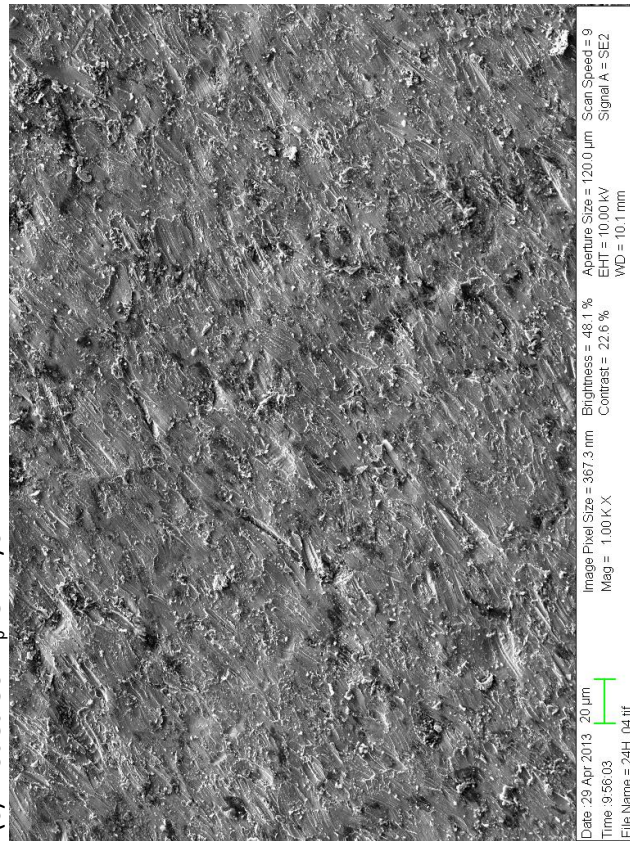
(a) Non eroded Kolsterising (original).



(b) Eroded 90° $V_p=52$ m/s.

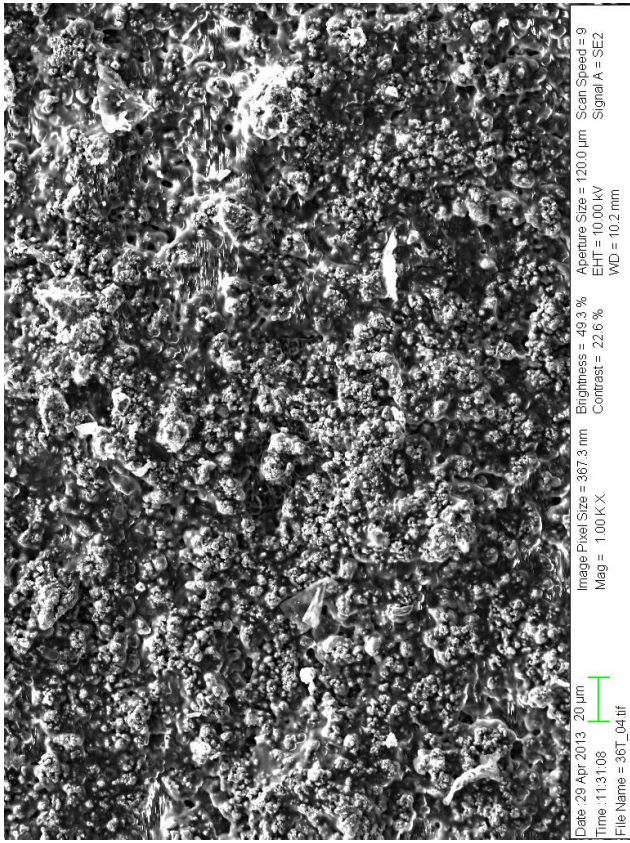


(c) Eroded 30° $V_p=52$ m/s.

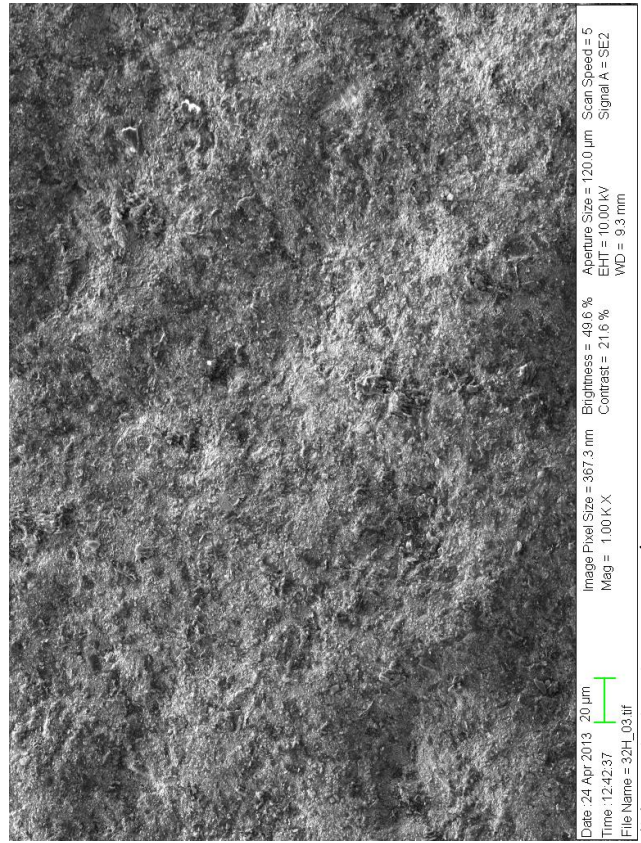


(d) Eroded 15° $V_p=52$ m/s.

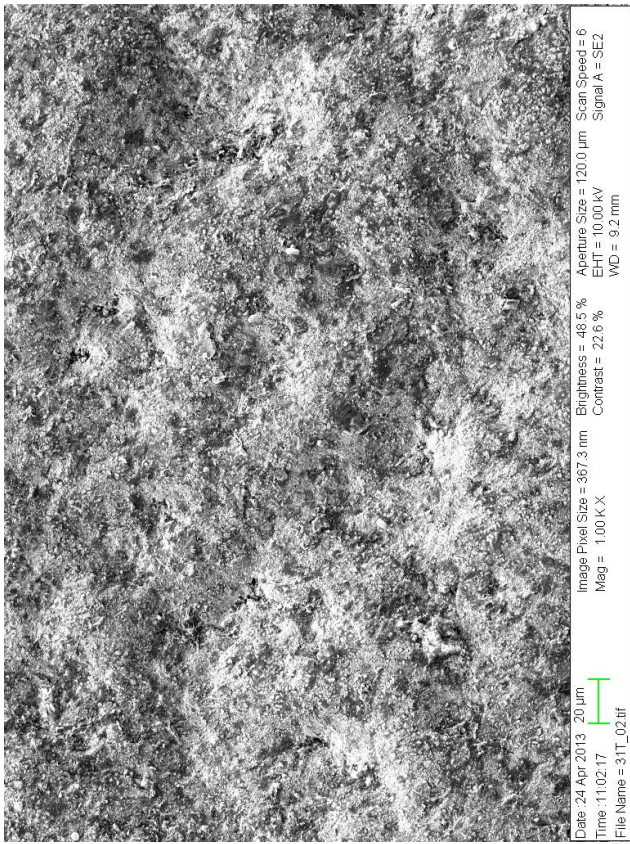
Figure 72. SEM images of Kolsterising (1000X) with a particle velocity of 52 m/s.



(a) Non eroded HVOF (original).

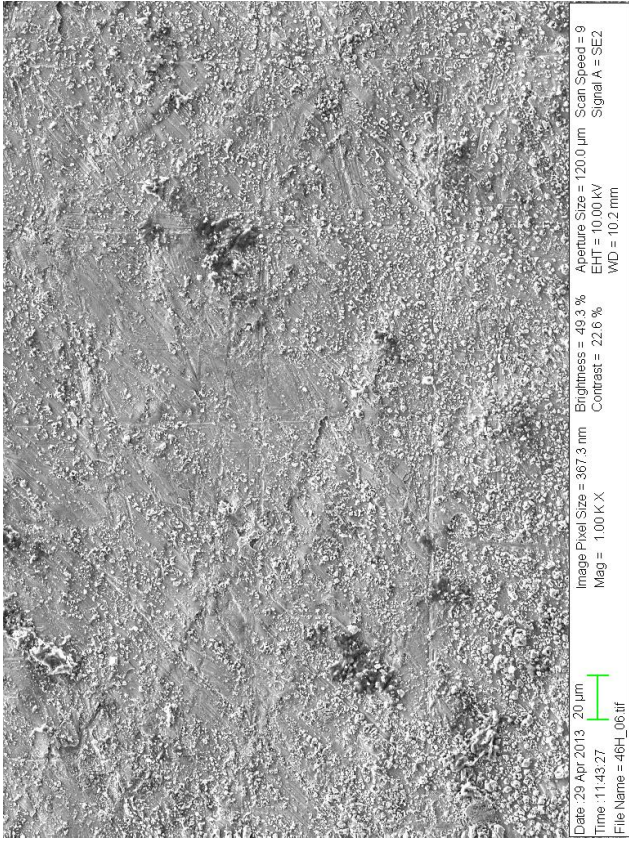


(b) Eroded 90° $V_p=52$ m/s.

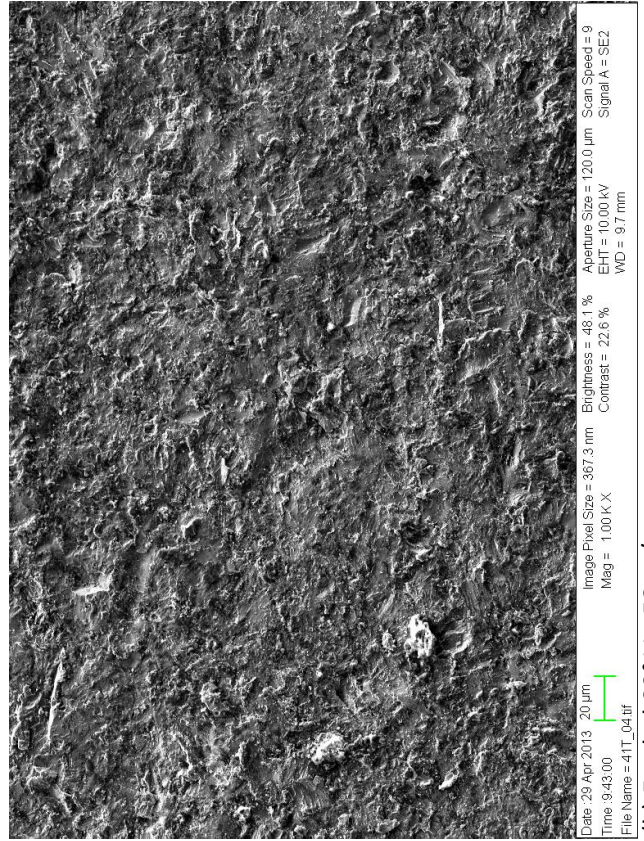


(c) Eroded 30° $V_p=52$ m/s.

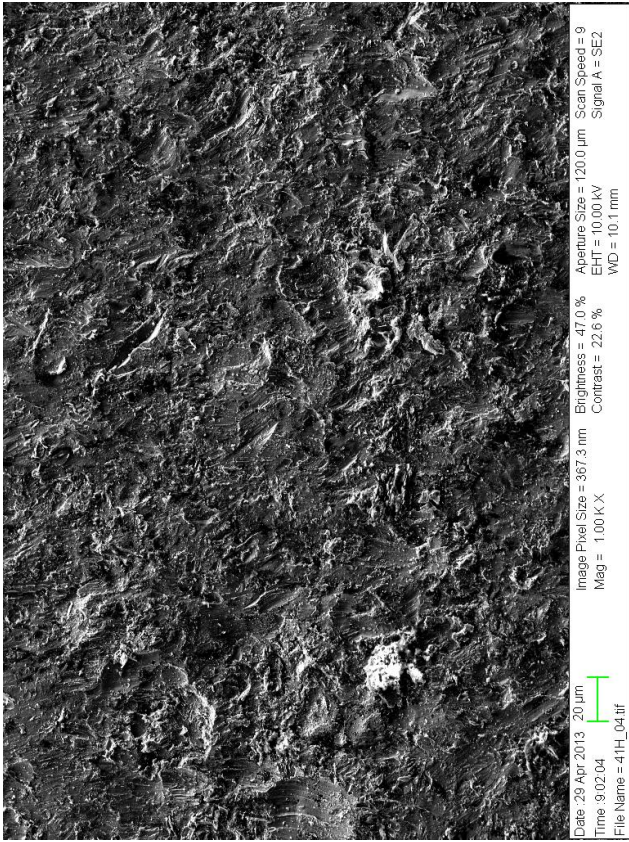
Figure 73. SEM images of HVOF (1000X) with a particle velocity of 52 m/s.



(a) Non eroded Sursulf duplex (original).

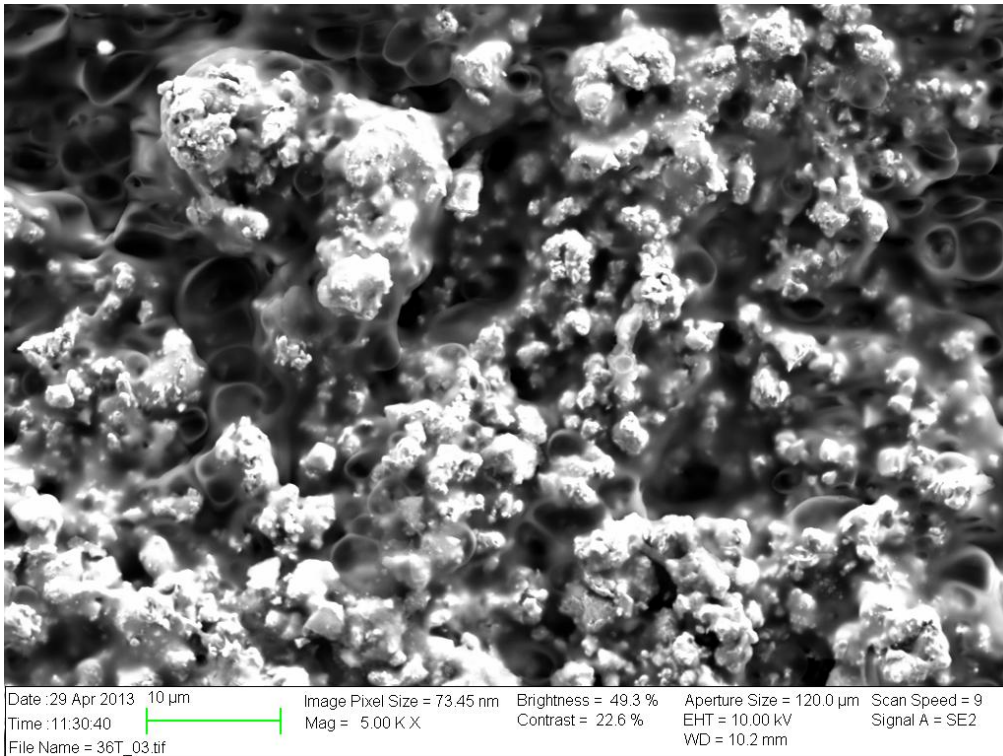


(b) Eroded 90° $V_p=52$ m/s.

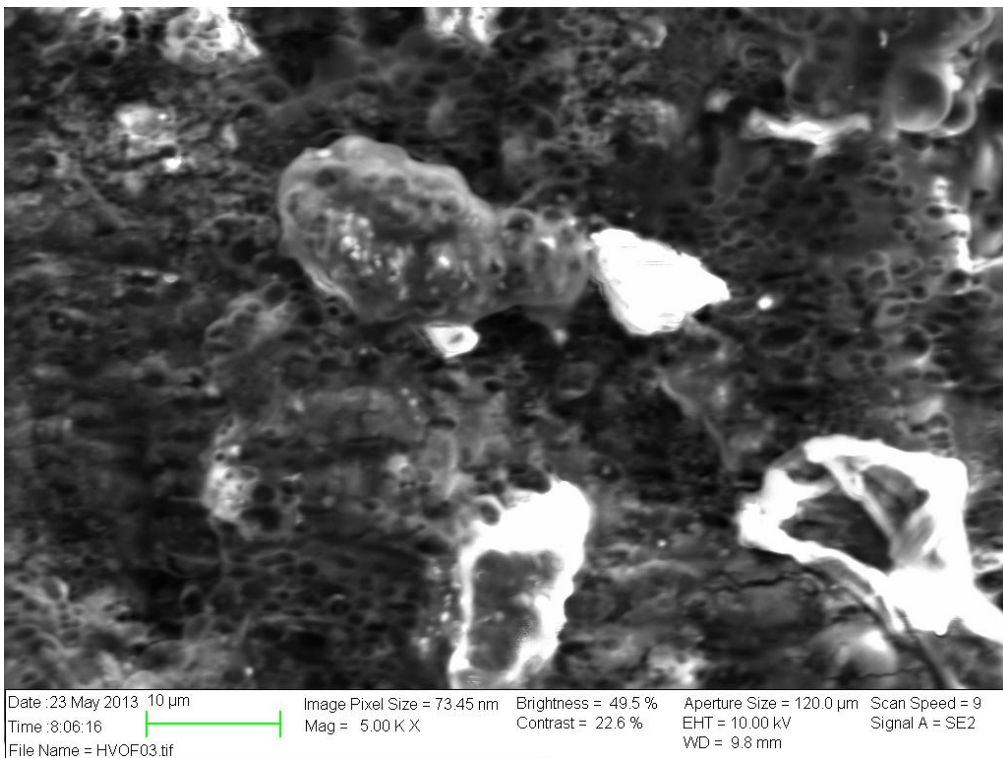


(c) Eroded 30° $V_p=52$ m/s.

Figure 74. SEM images of Sursulf duplex (1000X) with a particle velocity of 52 m/s.

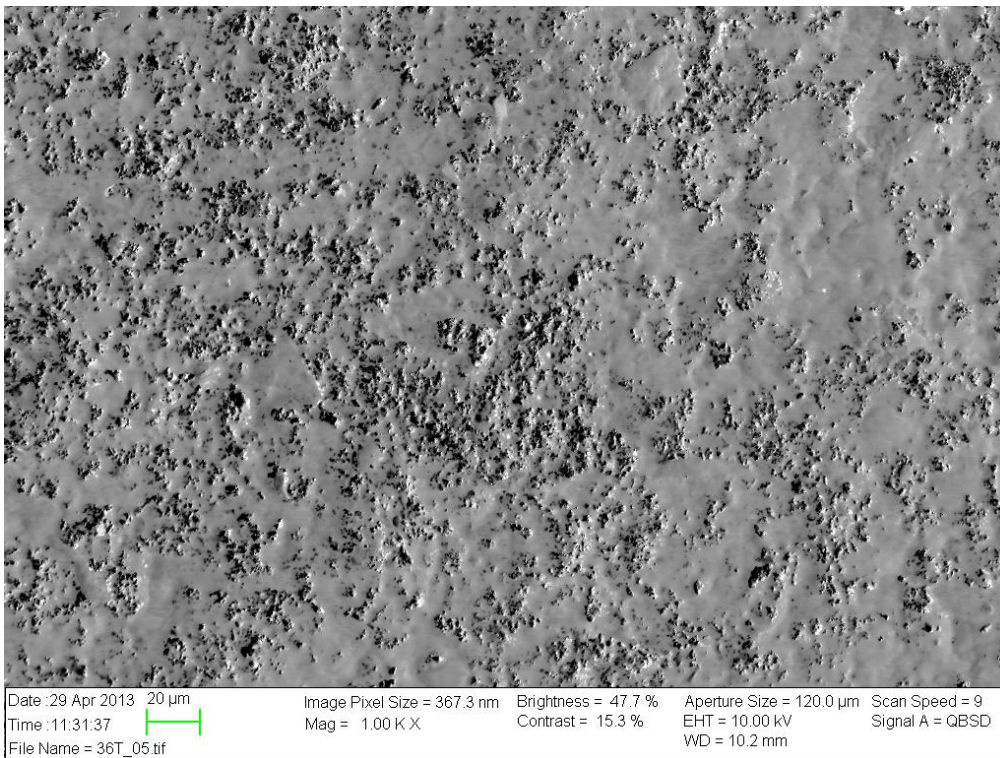
Attachment C: SEM images of HVOF surface – corrosion G48

(a)

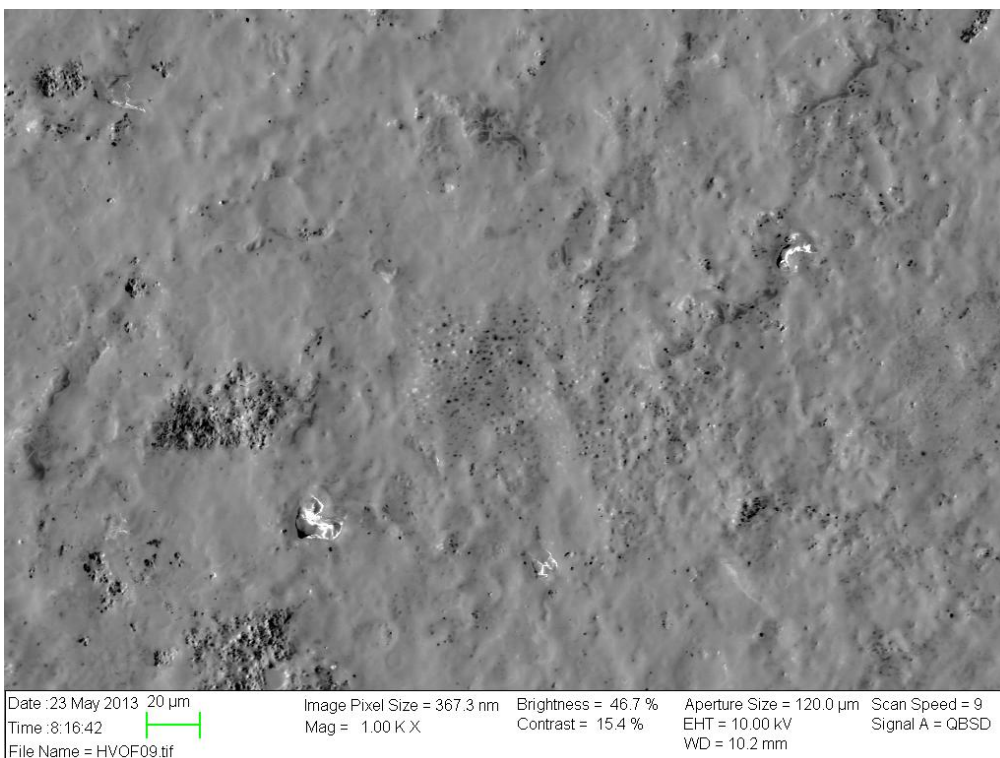


(b)

Figure 75. SEM images by use of secondary electron detector (5000X) showing HVOF surface (a) before and (b) after corrosion G48 test. A lot of the tungsten carbides have detached from surface due to material degradation of the binder.

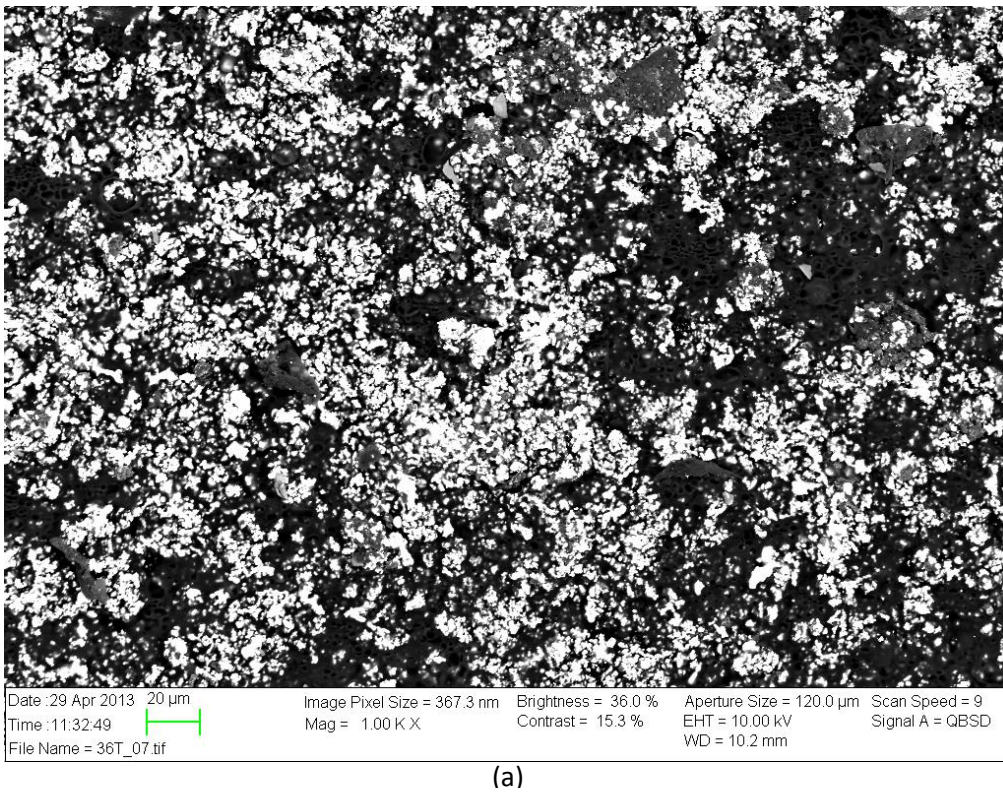


(a)

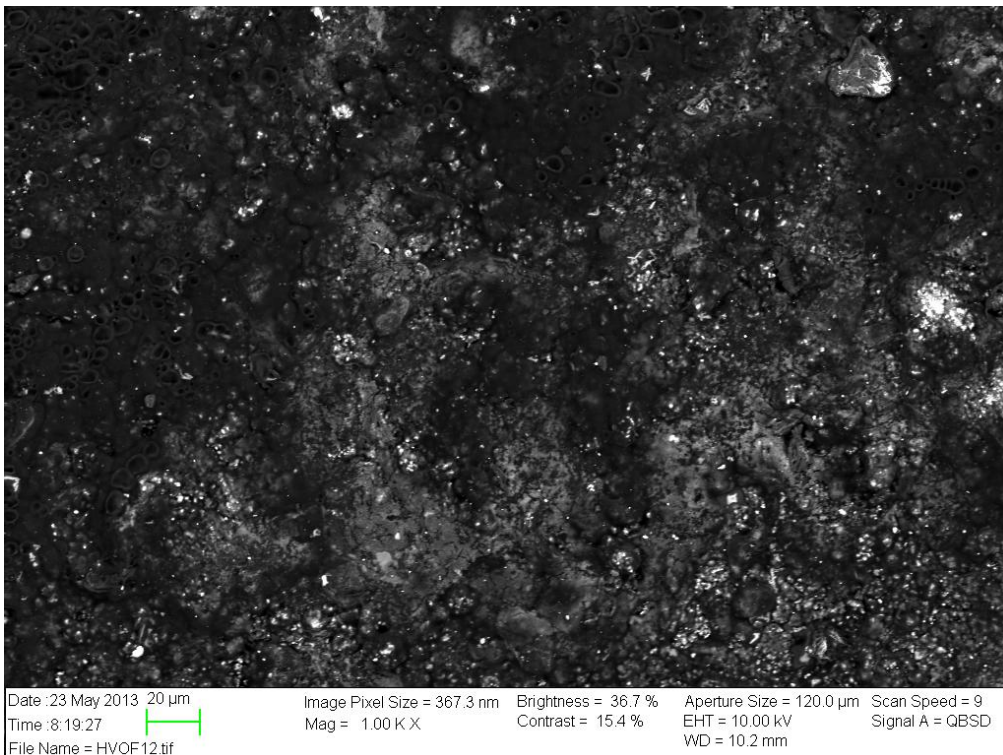


(b)

Figure 76. SEM images by use of the topographic mode of the backscatter electron detector (1000X) showing HVOF surface (a) before and (b) after corrosion G48 test. A lot of the tungsten carbides have detached from surface due to material degradation of the binder.



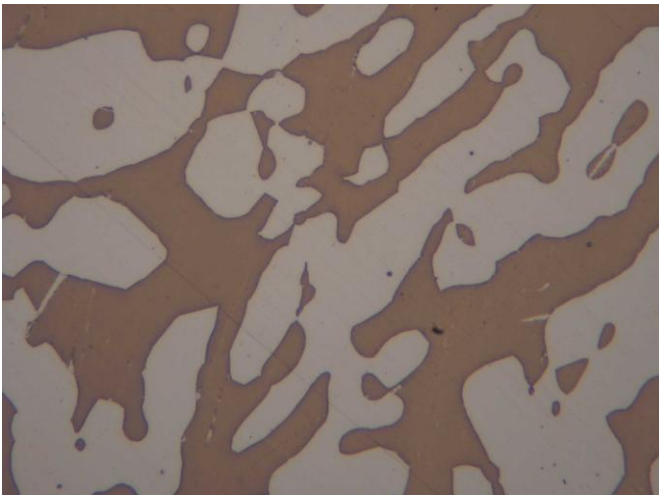
(a)



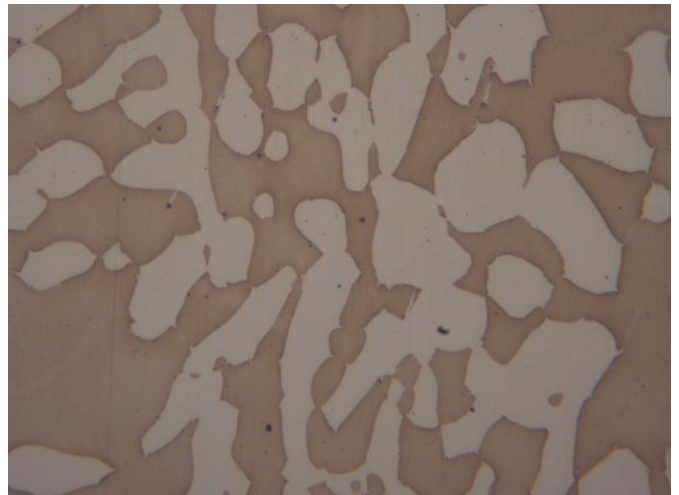
(b)

Figure 77. SEM images by use of the composition mode of the backscatter electron detector (1000X) showing HVOF surface (a) before and (b) after corrosion G48 test. Dark area represent binder and bright area represent tungsten carbide. The image taken after corrosion test reveal that a lot of the tungsten carbides have detached from surface due to material degradation of the binder.

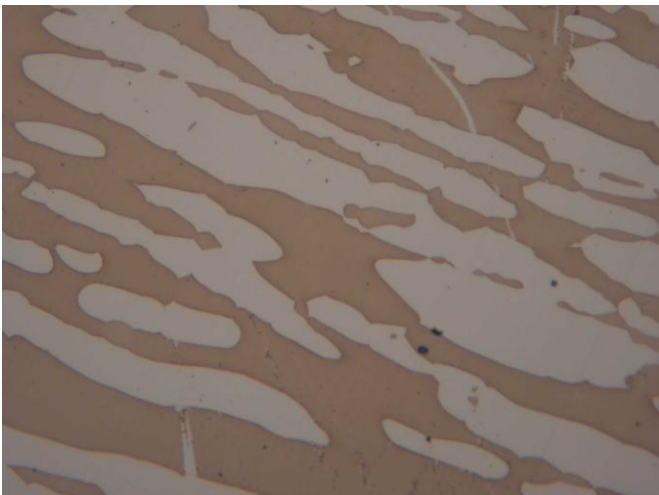
Attachment D: Optical micrographs of NaOH etched specimens



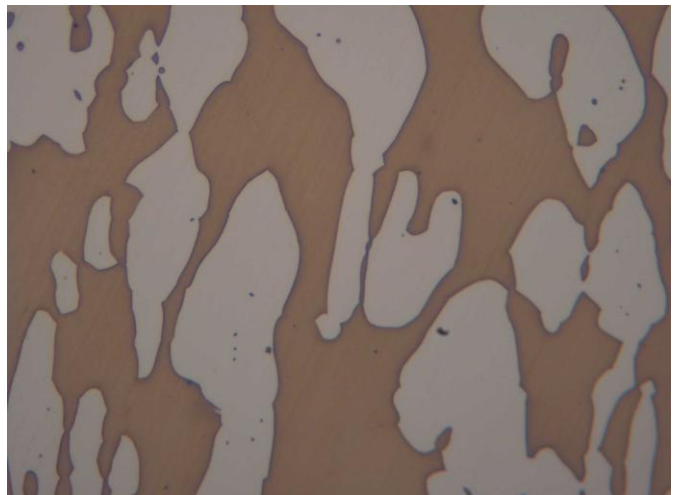
(a) untreated duplex



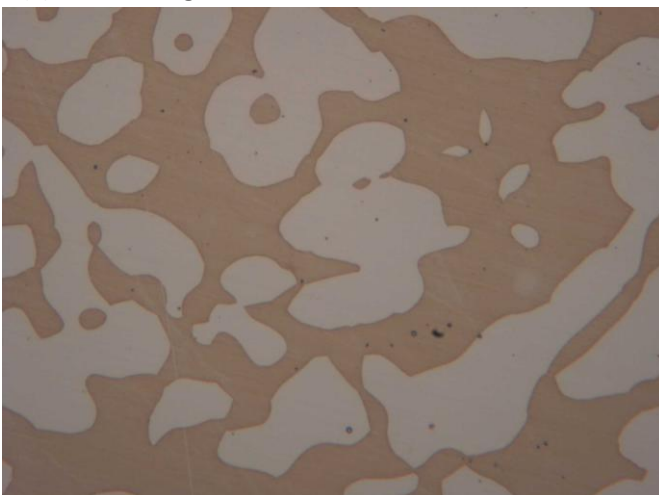
(b) Expanite



(c) Kolsterising



(d) HVOF



(e) Sursulf duplex

Figure 78. Optical micrographs of duplex base material etched with sodium hydroxide (NaOH).